Toward the Development of a Novel Mineralized Collagen Scaffold for Bone Repair and Regeneration

Brendan Hilton Grue

Submitted in partial fulfilment
of the requirements for the degree of
Doctor of Philosophy in Applied Science

at

Saint Mary's University
Halifax, Nova Scotia
Canada
July, 2020

Approved by:

Samuel P. Veres, PhD
Supervisor

Kathy Singfield, PhD
Supervisory Committee Member

Paul Gratzer, PhD
Supervisory Committee Member

Thomas Willett, PhD
External Examiner

Date: July 7, 2020

Toward the Development of a Novel Mineralized Collagen Scaffold for Bone Repair and Regeneration

By: Brendan Hilton Grue

Abstract

Due to an increasing demand for more functional bone-repair materials, implants composed of mineralized collagen have garnered interest. The process as to how collagen fibrils become mineralized both *in situ* and *in vitro* is not yet well understood. Additionally, preparing scaffolds possessing similar mechanical and structural features as those found within bone remains a difficult process. The benefit of preparing an implant composed of mineralized collagen that can be mechanically tailored and holds a chemical and structural profile similar to bone is widely recognized. The studies contained herein describe a novel process for preparing an acellular, naturally crosslinked mineralized collagen scaffold based on a tailorable alternate soaking mineralization procedure.

The developed mineralization procedure led to a close integration between bone-like mineral and aligned collagen fibrils in produced scaffolds. Through adjustments in the manufacturing procedure, the mechanics of both individual fibrils and whole sheets were able to be controlled, as determined through nanoindentation and flexural testing. It was found through *in vitro* investigations that mineralized scaffolds preferentially promoted the differentiation of pre-osteoblast cells, measured by ALP activity and OCN content.

Traditional methods of preparing mineralized collagen scaffolds often use reconstituted, randomly oriented collagen fibrils, mineralized in such a way that often ignores the specific mineral-collagen association found in nature. The motivation behind this work was to develop a mineralized collagen scaffold that paid particular attention to fibril alignment as well as mineral integration and subsequent material mechanics. The work described herein presents, for the first time, the ability to easily control the mechanics of mineralized collagen fibrils and aligned sheets in a predictable way through simple modifications in their mineralization procedure. Additionally, insights

gained from detailed structural and chemical analyses allow for a wider understanding of the effects various chemical additives have on prepared mineral crystals; widening our understanding on biomineralization.

July 7, 2020

Acknowledgments

It is without question that the year 2020 has brought with it many highs and lows, including unimaginable changes for our global community as we face the repercussions of COVID-19. Locally, my peaceful rural home community was confronted with a massive tragedy, leaving my friends and family shocked in horror and confusion. In response to these events, I feel that my community, defined in its largest sense, has come together like never before. I don't know where I would be without the continued support from friends and strangers alike in this grim and challenging time.

I'd like to thank my friends and family for their enduring support over the past five years and beyond; in particular my mom, who allowed me to move home and write this thesis from her basement during the pandemic. Thank you to my thesis committee for your encouragement and feedback throughout this process. I'd also like to extend a special thank you to all of the help I received from my research colleagues, including technical support from Darren Cole and Patricia Scallion, and mentors, particularly Dr. Laurent Kreplak for his extensive support. Finally, thank you, Sam. These past five years have been quite a transformative time in your life as well, however, from my perspective, your commitment and respect to me as your student has never fallen short.

I am dedicating this thesis to those who, for reasons due to circumstance or lack of support, are unable to be in my current position of privilege and opportunity. I aim to represent and give voice to you as a future clinician-scientist and shine light on injustices that feed cycles of inequity; understanding that this can only be done with open ears.

Contents

List of Abbreviations

ALP	alkaline phosphatase
ACP	amorphous calcium phosphate
AFM	atomic force microscopy
BMP	bone morphogenetic protein
CaP	calcium phosphate
CDE	common digital extensor
DBM	demineralized bone matrix
DMT	Derjaguin-Muller-Toporov
DCPD	di-calcium phosphate dibasic
DSC	differential scanning calorimetry
EDX	energy-dispersive X-ray spectroscopy
EDC	1-Ethyl-3-[3-dimethylaminopropyl]carbodiimide hydrochloride
ECM	extracellular matrix
FGF	fibroblast growth factor
FE	finite element

FTIR-ATR	Fourier transform infrared spectroscopy attenuated total reflection
FWHM	full-width half-max
GP	genipin
GTA	glutaraldehyde
GAG	glycosaminoglycan
HA	hydroxyapatite
Pi	inorganic phosphate
IGF	insulin-like growth factor
LOX	lysyl oxidase
MV	matrix vesicle
MSC	mesenchymal stem cell
MW	molecular weight
NHS	N-hydroxysuccinimide
NCP	non-collagenous protein
OCP	octa-calcium phosphate
ORIF	open reduction internal fixation
OCN	osteocalcin
OPN	osteopontin
PAA	polyacrylic acid
PTH	parathyroid hormone
PBS	phosphate-buffered saline

pAsp	polyaspartic acid
PCL	poly(ϵ-caprolactone)
PGA	poly(glycolic acid)
PLA	poly(lactic acid)
PLGA	poly(lactic-co-glycolic)
PLGU	poly-L-glutamic acid
PILP	polymer induced liquid precursor
PPi	pyrophosphate
PVPA	polyvinylphosphonic acid
QNM	quantitative nanomechanical mapping
RGD	tripeptide Arginine-Glycine-Aspartate
SEM	scanning electron microscopy
SBF	simulated body fluid
STMP	sodium trimetaphosphate
STP	sodium tripolyphosphate
TPP	sodium tripolyphosphate
TGF	transforming growth factor
TEM	transmission electron microscopy
TCP	tricalcium phosphate
VEGF	vascular endothelial growth factor
XRD	X-ray powder diffraction

List of Tables

List of Figures

Chapter 1

Introduction

1.1 Bone anatomy and physiology

The basic components of bone and bone-like tissues are a mineral phase, usually described as hydroxyapatite (HA), and an organic phase, mainly comprised of type I collagen[1,2]. Bones serve many important functions throughout our bodies and represent a very dynamic organ system. Humans utilize this mineralized matrix in many ways, including for mineral storage, as a site for cell development, enhanced locomotion, acid-base balance, and fat storage[2]. Bone is essential for overall bodily homeostasis. Our skeleton is also divided into many different unique structures such as the small bones in the middle ear responsible for coupling sound energy, to the largest bone in the body, the femur, which is vital for weight bearing and is an attachment point for many muscles involved in locomotion. Bone is also found in different forms even within the same bone structure, including both cortical (compact) bone and trabecu-

lar (spongy) bone, where composition can be split evenly, such as in the femoral head, or offset at a ratio of 25:75 in the vertebrae[3].

1.1.1 Organic portion of bone

The organic portion of bone makes up roughly 30% of bone by dry weight. Type I collagen accounts for roughly 85-90% of the total protein in bone, with various non-collagenous proteins (NCP)s contributing towards the remainder[1]. Type I collagen fibrils are made from the self-assembly of individual tropocollagen molecules. Tropocollagen is formed once associated propeptides are removed from precursor procollagen molecules by extracellular proteinases[4,5]. Type I collagen molecules are triple helical in structure, composed of two α1-chains and one α2-chain[4]. In fibrils, these 300 nm long collagen molecules are arranged in parallel to one another in a quarter staggered arrangement forming regions of gap and overlap with a 67 nm (D) banding periodicity in the hydrated state (Fig. 1.1)[4–6]. Gap regions, in which one-fifth of the collagen molecules are absent, are thought to be roughly 0.54D (36 nm) in length and 1-2 nm in depth (diameter of a single tropocollagen molecule)[5,7]. Individual collagen fibrils ultimately form macroscopic collagen fibers and organized networks found in larger tissues, such as bone. The orientation and specific patterns of collagen fibers found within bone also determines the bone type. Fibers arranged in a regular parallel array make up lamellar bone whereas woven bone is comprised of fibers possessing a much more disordered and overall mechanically weaker configuration[2].

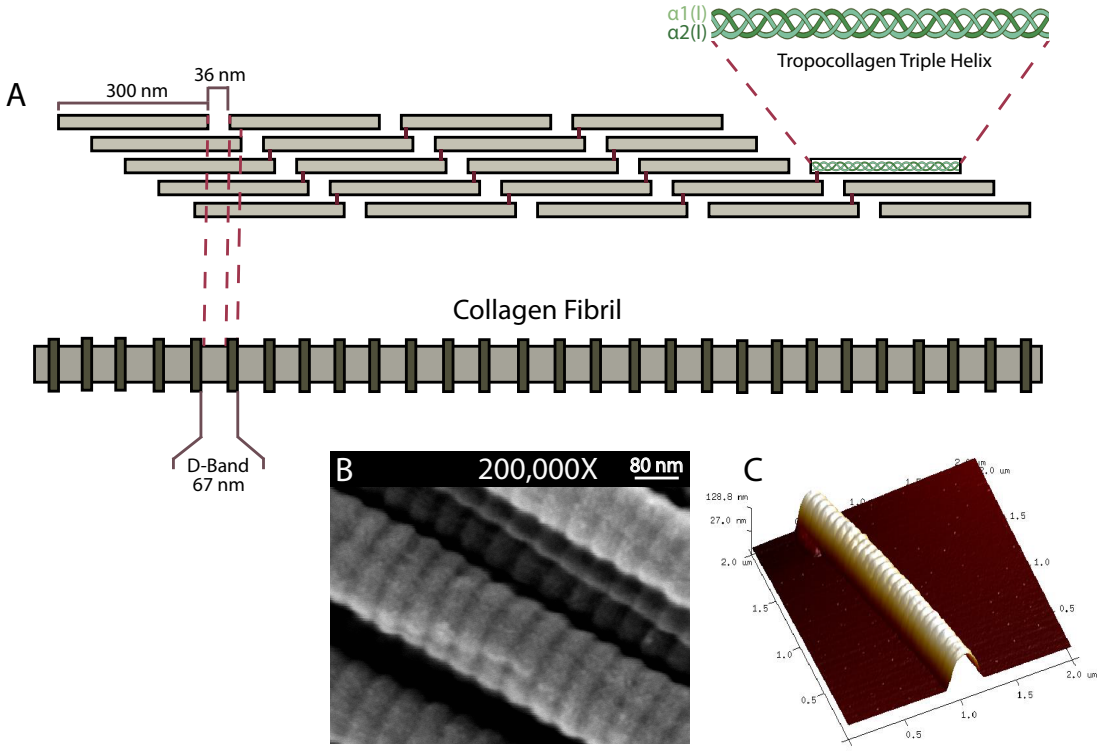

Figure 1.1: A. Schematic illustrating the arrangement of collagen molecules into a larger fibril structure with D-banding periodicity. B. Scanning electron micrograph of collagen fibrils isolated from a bovine common digital extensor forelimb tendon C. Atomic force micrograph of an individual collagen fibril. Adapted from[8].

1.1.2 Inorganic portion of bone

The inorganic mineral portion of bone is complex and dynamic in its state. The mineral phase of bone constitutes roughly 60% of the bone by dry weight[3]. This mineral phase, often referred to as HA, is actually poorly crystalline carbonated HA with various ion incorporations, such as magnesium, chloride, zinc, strontium, sodium, potassium, cobalt, and fluoride[9–11]. These mineral crystals possess a hexagonal crystal structure and are aligned with their c-axis ([001] crystallographic orientation) parallel

to the long axis of the collagen fibrils in which they are associated with[12]. Dimensions of these crystals are roughly 25-50 nm wide, 50-100 nm long, and 2-6 nm thick[13–15]. Aside from HA, other mineral phases exist which are thought by some to serve as precursors to mature bone mineral[12,16–19]. These phases include: amorphous calcium phosphate (ACP), octa-calcium phosphate (OCP), and di-calcium phosphate dibasic (DCPD)[1]. It is believed that ACP predominates the early phase of mineral formation in bone followed by OCP and finally HA or DCPD[1]. Due to the role of ACP and OCP as precursors to mature bone mineral, they are sometimes the target of biomimetic bone implants.

Crystallization of bone mineral is thought to proceed via a non-classical pathway where a transient kinetically driven mineral phase exists prior to the final thermodynamic apatitic crystal structure[13,20]. In this process, particles from single nucleation events combine to form mesocrystals, indistinguishable from classically mineralized crystals (Fig. 1.2)[21,22]. Various ionic and molecular species present in areas undergoing mineralization are thought to affect the surface energy of forming crystals at specific faces or may even prevent crystal formation altogether, instead forming a fluidic mineral phase as was described by Gower et al.[21,23]. In the non-classical crystallization pathway an initial amorphous mineral phase is thought to exist, which is kinetically stabilized by ions and small molecules in solution (Fig. 1.2)[21]. The exact precursor structures present during the non-classical pathway involved in biomineralization, and to some degree during bio-inspired mineralization, are difficult to observe however, largely due to their transient state[21].

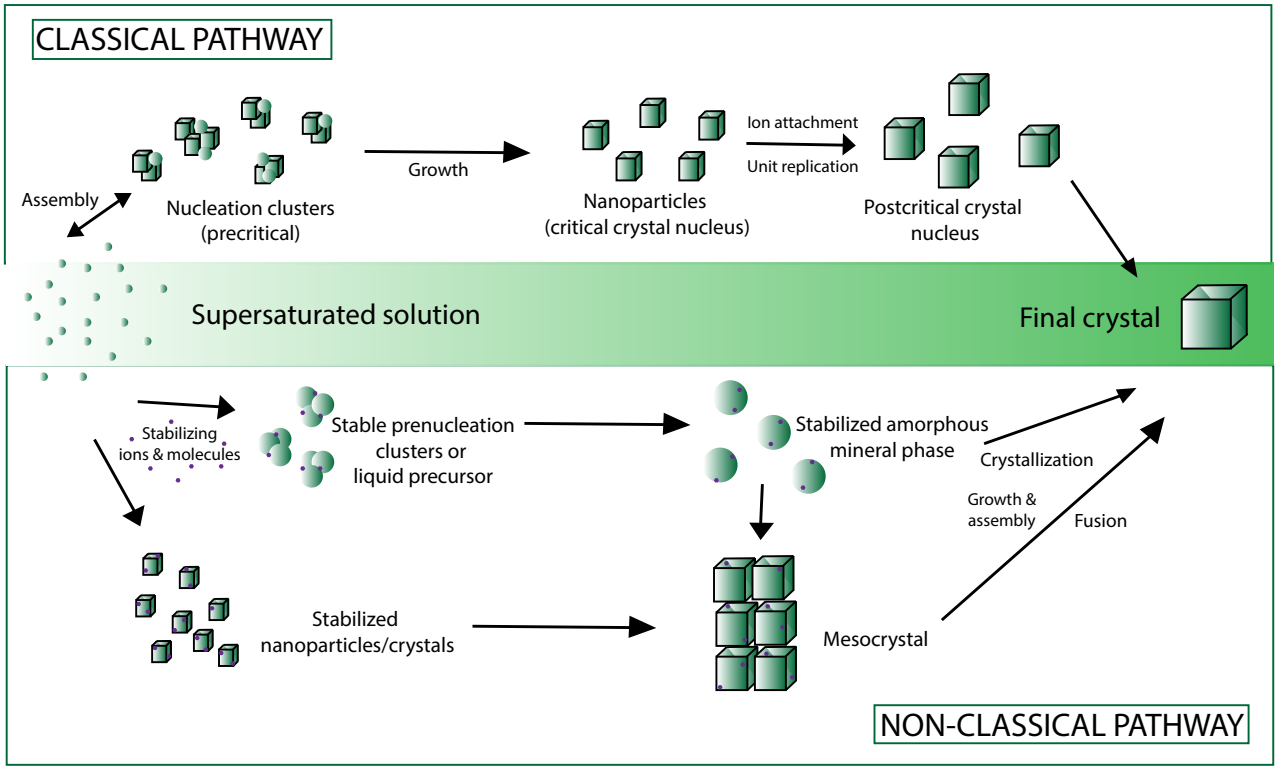

Figure 1.2: Top. Classical nucleation theory outlines mineral crystal nucleation proceeding through the addition of ions to a single precritical cluster. Bottom. The non-classical pathway proceeds through the aggregation of amorphous precritical clusters or nanocrystals forming mesocrystals or an amorphous mineral phase[21].

1.2 Bone mechanics and structure

Most of the mechanical differences observed in bone from different locations and across different individuals and species are a result of the degree of mineralization of collagen as well as variations in structure, such as collagen alignment, resulting in structural anisotropy[2,24]. Usually the mechanical profile of a particular bone region depends on the functional role of that bone in the body in a highly controlled structure-function relationship. Bone possesses a hierarchical structure spanning over multiple length

scales (Figs. 1.3, 1.4)[25]. Detailed understandings of these structural and mechanical features of bone are important as they may provide insight towards the development of devices aimed at bone repair and regeneration. Furthermore, mechanical evaluations of potential bone repair devices should be evaluated at both the nano- and macroscopic levels in order to gain a better understanding of their mechanics compared to bone and existing biomaterials. Nanomechanical testing allows for a characterization of the material properties without the influence of stabilizing effects from surrounding structures, while macromechanical tests allow for an identification of the overall mechanical features of the scaffolds.

1.2.1 Nanomechanics of mineralized collagen

Although multiple types of bone exist within the body, one commonality between each type is that of the mineralized collagen fibril. These fibrils contribute towards the unique stiffness, elasticity, strength, and energy dissipation capabilities of bone[27]. The structure of the mineralized collagen fibril first consists of mineral plates located within the characteristic gap regions of the fibril followed by interfibrillar mineralization[25]. From a mechanical standpoint, this mineral reinforcement of the organic fibril confers orthotropic qualities to the collagen[25,28]. Plastic deformation of mineralized collagen fibrils in bone can occur in many different ways depending upon the hierarchical scale in question. For example, intermolecular sliding or bond breaking can occur at the nanoscale[28]. Sliding between the collagen fibrils themselves or damage to intermolecular crosslinks can also occur giving rise to plastic deformation of the bone[28].

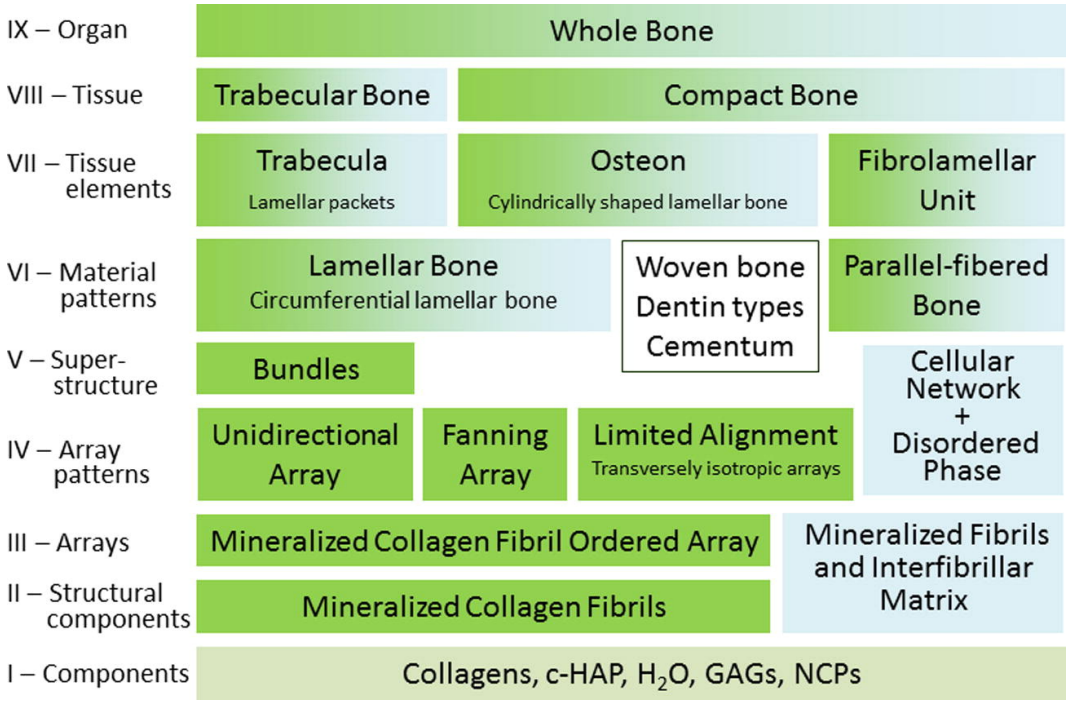

Figure 1.3: Schematic showing the hierarchical structure of bone. Organic and inorganic components combine to form mineralized fibrils which ultimately, through differing arrangements, form both trabecular and compact bone. From ref.[26] Reprinted with permission from Elsevier.

Few studies to date have examined the nanomechanical properties of isolated, individual mineralized collagen fibrils from bone, largely stemming from the difficulty of obtaining such specimens. Greater numbers of studies exist outlining the nanomechanical profile of collagen within bone, however still contained in its native macrostructural configuration. Comparing the mechanical properties of individual mineralized collagen fibrils, such as those produced in this project, to mineralized collagen in bone should be taken with caution as mineralized collagen in bone is often surrounded by stabilizing hierarchical structures which may make such a comparison difficult.

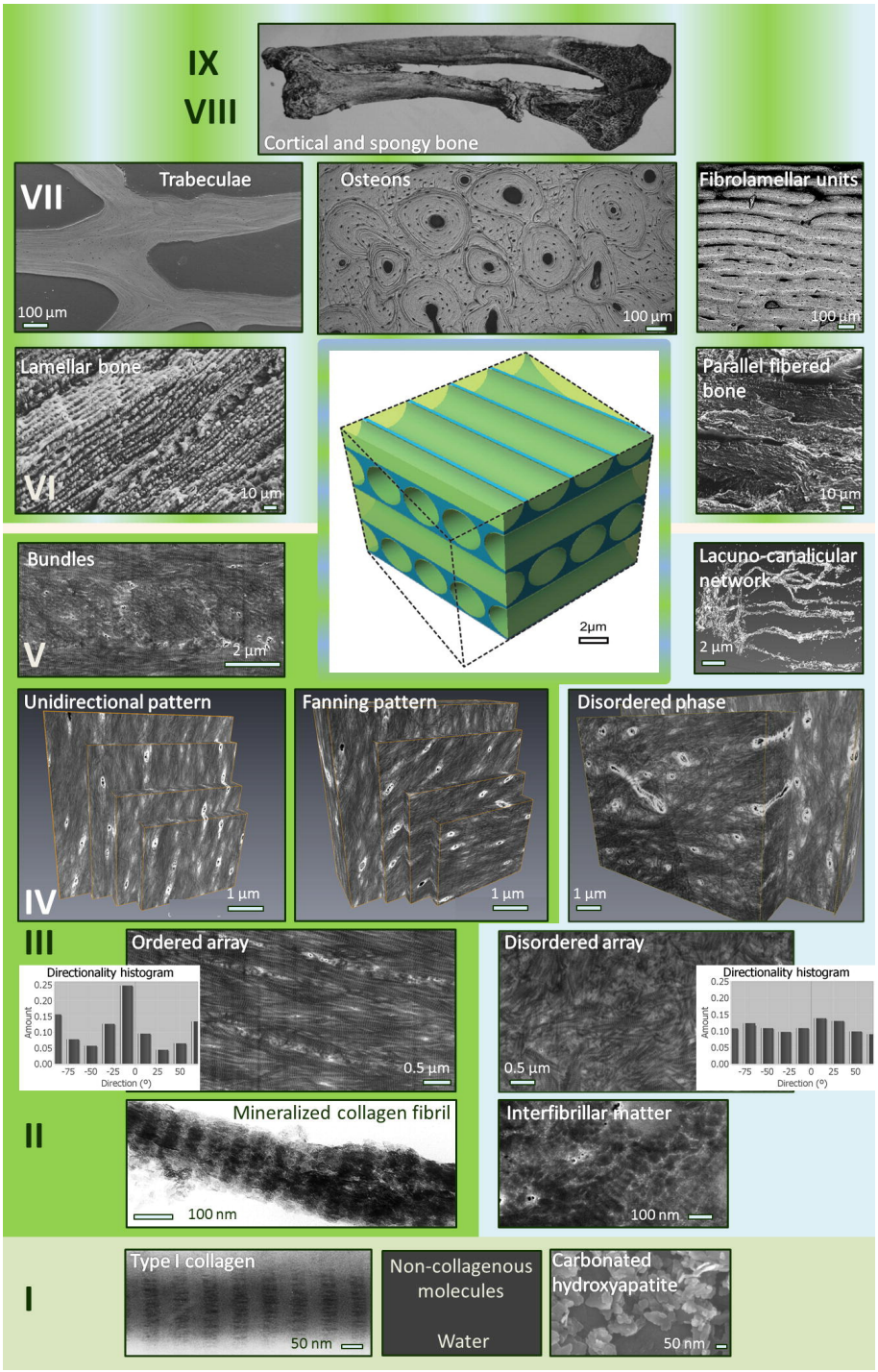

Figure 1.4: Schematic showing the hierarchical structure of bone. This figure is similar to the previous only now with representative images from each hierarchical level. From ref.[26] Reprinted with permission from Elsevier.

Using an *in silico* model with molecular dynamics simulation, Nair et al.[29] evaluated the tensile properties of mineralized collagen microfibrils. Higher modulus values were found as the mineral density of the fibrils increased, reaching 1.5-2.8 GPa for 40% mineral density samples (depending on strain)[29]. In order to better determine the effects mineral has on the nanomechanics of collagen fibrils in bone, Tai et al.[30] used atomic force microscopy (AFM) to determine the elastic modulus of bone during multiple stages of demineralization. It was found that mineralized collagen samples possessed modulus values 2-6X that of demineralized bone sections (7-12 GPa vs. 1.9 GPa)[30]. The relationship between the degree of mineralization of collagen and material stiffness was demonstrated by Mulder et al.[31] where this association was investigated in developing trabecular bone. A significant relationship was found between the stiffness of fetal and newborn trabecular bone and the degree of mineralization. Stiffness values obtained through nanoindentation ranged from 7.4-17.0 GPa for fetal and newborn bone samples[31]. Caution should be taken however when comparing mechanical values across multiple groups, particularly nanomechanical values, as a multitude of parameters may affect results, such as temperature, humidity, and substrate effects[32].

Computationally, work has been done to evaluate the mechanics of mineralized collagen fibrils using 3D finite element (FE) modelling. Hambli et al.[27] used such a model and found the stiffness of microfibrils to increase following mineral addition to collagen under tension, 0.25 GPa compared to 1.9 GPa. Values under compression were lower for pure collagen fibrils at roughly 0.1 GPa compared to higher values for mineralized fibrils at roughly 18 GPa[27]. Further, to highlight the importance of scale on resultant elasticity, they found the elastic modulus of single tropocollagen

molecules to be 2.8 GPa whereas the value for collagen microfibrils were found to be 0.25 GPa[27]. A study by Barkaoui et al.[33] expanded the hierarchical mechanical investigation further by looking at 3D FE modelling of both mineralized collagen microfibrils as well as fibrils and fibers. The researchers defined a microfibril as an arrangement of five tropocollagen molecules whereas a fibril was defined as collection of cross-linked microfibrils, and a fiber, a collection of fibrils surrounded by a mineral matrix[33]. It was found in this study that the resultant Young's modulus values depended upon the modulus values for constituent tropocollagen molecules and mineral. Elastic modulus values were found to be roughly 0.4-1.1, 40-95, and 50-115 GPa for mineralized microfibrils, fibrils, and fibers, respectively[33]. The authors reported these values as corresponding well with those reported by others using FE and alternative methods such as AFM and molecular dynamics computation.

1.2.2 Composite mechanics in relation to mineralized collagen

Bone is an anisotropic composite material consisting of an inorganic mineral phase intricately associated with organic material[34]. Mineral crystals within bone are stiff and strong, carrying relatively large amounts of stress[29]. On their own, these crystals are prone to brittle cracking, however reinforcement by the tough collagenous phase acts to prevent crack growth and propagation[29]. Collagen on its own lacks the rigidity needed to support compressive loads. Mineral addition to the collagen improves its mechanics while also increasing yield strength by limiting slippage between collagen molecules[29,35]. When the amount of collagen in bone decreases, and thus the relative

amount of mineral is increased, the area under the corresponding stress-strain curve and strain at yield experiences a decline, while Young's modulus is increased[36,37]. This mechanical response is a product of the ability for bone with a high collagen content to form microcracks that are restricted spatially, whereas in bone with relatively high mineral content, cracks are more likely to spread from one brittle mineral region to another, possibly leading to failure before remodelling can occur[36,38]. It has been proposed by Reilly and Burstein[37] that the mineral in bone is largely responsible for the initial stiffness (slope of the stress-strain curve) of the tissue in response to load, while the collagenous matrix determines the slope of the curve post-yield. Taken to an extreme, largely collagenous tissues, such as tendons, although very tough and strong, do not provide adequate rigidity for bone. Highly mineralized bone tissues, such as the whale tympanic bulla for example, are conversely highly brittle[36,39]. Other tissues, such as antler in red deer, have relatively high amounts of organic matrix in relation to mineral and can thus sustain extensive deformations before ultimate fracture[40].

At the nanoscale, it have been suggested by Nair et al.[29] through full-atomistic calculations of the 3D structure of mineralized collagen, that the specifically controlled shape and size of mineral crystals present within the gap regions of collagen fibrils control deformation mechanisms of the fibrils as well as the effective modulus. It was suggested that mineral crystals of such a small size no longer display brittle behaviour, rather they display highly ductile characteristics[29]. At the whole bone level, strength of the composite structure depends upon the total bone mass, the specific geometric distribution of microscopic components, and the composition of the tissue at specific locations[34].

Estimation of the mechanics of whole bone through analytical methods are sometimes made through its correlation to the properties of the individual components of bone[41]. For example, a relatively simple method for estimating these tissue mechanics, such as elastic modulus, in terms of individual components is the rule of mixtures (ROMs)[42]. In this method, there are two main models: the Voigt model applied to axial loading (strains constant), and Reuss model for transverse loading (stresses constant)[43]. ROMs, or the inverse ROMs, are sometimes applied to bone since bone can be thought of as a fibre composite. Due to the many fibre orientations in bone, its mechanical response should fall below the upper bound given by the Voigt model, and above the lower bound given by the Reuss model. This method applied to whole bone estimates that the stiffness of the tissue is greater in the direction parallel to the long axis of bone (the direction of osteons)[43].

The longitudinal elastic modulus estimated by the Voight model[44] is given by:

$$E = (E_c V_c) + (E_m V_m)$$

The transverse elastic modulus estimated by the Reuss model[45] is given by:

$$1/E = (V_c/E_c) + (V_m/E_m)$$

Where the subscripts c and m refer to collagen and mineral, respectively, and V is volume fraction.

Issues with these models may arise due to the heterogenous distribution of the individual components of bone within the whole structure, the complex directional orientation of collagen fibrils in some bone types, interpenetration of other tissue types, and the presence of various defects[46–49]. For example, the Voigt and Reuss models

only take into consideration volume concentrations of components, disregarding their specific geometry, and are thus usually limited to only first estimates of mechanical behaviour[48]. Due to these limitations, extensions to these models have been developed. In order to account for the arrangement of mineral platelets within collagen fibrils, the shear-lag model was introduced Jager and Frayzl in 2000[7]. Due to the complex architecture of bone, numerical approaches, such as finite element methods are sometimes applied to more precisely account for these effects when modelling bone[50]. Recently, Alizadeh et al.[51] estimated the anisotropic elastic properties of mineralized collagen fibril arrays using a 3D finite element analysis and compared these results to those calculated using the basic ROMs method and shear-lag model, as well as the Mori-Tanaka scheme and upper/lower bounds by Hashin and Shtrikman. In this study, the contribution of not only mineral plates was taken into consideration, but also the contribution of NCPs in an extrafibrillar matrix. It was found that stress distributions in both mineralized collagen fibril and fibril array models reflected results obtained from the shear-lag model[51].

1.2.3 Macromechanics of bone

Analyses of the mechanical properties of certain bone types offer convenient snapshots in time and allow for comparisons to be made. These measurements can sometimes fault however as they may ignore the dynamic nature of bone, i.e. the change in structure and resultant mechanics of bone over time. The macromechanical properties of bone also vary depending on the location within the body, the species, age, and disease status of the individual, as well as stage during the healing process, amongst

other parameters, including the testing method and direction. For example, mid-diaphyseal cylindrical cuts taken from human femurs of varying ages showed an elastic modulus of 15.2 GPa at age 35, which decreased by 2.3% per decade thereafter[52]. Modulus values presented by Baker and Haugh[53] for bones tested under flexion range from 0.6 GPa (rat femora) to 39.2 GPa (canine femora). It has also been reported that differences in bone mass, depending on the location within an individual's body, can result in cancellous bone stiffness varying by 100-fold (4-453 MPa)[54]. Collagen fibrils within bone align themselves according to specific mechanical demands placed upon the region of bone within the body. This is reflected in the complex hierarchical structure of bone and its variability throughout the body. Relative to an applied load, collagen fibrils aligned in a longitudinal direction resist tension much greater than fibrils aligned transversely, which preferentially resist compression[55]. For example, Riggs et al.[56] mechanically compared cranial and caudal cortices of the equine radius, a bone frequently subjected to bending, in an attempt to determine the influence collagen fibril orientation has on tissue mechanics. The cranial cortex is often placed under tension during physiological loading whereas the caudal cortex is loaded under compression[56]. The cranial cortex, with its collagen fibrils oriented predominately in a longitudinal direction, was stiffer and had a higher tensile strength but lower compressive strength than the caudal cortex, which has a largely oblique to transverse fibril orientation composition[56].

1.3 Bone formation

1.3.1 Bone cells

There exist three main cell types in bone tissue; osteoblasts, which build bone, osteoclasts, which resorb bone, and osteocytes, which support bone metabolism (Fig. 1.5)[2]. These cells types in reality however exist as many transient phenotypes as they progress towards terminal differentiation, sometimes defined as ranging from pre- to mature in appearance and function[57,58]. Osteoblasts, which are derived from mesenchymal stem cells (MSC)s found largely in the bone marrow stroma, make up roughly 4-6% of total resident bone cells[57,58] and possess a characteristic cuboidal appearance[58]. Osteoclasts are multinucleated cells derived from mononuclear cells responsible for bone resorption in response to signals from osteoblasts and osteocytes[57]. Once osteoblasts become embedded in their secreted osteoid and become resident within bone, they are termed osteocytes, which comprise roughly 90-95% of the total resident bone cells[57,58]. Osteocytes, housed in lacunae within bone, are interconnected with one-another through a series of elaborate networks throughout bone termed canaliculi, where protoplasmic cellular processes end in gap junctions just before that of the neighbouring cell (Fig. 1.5)[59]. Communication between osteocytes and osteoblasts may also occur through similar cytoplastic extensions allowing for intercellular transport[57]. These cellular connections allow for communication between osteocytes and are vital to the regulation of bone remodelling and many other bodily processes, including kidney function and ion homeostasis[59]. Other cell types exist more transiently during various stages of bone formation and healing, such as chon-

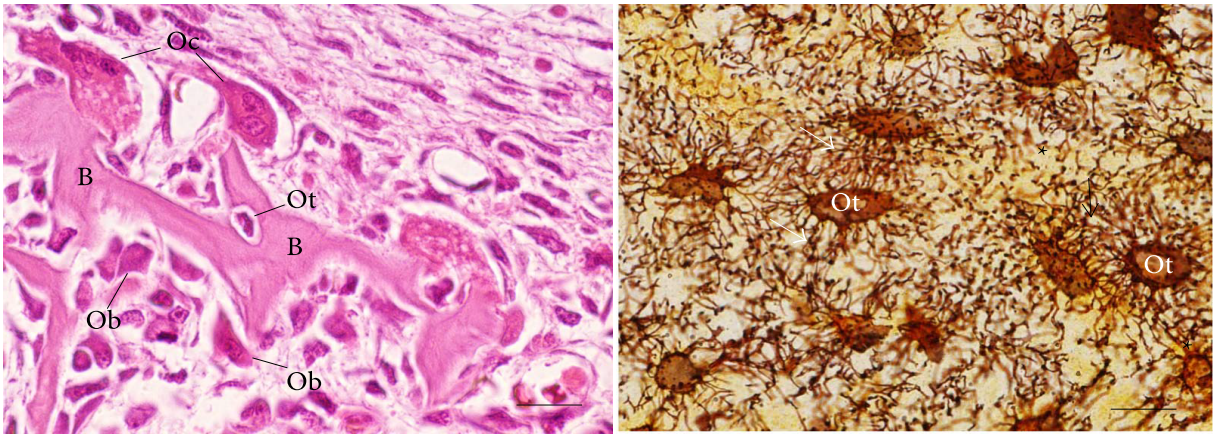

Figure 1.5: Left: HE-stained histological light micrograph of alveolar bone showing: B. bony trabecula, Ob. Osteoblasts, Oc. Osteoclasts, and Ot. Osteocytes. Right: Light micrograph of osteocytes with associated cytoplasmic processes (arrows) used for intercellular networking through canaliculi. Image obtained using the silver impregnation method. From ref.[57].

drocytes which are involved in endochondral ossification and various progenitor cells, including MSCs. All of these cell types orchestrate together, through direct contact, communication via paracrine signalling and gap junctions, the dynamic structure of bone[60].

1.3.2 Intramembranous and endochondral ossification

The formation of bone occurs through two mechanistically distinct processes; intramembranous (mesenchymal) ossification and endochondral (intracartilaginous) bone formation[2]. During the development of the early skeletal system, pluripotent mesenchymal cells of embryonic origin migrate to the sites which will later become bones[61,62]. These mesenchymal cells, now packed in regions of high cellular density, begin to form into arrangements representing the size and shape of the future

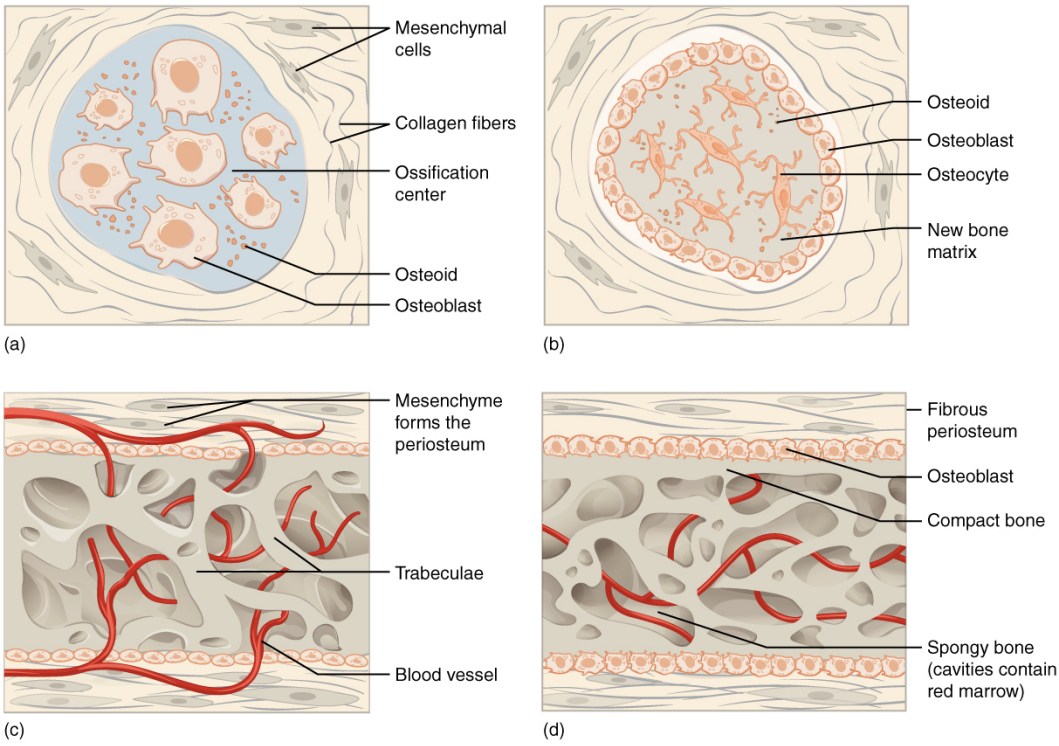

Figure 1.6: Schematic showing the four steps involved in intramembranous ossification. A. Precursor mesenchymal cells cluster together as ossification centers form. B. Osteoblasts become encased in surrounding osteoid forming osteocytes. C. The periosteum and bony trabecular matrix form. D. Compact bone forms. From ref.[63].

bones[61]. These highly dense clusters of mesenchymal cells then differentiate into either the cartilage forming cells, chondrocytes, which will form models of the soon-to-be bones (endochondral ossification), or osteoblasts, which contribute to intramembranous ossification (Fig. 1.6)[61]. Intramembranous ossification occurs predominantly in craniomaxillofacial regions and in fracture repair and proceeds without cartilage intermediate formation[1].

Endochondral ossification occurs in the early development of the limb and trunk bones

and during fracture repair[1]. In this process, the cartilage formed, or the early growth plate, is subsequently replaced with mature mineralized bone (Fig. 1.7)[61,62]. Endochondral ossification begins with the differentiation of chondrocytes found within the central portion of the cartilage model into a hypertrophic state followed by an infiltration of osteoclasts, osteoblast progenitor, endothelial, and hematopoietic cells from the perichondrium[61,64]. Osteoclasts that are recruited to the site of the hypertrophic chondrocytes resorb the cartilaginous matrix and secrete osteoid, which is the unmineralized component of bone tissue matrix[62]. The osteoblast progenitor cells then further differentiate and form both trabecular and cortical bone through the mineralization of the osteoid, while the hematopoietic and endothelial cells form the bone marrow, post resorption of the cartridge by the osteoclasts[61,62,64]. The previous ossification process is termed the primary ossification center whereas secondary ossification centers form on either end of bones undergoing development, which contributes to the longitudinal epiphyseal growth of fetal bones[61,62].

During bone remodelling and repair, these cell types are able to recognize and respond to various mechano-chemical stimulatory cues and alter their morphology and biochemical profile in response, a phenomenon first described as Wolff's law[65,66]. If bone is left under static, non-loading conditions, differentiation of osteoblasts is decreased along with an increased activity of osteoclasts[67]. Under dynamic loading conditions, the opposite is true, where bone formation is favoured. Beginning with the osteocytes, their morphology may differ from a rounded to elongated phenotype depending on if they reside in trabecular or cortical bone, respectively[24,57]. This adaptation can be summarized in a four-step model: Firstly, mechanocoupling allows

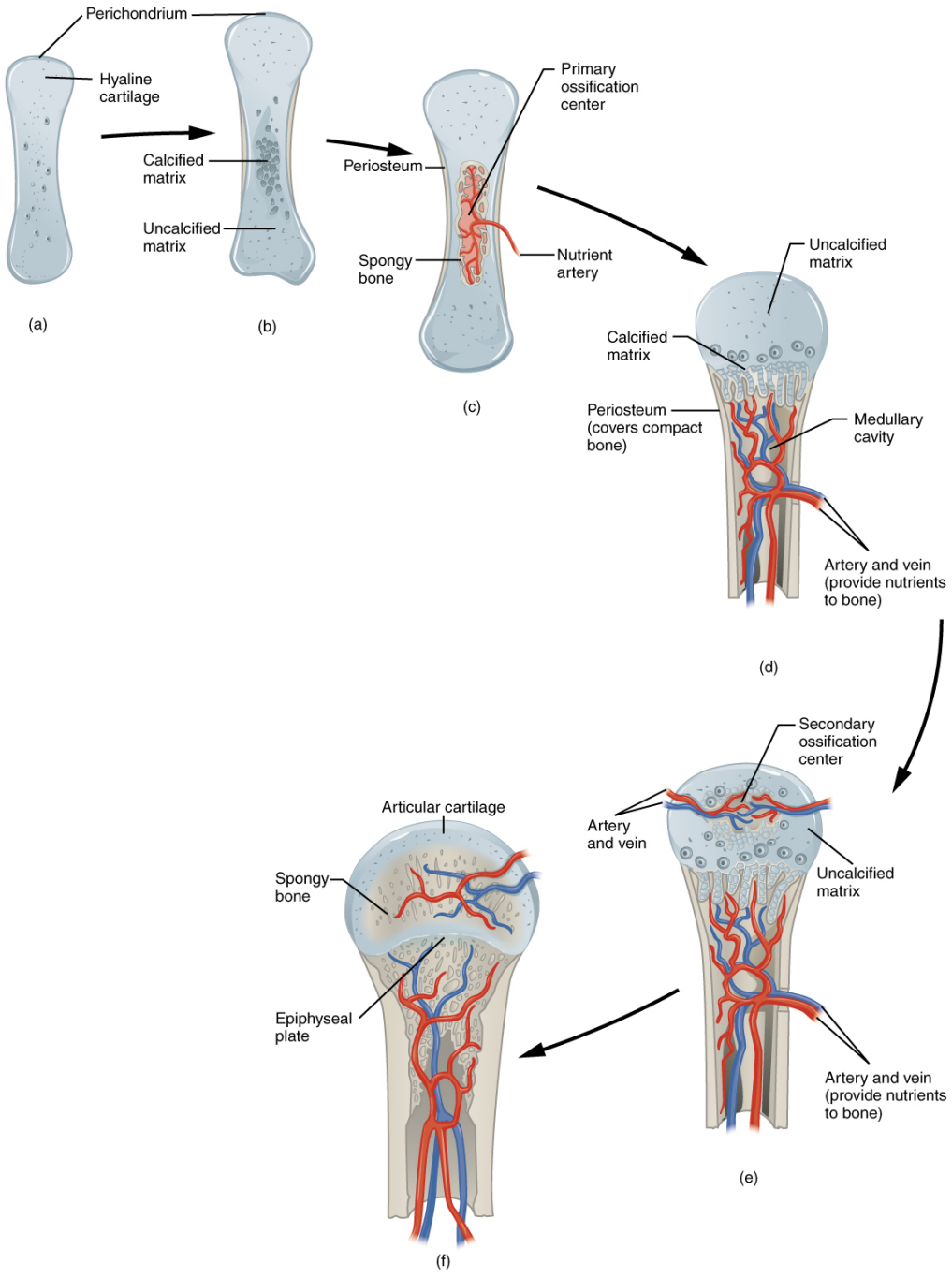

Figure 1.7: Schematic showing the steps involved in endochondral ossification. A,B. Recruited precursor cells differentiate into chondrocytes, which form a cartilage model of the future bone. C. Cells infiltrate from the perichondrium and begin to form the early ossification center. D-F. Ossification continues as chondrocytes continue to grow at bone ends, contributing towards secondary ossification. From ref.[63].

the forces applied to bone to be converted to signals recognizable to cells, typically through fluid shear stresses on osteocytes which are housed in interconnected fluid filled lacunae[68,69]. Next, mechanotransduction takes place where these forces are converted to biochemical responses. Third, transduction takes place where cells convert signals. Finally, cells, largely osteoblasts and osteoclasts, respond via various mechanisms including differentiation and protein secretion[65,67]. During the remodelling process of bone, osteoclasts begin to polarize, forming defined membrane phenotypes via actin cytoskeletal rearrangement[57]. These membrane phenotypes in turn determine the function of the osteoclast. Osteoblasts similarly respond to signals produced by the osteocytes in addition to cues given by osteoclasts. As osteoblasts mature, they either undergo apoptosis or begin to alter their cytoplastic organization in an attempt to begin their transition into resident osteocytes or more flattened bone lining cells[57,58].

1.3.3 Bone fracture types and natural repair

The regeneration of bone tissue is a complex process that requires the coordination of many cells and signalling molecules (Fig. 1.8). The temporality in which this process of repair occurs closely mimics that of initial embryonic bone formation, which was mentioned previously[70]. Modes of bone fracture healing can be separated into primary and secondary healing. The former of the two represents only reduced fractures (no movement between bone ends in fracture) and involves no callus formation while the latter represents the majority of fractures and involves the classical stages of tissue injury, which are outlined below[71].

Immediately post injury to bone, the disruption of the local vasculature results in the formation of a clot, which aims to provide hemostasis[72]. Associated platelets consequently release various pro-inflammatory molecules that recruit inflammatory cells, which enter the clot[72,73]. The major role of the recruited inflammatory cells, such as the lymphocytes, macrophages, eosinophils, and neutrophils, is to remove cellular debris and promote the formation of blood vessels (angiogenesis), and recruit fibroblasts to the callus[72]. Furthermore, a deficit in the inflammatory macrophage population was found to greatly delay the process of endochondral ossification[73]. Following inflammation, blood vessels and MSCs are recruited to the makeshift callus in a fibrovascular phase which precedes the differentiation of these MSCs into osteoblasts and osteoclasts[72]. The cellular differentiation pathways in which the mesenchymal precursor cells chart is dependent upon their chosen chondrogenic and osteogenic pathways[74]. During this initial course of cellular differentiation, and serving as prerequisite to additional tissue regeneration, angiogenesis takes place[71]. These newly formed effector cells, which were recruited from the local fracture site or more distantly from systemic circulation, lead to the formation of new bone through endochondral and intramembraneous ossification[70]. This immature woven bone is then remodelled via the recruitment of osteoclasts and mature intramembraneous bone formation[72]. These cellular processes in which mature bone formation results are controlled through the regulated use of various bio-molecular signals, such as transforming growth factor-β (TGF-β), bone morphogenetic proteins (BMP)s, and insulin-like growth factors (IGF)s[74]. The overabundance of cells present at the site of fracture is progressively decreased through a process of programmed cell death, or apoptosis[74]. In order to restore prior structure and function, the regeneration of bone must be completed through the application of

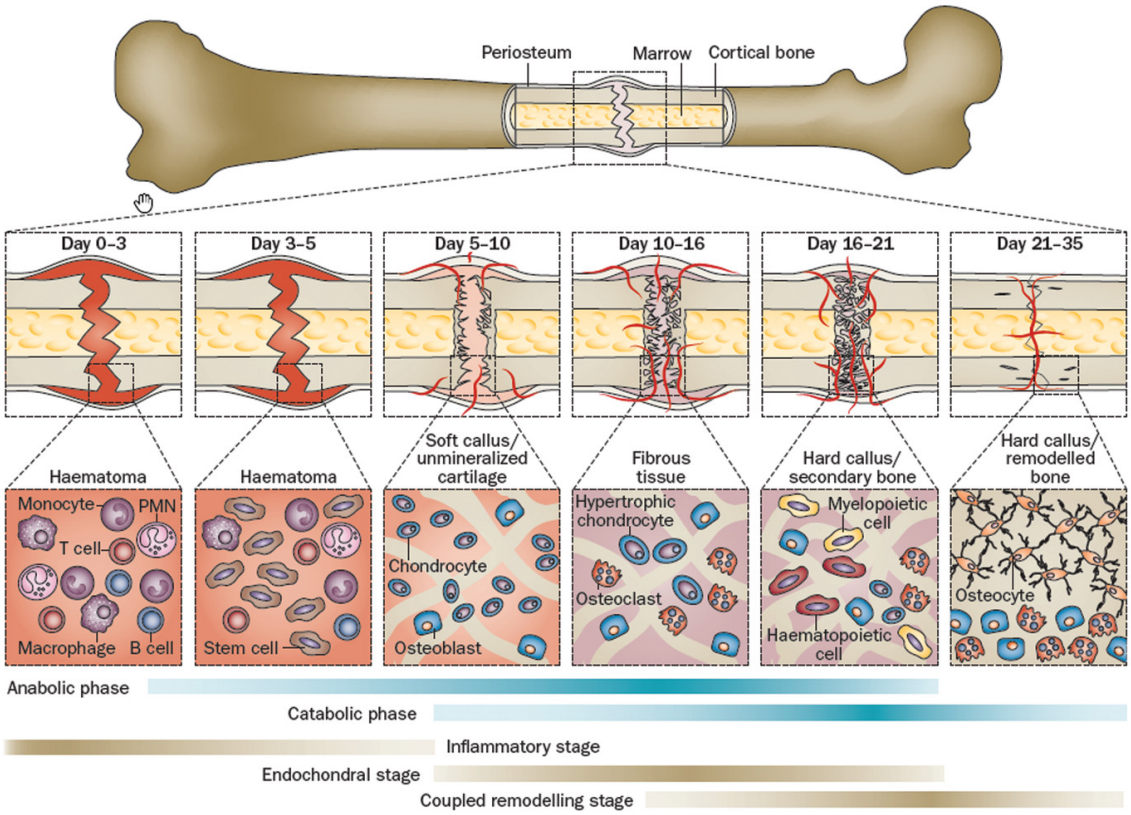

Figure 1.8: Schematic outlining the classical stages of bone healing post injury. From ref.[75] Reprinted with permission from Springer Nature.

mechanical loads to the bone tissue, which can be a lengthy process[72].

1.4 Biomineralization of collagen *in vivo*

As evidenced through transmission electron microscopy (TEM) investigations, the mineral phase of bone initially deposits within the gap regions of collagen fibrils[7,76]. Gap regions are thought to contain clusters of both positively and negatively charged amino acids, as well as side chains that provide favourable crystal nucleation environ-

ments[13]. Due to the confined nature of the gap regions, constrained growth of the mineral phase towards the naturally observed crystallographic orientation may also provide as an important mechanism towards collagen biomineralization[77–79]. *In vivo* studies supporting mineral formation beginning in the gap regions of collagen fibrils can be found in models analyzing biomineralization in the turkey leg tendon, which mineralizes in response to increased levels of applied stress[12]. Eventually, the mineral crystals outgrow these gap regions in collagen and begin to occupy regions between tropocollagen molecules and along the fibrils (extrafibrillar mineralization)[7,80].

1.4.1 Role of non-collagenous proteins, small molecules, and ions

Collagen is often combined with inorganic mineral to enhance its mechanics and biofunctionality when used towards bone repair. *In situ*, collagen is complexed with various NCPs to enhance its ability to become mineralized. Polyanionic domains within NCPs are thought to aid in this process[81,82]. Examples of NCPs include bone sialoproteins (BSP), osteopontin (OPN), and octeocalcin (OCN). BSPs are heavily glycosylated and sulfated flexible phosphoproteins and are members of the small integrin binding ligand N-linked glycoprotein (SIBLING) family of proteins, which also includes OPN[62,82,83]. BSPs contain a cell binding RGD motif, an N-terminal collagen binding region, as well as mineral interacting polyglutamic acid repeats[83]. It was recently found by Foster et al.[83] that loss of BSP affects severely the process of mineralization in bone of the alveolus and mandible, supporting the idea of its non-redundant role in bone biomineralization. OCN, in addition to matrix gla protein,

contains γ-carboxyglutamic acid, which is thought to aid in its ability to sequester and bind calcium in solution and on HA crystals[80,84]. OCN has been found to associate largely with mineralizing nodules in osteoid and is commonly used as a late-stage marker for osteoblast differentiation *in vitro*[84].

In addition to these NCPs, various small molecules and ions have also been suggested to contribute towards the enhancement of collagen mineralization *in situ*. Citrate for example is thought to aid in the stabilization of amorphous mineral precursors while also controlling the size and shape of nanocrystals[85]. This was highlighted recently by Gomez-Morales et al.[86] where type I collagen fibrils were mineralized with and without the addition of citrate. Citrate was found here to slow the transformation of amorphous calcium phosphate (ACP) to mature apatite, enhancing collagen-associated ACP stability[86]. Magnesium has been found to inhibit apatite crystallization through competition with calcium ions for structural sites, along with its role in osteoblast stimulation[87]. F^{-}, Sr^{2+}, and Zn^{2+} have also been shown to have roles in the mineralization process[11,88,89].

The exact mechanism as to how early mineral phases enter the gap region in collagen fibrils and subsequently expands is not yet completely understood. Gower et al.[90], proposed the idea that acidic polyelectrolytes in solution stabilize an amorphous precursor phase with a fluidic character that subsequently enters the collagen gap regions via capillary action. It is thought that NCPs fill this role during bone biomineralization *in vivo*. An *in vitro* method, termed the polymer induced liquid precursor (PILP) process, has been investigated broadly since and has been performed on both loosely and densely packed collagen substrates[12]. Negatively charged polymer-mineral com-

plexes have also been shown to interact with positive regions in the C-terminus end of the gap region in collagen fibrils, which allows the ACP phase to enter[13]. The acidic polymer used by Gower et al. to mimic the glycoproteins found naturally, specifically regions rich in acidic amino acids, was that of polyaspartic acid (pAsp)[23]. Chosen due to its availability over recombinant versions of NCPs, pAsp, although simplistic in nature, serves the role of mimicking the functional domains of the NCPs.

It was found that the gap regions of collagen fibrils exclude molecules larger than 40 kDa, while allowing the diffusion of molecules smaller than 6 kDa, which led to the theory of 'mineralization by inhibitor exclusion'[12,91,92]. NCPs, which are thought to prevent mineralization and stabilize ACP in solution, are therefore too large to enter these gap regions. The smaller ACP can then enter these gap regions where no inhibitor of mineralization is present and subsequently crystallize into larger mineral structures (Fig. 1.9). This proposed method may allow for the presence of initial nanoparticles as opposed to the required nanodroplet phase proposed in the PILP process[77].

1.4.2 Role of extracellular matrix vesicles

Traditionally, it was thought that biomineralization in animals occurred through the precipitation of mineral from a supersaturated solution, a method frequently employed *in vitro*[80,94]. Recent evidence has challenged this belief and has pointed towards the occurrence of more complex mechanisms and cellular/molecular interactions along with the presence of transient precursor mineral phases[1,95]. Matrix vesicles (MV)s play an important role in the mineralization of collagen[9,81,96]. MVs are small lipid

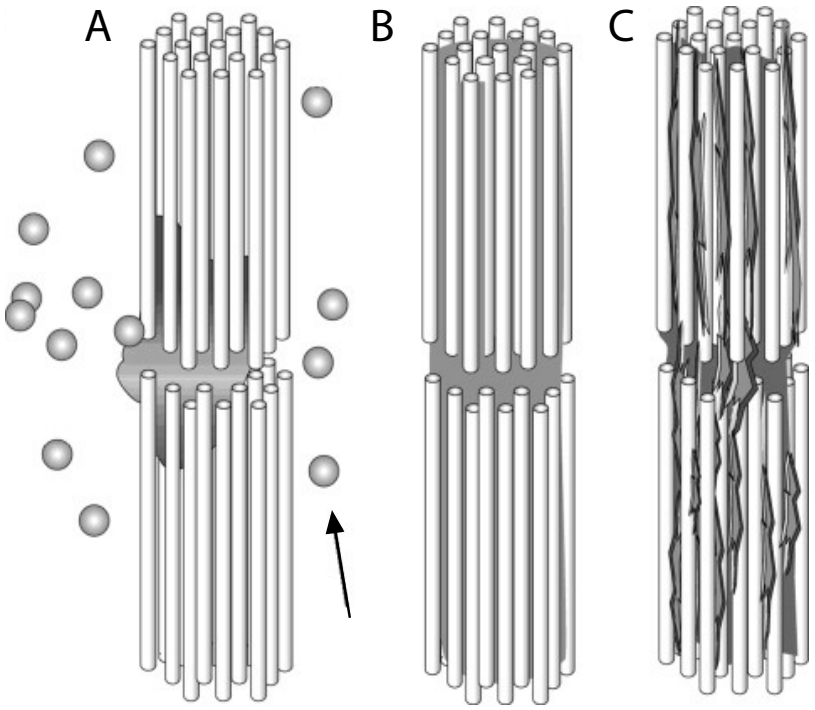

Figure 1.9: Schematic illustrating the proposed mechanism for the intrafibrillar mineralization of collagen fibrils resulting from the PILP process. A. Amorphous mineral precursors (arrow) are formed in solution and are attracted to the collagen fibril gap regions. B. The amorphous mineral phase enters the gap regions. C. The amorphous mineral phase crystalizes forming a more mature mineralized collagen fibril. From ref.[93]. Reprinted with permission from Elsevier.

bound spherical bodies roughly 40-200 nm in diameter thought to be derived from the plasma membrane of hypertrophic chondrocytes and osteoblasts and were initially discovered when observing the early stages of matrix mineralization in bone[9,97]. As an inhibitor of pyrophosphate (PPi), which is the inhibitor to mineral precipitation in serum, alkaline phosphatase (ALP) is important in the process of biomineralization in bone where it cleaves PPi into Pi (inorganic phosphate, which is subsequently used in bone mineral formation). Along with various other molecules, including calcium

channel forming annexins and calcium binding entities, ALP has been found in the membranes of MVs and has been determined to be important in collagen mineralization[97]. Other molecules present on MVs are thought to inhibit mineral formation externally, such as through increases in PPi concentrations, which allow preferential mineral formation intravesicularly[97,98]. It has been shown that these MVs can bind to the native structure of type I collagen, possibly through RGD cell binding domains[98].

1.5 Collagen mineralization *in vitro*

Traditionally, to achieve collagen mineralization *in vitro*, collagen is immersed in a simulated body fluid (SBF)[80,96]. Other methods include direct blending (mixing collagen and mineral nanoparticles together[99]) and co-precipitation (mineral association during collagen fibrillogenesis)[80,96,100]. In the co-precipitation method, solutions of both collagen molecules and Ca^{2+} and PO_4^{3-} are combined in suspension followed by raises in the pH in order to promote HA nucleation onto the assembling collagen fibrils[96]. Mineralized collagen from co-precipitation techniques may additionally be freeze dried to produce scaffolds of varying structures[101,102].

Modifications to these methods often include various ionic or molecular additives to either the substrate or the mineral phase to better mimic natural bone mineral, or to mimic extracellular molecules thought to modify and aid in the organization of crystal size and shape. For example, during SBF immersion techniques, enrichment with various metal ions including, Ca^{2+}, Ni^{2+}, Zn^{2+}, Fe^{3+}, Mn^{2+}, and Cu^{2+}, is done in an attempt to incorporate these ions within the mineral structure[80].

1.5.1 Mechanisms of sequestering and templating agents on biomineralization

As was mentioned, during the biomineralization of bone *in vivo*, nanoscopic mineral deposits accumulate within the gap regions of individual collagen fibrils, in addition to further accumulation between fibrils, termed both intrafibrillar and extrafibrillar mineralization, respectively. Regulation of this process is thought to be achieved through first, sequestering of ions from solution to form the initial ACP phase, and second, templating of this early mineral phase onto collagen, encouraging its nucleation and crystallographic transformation[80,92]. Polyanionic domains containing polycarboxylic acid and phosphate functional groups are the active regions of NCPs that are thought to aid in this sequestration mechanism and collagen binding[92]. It has been proposed by Liu et al.[92] that biomimetic collagen mineralization requires the reproduction of noncollagenous matrix molecules found in bone that act as both sequestration and templating agents[92]. This led the researchers to include a collagen phosphorylation step prior to mineralization using the polyphosphate sodium trimetaphosphate (STMP) as a templating agent. The authors found that only when both methods were employed, polyphosphate treatment along with polyacrylic acid (PAA) addition to SBF as a sequestering agent, were mineralized collagen fibrils with intrafibrillar mineral deposition able to be produced possessing levels of structural hierarchy found in nature[92].

Mechanistically, *in vitro* sequestering agents, such as pAsp or the previously mentioned PAA, are thought to contribute to collagen biomineralization similar to the mechanisms occurring during NCP mediated collagen mineralization *in vivo*. Briefly,

NCPs (and their sequestering agent mimics) possess a high density of negatively charged regions, largely acidic carboxylated and phosphorylated domains[103]. These functional regions are thought to alter crystallization pathways, including the structure and stability of a mineral precursor phase(s), in addition to aggregation kinetics[103]. As initially suggested by Gower et al.[90], this stabilized amorphous liquid-like mineral precursor phase is able to enter the small gap regions within collagen fibrils where it can then crystallize.

Post-translational modifications to collagen, prior to extracellular secretion, include the formation hydroxylysine and its glycosylation[104]. Following secretion, individual collagen molecules self-assemble into collagen fibrils in an entropy driven process, followed by covalent crosslinking via lysyl oxidase action[105]. In addition to the previously mentioned post-translational modifications, phosphorylation of collagen, specifically Ser residues in type I collagen, is increasingly being investigated in regards to bone mineralization[106]. Phosphorylation of various NCPs found in the mineralized matrix of bone is important in order to promote their ability to facilitate bone mineralization[106]. For example, the ability to nucleate HA by BSP has been enhanced through phosphorylation of Ser[107]. It then follows that post-translational phosphorylation of type-I collagen may be vital in regard to its ability to become mineralized in bone[106]. *In vitro*, phosphorylation of collagen has been shown to be achieved through the use of STMP, specifically via phosphoesterification of hydroxyl amino acids, which may indicate a role for STMP in the preparation of collagen that is to become mineralized[108]. Importantly, it has been found that following the hydrolysis of the six-membered ring configuration of STMP to sodium tripolyphosphate (STP) in alkaline conditions, the

covalent binding of STP to free hydroxyl groups in collagen can only occur if the hydroxyl groups are kept highly reactive under alkaline conditions with a pH greater than 9[109].

1.5.2 Effects of pAsp molecular weight on biomineralization

The contribution of pAsp to the promotion of collagen intrafibrillar biomineralization is highly dependent upon the molecular weight (MW) of the polymer. For example, Jee et al.[110] found that in the mineralization of bovine tendon, which was suggested to contain calcification inhibitors, bone-like mineral was only formed when a MW of 32,200 Da was used, in comparison to MWs of 5,500 Da and 10,300 Da[110]. The lower MW pAsp polymers resulted in lack of XRD peaks for both HA and amorphous calcium phosphate, lack of intrafibrillar mineral crystals, and resulted in an overall lack of mineral content overall compared to tendon mineralized with pAsp at a MW of 32,200 Da[110]. Additionally, in a study by Thula et al.[111], the PILP mineralization process was applied to a dense collagen substrate, that of demineralized manatee bone. The influence of pAsp MW was investigated to the degree of collagen remineralization using MWs of either 10,500 Da or 27,000 Da[111]. It was found that the higher MW pAsp resulted in a greater degree of remineralization, 43 wt.% compared to 30 wt.%[111].

The findings that relatively higher MW polyanionic molecules support the mineralization of collagen, including intrafibrillar mineral penetration, greater than their lower MW counterparts may relate to their greater similarity to the MW of the NCPs found within bone that they are suggested to mimic. For example, Goldberg et

al.[112] investigated the binding ability of the flexible and disordered phosphorylated acidic glycoproteins BSP and OPN to HA. In this investigation, the MW of BSP and OPN obtained through porcine calvaria extraction were reported to be 32,800 Da and 31,900 Da, respectively[112]. These MWs are similar to the MWs of the PILP process directing agent, pAsp, that were found to result in the highest degree of collagen mineralization, in particular intrafibrillar mineralization[110,111]. Perhaps mimicking the polyanionic domains of the NCPs found within bone is not the sole factor of importance when attempting to mimic their intrafibrillar collagen mineralization ability. The close resemblance of the MW of pAsp to the MW of similarly active NCPs in bone may also be of great importance towards biomimetic mineralization of collagen *in vitro*.

1.5.3 Alternative PILP process directing polymers

In addition to pAsp, various other polymers have been suggested and used as PILP process directing agents, such as poly-L-glutamic acid (PLGU), polyvinylphosphonic acid (PVPA), and as previously mentioned, PAA[113,114]. Thula et al.[115] investigated the use of these three anionic polymers, PGLU, PVPA, and PAA, in comparison to pAsp towards the mineralization of collagen scaffolds via the PILP process. It was found that although PGLU alone did not result in mineralization, its combination with pAsp could yield highly mineralized collagen scaffolds (65% w/w)[115]. Additionally, it was found that PVPA and PAA, despite yielding success in achieving intrafibrillar collagen mineralization in a demineralized human dentine model by Tay / Pashley[116], resulted in very little collagen mineralization[115]. Qi et al.[113] similarly investigated the

use of PAA in the preparation of mineralized collagen scaffolds. The authors suggest that the carboxylate groups present in PAA allow it to serve as a polyelectrolyte NCP analog, acting to stabilize fluidic ACP nanoprecursors[113]. It was found that at a relatively high concentration (50 mg/L) in combination with a relatively low MW (2 kDa), PAA did not produce mineralized collagen[113]. Conversely, when the MW of PAA increased greatly to 450 kDa and the concentration was decreased to 10 mg/L, complete mineralization of collagen occurred in a relatively unstable mineralization solution[113]. The authors suggested that there exists a 'sweet spot' in regards to PAA MW and concentration that allows for exclusive intrafibrillar mineralization of collagen fibrils[113].

1.6 Cellular interactions with materials

It is not surprising, given the sensitivity of bone cells, that many implant parameters, including surface roughness and rigidity, determine the ability for cells to be recruited to the defect site and further differentiate into cells capable of remodelling the bone defect. Cells that adhere to an implant generate cytoskeletal forces in accordance to the underlying substrate material stiffness[117]. These forces contribute to the overall cell shape, which in turn, dictates the biochemical profile of the cell[117–119]. Cell morphology has been linked to the growth pattern a cell adapts throughout its life cycle in addition to its differentiation and associated gene expression[120]. In general, cells respond with an elongated shape over a rounder phenotype when encountering stiffer surfaces[117]. MSCs observed to adopt a rounded morphology were found to specify to an adipogenic lineage, whereas MSCs flattened and more well-spread underwent os-

teogenic differentiation[121–123]. The stiffness of a substrate has even been suggested to provide more of a selective cue towards stem cell differentiation than soluble induction factors[124].

Scaffolds hold the potential to provide an environment that facilitates the bodies innate capacity to repair bone tissue, such as through the recruitment and differentiation of surrounding stem cells. This innate ability to repair itself points towards the importance of implantable devices to exploit this process, through careful consideration of substrate mechanics, and refrain from unnecessary complexity that may equate to expensive or prohibitive redundancy.

1.7 Bone repair materials

After injury, such as that due to trauma or disease, bone may undergo a substantial loss of structural integrity and mechanical and biological function. Roughly 20 million orthopaedic surgeries occur each year worldwide, of which 70% require the use of bone biomaterials for filling and repairing defects[1] Table 1.2. Bone harvested from a patient at a healthy site distant from their injury, such as from the ilium, tibia, fibula, or mandible, may be used in repair[125]. These autologous bone grafts are currently the gold standard in grafting material and are optimal in terms of avoiding graft rejection[1]. Due to complications and the limited supply of autologous grafting tissue, it may be used in combination with metallic devices or various biomaterials or replaced with tissue from another human or species.

Traditionally, defects to bones substantial or complex enough to require surgical inter-

vention were first reduced to bridge displaced bone segments followed by rigid fixation in attempt to regain some mechanical stability as well as to allow the bone segments to fuse. This method is termed open reduction internal fixation (ORIF) and is typically done through the use of metallic devices, with use of such devices dating back to the late 19th century[126]. These early metallic devices were, however, prone to corrosion, which prompted researchers to develop devices made of non-corrosive, bio-inert metals, such as stainless steel and titanium. As time went on it was observed that the bone underneath these passive metallic implants had experienced a deterioration in quality. This atrophy was later deemed to be a product of stress shielding caused by the metallic devices. It is a requirement for the structural integrity of bone tissue to be loaded in a delicate structure-function relationship, some bone regions more so than others[66,127]. Bone holds the ability to increase in size in order to accommodate and adapt to excessive or increasing loads, or conversely, become resorbed when mechanical function is reduced, such as during immobilization[127]. Metallic implants may provide for early mobility, however, at the expense of accompanied future complications and possible need for eventual device retrieval due to bone atrophy.

An ideal engineered scaffold for use as a bone tissue repair device should possess many characteristics. The scaffold should be osteoconductive in its surrounding tissue environment, that is, it should act as a substrate to promote new bone growth and prevent encapsulation. The scaffold should be osteoinductive, meaning that it should stimulate the development of pre-osteoblastic cells into bone forming osteoblasts. The scaffold should possess the ability to degrade in the implanted physiological setting not only into non-harmful by-products, but also at a rate that exposes the healing

bone to gradual loading. The scaffold should possess mechanical properties that allow it to adequately support the bone defect site under external mechanical loading but no so much as to prevent all micromotion and cause stress shielding. Aside from being functionally and biochemically ideal, the scaffold should be prepared in such a way that allows for an ease of fabrication, including the production of complex geometric shapes that can be tailored to individual patients[128]. Finally, the ideal scaffold should allow for reliable commercialisation and potential for clinical integration through various reimbursement measures and regulatory adherence.

Table 1.1: Comparison between materials currently used or targeted for use towards bone repair and regeneration. Arrows signify the relative degree to which the corresponding material is either favourable in a particular category (↑), unfavourable/lacking (↓), or is relatively neutral (↑↓). The number of arrows corresponds to the degree in which the material is either favourable/lacking, with three arrows signifying the most extreme cases. Information used for this relative comparison was obtained from references cited in each corresponding subsection.

Material	Safety	Biocompatibility	Biofunctionality	Biodegradable	Availability	Osteoconductive	Osteoinductive	Osteogenic	Mechanics
Autograft	↑↑↑	↑↑↑	↑↑↑	↑↑↑	↓↓↓	↑↑↑	↑↑↑	↑↑↑	↑↓
Allograft	↑	↑↑	↑	↑↑↑	↑	↑↑↑	↑	↑↓	↑↓
Xenograft	↑	↑↑	↑	↑↑↑	↑↑	↑↑↑	↑	↓	↑↓
Metallic Implants	↑	↑↓	↓↓↓	↓↓	↑↑	↑↓	↓↓↓	↓↓↓	↑↑↑
Synthetic Polymers	↑↑	↑	↓	↑	↑↑↑	↑↑	↑↓	↓	↑↓
Natural Polymers	↑↑	↑↑	↑↓	↑↑	↑↑↑	↑↑	↑↓	↓	↑↓
Bioactive Glasses	↑↑	↑	↑	↑	↑↑↑	↑↑	↑	↓	↑
Ceramics	↑↑	↑	↑	↑	↑↑↑	↑↑	↑	↓	↑
Biologic Devices	↑	↑↑	↑↑	↑	↑	↑↑↑	↑↑	↑↑↑	↑↓
Mineralized Collagen	↑↑	↑↑	↑	↑↑	↑↑↑	↑↑↑	↑	↓	↑↓

1.8 Current bone repair materials and devices

The structure of bone varies depending upon the location within the body. For these different bone structures and types, different bone-repair materials are needed. Aside from mineralized collagen-based devices, which will be outlined below, there are many different medical devices and grafts aimed at the surgical repair of damaged bone. Such devices and grafts include auto-, allo-, and xenografts, metallic devices, synthetic polymeric implants, bioactive glass and ceramic implants, various composite devices, and biologic-based implants[125] Table 1.1.

1.8.1 Autografts, Allografts, and Xenografts

As mentioned, autografts are often considered the 'gold standard' implants for the replacement and repair of bone defects due to their inherent osteoconductive, osteoinductive, and osteogenic properties[88]. These bone grafts make use of tissue found elsewhere in the patient's own body, and as such, are completely biocompatible and eliminate the risk for transmissible infections or graft rejection. Types of autologous graft material includes cancellous bone, cortical bone, bone marrow aspirates, and other blood-based products[88]. Cancellous bone may be used to fill various bone defects, is highly osteogenic, and is rapidly incorporated into a recipient site, however it does come with poor mechanical properties[129,130]. Cortical grafts on the other hand provide increased mechanics, which is why they are more often used in regions exposed to great forces, however they contain few cells and revascularization of these grafts is difficult given their dense structure[129,130]. Bone marrow aspirates or other blood products may contain an abundant supply of osteogenic factors and stem cells,

however their localization can be difficult, which is why they are often used with carriers, such as demineralized bone matrix[129]. Downsides to autograft use are the limited availability of donor bone, potential for donor site pain, and complications including hematoma formation, infection, or fracture, as well as increased time under anesthesia[88,125]. In order to avoid some of these limitations, allograft or xenograft bone may be used.

Allograft bone is tissue that is harvested from another individual and stored until future use. Allograft bone is processed through defatting and bone marrow removal, and sterilized, which may reduce the levels of various osteoinductive factors as well as potentially compromising some of the mechanical integrity of the implant[125,131]. Allografts may be stored as frozen or freeze-dried at room temperature, with the latter reducing the mechanical stability of the graft[131]. Due to allograft tissue being from another individual, there also exists the possibility for disease transmission, however this risk is quite low due to screening and processing techniques[132]. Types of allogenic grafts include both cancellous and cortical bone as well as demineralized bone matrix (DBM) among other tissues, which are included in the section below on biologic devices[88].

Xenografts are tissue grafts that originate from a species other than human; often of porcine or bovine origin. These grafts allow for much greater tissue availability at a reduced cost, however concerns have been raised in regards to possible disease transmission and immune responses in the recipient patient[88]. Often xenograft tissue is used as part of a composite repair device, such as the use of bovine collagen in various mineralized collagen devices described below.

1.8.2 Bone healing in response to allograft implantation

Allografts, and related xenografts, present as viable alternatives to autologous grafts, largely due to the limited supply and related surgical complications associated with autografts and their harvesting. Allograft tissue can be obtained from living donors, such as done during hip replacement, or from post-mortem donors[133]. Processing of this grafting tissue is done to reduce implant immunogenicity as well as to form the graft into desirable dimensions. This processing is often done through the use of detergents, ethanol, and other chemical methods, followed by sterilization, such as through irradiation[133]. Healing in response to allografts differs from when autologous grafts are used in many ways, including the observation that autograft treated defects heal through both endochondral and intramembranous ossification, whereas allograft treated bones heal largely through only the former mode[134]. The healing response to an implanted allograft also relies partially upon the proper preparation of the host site by the surgeon[133]. For example, the interface between host and graft should be mechanically stable and the exposed tissue bed should be modified to provide bleeding bone[133].

As mentioned, allografts may be obtained and processed into many forms, including both cortical and cancellous bone, and DBM. Cortical allografts allow for rigid fixation to take place thus restoring load-bearing ability to the donor tissue site relatively quickly, such as during spinal augmentation procedures[88,135]. Cortical strut allografts, which are diaphyseal segments of donor bone, are sometimes used as biological plates to reinforce periprosthetic fractures[136,137]. Following implantation of cortical allografts, appositional bone growth begins into the graft beginning with inflamma-

tion and progenitor cell recruitment, followed by osteoid production by osteoblasts onto the graft surface and subsequent osteoclastic resorption in a remodelling process termed "creeping substitution" [88,134,135]. The union rates associated with cortical strut allografts have been reported to range from 89% to 99% when used in treating periprosthetic femoral fractures and as high as 100% in the treatment of distal femoral non-unions when combined with internal fixation and autologous grafts [138].

Cancellous allografts may become remodelled via a similar process to cortical allografts [88]. Cancellous allograft resorption however is likely to occur much more quickly than their cortical counterparts, yet fibrous encapsulation and lack of resorption may still occur [88]. DBM on the other hand is limited to bone filling applications; often used as an adjunct to other implants [88,135] DBM has been shown to be osteoinductive, however this property is highly dependent upon the preparation technique [135].

Incorporation of bone allografts depends highly upon the structural form of the graft tissue and the location of the donor site. For example, allograft chips have been shown histologically to incorporate completely, resulting in new bone growth, whereas fully intact (structural) allografts have been found to result in limited remodelling, with lack of complete incorporation observed many years after implantation [139]. This limited remodelling capacity for structural allografts is due in part to the lack of access remodelling cells have beyond a limited depth on the surface of the graft [139]. It has been identified through observations of retrieved allografts in humans, that union is largely achieved through external callus formation bridging the implant-host interface [134]. Although creeping substitution/replacement of the allograft proceeds towards the interior of the graft, complete remodelling is often not achieved, leaving

avascular tissue within the graft[134]. It has been reported by Judas et al.[136] that although some degree of creeping substitution occurs at the interface between the host bone and allograft surface, the bulk of the cortical allograft remains dead, yet structurally intact. Due to this lack of vascularization and host cell repopulation, damage to this bone goes unresolved and microcracks eventually begin to accumulate as a result of cyclic loading. This accumulation of microdamage may eventually lead to complete mechanical failure at the graft site[134].

The mode of failure associated with allograft use depends upon the type of allograft used, implant location, surgical technique, along with many other physiological factors. In a review by Lash et al.[140], the rates of complications and delayed union were investigated for the use of various void fillers for opening-wedge osteotomies of the knee. Delayed union/non-union rates were found to be significantly higher for allografts compared to autografts (4.6% vs. 2.6%)[140]. Allografts in turn had higher rates of union than the synthetic bone graft substitutes investigated, with the latter having varying rates depending upon the material used[140]. In regard to the specific mode of implant failure, as was mentioned, due to the difficulty of remodelling allograft tissue completely post implantation and also the use of sterilizing techniques, such as gamma radiation, fatigue microcrack growth may occur, leading to eventual graft failure[141].

Additional complications associated with allograft use include the risk for an undesirable immunogenic response which may lead to device failure[88]. This immune response would reduce any osteoinductive properties inherent to the implant as infiltrating immune cells would result in implanted tissue necrosis and encapsulation[88]. Disease

transmission is also a possibility associated with allograft use. Diseases that are difficult to identify and track include viruses, such as hepatitis C virus and HIV, as well as possible prion exposure[133]. Advances in tissue bank screening and processing protocols have led to a reduction in disease transmission to recipients from donor allograft tissue[88,133].

1.8.3 Metallic implants

Metals are amongst the oldest bone repair device materials used and offer great mechanical stability to bone defect sites and often allow a restoration of mobility quicker than most non-metallic implants. The devices may be used for many different applications, including hip, knee, shoulder, or other joint replacement, spinal fixation, as well as for the fixation of many bone fractures. Most commonly these implants are composed of either stainless steel (typically 316L), titanium (Ti) and its alloys (typically Ti-6Al-4V), or cobalt-chromium alloys[142–145]. Although metallic implants offer mechanical advantages, they are prone to stress shielding[66,146,147], implant migration[148], and toxic ion leaching leading to metallosis[149,150], which may require revision surgery for device retrieval. Ion toxicity has been well reported and includes characterized toxicity of V, Co, and Ni ions[145].

Metallic implants lack the enhanced bioactivity many of the polymeric, ceramic, or biologic implants possess. In response to this lack of bioactivity, various metallic implants under development or recently placed on the market have been functionalized with coatings, including those of ceramic and bioactive glass origin[142,143]. Additionally, recently entering the marketplace are metallic implants based on alter-

native metals, such as magnesium, iron, and zinc, which may allow for biodegradation[142,144,145,151]. These metals may offer enhanced bioactivity as well as providing an implant that better matches the mechanics of the underlying bone, such as a pure Mg implant which has a Young's modulus of 45 GPa vs. 15-30 GPa for cortical bone and upwards of 200 GPa for stainless steel and cobalt-chromium implants[143]. In response to the high elastic modulus of Ti-based implants, Takizawa et al.[152] are developing bone repair plates composed of Ti fibers. These plates have a Young's modulus closer to that of cortical bone than traditional Ti plates[152]. Issues surrounding fast degradation rates plague Mg-alloy implants however, leading to investigations towards surface coating, such as with HA[143,145]. Other biodegradable metals proposed include pure iron as well as iron and zinc alloys[145]. These metals are often alloyed with other metals to better control degradation rates. In addition to the example of Mg-alloys above, Fe is often alloyed to shorten its degradation rate, such as in Fe-35Mn and Fe-Mn-Pd alloys[153,154].

1.8.4 Bioactive glasses and ceramics

Many devices currently on the market have aimed to replicate the mineral phase within bone. These materials include HA, calcium aluminate, tricalcium phosphate, dicalcium phosphate dehydrate, calcium carbonate, octacalcium phosphate, calcium sulfate, and biphasic calcium phosphate, and ceramic or bioactive glass-based cements, among other products[88,125,155,156]. Ceramic constructs can also be tailored to conform to various specific shapes, such as spheres, rods, sheets, or other 3D conformations[155]. Ceramics serve as a source of Ca and P ions to the local environment surrounding

osteogenic cells during bone tissue repair and regeneration. In addition to providing materials necessary for natural apatite deposition, it was found that nano-CaP resulted in an upregulation of various osteogenic factors, such as BMP-2, Runx2, and OP, indicating osteoblastic differentiation[155]. In addition to the CaP based ceramics, researchers have begun experimenting with ion doping, such as Mg incorporation within apatite, which has been found to enhance osteogenesis due to reduced crystallinity of the ceramic, better mimicking the ceramic phase of natural bone[157]. These materials are commercially available in granular form, blocks, or even as injectable systems[125]. Strength of ceramic only implants is one of the major limiting factors of these products.

Originating with the work of Hench et al.[158] in 1969, various silicate-based glass compositions have been found to possess heightened levels of biocompatibility as well as the ability to bond with native bone tissue. Bioactive glasses, that is glasses with the ability to form bonds between tissue and material surface, as Class A bioactive materials, hold both osteoconductive and osteoinductive properties[159,160]. 45S5 Bioglass, the first described bioactive glass discovered[161], is a biodegradable glass possessing a Na_2O-CaO-SiO_2-P_2O_5 system. Bioglass implants have since expanded into many different formulations and include the addition of elements such as fluorine, magnesium, strontium, iron, silver, boron, potassium, and/or zinc into the silicate network[160]. An example of a device using 45S5 bioglass is the Ossimend® scaffold by Collagen Matrix, Inc., which is composed of bovine collagen and bone mineral and is indicted for use in bony voids and/or gaps not intrinsic to stability (Table 1.2).

Although these single-phase ceramic systems may prove biocompatible or even osteo-

conductive *in vitro*, there is benefit towards their incorporation with various biopolymers. These composite preparations have been investigated widely in recent literature and are generally found to possess heightened levels of osteogenic potential and mechanical stability as they are more biomimetic in nature and reinforce the brittle nature of ceramics alone[155].

1.8.5 Biologic devices

Biological devices are those that may be derived from donor tissue, such as DBM, those that contain added biologics, such as growth factors, and blood products, such a bone marrow aspirate[88,125]. These materials have been introduced largely to address the lack of osteoinduction and osteogeneity of synthetic biomaterials. In regard to the addition of biologics to existing devices, relatively few factors have seen clinical testing and trials to date. These include various BMPs, fibroblast growth factors (FGF)s, vascular endothelial growth factors (VEGF), parathyroid hormone (PTH), and blood products, such as bone marrow and platelet rich plasma[75,88]. These products offer inherent osteoinductive capabilities, yet come at an increased cost as well as manufacturing/storage difficulties, and sometimes unpredictable responses within the body post implantation. Current products on the market include various allografts as well as DBM products such as InterGro® (Zimmer Biomet Spine Inc., CO, USA) and Indux™ (Zimmer Biomet Spine Inc., CO, USA) and products containing growth factors such as the INFUSE® bone graft (Medtronic, TN, USA) which delivers BMP-2 via a resorbable collagen sponge vehicle. Examples of biologic devices currently under development include a BMP-2-HA-collagen based scaffold by Cai et

al.[162] and a 3D-printed HA scaffold coated with BMP-2-PCL nanoparticles by Kim et al.[163].

1.8.6 Synthetic polymeric materials

Polymer-based implants offer a wide range of mechanical, compositional, and structural properties and may be further subdivided into naturally derived or synthetic polymers. Synthetic polymers may include the surface erodible polymers (polyphosphazene, Poly(anhydrides), Poly(propylene fumarate), and Poly(ortho-esters)) and saturated aliphatic polyesters (poly(lactic acid) (PLA), poly(glycolic acid) (PGA),poly(ϵ-caprolactone) (PCL), and poly(p-dioxanone)[164]. Saturated poly-α-hydroxy esters, such as PLA, PGA, and their co-polymer, poly(lactic-*co*-glycolic) acid (PLGA), constitute the most frequently used synthetic biodegradable polymers[164]. Degradation of these products at an undesired rate may however lead to premature device failure along with the formation of an acidic environment caused by monomeric accumulation leading to inflammation and a delay in bone tissue regeneration and repair[164]. Surface eroding polymers are hydrophobic and undergo a heterogeneous hydrolysis course degrading from their exterior surface before internal degradation[165]. As these polymers are not degraded in bulk they offer the unique properties of retaining their structural integrity over a longer period of time along with diminished acidic environment production and enhanced bone ingrowth[165].

1.8.7 Natural polymeric materials

Naturally sourced biomaterials may include various polysaccharides (cellulose, chitosan, alginate)[166–169] and proteins (collagen, silk fibroin, soy)[170–175]. Chitosan is a deacetylated derivative of the high molecular weight biopolymer found in marine crustacean shells, mushrooms, jellyfish, coral, and cell walls of fungi, chitin[168,176]. Chitosan may interact with various negatively charged molecules, such as proteoglycans found naturally within bone. Complexing of chitosan with growth factor linked glycosaminoglycans may enhance its use in bone tissue engineering[176]. Recently, Zhao et al.[177] developed a porous chitosan/nano-hydroxyapatite scaffold aimed at bone repair. The compressive strength of the scaffold was found to be similar to trabecular bone and the material demonstrated good biocompatibility when cultured with MC3T3-E1 cells[177]. Alginate polymeric materials may provide beneficial in terms of bone tissue engineering due to their ability to delivery necessary cells and/or osteoinductive factors along with their ability to form complexes with cell adhesion peptides[178–180]. Alginate gels may also offer benefit as they possess easily customizable geometries, allowing their incorporation into irregularly shaped defects[181].

Of the natural polymers, collagen predominates as the most widely used in commercially available products, as it is the main organic component of bone. Collagen, along with many other biopolymers, is often combined with a mineral or bioactive glass phase to increase mechanical properties as well as osteoconduction. Collagen also degrades into by-products found naturally within the body and has even been found to exhibit osteoinductive characteristics[182]. Examples of these collagen-based composite devices can be found in Table 1.2 and are described below. Another protein

under investigation for use as a bone repair material is silk[183,184]. Silk, which can be processed into films, fibers, hydrogels, and sponges, and has heightened mechanicals stiffness and toughness over many other natural biomaterials[183].

1.8.8 Mineralized collagen devices

Multiple materials may be complexed together to create more advanced biomimetic devices. These devices typically employ the use of a mineral phase, predominantly HA, and biopolymers[1,185]. Synthetic polymeric composites with mineral offer a wide range of customizable properties, however if bioinert, they may fail to degrade properly within the body and may promote an unfavourable response due to their foreign composition. Due to reduced toxicity and increased similarly to native tissue, natural polymeric composites with mineral are undergoing increasing investigation for use in bone repair[1,186,187].

Although still a relatively new material system within the area of bone tissue engineering, mineralized collagen is emerging rapidly as an alternative to many existing materials[188]. One of the obvious reasons for this is the similarity of these devices to bone. This bio-inspired approach has been shown to enhance the ability for the body to recognize the implant as a bone-like material which in turn promotes the migration and differentiation of osteogenic cells and subsequent bone defect repair[189,190]. Additionally, biocompatibility is enhanced by using materials found naturally within bone, which leads to desirable degradation products[191]. Mineralized collagen-based devices currently available on the market largely target bone defects caused by traumatic injury and surgical wounds, including those from tumor resection[191]. Within these

available products there exists a fair degree of structural heterogeneity, as pore sizes, surface roughness, composition, and target defect site may vary greatly[191]. Table 1.2 summarizes mineralized collagen based medical devices currently on the market aimed at bone repair and regeneration.

Indications of use for products summarized in Table 1.2 typically state regions of the skeleton not essential to load bearing or stability as device target sites. Examples of this include CopiOs® bone void filler (Centerpulse Spine-Tech Inc., MN, USA), OssiMend™ (Collagen Matrix Inc., NJ, USA), Vitoss® (Orthovita Inc., PA, USA), MASTERGRAFT® (Medtronic, TN, USA), Integra MAZAIK™ (Integra LifeSciences Corp., NJ, USA), PlatFORM™ (Zimmer Biomet, IN, USA), and NovaBone bioactive strip bone graft (NovaBone Products, FL, USA), all of which state: "-indicated for bony voids or gaps, that are not intrinsic to the stability of the bony structure" (Table 1.2). Most refer to regions of the skeletal system including the extremities, pelvis, and spine that are a result of trauma or as a result of surgery. Others are specifically targeted to dental and/or maxillofacial applications including HEALOS® (DuPuy Spine Inc., MA, USA), Bio-Oss Collagen® (Geistlich, Switzerland), and SynOss™ (Collagen Matrix Inc., NJ, USA) (Table 1.2). These indications may include augmentation or reconstruction of the alveolar ridge, filling of periodontal defects and extraction sockets or defects resultant from root resection, apicocectomy, and cyctectomy, or elevation of maxillary sinus floor. Other products have less specific indications for use or are indicated to be used as a graft extender for regions not vital to overall stability, such as BonGold™ (Allgens Medical Inc., China) and ReFit (Hoya, Japan).

One of the major limitations of mineralized collagen use in bone repair systems is its undesirable mechanical properties for use in certain load bearing regions within the body[188]. The ability to tailor the mechanical properties of such materials has been limited to date. As such, mineralized collagen based devices are still in their clinical infancy. This can be seen with the devices listed in Table 1.2. Most, if not all, of these devices are limited to regions not essential for overall skeletal stability. This is a major area that products under development are aiming to address. By allowing mineralized collagen devices to be targeted towards areas intrinsic to major load bearing functions within the skeleton, a much greater market space opens up and the replacement of many currently used products may be achieved.

Table 1.2: Commercially available mineralized collagen based devices for bone repair and regeneration.

Product	Composition	Form	FDA Market Approval	Handling	Indications	Company	510(K) Number
CopiOs® Bone Void Filler	Type I bovine collagen, 67wt% calcium phosphate	Sponge, paste (hydrated powder discs)	2004, 2007	Combined with autologous blood products (bone marrow)	Bony voids or gaps in skeletal system not intrinsic to stability	Zimmer Biomet, USA	K033679, K071237, K072384
HEALOS®	30wt% HA, type I bovine collagen	Strips or pads	2001, 2005, 2008	Direct application	Treat periodontal or bony defect of upper and lower jaw	DePuy Spine, Inc. MA, USA	K012751, K043308, K081432
OssiMend™	45% bovine type I collagen, 55% bovine bone mineral	Strips, pads, or granular	2006	Hydrated with autogenous bone marrow prior to use	Bony gaps (strips, pads), bone voids (granular) in skeletal system that are not intrinsic to stability	Collagen Matrix Inc. NJ, USA	K052812
Bio-Oss Collagen®	10% porcine type I collagen with 90% bovine bone mineral	Block	1998, 2004	Trim and apply directly to defect dry or moistened with saline	Augmentation of alveolar ridge, filling periodontal, root resection, apicoectomy, cystectomy, and extraction defects, and elevation of the maxillary sinus floor	Geistlich, Switzerland	K033815, K974399
BonGold™	Type I bovine collagen and HA	Strip, granule, block, putty, sponge, screw hole back filler	2015	Used with autograft as a bone graft extender	Bony voids or gaps	Allgens Medical Inc.(TM), China	K141725
Vitoss® Bioactive, Scaffold Foam	Type I bovine collagen with B-TCP	Cylinders, strips	2003, 2007, 2008	Direct application	Bony voids or gaps in skeletal system not intrinsic to stability	Orthovita, Inc., Pennsylvania USA	K032288, K072184, K081439, K083033
MASTERGRAFT® Putty, Strip, UltraMatrix	Type I bovine collagen and biphasic calcium phosphate ceramic (15% HA, 85% B-TCP)	Strip	2007, 2009, 2013, 2014	Strip combined with autogenous bone marrow	Bony voids or gaps in skeletal system not intrinsic to stability	Medtronic, Tennessee, USA	K082166, K071813, K082166, K140375
Ossimend® Mineral Collagen Composite Bioactive Bone Graft Matrix	Bovine tendon type I collagen, 45S5 Bioactive Glass, bovine bone mineral	Strip or cylindrical matrix	2019	Combined with autogenous bone marrow or autograft with saline	Bony voids or gaps in skeletal system not intrinsic to stability	Collagen Matrix, Inc., NJ, USA	K182074

Table 1.2: **Continued.** Commercially available mineralized collagen based devices for bone repair and regeneration.

Product	Composition	Form	FDA Market Approval	Handling	Indications	Company	510(K) Number
Integra MAZAIK™	Bovine type I collagen, B-TCP	Strip	2007, 2014	Combined with bone marrow aspirate	Bony voids or gaps in extremities, spine, and pelvis not intrinsic to stability	Integra LifeSciences Corp. NJ, USA	K063124, K141841
ReFit	20wt% porcine type I collagen, 20wt% poorly crystalline HA	sponge	2010	Direct application	Bony voids	Hoya, Japan	
SynOss™	Bovine tendon type I collagen, synthetic calcium phosphate	Granular, block/plug, putty	2007, 2009	Direct application	Augmentation of alveolar ridge, filling periodontal, root resection, apicoectomy, cystectomy, and extraction defects, and elevation of the maxillary sinus floor	Collagen Matrix, Inc. NJ, USA	K072397, K083742
NovaBone Bioactive Strip Bone Graft	Type I collagen, bioactive synthetic granules	Strip	2014	Direct application	Bony voids or gaps in extremities, spine, and pelvis not intrinsic to stability	NovaBone Products, Florida, USA	K141207
PlatFORM™ CM Blocks and Strips	Carbonate apatite mineral (80%) with bovine type I collagen (20%)	Blocks, strips	2013	Hydrated with autologous bone marrow at time of use	Bony voids or gaps in extremities, spine, and pelvis not intrinsic to stability	Zimmer Biomet, Indiana, USA	
PlatFORM™ CM Pads and Putty	Bone mineral (55%), collagen (45%)	Pads, granular	2012	Hydrated with autologous bone marrow at time of use	Bony voids or gaps in extremities, spine, and pelvis not intrinsic to stability	Zimmer Biomet, Indiana, USA	

Chapter 2

Thesis Rationale and Objectives

2.1 Thesis rationale

Autologous and allogenic bone grafts remain the gold standard materials used for bone repair procedures due to not only their associated biocompatibility and osteogenic potential, but also due to their mechanical similarities to the host bone site[192–194]. As was outlined in Chapter 1, there exists many limitations however for the use of such grafting materials in bone repair, largely stemming from tissue availability[88]. Due to these restrictions, and a general lack of alternative materials, there currently exists an unmet demand for functional load-bearing graft material[195,196].

The development of orthopaedic devices constructed from mineralized collagen has gained increasing attention over the past decade due to the increasing demand for functional implants and similarity of these devices to bone[196]. While there is demonstrated efficacy in the use of mineralized collagen constructs for bone repair/regeneration[188,191],

the structure of these constructs currently limits them to non-load bearing applications[195,196]. This is due in part to the structure of the collagen template used in these devices and the collagen mineralization technique. Most mineralized collagen constructs produced to-date have been constructed from reconstituted collagen, and as such, lack well ordered fibrils.

which lacks the ordered alignment found within bone and natural crosslinking. In addition, mineralization of this collagen template typically lacks intrafibrillar incorporation and may be limited to a thin superficial region.

The work described herein identified a sustainable source of collagen for such a device, which was comprised of well-aligned, naturally crosslinked collagen fibrils, that served as a suitably robust template for scaffold construction. Knowing that sourcing of collagen, particularly natively crosslinked, tissue derived collagen, is an important issue facing mineralized collagen scaffold development, I chose to utilize a waste product from the food processing industry as a collagen source. Biomineralization of collagen was performed in such a way as to take advantage of natural processes known to achieve intrafibrillar collagen mineralization; largely collagen phosphorylation and the incorporation of polyanionic molecules and other crystal modifying agents during the mineralization process. This work provides a better understanding to the effect various crystal modifying agents have on the mineralization of dense collagen substrates, in particular, the role pAsp and citrate have to the final size of calcium phosphate crystals and their integration with collagen fibrils.

Achieving an appropriate mechanical profile for an orthopaedic implant is important, as cells respond differently to varying degrees of substrate stiffness[117]. Additionally,

the ability to control device mechanics over multiple scales in a predicable way is advantageous as the mechanical requirements for a bone repair device vary greatly depending upon the body location, bone type, disease state and age of the patient. This thesis aimed to achieve, for the first time, the creation of a highly aligned, naturally crosslinked mineralized collagen scaffold with tailorable mechanical properties, as evidenced at both the nano- and macro-scales. It is thought that this developed mineralized collagen scaffold may serve as a base technology on which higher order multilaminate constructs can be designed, ultimately reaching the goal of creating a viable load-bearing bone graft material. The goal of this multilaminate graft material would be to maintain the load-bearing requirements for a bone defect site as the graft is gradually remodelled by surrounding bone cells, thus extending its use to multiple defect sites. This approach is somewhat in contrast to existing bone scaffold preparation methods where a biodegradable scaffold is developed with the goal of degrading at a rate matching the infiltration of new bone tissue, usually at very specified defect locations.

2.2 Thesis objectives

The central objective of this work was to develop and characterize a novel, naturally crosslinked mineralized collagen scaffold, with a focus on mineral chemistry, resultant mineralized collagen fibril and scaffold mechanics, and *in vitro* biocompatibility.

Specific objectives were to:

1. Develop a method of mineralizing decellularized sheets of bovine tendon that

leads to close integration of mineral with collagen and a mineral phase that compares favourably with that found in bone.

2. Determine the degree to which the mechanics of the mineralized collagen scaffolds produced using the system developed under objective one can be controlled through small adjustments to the manufacturing process.

3. Evaluate the response pre-osteoblastic cells have to the prepared scaffolds and determine the degree to which alterations of scaffold mechanics, as achieved under objective two, influence cellular phenotypic and osteogenic biochemical profiles.

Chapter 3

Use of Tendon to Produce Decellularized Sheets of Mineralized Collagen Fibrils for Bone Tissue Repair and Regeneration*

*The experiments presented in this chapter have been published in the Journal of Biomedical Materials Research Part B: Applied Biomaterials[258].

3.1 Introduction

Critical size defects in bone are those sufficiently large to prevent spontaneous healing and can occur due to injury, illness, or through surgical procedures, such as osteotomy[198,199]. Defects that are large enough to require surgical intervention are typically filled using autologous bone tissue, usually taken from the iliac crest[140]. While success rates using autologous grafts are high, limited graft availability and donor site morbidity remain serious concerns. To overcome these limitations, alternatives including allografts, xenografts, and engineered materials have been used. Other issues, however, exist for the currently available alternatives, including immunogenicity, undesirable degradation rates or by-products, and unfavourable mechanical characteristics.

As an alternative to synthetic void filler materials, such as poly lactic acid, poly glycolic acid, polyurethanes, and others[200], interest in engineered mineralized collagen composite scaffolds is increasing. Commonly used methods for preparing mineralized collagen scaffolds include formation of matrix from soluble collagen followed by exposure to a mineral containing solution for several hours[188], or co-precipitation of mineral and collagen mixtures[80]. Mineralized collagen scaffolds may be ideal materials for bone defect repair due to their chemical, structural, and mechanical similarity to native bone. In a study conducted by Lyons et al.[201], a collagen-hydroxyapatite (HA) scaffold exhibited comparable healing to autologous bone grafts in a rabbit radius osteotomy defect model. These scaffolds were prepared through the dissolution of collagen in an acidic solution followed by freeze-drying a mixture of mineral and collagen[201]. Pugely et al.[202] investigated two bone void fillers composed of HA, tri-

calcium phosphate (TCP), and bovine collagen, with one also containing Bi-Ostetic bioactive glass foam. Both fillers exhibited biocompatibility and efficacy in bone healing using an established rabbit posterolateral fusion model[202]. In a study conducted by Zheng et al.[203], a β-TCP/collagen composite filler (Cerasorb® Orhto Foam) was tested in a rabbit distal femoral condyle model and resulted in complete resorption and bone formation without toxic or immunologic effects. A bilayered biomimetic scaffold composed of an inner type I collagen layer and an outer layer of mineralized collagen (30%) and Mg doped HA (70%) was evaluated by Calabrese et al.[204] through subcutaneous implantation in mice. This bilayered scaffold was able to recruit host cells and produce new mineral formation by the host tissue throughout its ectopic location as well as neovascularization[204]. Weisgerber et al.[205] prepared mineralized collagen-glycosaminoglycan (GAG) scaffolds through the lyophilization of a collagen-calcium salt suspension in custom molds. These scaffolds were then crosslinked in a solution of EDC and NHS before culturing with human MSCs where they exhibited enhanced osteogenesis compared to non-mineralized controls[205]. In a study by Lin et al.[206], composite type I collagen-hydroxyapatite scaffolds were produced through low-temperature additive manufacturing. Through in vitro investigations, these scaffolds showed enhanced bone marrow stromal cell proliferation compared to non-printed scaffolds (molded) and were remodeled successfully when used in a rabbit femoral condyle defect model[206]. Additionally, Wang et al.[188] constructed a mineralized collagen scaffold through the immersion of type I collagen in a mineral containing solution for 48 hours. This scaffold was found to promote MSC adhesion, proliferation, and osteogenic differentiation *in vitro* as well as ectopic bone formation and enhanced bone growth in a skull-penetrating SD rat defect model when compared to blank control

and collagen membrane groups at both 4 and 12 week timepoints[188].

While the engineered mineralized collagen scaffolds mentioned above have shown promise in their ability to aid tissue regeneration, further benefits and new surgical applications may be realized by developing scaffolds that: (i) possess mineral that more closely mimics that present in native bone, and (ii) offer improved structural control of the organic collagen phase.

Achieving the correct mineral structure when creating mineralized collagen scaffolds may be biologically important. The mineral phase found within native bone tissue has a non-stoichiometric, poorly crystalline apatite structure, close to that of hydroxyapatite (HA), $Ca_5(PO_4)_3(OH)$[93]. The poorly crystalline nature of the mineral phase is partly due to the incorporation of various chemical and ionic species within the apatitic mineral, including carbonate (4-6%), Na (0.9%), and Mg (0.5%)[93]. Bone graft substitutes have largely focused upon the use of CaP materials, such as HA, to induce device integration at the defect site. Incorporation of cationic or anionic additives into these CaP based mineral preparations has received much less study. These minor constituents may act to enhance recognition and remodelling of the implanted materials via their interactions with native osteogenic cells. For instance, Mg^{2+} may play an important role in the production of nitric oxide, which aids in the modulation of angiogenesis[96]. Mg^{2+} may also help stimulate osteoblast proliferation[207]. When added to HA, carbonate was found to enhance osteoconductivity and bioresorption of mineral[96].

Current mineralized collagen fillers are typically produced from aqueous collagen suspensions or slurries that are precipitated or moulded into shape[99–101,208–214]. The

resulting fillers are composed of randomly oriented collagen fibrils, which may additionally lack native enzymatic crosslinking if produced from suspensions of collagen monomers. Because the mechanics of collagen materials depend highly on collagen fibril alignment, improved control of collagen fibril alignment in mineralized fillers would be highly advantageous. In terms of maintaining native intermolecular crosslinking within fibrils, this may have biological in addition to mechanical importance. While intermolecular crosslinking is required to both limit the rate of scaffold degradation and improve mechanical stability, various forms of exogenous crosslinking have been shown to promote proinflammatory response[215], suggesting that incorporation of native lysyl oxidase (LOX)-mediated crosslinking may be important for optimization of a scaffold's regenerative potential. LOX crosslinking may also influence osteoblast and osteoclast differentiation[216], providing an additional means to influence osteogenesis.

Biomimetic mineralization of well-structured collagen fibrils presents various challenges, however. First, in isolation from other matrix components, collagen fibrils may lack the molecular functionality required to induce both intra- and extra- fibrillar mineralization. For example, various acidic non-collagenous proteins rich in aspartic and glutamic acid residues are found throughout the bone tissue micro-environment and are thought to play a role in intrafibrillar mineralization of collagen fibrils. The action of these proteins was simulated by Gower et al.[90] where only after the addition of polyaspartic acid (pAsp) to the mineral containing solutions was intrafibrillar mineralization achieved. It was thought that these process directing polymers caused the mineral phase to form a polymer induced liquid-phase precursor (PILP) which

was able to penetrate the small gap regions in the collagen fibrils before further nucleation, forming mineralized collagen fibrils better resembling those found within native bone tissue[23,217]. Second, the exact chemical structure and geometry of the poorly crystalline, carbonated HA found within bone has proved difficult to reproduce *ex vivo*[93,96]. For intrafibrillar mineral integration and deposition to occur, the geometry in which the incoming mineral phase exists as must be carefully regulated. If the incoming mineral phase can nucleate and crystallize into relatively large crystals, size constraints will inhibit occupancy within collagen fibrils[23]. Modifications to crystal size and composition may affect how well a scaffold integrates with bone as well as degradation rate and by-products.

In this study we describe a process for preparing mineralized collagen sheets, with organic phase composed of highly aligned, natively-structured collagen fibrils, and mineral phase sharing chemical similarities to that found in native bone. In characterizing the resulting scaffold structures, the effects of pAsp and citrate additions during the mineralization process are explored. Evaluations of scaffold mineralization and surface architecture were made through use of scanning electron microscopy (SEM) and transmission electron microscopy (TEM). Mineral phase identification and characterization was performed using energy-dispersive X-ray spectroscopy (EDX), X-ray powder diffraction (XRD), and Fourier transform infrared spectroscopy attenuated total reflection (FTIR-ATR). The process that we describe for producing single, mineralized collagen sheets may be useful for creating larger, load-bearing, regenerative orthopaedic devices.

3.2 Materials & Methods

3.2.1 Tendon acquisition and decellularization

Common digital extensor (CDE) tendons were dissected from the forelimbs of steers aged 24-36 months, killed for food at a local abattoir. Dissected tendons were stored in phosphate-buffered saline (PBS) solution at 4° C to await decellularization treatment, which was started within 12 h of dissection.

Decellularization treatment was conducted following a method previously described by Woods and Gratzer[218]. Briefly, tendons were first exposed to a hypotonic 10 mM tris buffer, containing serine and metalloprotease inhibitors, along with 1% penicillin/streptomycin and 1% amphotericin B for 36 h at room temperature. Tendons were then moved to a high saline 50 mM tris buffer containing 1% Triton X-100 along with antibiotics and protease inhibitors for 48 h at room temperature, followed by Hanks' buffer rinse and wash in a DNase/RNase solution. This was followed by a 48 h, room temperature soak in 1% Triton X-100 solution with 50 mM TRIZMA® base and antibiotics. Finally, the tendon samples were rinsed in PBS with antibiotics and stored in a similar solution at 4° C until further use.

3.2.2 Cryosectioning and phosphorylation

Decellularized tendons were cryosectioned using a Leica SM2000R sliding microtome. Tendons were cut into 2-cm-long segments, mounted on a steel block using OCT compound, frozen in liquid nitrogen, and sectioned longitudinally to produce 200-μm-thick collagen sheets. The collagen sheets were then phosphorylated via treatment

with STMP in order to enhance mineralization[108,219]. A solution of 2.5 wt% STMP was hydrolyzed at pH 12 for 5 h[220]. The solution was then adjusted to pH 10. Collagen sheets were treated in STMP solution for 1 h at room temperature under constant agitation. The sheets were then rinsed in ddH_2O before beginning the alternate soaking mineralization procedure.

3.2.3 Mineralization

Mineralization of the phosphorylated collagen sheets was performed using a modified form of the alternate soaking process described by Taguchi et al.[221]. Using a stainless-steel mesh basket, sheets were first soaked in 200 mL ddH_2O before soaking in 200 mL of a magnesium doped (0.01M) calcium solution ($CaCl_2/MgCl_2$, 200 mM) within a temperature-controlled water bath at 37° C for 120s at pH 7.4. The sheets were then briefly rinsed in ddH_2O before soaking for an additional 120s in a 120 mM sodium phosphate solution containing 0.025M sodium carbonate at 37° C at pH 7.4. The progression of collagen sheets through these four solutions constituted a single mineralizing cycle (Fig. 3.1). For this study, sheets underwent 10 mineralization cycles.

3.2.4 pAsp and citrate additions to the mineralization process

To promote intrafibrillar mineralization, pAsp (mean MW 29 kDa, Alamanda Polymers, AL, USA) was added to the alternate soaking process during the mineralization of some of the collagen sheets. For the mineralization of those sheets, the calcium and

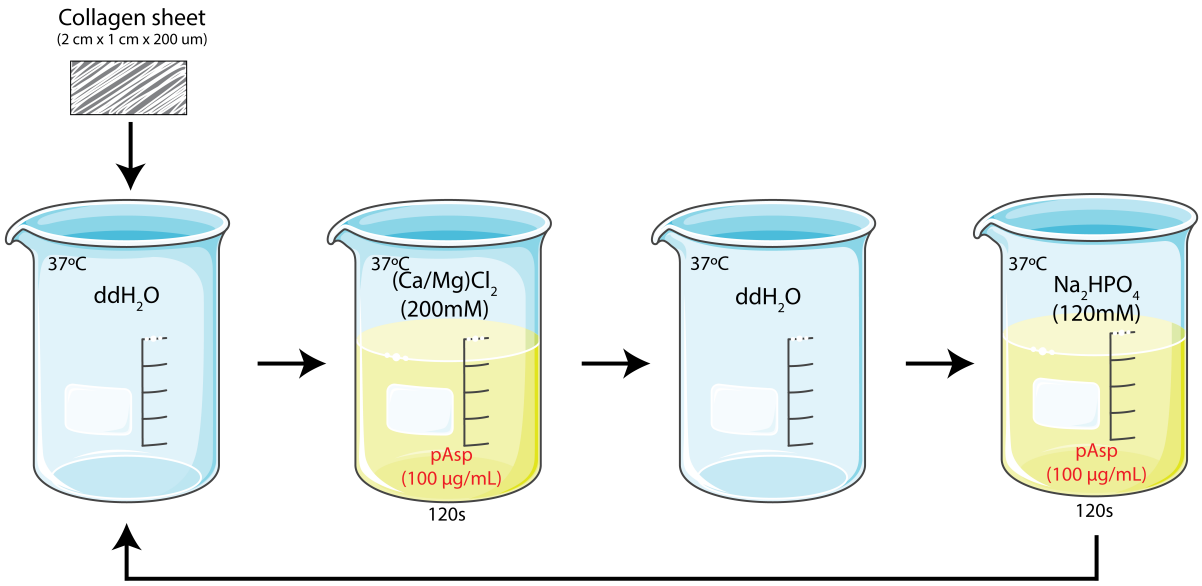

Figure 3.1: Schematic of the alternate soaking process used to mineralize sheets of highly aligned, natively structured collagen fibrils derived from decellularized bovine tendon.

phosphorous solutions each contained 100 μg/mL of pAsp. To better match the chemical environment of natural bone tissue, citrate (Sigma-Aldrich, Ontario, Canada) was also added to the alternate soaking process during the mineralization of some collagen sheets. Citrate was only added to the calcium solution, at a concentration of 0.02M.

3.2.5 Sample groups

With the addition of pAsp and citrate to the mineralization process, the study included four sample groups:

Mineralized +pAsp/+citrate group: these scaffolds were mineralized with additions of both pAsp and citrate to treatment process.

Mineralized +pAsp/-citrate group: these scaffolds were mineralized with addition of pAsp, but without citrate addition.

Mineralized -pAsp/+citrate group: these scaffolds were mineralized with addition of citrate, but without pAsp.

Unmineralized group: these scaffolds consisted of cryosectioned sheets of decellularized tendon that were phosphorylated, but did not undergo subsequent mineralization.

3.2.6 SEM & EDX

Ultrastructural and elemental analyses of both mineralized and unmineralized collagen sheets were performed using a scanning electron microscope (model S-4700, Hitachi, Tokyo, Japan) and integrated energy dispersive x-ray spectroscopy with precision approaching 0.1% (model X-Max, Oxford Instruments, Abingdon, UK). The collagen sheets were prepared for analysis by fixation in 2.5% electron microscopy-grade glutaraldehyde in PBS for 1 h at room temperature under constant agitation, followed by rinsing in ddH_2O and dehydration in graded ethanol. Sheets were then critical point dried, mounted on SEM stubs using carbon tape, and coated with gold-palladium. The coated samples were viewed under SEM at 3-5kV, 10-15μA. To better visualize the relationship between collagen fibrils and the introduced mineral phase, some scaffolds were etched prior to glutaraldehyde fixation using 0.1M HCl under constant agitation

for 2 min before rinsing in ddH_2O. For each of the four sample groups, three scaffolds prepared from the CDE tendons of different animals and mineralized in different treatment batches were examined using SEM. Only the mineralized +pAsp/+citrate scaffolds were assessed via EDX, which was conducted at 10kV. For the three mineralized +pAsp/+citrate scaffolds assessed under SEM, EDX measurements were taken at a total of eight locations, the results of which were then averaged.

3.2.7 TEM

Mineralized and unmineralized sheets were also assessed using a FEI Tecnai 12 TEM. Samples were pulverized in liquid nitrogen, dispersed in ethanol, collected on copper TEM grids, and examined unstained at 120 kV. For each of the three mineralized sample groups, samples from three scaffolds prepared from the CDE tendons of different animals and mineralized in different treatment batches were examined using TEM. A sample from an unmineralized scaffold was also examined.

3.2.8 XRD & FTIR-ATR

Mineralized +pAsp/+citrate scaffolds were assessed using XRD and FTIR-ATR and compared to samples of bovine cortical bone and pure HA. Cortical bone samples were prepared from the mid-diaphysis of metacarpals 3 and 4 from the collected bovine forelimbs. 2-cm-long samples were cut, boiled in ddH_2O for 30 min, dried at 100° C for 22 h, processed into a coarse powder using a hacksaw, and then fine powder using a mortar and pestle. A mortar and pestle was similarly used to produce fine powders from the pure HA and prepared mineralized scaffolds. XRD was conducted using

Cu-Kα X-ray radiation from a Siemens D500 Diffractometer at 30 kV and 30 mA, using a step size of 0.05° over a 2θ range of $20 - 50°$. XRD peaks were recognized by referring to JCPDS file number 00-009-0432 (hydroxylapatite, syn). FTIR-ATR was conducted using a Bruker Alpha Platinum-ATR FTIR spectrometer in the 400-4000 cm^{-1} range averaged over 24 scans per sample with a resolution of $4cm^{-1}$. For each of the three mineralized sample groups, samples from three scaffolds prepared from the CDE tendons of different animals and mineralized in different treatment batches were assessed using XRD and FTIR-ATR.

3.3 Results

All numerical data are presented as mean ± SD.

3.3.1 Scaffold ultrastructure

SEM and TEM were performed on collagen sheets mineralized with additions of both pAsp and citrate (mineralized +pAsp/+citrate group), without citrate (mineralized +pAsp/-citrate group), and without pAsp (mineralized -pAsp/+citrate group). Unmineralized collagen sheets were also assessed.

SEM examination of unmineralized collagen sheets showed that the highly aligned fibril arrangement typical of tendon was preserved during decellularization treatment and cryosectioning (Fig. 3.2A,B). SEM examination of the mineralized +pAsp/+citrate sheets showed that the introduced mineral phase formed plate-like crystals covering the fibrils, with accumulation of extrafibrillar spherulites (Fig. 3.2C,D). Similarly

prepared sheets etched prior to preparation for SEM using dilute HCl to better visualize the underling mineral-collagen interface showed mineral bridging between adjacent collagen fibrils (Fig. 3.3A,B). When samples from the mineralized +pAsp/+citrate scaffolds were viewed unstained under TEM, individual mineralized collagen fibrils were observed with plate-like crystals longitudinally aligned with the fibrils (Fig. 3.4A,B). Unlike the fibrils from scaffolds mineralized without pAsp or citrate, described below, D-banding could not be seen on these fibrils under TEM, possibly due to the abundance of mineral present.

For samples prepared with the absence of citrate only (mineralized +pAsp/-citrate scaffolds), SEM after acid-etching revealed the presence of much larger plate-like crystals than were observed when citrate was present (Fig. 3.3C,D) vs. (Fig. 3.3A,B). TEM similarly showed that these samples contained larger plate-like crystals when compared to the mineralization treatments that included citrate (Fig. 3.4C,D) vs. (Fig. 3.4A,B).

Acid-etched sheets that were prepared in the absence of only the process directing agent, pAsp, (mineralized -pAsp/+citrate scaffolds) were found to contain greater amounts of extrafibrillar spherulites when observed under SEM (Fig. 3.3E,F). In TEM, it was evident that the absence of pAsp greatly reduced the amount of mineral associated with the collagen fibrils. Compared to fibrils from the mineralized +pAsp/+citrate scaffolds (Fig. 3.4A,B), those from the scaffolds prepared without pAsp possessed noticeably fewer plate-like crystals (Fig. 3.4E,F).

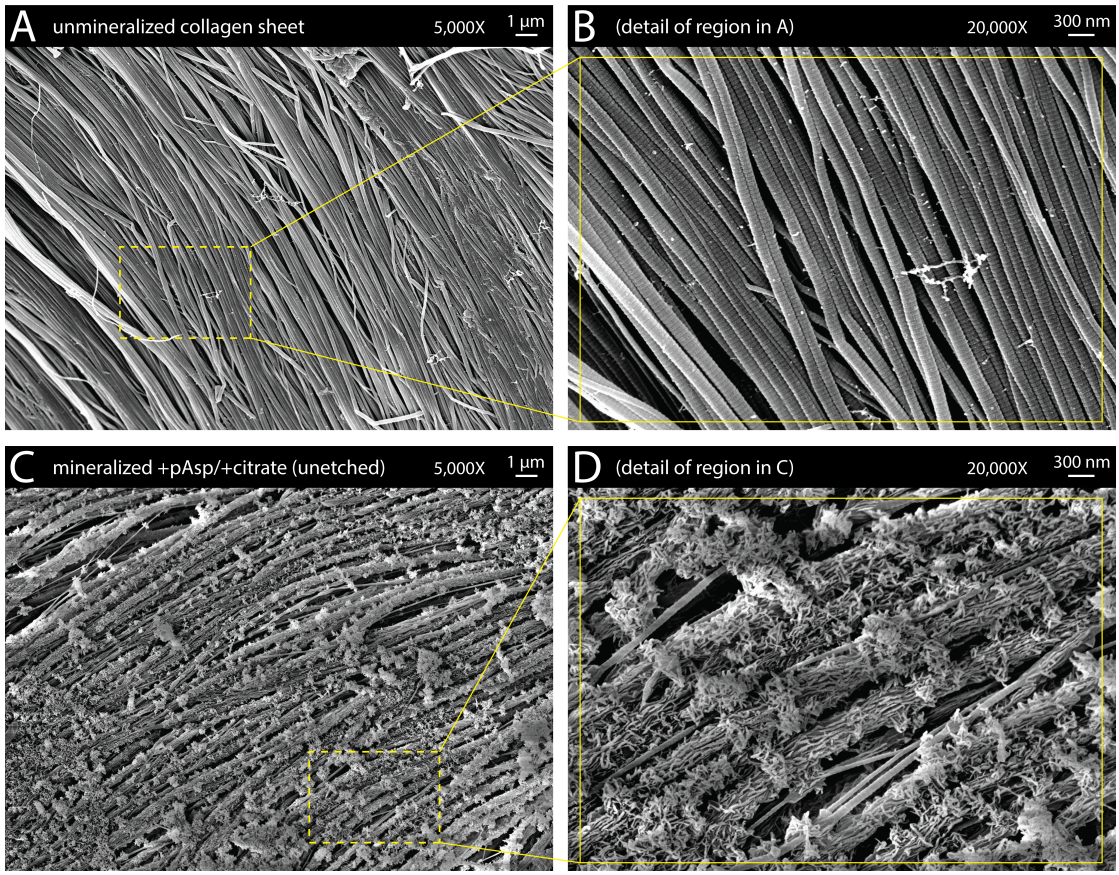

Figure 3.2: A, B: Low and high magnification SEM images of a decellularized sheet of collagen fibrils from bovine tendon prior to mineralization. C, D: Low and high magnification SEM images of a similar collagen sheet after mineralization via 10 cycles of alternate soaking with both pAsp and citrate additives. Individual collagen fibrils are covered in plate-like crystals, with larger spherical clusters of mineral frequently occurring. Unlike the sheets shown in (Fig. 3.3), the sheets shown here are unetched.

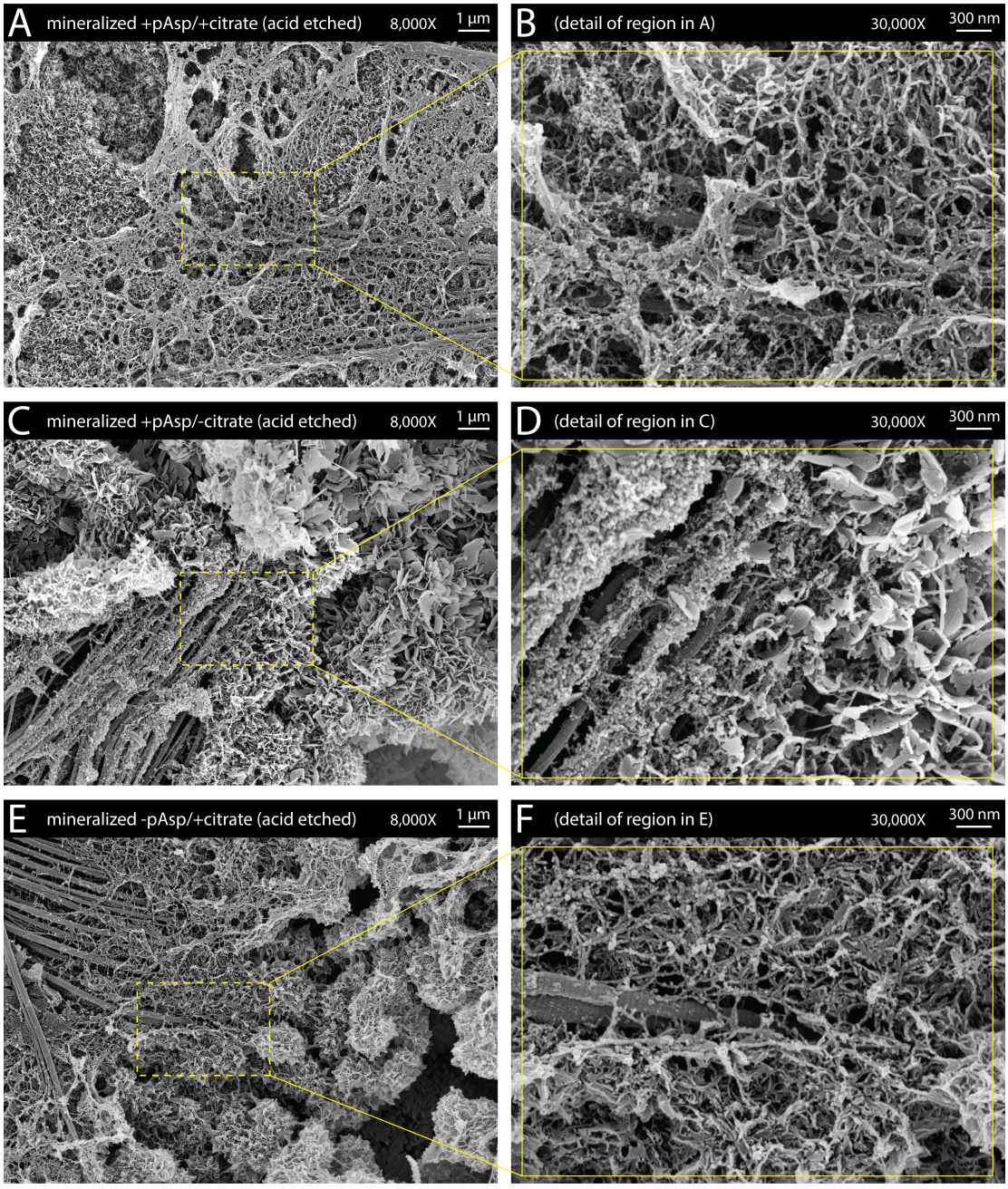

Figure 3.3: SEM images of acid-etched mineralized collagen sheets. A, B: Sheets prepared with pAsp and citrate additions to the mineralization treatment process showed mineral bridging between collagen fibrils. C, D: Absence of citrate from the mineralization process led to extrafibrillar plate-like crystals growing much larger in size. E, F: Absence of pAsp from the mineralization process led to excessive accumulation of extrafibrillar spherulites.

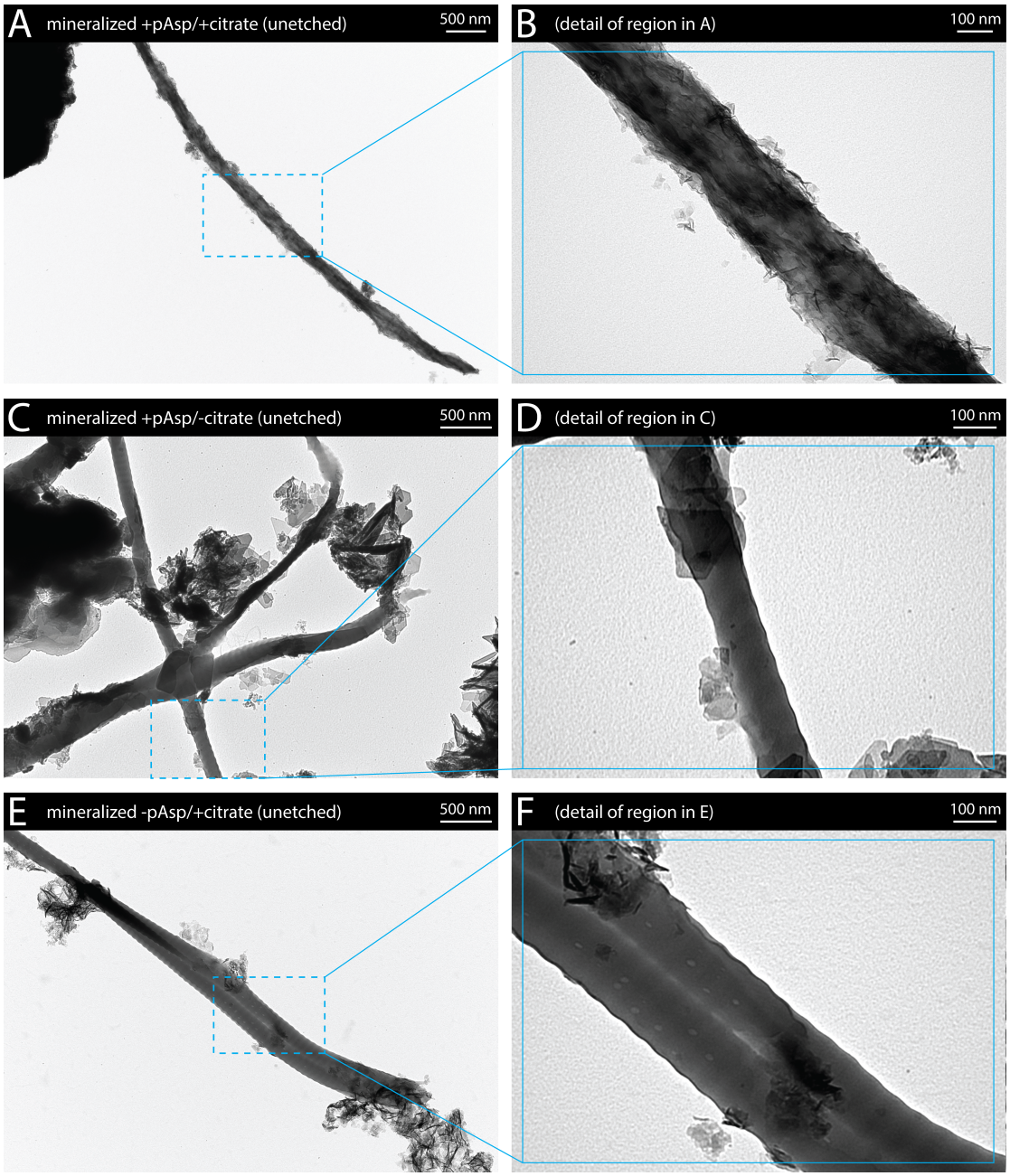

Figure 3.4: TEM images of collagen fibrils removed from the unetched mineralized collagen sheets. A, B: Sheets mineralized with pAsp and citrate additions contained collagen fibrils incorporating a high density of small, longitudinally aligned crystals. D-banding was not apparent, presumably due to the quantity of mineral present. C, D: For sheets mineralized without citrate, much larger plate-like crystals were seen. E, F: Sheets prepared without addition of the PILP process directing agent pAsp contained fibrils with a reduced quantity of closely associated mineral.

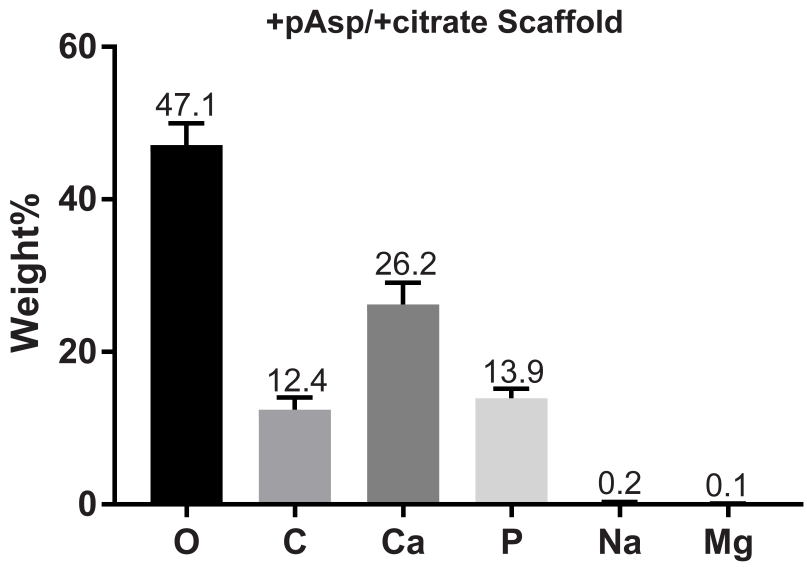

Figure 3.5: EDX-derived elemental composition of collagen sheets mineralized with pAsp and citrate additions showed a Ca/P wt% ratio of approximately 1.89, similar to native bone, with small quantities of Mg and Na present within the prepared mineral phase.

3.3.2 Mineral phase analysis

3.3.3 EDX

Elemental compositions for three mineralized +pAsp/+citrate scaffolds were assessed by EDX. Mean weight percent (wt%) for O, C, Ca, P, Na, and Mg within the mineral phase of the sheets was 47.13, 12.42, 26.23, 13.90, 0.25, and 0.08 wt%, respectively (Fig. 3.5), yielding a Ca/P ratio of 1.89.

3.3.4 XRD

XRD was performed on the mineralized +pAsp/+citrate scaffolds, cortical bone powder, and pure HA. XRD patterns for the mineralized +pAsp/+citrate scaffolds were similar to those of native cortical bone, with peak positions similar to pure HA but significantly broadened (Fig. 3.6), indicating small crystallite size and presence of chemical substitutions. Both cortical bone and mineralized scaffolds contained the (002) peak found at approximately 26° for pure HA, and the (211), (112), and (300) peaks for pure HA appeared as a single broadened peak in both bone and mineralized scaffolds. Compared to cortical bone, peaks for the mineralized scaffolds were somewhat weaker and broader. While both bone and pure HA contained smaller peaks near 40°, 47°, and 50°, these were not observed for the mineralized scaffolds.

3.3.5 FTIR-ATR

Absorption bands for the mineralized +pAsp/+citrate scaffolds, cortical bone, and pure HA were obtained through FTIR-ATR. The characteristic banding of the $PO4^3$ groups was visible in all three samples (Fig. 3.7), with the asymmetric O-P-O bending modes occurring at approximately 560 cm^{-1} and the asymmetric P-O stretching mode visible at approximately 1020 cm^{-1} [222,223]. As expected, weak intensity bands between 3100 and 3500 cm^{-1} attributed to the N-H of the amide of collagen, were observed for both cortical bone and mineralized scaffolds. Doublet peaks at around 1450 and 1640 cm^{-1} and a peak at 873 cm^{-1} were also present, attributable to the vibrational frequencies of carbonate ions substituted into apatite at the phosphate and OH- sites[223,224]. The band at approximately 1650 cm^{-1} on both cortical bone

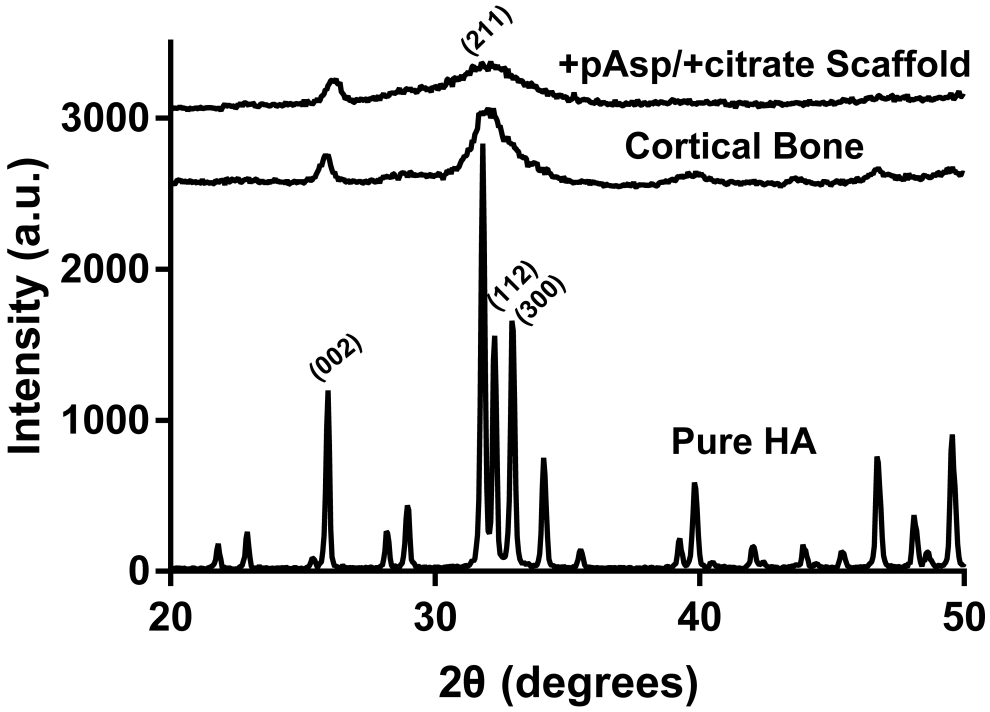

Figure 3.6: XRD peaks of collagen sheets mineralized with pAsp and citrate additions, compared to those from native bovine cortical bone and pure HA.

and mineralized scaffold spectra is most likely attributable to OH^-, carbonate ions, H_2O, or a combination of the former with contribution from the amide I band of collagen[222,225–227].

3.4 Discussion

Many of the previous approaches to creating mineralized collagen scaffolds for bone tissue repair and regeneration have relied upon the use of reconstituted collagen, with the mineral phase either incorporated into the scaffold during tropocollagen aggrega-

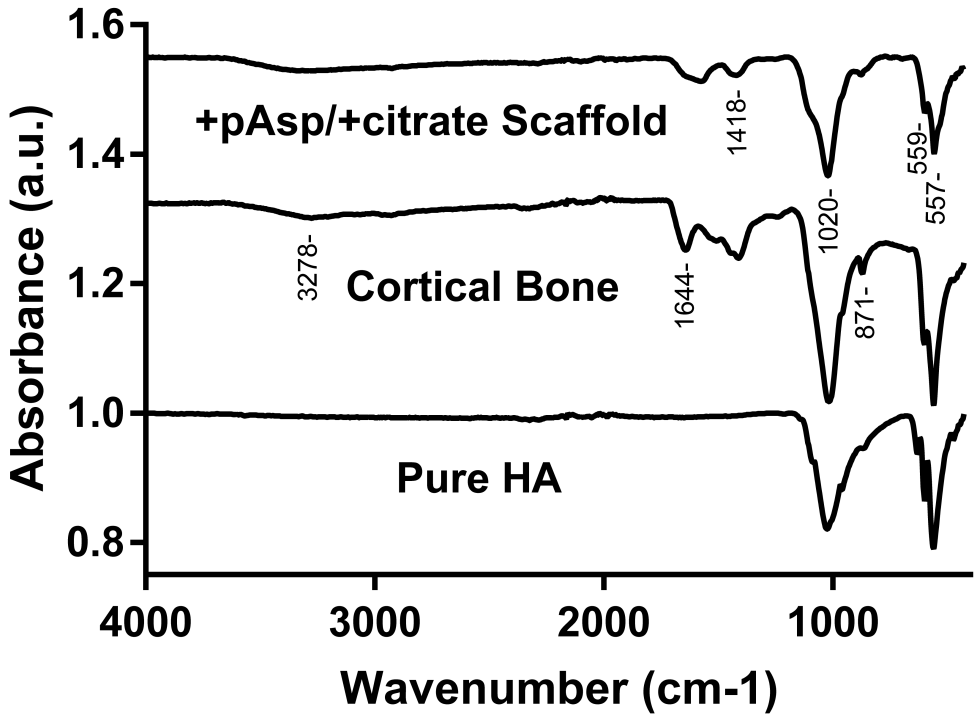

Figure 3.7: FTIR-ATR spectra of collagen sheets mineralized with pAsp and citrate additions, compared to those from native bovine cortical bone and pure HA.

tion[99–101,208,212,214] or following assembly of a collagen template[209–211,213]. Although desirable from an ease-of-manufacturing standpoint, approaches based on reconstituted collagen monomer assembly have not been able to re-create scaffolds of well-aligned, natively crosslinked collagen fibrils, potentially limiting their functionality. In this work we have taken a different approach, using cryosectioned sheets of decellularized bovine tendon to provide an acellular template of highly-aligned, well-crosslinked collagen fibrils into which carbonated hydroxyapatite has subsequently been incorporated. By combining sheets of densely packed, uniaxially aligned collagen fibrils to

form a multi-laminate construct, it may be possible to produce a scaffold with the regenerative potential inherent to mineralized collagen[201], and load-bearing capacity required to effectively support the defect site.

Early crystal nucleation on the surface of collagen fibrils *in vivo* is thought to be inhibited by various ionic or macromolecular constituents, allowing amorphous mineral phases to penetrate the gap regions of collagen fibrils, resulting in intrafibrillar mineralization[90]. Non-classical crystallization pathways may allow for kinetically rather than thermodynamically driven crystal formation mechanisms, leading to development of the complex crystal structures found in bone and elsewhere in nature[21]. Kinetically driven crystal formation is usually supported through the presence of polyelectrolytes, or other soluble macromolecules or ions, that affect the surface energy of forming crystals at specific faces or, as is thought to be the case for bone, may initially prevent crystal formation altogether by creating a liquid precursor[21]. In the current study, mineralization treatment of the collagen sheets without addition of pAsp led to the development of extrafibrillar spherulitic clusters (Fig. 3.3E,F), consistent with the work of others[77,228]. When mineralization was conducted with pAsp, fewer extrafibrillar spherulites were formed and an increase in plate-like crystals intimately associated with individual collagen fibrils was observed (Figs. 3.2B, 3.4B). These observations are consistent with previous experiments where reduction in crystal size and increase in intrafibrillar mineralization were thought to be promoted by the addition of pAsp to the mineralization solutions through a crystal nucleation-limiting mechanism[23,229,230].

Along with pAsp, it is likely that citrate and inorganic ions, such as Mg^{2+} and $PO4^{3-}$,

contributed to the crystal structures seen in the current study. It has been proposed that citrate penetrates collagen fibrils where it then provides additional nucleation sites for intrafibrillar calcium-phosphate crystal growth[231]. Additionally, when adsorbed on collagen fibrils, citrate has been reported to improve wetting between collagen and the mineral precursor phase[231]. These effects appear to promote intrafibrillar mineralization, even in the absence of pAsp[85]. It has also been reported that the presence of citrate during mineralization contributes to a reduction in extrafibrillar mineral plate size[232–234]. This was indeed observed in the current study, where mineralization solutions containing pAsp but lacking citrate lead to the formation of large extrafibrillar mineral plates (Fig. 3.4D) vs. (Fig. 3.4B). Use of citrate during collagen mineralization for scaffold production may be important for increasing intrafibrillar mineralization, increasing scaffold homogeneity, and increasing potential sites for cellular interaction through reduction in extrafibrillar mineral plate size. As with other additives to the mineralization solutions, further investigations however towards the extent and complete characteristic profile of citrate incorporation within the mineral phase structure may be warranted, along with a complete analysis of its effects on scaffold functionality, to support its use in the manufacture of future bone repair devices.

In addition to pAsp and citrate incorporation into the mineralization process, the present study also used phosphorylation via STMP treatment, and Mg and carbonate additives. Unlike pAsp and citrate, these were used in the preparation of all mineralized scaffolds produced, and no attempt was made to assess their individual contributions to the mineralized structures produced. STMP has a long history

for phosphorylation of proteins in the food industry[235,236], and phosphorylation of collagen using STMP has previously been described in detail[108,219,220]. Under alkaline conditions, STMP is hydrolyzed to produce sodium tripolyphosphate, which is believed to phosphorylate serine, threonine, and tyrosine residues through covalent bonding with side chain oxygens[219]. That STMP is effective in aiding collagen mineralization, likely via the ability of phosphate groups to attract amorphous calcium phosphate precursors, is supported by prior studies of in vitro mineralization of dentin and dermal collagen[219,236]. Meanwhile, the presence of Mg^{2+} during mineralization has been shown to improve the stability of PILP and amorphous mineral phases[237,238], and allow wetting of protein matrices by PILP[239], while incorporation of carbonate during synthetic apatite formation has been shown to result in crystal structures with high similarity to those present in native bone[214,240–242].

To examine the atomic composition and crystallographic structure of the mineral phase within the prepared collagen sheets, EDX, XRD, and FTIR-ATR were employed. EDX analysis of the scaffolds indicated a Ca/P molar ratio of 1.46, close to known Ca/P molar ratios for various forms of calcium phosphates: 1.33 for octocalcium phosphate, 1.5 for amorphous calcium phosphate and calcium deficient hydroxyapatite, 1.67 for precipitated hydroxyapatite, 1.8 for Na and carbonate containing apatite and 2.0 for heavily carbonated hydroxyapatite[243]. For human bone, Ca/P molar ratios typically range from 1.19-2.28[244–246]. Contribution from the underlying phosphorylated collagen to the EDX peaks is unlikely due to the thickness of the mineral coating on samples.

As summarized by Driessens and Verbeeck[247], the atomic fraction by wt% of O, C, Ca,

P, Na, and Mg in bone are 43.5, 15.5, 22.5, 10.3, 0.1, and 0.2, respectively, similar to the mineral phase composition of the scaffolds that were produced in the current work (Fig. 3.5). XRD comparisons between the prepared sheets and bovine cortical bone indicated similar broad profiles with conserved hydroxyapatite-like peaks at around 26° (002) and 32° (211, 112, 300) indicating that both mineral phases consisted of poorly crystalline or amorphous hydroxyapatite. XRD profiles for the mineralized collagen sheets were somewhat duller and possessed broader peaks, perhaps indicating a more amorphous mineral composition compared to that of the 2 to 3-year-old bovine cortical bone (Fig. 3.6). Greater content of amorphous mineral would be representative of that found earlier in bone tissue development[17,89], which may benefit healing by providing starting materials more similar to those found naturally.

3.5 Conclusion

Using an alternate soaking procedure, it is possible to use decellularized sheets of natively structured collagen fibrils to produce a scaffold of mineralized collagen reasonably matching the chemical makeup and structural organization seen in native bone, as determined using EDX, XRD, ATR-FTIR, SEM, and TEM. During the mineralization process, use of pAsp was confirmed to be important for close integration between collagen fibrils and the introduced mineral phase, as was citrate for limiting the plate size of crystals. The process described here may be a useful alternative approach for the development of bone regeneration scaffolds.

3.6 Contributions

3.6.1 Author contributions

The original conception of the research goal described in this chapter was carried out by myself and Dr. Samuel Veres. Detailed experimental and procedural design were carried out by myself. More specifically, tendon acquisition, decellularization, cryosectioning, collagen mineralization, SEM, EDX, TEM, FTIR-ATR, and data analysis and presentation, including chapter writing and illustration, were completed myself with minor technical support (initial set-up) from Patricia Scallion for SEM and EDX and Dr. Ping Lee for TEM. Dr. Veres acted as a mentor for this chapter, providing feedback, editing, and formal analysis assistance where required, in addition to Dr. Kathy Singfield and Dr. Paul Gratzer. Detailed experimental design, set-up, and execution of the collagen mineralization process was carried out myself.

3.6.2 Contributions to the field

The work described in this chapter offers, to the best of my knowledge, the first description of alternate-soaking mineralization of tendon. Additionally, as most biomineralization studies focus upon the use of reconstituted collagen or mineralization during fibrillogenesis, this work highlights an ability to mineralize natively structured and crosslinked, highly aligned collagen fibrils, which better resembles biomineralization *in vivo*. Insight to the effect both pAsp and citrate have to final crystal morphology in biomineralization gained from this work is applicable to not only collagen mineralization, but also to the fabrication of many other mineral coated orthopaedic

implants.

Chapter 4

Alternate Soaking Enables Easy Control of Mineralized Collagen Scaffold Mechanics from Nano- to Macro-scale*

*The experiments presented in this chapter have been published in the Journal of the Mechanical Behavior of Biomedical Materials[197].

4.1 Introduction

The mechanical properties of biological scaffolds are critical to cellular interactions and hence functional response within the body[119]. For adherent cells, cytoskeletal

forces generated depend on substrate stiffness[117], with cell shape changing accordingly[118]. In turn, cell shape can be a defining factor for biochemical profile, including programmed death and differentiation pathway[117–119]. Material stiffness may even be more selective towards stem cell differentiation than soluble induction factors[117,124]. In the case of scaffolds developed for bone regeneration, mechanical property requirements must consider both the ability to provide an appropriate level of structural support, as well as the ability to optimally trigger cell differentiation and promote proliferation[117,118,124,248]. With differing requirements, an ability to control the mechanics of scaffold materials is crucially important to scaffold design.

Along with the mechanical properties of scaffolds influencing cellular responses, structural and chemical features also strongly influence how cells will interact with the material post implantation. Structurally, nanofibrous materials tend to better promote osteogenesis than their flat material counterparts[249], most likely due to their ability to better facilitate protein adsorption and cell attachment[250]. It is known that cells adhere to and proliferate better on fibrillar surfaces, particularly those containing Arginine, Glycine, Aspartate (RGD) adhesion sites, and may even alter their differentiation pathway dependent on surface roughness[251]. Additionally, increases in nanophase roughness and surface texture will likely result in greater surface wettability, which in turn results in greater protein adsorption and subsequent cell adhesion[252]. In a study by Dalby et al.[253], it was found that mesenchymal stem cells (MSCs) could be directed to an osteogenic phenotype by modification of surface topography alone in poly(methyl methacrylate) scaffolds.

Being the predominant organic component of bone, collagen is a highly desirable al-

ternative to other resorbable polymeric materials for creating the basic structure of scaffolds. Many of the collagen-based scaffolds produced to date have used aqueous collagen suspensions or slurries that are molded into desired shapes[99–102,209,210,213,214]. Rather than highly organized collagen fibril arrays, as found in bone, these methods produce randomly oriented collagen fibers that lack well-structured nanoscale fibrils. In order to tailor degradability and mechanical stability, these scaffolds are often exogenously crosslinked, which can result in the accumulation of toxic residues that promote proinflammatory responses post-implantation[215,254]. While physical crosslinking methods such as dehydrothermal treatment may be used to avoid such responses, heat treatments may cause molecular denaturation[255]. Thus, use of natively assembled and crosslinked collagen, such as the well-aligned tendon-derived collagen used in this work, is desirable.

Along with crosslinking, modification to collagen-based scaffold mechanics has been achieved through the introduction of a mineral phase[1,256]. An advantage of incorporating a mineral phase within collagen-based scaffolds is increased osteoconductive and osteoinductive potential due to a resulting microstructural organization and chemical profile resembling bone[257]. Collagen mineralization *in vitro* has traditionally been accomplished through immersion of collagen in a simulated body fluid (SBF)[77,80,92]. Other methods for mineralizing collagen include direct blending (mixing collagen and mineral nanoparticles together) and co-precipitation (mineral association during collagen fibrillogenesis)[80,96,99,100]. A somewhat more recent method of preparing mineralized-collagen materials has come largely from the work of Gower et al.[23,90] where an acidic polymer is added to the mineralization solution in an attempt to

mimic the role of various non-collagenous proteins during the intrafibrillar mineralization of collagen within bone *in vivo*. This method has been termed the polymer induced liquid precursor (PILP) process, indicating the role these acidic polymers have in stabilizing an amorphous liquid mineral precursor phase that is thought to enter the gap regions within individual collagen fibrils and promote intrafibrillar mineralization[12,77]. In addition to acidic polymers, other additives such as magnesium, carbonate, and citrate have been included in an attempt to create a mineral phase closely matching that in bone[258].

The ability to control scaffold mechanics in a predictable way over multiple scales would be useful in the creation of scaffolds, but to date such an ability has not been well demonstrated. Heinemann et al.[259], described an increase in compressive modulus when collagen was mineralized with hydroxyapatite (HA) through a sol-gel process. However, mechanical properties were only tested for 25 wt% HA incorporation, and therefore whether mechanically tailored scaffolds can be produced using this method is unclear. Cunniffee et al.[260] found an increase in scaffold modulus values following additional mineral incorporation to collagen-nanoHA scaffolds, however a clear predictable relationship between nanoHA wt% and Young's modulus was not evident.

From a chemical and structural standpoint, mineralized collagen fibrils offer significant advantages as a scaffold material for bone regeneration. Needed now is a means for tailoring the mechanical properties of these next generation scaffold materials. Here we describe a process for producing sheets of well-ordered, mineralized collagen fibrils that allows easy control of macroscale flexural modulus of the sheets and nanoscale

radial indentation modulus of the constituent collagen fibrils.

4.2 Materials & Methods

4.2.1 Collagen acquisition and initial processing

Forelimbs of steers aged 2-3 years, killed for food at a local abattoir, were used as the source for common digital extensor (CDE) tendons. Tendons post dissection were stored in a phosphate-buffered saline (PBS) solution at 4°C until decellularization treatment begun, which was started within 6 h of dissection.

Decellularization treatment followed a method previously described by Woods and Gratzer[261]. The CDE tendons were first exposed to a hypotonic 10 mM tris buffer, containing serine and metalloprotease inhibitors, along with 1% penicillin/streptomycin and 1% amphotericin B for 36 h at room temperature. Tendons were then moved to a high saline 50 mM tris buffer containing 1% Triton X-100 along with antibiotics and protease inhibitors for 48 h at room temperature, followed by Hanks' buffer rinse and wash in a DNase/RNase solution. This was followed by a 48 h, room temperature soak in 1% Triton X-100 solution with 50 mM TRIZMA base and antibiotics. Finally, the tendons were rinsed in PBS containing antibiotics and stored in a similar PBS solution at 4°C until further use.

Decellularized tendons were cryosectioned using a Leica SM2000R sliding microtome. Tendons were cut into 2-3 cm long segments, mounted on a steel block using optimal cutting temperature compound (Fisher Healthcare, Ottawa, ON), frozen in liquid nitrogen, and sectioned longitudinally to produce 200-μm-thick sheets of collagen for

AFM, SEM, and TEM work and 300-μm-thick sheets for macroscale flexural testing. As previously done[258], the collagen sheets were then phosphorylated via treatment with sodium trimetaphosphate (STMP) in order to enhance mineralization[108,219]. A solution of 2.5 wt% STMP was hydrolyzed at pH 12 for 5 h[220]. The solution was then adjusted to pH 10. STMP treatment of collagen sheets occurred for 1 h at room temperature under constant agitation. The sheets were then rinsed in distilled deionized water (ddH_2O) prior to the start of the alternate soaking mineralization procedure.

4.2.2 Alternate soaking mineralization

Mineralization of the phosphorylated collagen sheets was performed following the method of Grue & Veres[258]. Using a stainless steel mesh basket, sheets were first soaked in 200 mL ddH_2O before soaking in 200 mL of a magnesium (0.01 M) and citrate (0.02 M) doped calcium solution ($CaCl_2/MgCl_2$, 0.2 M) within a temperature-controlled water bath at 37°C for 120 s at pH 7.4. The sheets were then briefly rinsed in ddH_2O before soaking for an additional 120 s in a 0.12 M sodium phosphate solution containing 0.025 M sodium carbonate at 37°C at pH 7.4. Both the calcium and phosphate solutions contained 100 μg/mL pAsp (mean MW 29 kDa, Alamanda Polymers, AL, USA). This concentration and MW of pAsp was chosen based upon their successful use in achieving intrafibrillar mineralization of collagen fibrils by others[115,262–264]. Previous evidence suggests that higher MW pAsp promotes collagen mineralization to a greater extent than lower MW pAsp[263,264]. Additionally, MWs greater than the one used here are not typically used in PILP systems, possibly due

to the risk of their precipitation out of solution[23]. The progression of collagen sheets through these four solutions constituted a single mineralizing cycle.

4.2.3 Sample groups

Four sample groups of scaffolds were created by varying the number of mineralization cycles that the collagen sheets underwent, with scaffolds produced using 0, 5, 10, or 20 mineralization cycles.

4.2.4 Scaffold surface architecture under SEM

Surface architecture of scaffolds from the four sample groups (0, 5, 10, or 20 mineralization cycles) was assessed using a Hitachi S-4700 scanning electron microscope (SEM). For each of the four samples groups, three scaffolds were examined using SEM. Scaffolds were prepared for analysis by fixation in 2.5% electron microscopy-grade glutaraldehyde in PBS for 1 h at room temperature under constant agitation, followed by rinsing in ddH_2O and dehydration in graded ethanol. Sheets were then critical point dried, mounted on SEM stubs using carbon tape, and coated with gold-palladium. The coated samples were viewed under SEM at 5 kV, 10 μA.

4.2.5 Collagen fibril ultrastructure under TEM

Ultrastructure of individual collagen fibrils from the scaffolds of each sample group were assessed using a FEI Tecnai 12 TEM. Scaffolds were pulverized in liquid nitrogen and dispersed in ethanol. Collagen fibrils were then collected on copper TEM grids and examined unstained at 120 kV.

4.2.6 Nanomechanics of scaffold fibrils using AFM

Nanomechanics of individual collagen fibrils extracted from the prepared scaffolds were assessed using AFM. 12 fibrils from each of the 0, 5, 10, and 20 mineralization cycle groups were tested, with the 12 fibrils in each group extracted from scaffolds prepared in four separate processing batches. To extract fibrils, scaffolds were pulverized in liquid nitrogen, dispersed in 95% ethanol, allowed to adsorb onto the bottom of glass dishes, and then dried under nitrogen gas.

All AFM experiments were performed with a Bioscope Catalyst atomic force microscope (Bruker, USA) mounted on an IX71 inverted microscope (Olympus, Tokyo, Japan). AFM cantilevers (BudgetSensors, Bulgaria) were made of silicon with a nominal spring constant of 7.2 N/m. Each cantilever was calibrated using the thermal noise method yielding an average spring constant of 8.04 $\pm$ 1.33 N/m (n = 6). The radius of the tip was determined by imaging a titanium surface in PeakForce Quantitative Nanomechanical Mapping (QNM) mode at a peak force set point of 40 nN, an oscillation frequency of 1 kHz, a peak-force amplitude of 200 nm, and a raster scan frequency of 0.5 Hz. The image used for the tip reconstruction had 512x512 pixels and a size of 1.5x1.5 μm (Tip Check routine in NanoScope Analysis, v1.40, Bruker, USA). The average tip radius was 10.06 $\pm$ 1.80 nm at an indentation depth of 10 nm and 17.57 $\pm$ 3.35 nm at a depth of 20 nm. Relative humidity ranged from 15-26% during testing with an average ambient temperature of 21°C.

Each fibril to be assessed was first imaged. A 256x256 pixel image covering 2x2 μm was taken using a peak force set point of 60 nN, oscillation frequency of 1 kHz, a peak-force amplitude of 200 nm, and raster scan frequency of 1 Hz. Using this image,

10 points were randomly chosen along the longitudinal axis of the collagen fibril for nanomechanical assessment via point-and-shoot indentation. At each point, force-distance curves were acquired using a ramp speed of 100 nm/s and ramp size of 500 nm, with max force set to 300 nN. The radial modulus at each point was calculated using SPIP software (Image Metrology, Lyngby, Denmark) with sphere indentation, using the Derjaguin-Muller-Toporov (DMT) model of fitting including adhesion, along with a baseline and hysteresis correction, as previously used for studying collagen fibrils via PeakForce QNM[265,266]. The DMT model, which is based on the Hertz model, uses the unloading region of the force-separation curve and accounts for adhesive interactions between collagen fiber and AFM probe[265,267]. Calculation of a fibril's radial modulus using the DMT model is described by the following equation:

$$F = \left(\frac{4}{3}\frac{E}{(1-\nu^2)}\sqrt{R(d-d_0)^3}\right) + F_{ADH}$$

Where F is the force acting on the AFM tip from the sample, E is the radial modulus, ν is Poisson's ratio (0.5), R is tip radius, d – d_0 is the deformation of the sample, and F_{ADH} is the adhesive force between the AFM probe and the surface during contact. Bueckle's rule of only fitting indentations up to 10% of the fibril height in order to avoid any influence of underlying stiff substrates was adhered to for all modulus measurements[268].

4.2.7 Fibril and mineral volume quantification

Using the previously described 2x2 μm AFM images, fibril volumes were calculated using Gwyddion software (Version 2.51, Czech Metrology Institute, Czech Republic). Briefly, height images of control (0 cycle) and mineralized (5, 10, and 20 cycle) collagen fibrils were first levelled, followed by a line by line background subtraction using linear fit. Height profiles were then taken across the width of each fibril over a length of 1 μm, which were then averaged and integrated giving fibril volume per unit length. To estimate the amount of extrafibrillar mineral attached to the mineralized fibrils, median volume of the unmineralized control fibrils was subtracted from the corresponding value for the mineralized fibrils in each treatment group.

4.2.8 Macroscale scaffold mechanics under flexural testing

Flexural testing was conducted on 12 scaffolds from each of the 5, 10, and 20 mineralization cycle groups (the 0 cycle group lacked sufficient rigidity to be tested), with the 12 scaffolds in each group prepared in four separate processing batches. Following mineralization, scaffolds destined for flexural testing were placed into the bottom of 6-well plates and dried under a weighted PLA mesh to ensure that scaffolds remained flat prior to mechanical testing. The flexural mechanics of rehydrated scaffolds were assessed following the ASTM D790 standard[269]. Testing was done in room temperature PBS using a custom-built electro-mechanical system with series A1 Servo Cylinder (Ultra Motion, NY), GS0-1K load cell (Transducer Techniques, CA), and cylindrical loading nose and sample supports with 5-mm-radius. More information on the three-point bending system can be found in Appendix B. Scaffold samples for

testing were prepared from 300-μm-thick collagen sheets, cut to 7.0 mm width and 18.0 to 22.0 mm length. Testing was done using a support span length of 15.0 to 18.0 mm, fixed strain rate of 0.1 mm/mm/min, and maximum strain of 0.05 mm/mm. After rehydration for 5 minutes, each sample underwent 8 repeated flexion cycles, with average material properties calculated for the final 3 cycles.

Deflection data, measured at the sample midpoint using actuator displacement, and force data were converted to strain and stress following the D790 standard. Strain was calculated as:

$$\epsilon = 6Dd/L^2$$

Where D is deflection, d is the sample thickness, and L is support span. Stress was calculated as:

$$\sigma = \left(\frac{3PL}{2bd^2}\right)\left[1 + 6\left(\frac{D}{L}\right)^2 - 4\left(\frac{d}{L}\right)\left(\frac{D}{L}\right)\right]$$

Were P is load and b is the width of the scaffold tested. Modulus of elasticity was calculated as the tangent modulus of the steepest portion of each stress-strain curve.

4.2.9 Presentation and statistics

Numerical data are presented as mean ± SD. Box plot whiskers show maximum/minimum values. Differences between quantitative measurements for the scaffold groups were tested using one-way ANOVA with post hoc Tukey-Kramer HSD test, with results of $p \leq 0.05$ considered statistically significant.

4.3 Results

4.3.1 Scaffold ultrastructure

SEM was used to assess the surface architecture of the prepared collagen scaffolds. Unmineralized (0 cycle) sheets showed that the native, highly aligned arrangement of collagen fibrils characteristic of tendons was conserved after processing treatments, i.e. decellularization, sectioning, and phosphorylation (Fig. 4.1A,B). After 5 mineralization cycles, whole scaffold surface architecture was variable, with collagen fibrils completely occluded by mineral in some regions and absent of mineral in others (Fig. 4.1C,D). After 10 cycles, few instances of exposed fibrils existed. In numerous locations, the trajectory of individual fibrils could be seen, though the fibril surface was completely covered with mineral (Fig. 4.1E,F). After 20 cycles, collagen fibrils were completely hidden from the scaffold surface (Fig. 4.1G,H).

TEM images taken of isolated fibrils from unmineralized and mineralized sheets showed a greater abundance of mineral present as the number of mineralization cycles increased (Fig. 4.2A-H). The mineral phase was observed as multiple plate-like structures which tended to be aligned with the longitudinal axis of the collagen fibrils. As

the number of mineralization cycles increased, a greater abundance of extrafibrillar mineral spherulites adjoined to fibrils were seen. (Fig. 4.2A-H).

Topography of individual fibrils extracted from scaffolds were quantified by AFM (Fig. 4.3). For fibrils from the 0 cycle (unmineralized) group, fibril height was 130 ± 27 nm for collagen fibrils from the 0 cycle (unmineralized) scaffolds (Fig. 4.4A), consistent with previous assessments of collagen fibrils from similar tissue sources[270,271]. While fibril heights from the different scaffold groups were statistically similar, median fibril height and mineralization cycles completed nearly reached a significant linear relationship (Fig. 4.4B). Being less sensitive than height to the uniformity of mineral growth, the relationship between fibril volume and progressive mineralization treatment was stronger, with statistically significant increases in collagen fibril volume seen with increasing number of mineralization cycles completed (Fig. 4.5A). When the median volume of the unmineralized fibrils was subtracted from those for the mineralized groups to provide a measurement of mineral volume only, a significant linear relationship with increasing mineralization cycles was observed (Fig. 4.5B).

4.3.2 Change in nano-scale mechanics with progressive mineralization cycles

The nanomechanics of individual collagen fibrils extracted from scaffolds prepared with differing numbers of mineralization cycles (0, 5, 10, and 20) were assessed using AFM. Radial modulus for fibrils from unmineralized (0 cycle) scaffolds was 215 ± 125 MPa and increased significantly following 5, 10, and 20 mineralization cycles to 334 ± 177 MPa, 596 ± 387 MPa, and 778 ± 302 MPa, respectively (Fig. 4.6A). Plotting

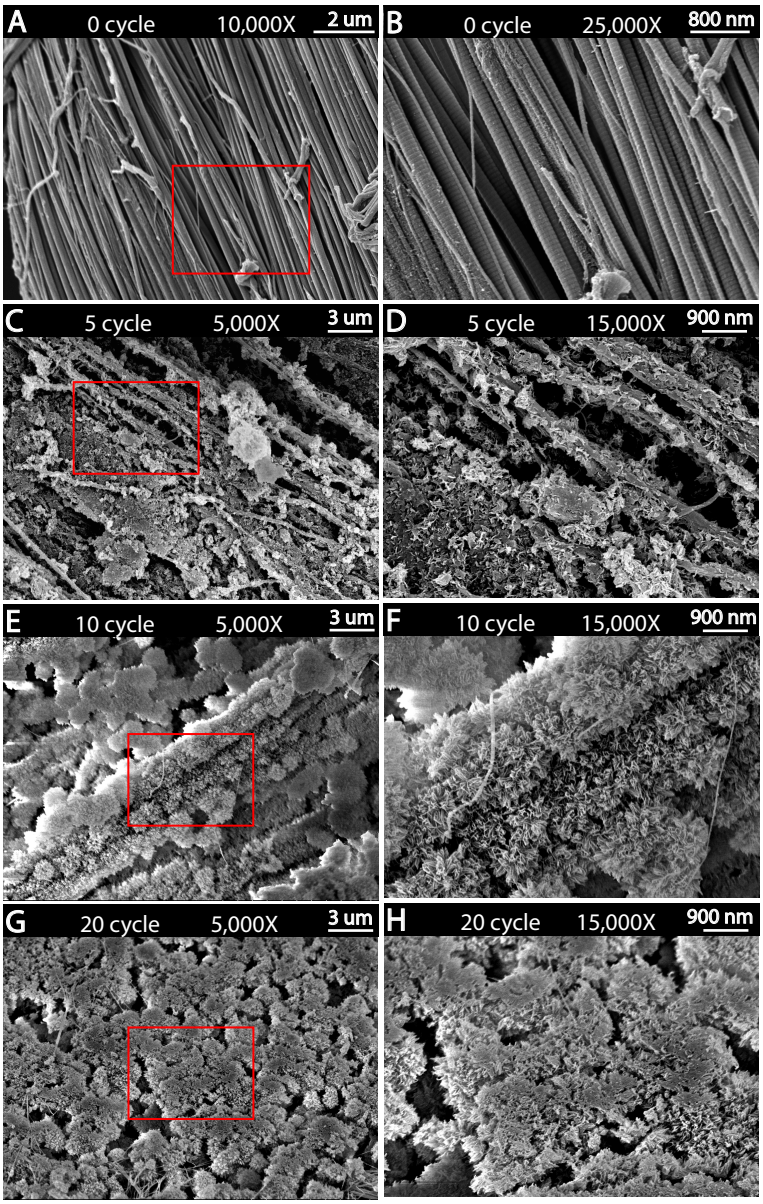

Figure 4.1: A, B: A 0 cycle (unmineralized) collagen sheet showing the highly aligned native collagen fibril arrangement characteristic of tendon. C, D: Scaffolds that underwent 5 mineralization cycles showed heterogenous regions of mineral association with collagen fibrils. E, F: 10 cycle mineralized collagen scaffold. While fibrils are completely occluded with mineral the longitudinal trajectory of fibrils is still visible. G, H: 20 cycle mineralized collagen scaffold where mineral has completely obscured the underlying collagen fibrils. Images on the right show magnified views of the boxed regions in images on the left.

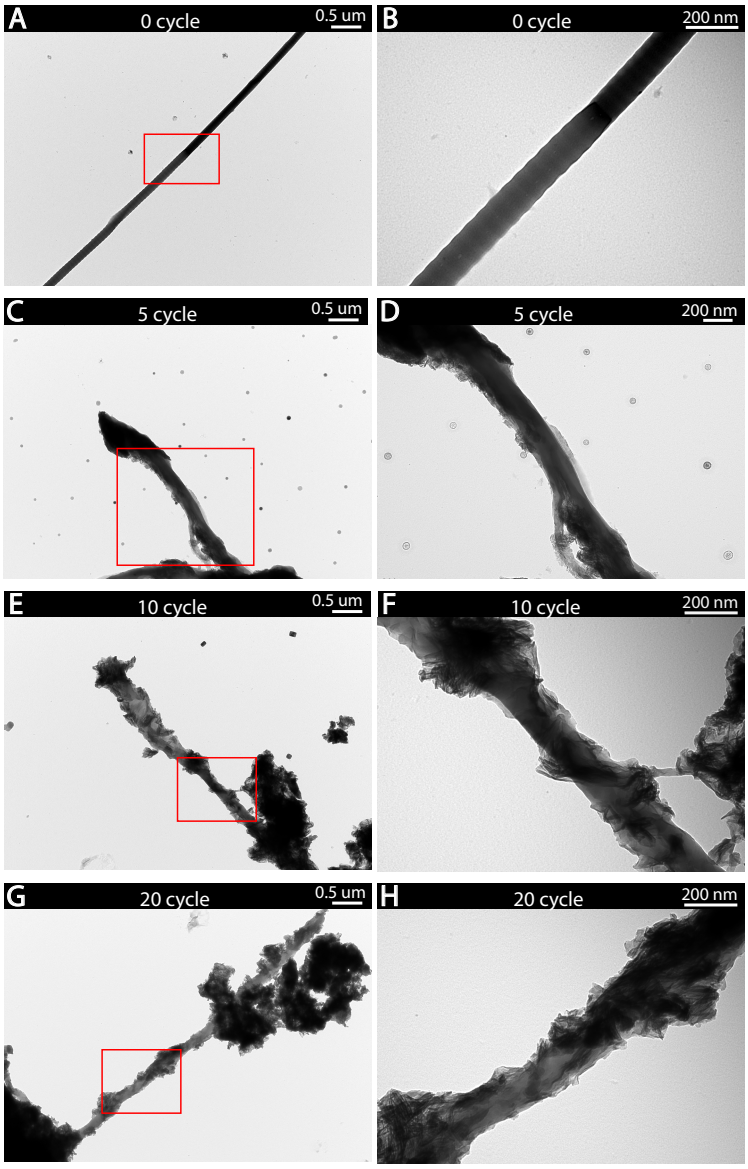

Figure 4.2: A, B: A collagen fibril extracted from a 0 cycle (unmineralized) scaffold showing native collagen fibril structure. C, D: Collagen fibrils extracted from scaffolds that underwent 5 mineralization cycles showed heterogenous mineral association. E, F: Collagen fibrils from 10 cycle scaffolds showed increased mineralization. G, H: For scaffolds that had undergone 20 mineralization cycles, extracted collagen fibrils showed an abundance of plate-like crystals closely associated with the fibrils, as well as an increase in extrafibrillar spherulites. Images on the right show magnified views of the boxed regions in images on the left.

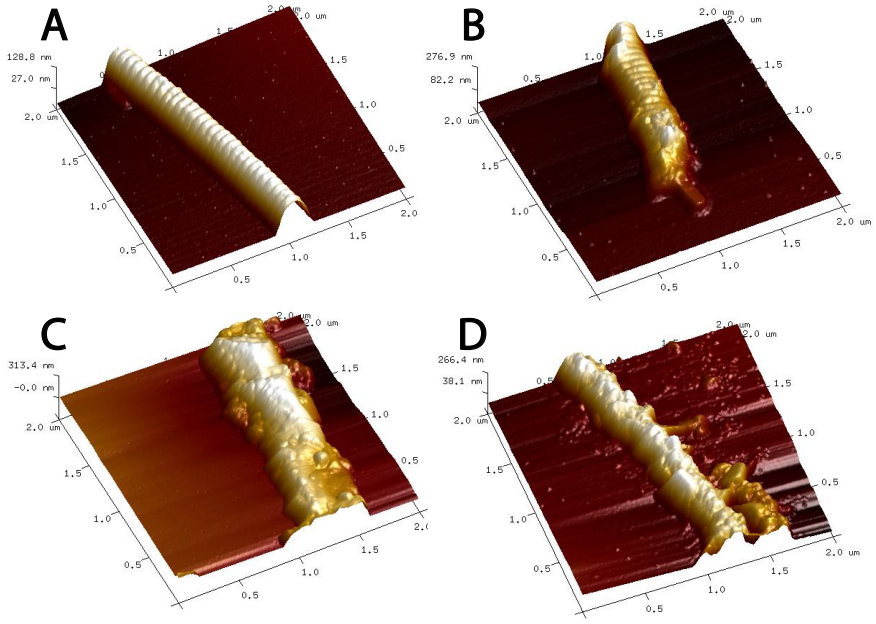

Figure 4.3: Representative 3D height images of collagen fibrils extracted from the prepared scaffolds. A: Collagen fibril from a 0 cycle (unmineralized) scaffold showing native collagen structure. B: After 5 mineralization cycles, many fibrils had regions of exposed collagen and mineralized collagen. C: Following 10 cycles, fibrils were completely covered in mineral, with none of the fibrils D-band showing. D: Fibrils from scaffolds that had undergone 20 mineralization cycles appeared similar to those from the 10 cycle scaffolds.

median fibril radial modulus vs. number of mineralization cycles showed a highly significant linear relationship with $p = 0.0004$ and $R^2 = 0.9993$ (Fig. 4.6B). Plotting median fibril radial modulus vs. fibril mineral content similarly showed a significant linear relationship, with $p = 0.0128$ and $R^2 = 0.9746$ (Fig. 4.7).

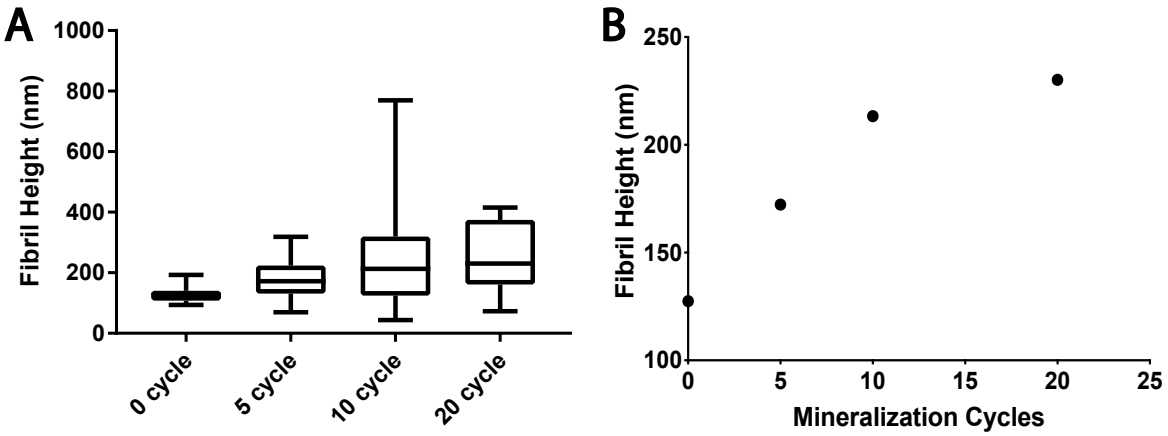

Figure 4.4: A: While the volume and radial modulus of fibrils both increased significantly with mineralization cycles completed (Figs. 4.5, 4.6), fibril height did not. B: Median fibril height measurements vs. mineralization cycle. A linear fit to the data was not significant with $p = 0.0684$.

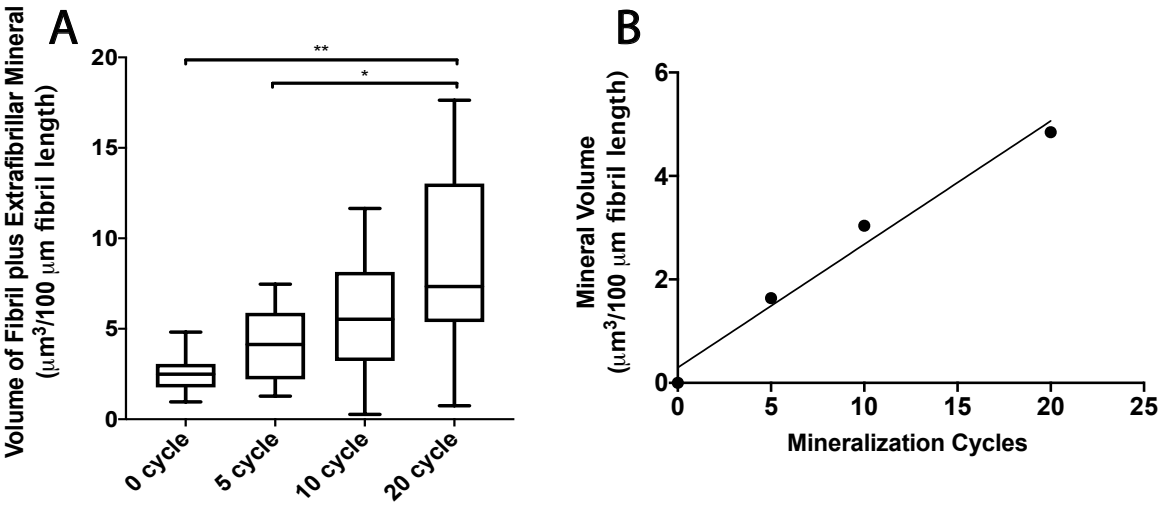

Figure 4.5: A: Volume measurements for single collagen fibrils taken from scaffolds following progressive mineralization. For mineralized groups (5, 10, 20 cycle), volume measurements include fibril plus attached extrafibrillar mineral. Whiskers represent min/max values. *$p \leq 0.05$, **$p \leq 0.01$. B: Linear regression of median mineral volume vs. mineralization cycle. $p = 0.0113$, $R^2 = 0.9775$.

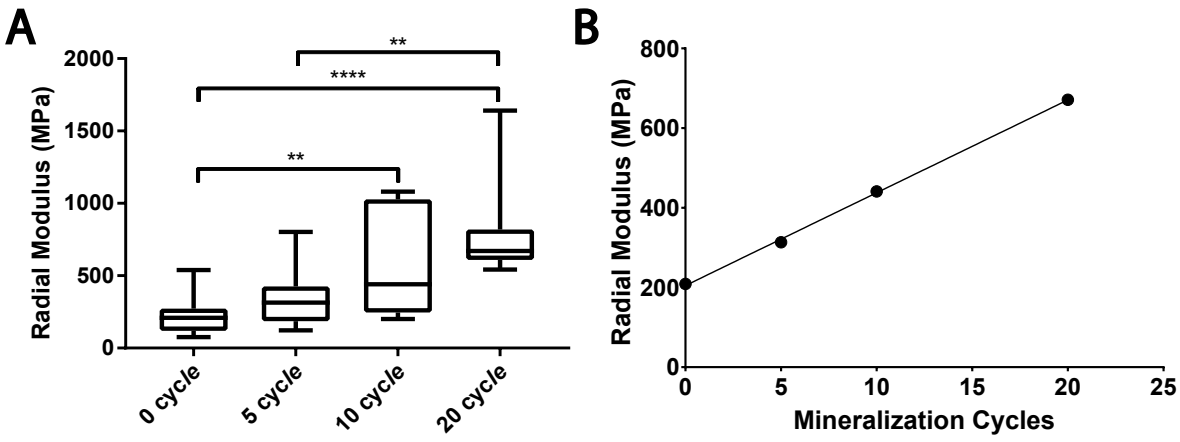

Figure 4.6: A: As measured by AFM, radial modulus of single collagen fibrils extracted from the prepared scaffolds increased significantly with increasing number of mineralization cycles. Whiskers indicate min/max values. $^{**}p \leq 0.01$, $^{****}p \leq 0.0001$. B: Linear regression of median fibril radial modulus vs. mineralization cycles. $p = 0.0004$, $R^2 = 0.9993$.

4.3.3 Change in macro-scale mechanics with progressive mineralization cycles

The macroscale mechanics of scaffolds produced using 5, 10, and 20 mineralization cycles were assessed using flexural testing. Scaffolds prepared without mineralization (0 cycles) lacked the required rigidity for testing. Representative stress-strain curves can be found in (Fig. B.17) as well as hysteresis data in (Fig. B.18) in Appendix B. Flexural stiffness increased significantly with increasing mineralization, from 18 ± 7 MPa for the 5 cycle group, to 156 ± 50 MPa for the 20 cycle group (Fig. 4.8A). Again, plotting median modulus vs. mineralization cycles completed showed a significant linear relationship with $p = 0.0227$ and $R^2 = 0.9987$ (Fig. 4.8B).

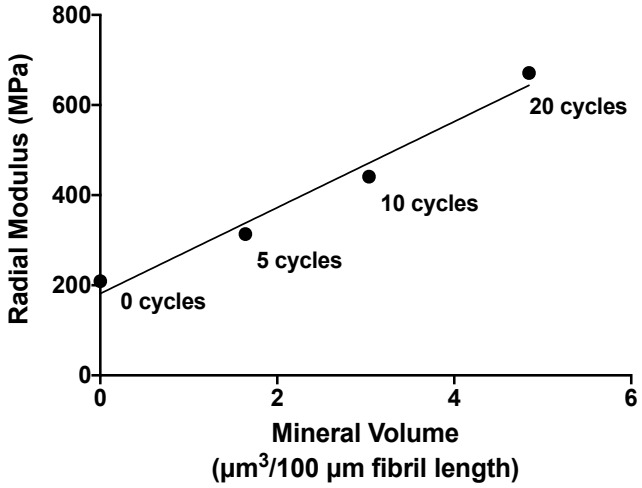

Figure 4.7: For single collagen fibrils extracted from scaffolds progressively mineralized via alternate soaking (0, 5, 10, or 20 mineralization cycles), a significant linear relationship was observed between median fibril radial modulus and fibril mineral content. $p = 0.0128$, $R^2 = 0.9746$.

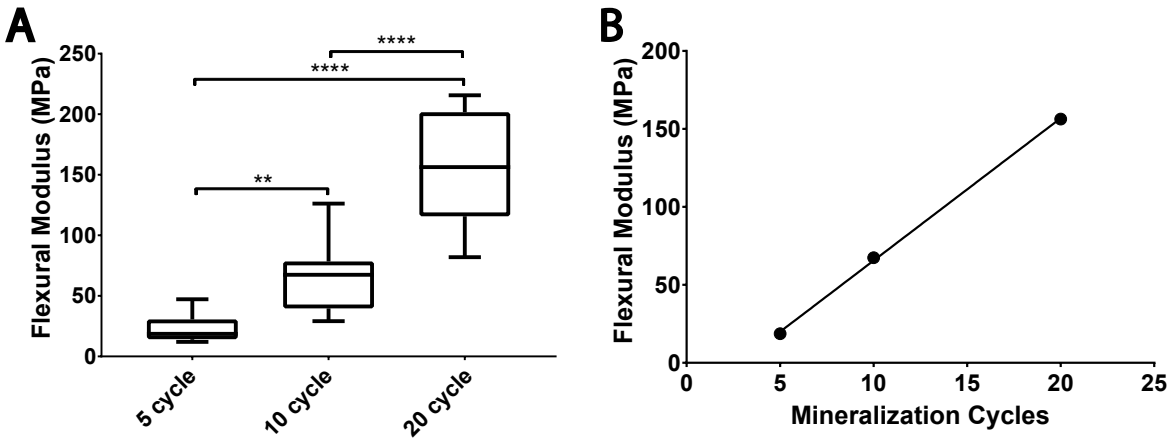

Figure 4.8: A: Box plot showing the relationship between the number of mineralization cycles and the flexural modulus of mineralized scaffolds. Whiskers represent min/max values. $^{**}p \leq 0.01$, $^{****}p \leq 0.0001$. B: Linear regression of median fibril flexural modulus measurements vs. mineralization cycle. $p = 0.0227$, $R^2 = 0.9987$.

4.4 Discussion

There has been a shift in bone scaffold technology towards providing bioactivity in addition to stability. It has been shown extensively in previous research that scaffolds composed of materials similar to those of native bone provide cues for the surrounding bone forming cells to begin repairing the associated bone defect[157,272–279]. The ability to draw pre-osteoblastic cells towards the repair site and promote their differentiation as well as provide an adequate housing environment is termed osteoinduction and osteoconduction, respectively. The focus of the current research was to construct a biologically inspired biphasic scaffold composed of natively structured collagen and inorganic mineral using a production process that would allow easy control over the resulting mechanical properties. Our process for treating tendon-derived collagen sheets using an alternating soaking technique achieves this, with both nanoscale and macroscale scaffold mechanics increasing in a linear fashion with mineralization cycles completed.

Cells interact with scaffolds post-implantation in a multitude of ways, one of which is through cytoskeletal interactions with the substrate—a parameter that is influenced by scaffold mechanics. Cytoskeletal interactions in turn affect migration, morphology, and differentiation of cells[117]. This was highlighted by Khatiwala et al.[280] in an experiment where MC3T3-E1 pre-osteoblastic cells were cultured on collagen-modified hydrogels with varying mechanical properties. The migration, proliferation, and differentiation of the cells were assessed in relation to scaffold mechanics. Cell migration and proliferation were found to increase following an increase to ECM stiffness[280]. Osteoblastic differentiation was also found to favour stiffer scaffolds (tensile modu-

lus of 39 kPa vs. 22 kPa)[280]. Engler et al.[124] found that stiffer materials (25-40 kPa) promoted the lineage specification of stem cells towards an osteogenic phenotype compared to softer collagen-coated gels that promoted neurogenic (∼0.1-1 kPa) and myogenic (∼8-17 kPa) differentiation. This highlights the importance of designing scaffolds that mimic the stiffness of the tissue type to be repaired. Ideally, bone scaffold mechanics should match those of the developing bone tissue. Prior measurements of a repairing rat fracture callus by nanoindentation have shown moduli of 0.6-1.3 MPa for granulation tissue, 1.4-4.4 MPa for chondroid tissue, and 27-1010 MPa for woven bone[281]. The radial moduli measured for mineralized collagen fibrils in the current study fall within the range for woven bone at the fracture callus site (Fig. 4.6). With an ability to easily control the stiffness of scaffolds through altering the number of mineralization cycles, substrate stiffness-based influence on cell differentiation can be taken advantage of. This may allow for the production of scaffolds that select for osteogenesis over the formation of other tissue types.

Along with responding to external loads, the mechanical environment within a scaffold and its effect on cellular response is an important design parameter[282,283]. Bruels et al.[117] distinguishes these effects as "active" vs. "passive" mechanical stimulation. Active mechanical stimulation arises from external forces that act on the implanted scaffold during physiological movement, whereas passive stimuli describe the response cells have to material stiffness post implantation[117]. In referencing various modes of stimulation that promote the differentiation of stem cells to the osteoblastic lineage, it is understood that soluble factors, cell-ECM interactions (stemming largely from nanostructural characteristics of the scaffold, such as porosity and roughness), as well

as mechanical stimulation all play key roles[117,124,284–287]. With a means of controlling passive stimulus in a material with innate chemical and structural advantages, our process for controlling mineralized collagen scaffold mechanics offers the potential to harness the intrinsic mechanotransduction pathways of stem cells.

Our ability to easily control the stiffness of the scaffolds was confirmed at both the nano- and macro-levels (Fig. 4.6, 4.8). This is likely a direct reflection of the degree to which alternate soaking allows control of the volume of mineral deposited on individual collagen fibrils (Fig. 4.5). Previous studies have shown that the mechanics of collagen scaffolds are altered on mineral incorperation but have not shown a process for doing this in a controlled way. For example, Heinemann et al.[259] constructed collagen scaffolds mineralized with silica and/or hydroxyapatite (HA) powder through a sol-gel process. Mineralization with HA (25 wt%) increased compressive modulus values by a factor of roughly 3. Cunniffee et al.[260] produced collagen-nanoHA scaffolds through both suspension and immersion methods. No significant improvement in compressive modulus was found when nanoHA was added during suspension methods at 100 wt% (relative to collagen weight used). An 18-fold increase, however, was found when 500 wt% nanoHA was used[260]. Kane et al.[288] prepared HA containing freeze-dried collagen scaffolds with varying degrees of HA incorporation. It was found that the compressive modulus significantly increased following increases to the collagen:HA weight ratio, with values ranging from roughly 20 kPa for 1:1 collagen:HA scaffolds to 200 kPa for 1:4 collagen:HA scaffolds[288]. Liu et al.[289] described the preparation of mineralized collagen using poly(acrylic acid) and sodium tripolyphosphate as sequestration and templating analogs, respectively. AFM-based nanoindentation measurements of their

mineralized collagen fibrils gave radial moduli of 13.7 ± 2.6 GPa; significantly greater than for non-mineralized collagen at 2.2 ± 1.7 GPa[289].

Relatively few studies have examined the nanomechanical properties of natively mineralized collagen fibrils. Balooch et al.[290] used AFM-based nanoindentation to determine the mechanical properties of mineralized collagen fibrils in human molar during demineralization. Modulus values reduced from 1.5 GPa to 50 MPa as collagen fibrils were gradually demineralized[290]. These values correspond reasonably well with those obtained in the current experiment: 778 ± 302 MPa for fibrils from scaffolds that underwent 20 mineralization cycles down to 215 ± 125 MPa for the fibrils from the unmineralized scaffolds(Fig. 4.6). Using AFM to perform tensile experiments, Hang and Barber[291] described the nanomechanical properties of individual mineralized collagen fibrils from antler. It was found that these mineralized fibrils exhibited tensile moduli of roughly 2.4 GPa[291]. Tai et al.[30] used AFM-based nanoindentation to determine the elastic modulus of bone during demineralization. It was found that mineralized collagen samples possessed modulus values 2-6x that of demineralized bone sections ranging from about 7-12 GPa vs. 1.9 GPa[30].

In terms of the micro- or macromechanical properties of bone, 3-point micro-bending tests by Choi et al.[292] of subchondral, trabecular, and cortical bone samples gave flexural modulus values of 1.2 GPa, 4.6 GPa, and 5.4 GPa, respectively[292]. Ascenzi et al.[293] investigated the mechanics of single osteons through bending tests and found flexural moduli of roughly 2-3 GPa. Lettry et al.[294] used 3-point bending to determine the Young's modulus of bone obtained from the human mandible, which ranged from 4.7 – 16 GPa. Using a similar 3-point testing set-up, Lee et al.[295] found the bending

modulus of human skull bone to be roughly 1 – 4 GPa. Rahmoun et al.[296] found the elastic modulus of human cranial bone through 3-point testing to range from about 2 – 6 GPa, with highest values found in the left temporal region and the lowest found in the coronal suture region. From these values, the flexural moduli of our 20-cycle mineralized collagen sheets appear to be about an order of magnitude below that of mature bone (Fig. 4.8). How much this could be further increased with additional mineralization cycles remains to be seen, as does whether matching the modulus of mature bone, or a lower modulus for developing bone is of greatest benefit to healing.

4.5 Conclusion

We have developed a process for easily producing sheets of mineralized collagen fibrils with tailorable mechanics. The mechanics of individual collagen fibrils from the sheets are comparable to natively mineralized collagen fibrils, while the flexural modulus of whole sheets is about an order of magnitude below that of native, mature bone. With chemical and structural characteristics of mineralized collagen fibrils having innate osteoinductive qualities, and now with a means of additionally controlling their mechanics, the sheets we describe may be of use in creating larger, multilaminate constructs with physiologically relevant mechanical profiles.

4.6 Contributions

4.6.1 Author contributions

The original conception and experimental design of the research described in this chapter was carried out by myself and Dr. Samuel Veres. More specifically, tendon acquisition, decellularization, cryosectioning, collagen mineralization, SEM, TEM, and data analysis and presentation, including chapter writing and illustration, were completed myself. Nanomechanical evaluation of collagen fibrils through AFM was carried out by myself after initial equipment training and assistance in selecting appropriate testing conditions by Dr. Laurent Kreplak. Collagen fibril and mineral volume quantification was carried out myself with minor technical assistance from Dr. Laurent Kreplak. All procedural work, including data analysis and figure presentation, for the flexural testing of whole mineralized collagen sheets was carried out myself after initial equipment set-up and software design by Research Assistant Luke Vincent.

4.6.2 Contributions to the field

This work describes, to the best of my knowledge, the first evidence for the ability to control the mechanics of *in vitro* mineralized collagen. Control over mechanical properties of mineralized collagen was demonstrated to be possible at both the nano- and macro-scale. Tailoring of scaffold mechanics over multiple scales is an important design parameter, as bone mechanics is highly variable depending on the location within the body, stage in healing, and individual. Additionally, this control of scaffold mechanics is crucial for optimizing the cellular response to the implant. The

nanomechanical evaluation of mineralized collagen fibrils is an area of little dedicated research, thus, this work allows for an expansion of the current knowledge base in the area. This work also highlights important design parameters that others may utilize to perform similar mechanical testing on related biomaterials.

Chapter 5

Effect of Increasing Mineralization on Pre-osteoblast Response to Native Collagen Fibril Scaffolds for Bone Tissue Repair and Regeneration

5.1 Introduction

Serving as the current gold standard bone repair material, autografts offer many advantages over alternative materials, including inherent biocompatibility and osteogenic potential[1,297]. Availability of autograft tissue remains a strong limitation for

its use however, along with donor site morbidities and extended time under anesthesia for tissue harvesting. While allografts are available in larger quantities, supply remains limited and concerns regarding disease transmission exist[1,205]. Alternative materials, including various synthetic and natural biopolymers, are under widespread investigation to fulfill the increasing clinical demand for bone scaffolds and to avoid limitations associated with graft use[298]. With the potential to use these scaffolds for a wide variety of defect treatments that require different levels of load-bearing ability, methods for creating mechanically tailored scaffolds are required, and an understanding how such changes impact cellular response developed.

Bone grafts for internal fixation may be indicated for use in some fractures to bridge bone ends and provide stability to the fracture site in an attempt to facilitate repair and regeneration. The specific healing processes that occur following surgical intervention are directed in part by the origin of bone graft material selected and bone type, i.e. cortical or cancellous[299,300]. Remodelling of autologous bone grafts proceeds similarly to normal physiological bone remodeling due to the presence of preserved mesenchymal stem cells (MSC) and osteogenic proteins[301–303]. This process begins by apposition of bone, including initial osteoclast resorption followed by graft vascularization and fibroblast ingrowth[299,300]. Osteoblasts fill resorption pits created by the osteoclasts with osteoid, which eventually becomes mineralized and subsequently remodelled[299,304]. Complete resorption and replacement of the autograft with new bone typically occurs within 6-12 months but may take years if the graft is derived from dense cortical bone[88,300]. A subset of autograft tissue includes bone marrow aspirate (BMA). BMA contains many similar osteogenic factors as bone autografts

and is often used along with other graft materials as an extender[302].

Grafts foreign to the recipient host include xeno- and allografts, including demineralized bone matrix, which is available in fresh, frozen, or freeze-dried forms[302]. Due to the foreign nature of these grafts and depending on processing techniques, the initial stages of remodelling may involve undesirable immune responses[88]. As a result, integration of allografts or xenografts may be delayed in comparison to autografts[305]. For example, Zhang et al.[306] compared the use of autograft to allograft for instrumented atlantoaxial fusions in 32 pediatric patients. Although similar fusion rates were observed with both grafting materials, fusion time was 3 months longer when allografts were used[306]. Interestingly, the overall incidence of surgery-related complications was significantly higher for the autograft group, including a seroma formation and pelvic fracture associated with the donor site[306]. In a comparative study by Shibuya et al.[307] of 61 foot and ankle surgery patients, xenograft incorporation into human bone was found to be slower than incorporation of autografts and allografts. For xenografts, while supply is significantly less constrained compared to allografts, processing methods, including decellularization and sterilization techniques vary greatly, which may result in variable clinical outcomes[299,308].

Materials being explored as graft substitutes include various synthetic and natural polymers, bioactive glasses, minerals, ceramics, and many composite preparations thereof[302]. Cellular responses to these graft substitutes vary depending on their chemical composition, structure, and mechanics[309]. While some graft alternatives have been shown to allow progressive healing similar to that occurring with graft use, healing typically progresses more slowly due to a general lack of osteoinduc-

tive potential[88]. To accelerate repair and remodelling, various biological factors have been incorporated into graft substitutes. These include bone morphogenetic proteins (BMP), fibroblast growth factors (FGF), vascular endothelial growth factors (VEGF), platelet-rich plasma (PRP), and many bioinorganic ions such as zinc, magnesium, cobalt, and strontium[88,310]. Biologic incorporation within graft substitutes may improve the rate of bone formation and remodelling, however their use comes with increased cost and possible post-operative complications, including heterotopic bone growth and oncogenic concerns[88,302,310,311].

Aside from collagen, the extracellular matrix (ECM) of bone contains various proteins involved in important osteogenic processes; more than 200 of which have been reported to date[1]. Some of the major non-collagenous proteins (NCP) found within bone include, osteonectin, osteocalcin (OCN), fibronectin, osteopontin, and bone sialoprotein[1,312]. Of these, OCN in particular has been widely used as a late stage biomarker for osteogenic differentiation[1]. OCN is thought to bind bone mineral with its N-terminal domain, contributing towards the rate of mineral crystal growth or maturation, while aiding in the regulation of bone matrix production via its C-terminal domain[313,314]. Another widely used marker for osteogenic differentiation is alkaline phosphatase (ALP), otherwise known as tissue non-specific alkaline phosphatase (TNAP)[315]. ALP is expressed early on in the development of bone and decreases as development progresses[315]. ALP is thought to play a role in promoting collagen mineralization through its hydrolysis of pyrophosphate (PPi), a mineralization inhibitor[316]. Additionally, NCPs and various ions and small molecules, such as magnesium and citrate, are thought to alter crystallization kinetics and promote the intrafibrillar

mineralization of collagen during bone formation and repair[191]. To mimic the role of these NCPs, polyanionic macromolecules of varying molecular weights (MW) are frequently used during mineralization, including poly(acrylic acid) and poly(aspartic acid) (pAsp)[191,298].

Our laboratory recently developed a process for producing mineralized collagen scaffolds that feature highly aligned and natively crosslinked collagen fibrils combined with a mineral phase closely matching that of native bone[258]. We subsequently demonstrated that the mineral content of these scaffolds can be easily controlled during production, allowing tuning of the scaffolds resulting mechanical properties, both in terms of macroscale flexural modulus and nanoscale collagen fibril stiffness[197]. In the present study, we make use of our developed scaffold production process to investigate how variations in the mineral content of aligned, natively crosslinked collagen scaffolds affect the osteogenic activity of cells. Our results provide new insights into how variations in scaffold mineralization may alter the functional response of osteoblasts.

5.2 Materials & Methods

An overview of the experimental design is shown in Figure 1.

5.2.1 Collagen acquisition and initial processing

Common digital extensor (CDE) tendons were dissected from the forelimbs of steers aged 2-3 years, which were killed for food at a local abattoir. Tendons were stored immediately in phosphate-buffered saline (PBS) solution at 4° C to await decellular-

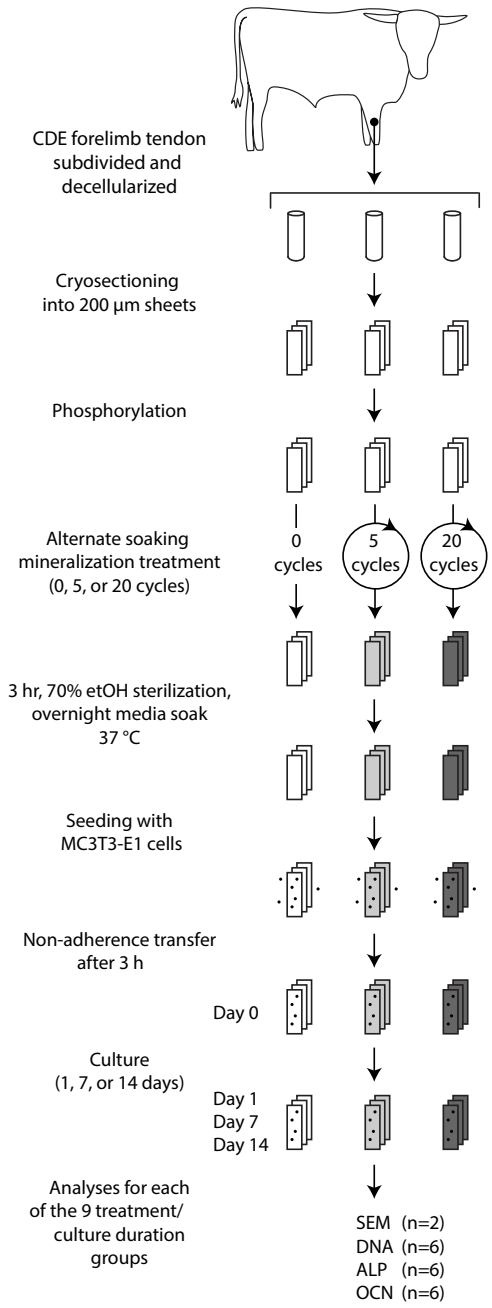

Figure 5.1: Overview of the experimental design. Collagen sheets underwent three different treatments (0, 5, or 20 mineralization cycles) with samples from each treatment cultured for three durations (1, 7, or 14 days) yielding 9 sample groups for analysis.

ization treatment, which was started within 8 h.

Decellularization was conducted following a method previously described by Woods and Gratzer[261]. Briefly, tendons were first exposed to a hypotonic 10 mM tris buffer, containing serine and metalloprotease inhibitors, along with 1% penicillin/streptomycin and 1% amphotericin B for 36 h at room temperature. Tendons were then moved to a high saline 50 mM tris buffer containing 1% Triton X-100 along with antibiotics and protease inhibitors for 48 h at room temperature, followed by Hanks' buffer rinse and wash in a DNase/RNase solution. This was followed by a 48 h, room temperature soak in 1% Triton X-100 solution with 50 mM TRIZMA base and antibiotics. Finally, the tendon samples were rinsed in PBS with antibiotics and stored in a similar solution at 4° C until further use.

Decellularized tendons were cut into 2-cm-long segments, mounted on a steel block using optimal cutting temperature compound (Fisher Healthcare, Ottawa, ON), frozen in liquid nitrogen, and cryosectioned longitudinally using a Leica SM2000R sliding microtome to produce 200-μm-thick collagen sheets. As previously done[258], the collagen sheets were then phosphorylated via treatment with STMP in order to enhance mineralization[108,219]. A solution of 2.5 wt% STMP was hydrolyzed at pH 12 for 5 h[220]. The solution was then adjusted to pH 10. Collagen sheets were treated in STMP solution for 1 h at room temperature under constant agitation. The sheets were then rinsed in ddH_2O before beginning the alternate soaking mineralization procedure.

5.2.2 Alternate soaking mineralization

Mineralization of the phosphorylated collagen sheets was performed following the method of Grue & Veres[258]. Using a stainless steel mesh basket, sheets were first soaked in 200 mL ddH_2O before soaking in 200 mL of a magnesium (0.01 M) and citrate (0.02 M) doped calcium solution ($CaCl_2$/$MgCl_2$, 0.2 M) within a temperature-controlled water bath at 37° C for 120 s at pH 7.4. The sheets were then briefly rinsed in ddH_2O before soaking for an additional 120 s in a 0.12 M sodium phosphate solution containing 0.025 M sodium carbonate at 37° C, pH 7.4. Both the calcium and phosphate solutions contained 100 μg/mL pAsp (mean MW 29 kDa, Alamanda Polymers, AL, USA). The progression of collagen sheets through these four solutions constituted a single mineralization cycle. Scaffolds were prepared with either 5 or 20 mineralization cycles, or without mineralization (0 cycle control). Prior to cell culture, scaffolds were sterilized in 70% etOH for 3 h followed by rinsing in complete media overnight at 37° C and 5% CO_2.

5.2.3 Cell culture

MC3T3-E1 osteoblast precursor cells derived from mouse calvaria (Sigma-Aldrich, MO, USA) were cultured in α-minimum essential medium, supplemented with 10% heat inactivated fetal bovine serum, 50 mg/mL ascorbic acid (AA), and 5% antibiotic/antimycotic mixture. The cells were maintained at 37° C and 5% CO_2 with media changes every 2 days. Cells used for scaffold seeding were obtained from passage 6. The MC3T3-E1 cells were seeded on scaffolds with a density of 150,000 cells/well for morphological evaluations and 50,000 cells/well for subsequent cell proliferation, ALP

activity, and OCN content measurements. Cells were allowed to adhere to scaffolds for 3 hours prior to conducting a non-adherence transfer to fresh 24-well ultra-low adhesion cell culture plates.

5.2.4 Visualization of cell morphology on scaffolds

Two scaffolds from each treatment group (0, 5, and 20 mineralization cycles) were examined under SEM following 1, 7, and 14 days of culture. Scaffolds were removed from the culture plates and transferred to fresh 24-well plates and fixed in 2.5% electron microscopy-grade glutaraldehyde in PBS for 1 h at room temperature under constant agitation, followed by rinsing in ddH_2O and dehydration in graded ethanol. Scaffolds were then critical point dried, mounted on SEM stubs using carbon tape, coated with gold-palladium, and examined at 5 kV, 10 μA using a Hitachi S-4700 SEM.

5.2.5 Sample groups for biochemical analyses

Biochemical analyses for dsDNA content, ALP activity, and OCN content were undertaken. For each of the three culture durations (1, 7, and 14 days), the tests were performed on n=6 scaffolds from each treatment group (0, 5, and 20 mineralization cycles). In addition to these 54 scaffolds, an additional 6 scaffolds per treatment group were prepared and cultured for 14 days without the addition of AA. As a no-cell control, analyses were also performed on a single scaffold for each of the 9 treatment/culture duration combinations that was prepared and maintained under the same conditions, but in the absence of cells. For each scaffold, biochemical mea-

surements were made in duplicate and then averaged.

5.2.6 Cell proliferation

DNA, measured via Quant-IT^{TM} PicoGreen® dsDNA assay kit (Invitrogen-Thermo Fisher Scientific, Berlin, Germany) was used as a proxy for the number of cells present on scaffolds[317,318]. At days 1, 7, and 14, scaffolds were transferred to a new 24-well plate, washed with sterile PBS, and incubated in TrypLE Express reagent (Invitrogen-Thermo Fisher Scientific, Berlin, Germany) for 30 minutes. Cell-TrypLE suspension was drawn off and centrifuged at 3000 rpm for 15 minutes followed by resuspension of cells in sterile PBS. The cells were then lysed through three freeze-thaw cycles followed by further centrifugation at 3000 rpm for 15 minutes to remove cellular debris. From the supernatant, 50 μL samples were used for dsDNA measurement.

Cellular dsDNA measurement was performed according to the kit manufacturer's instructions. Briefly, lambda DNA standards were prepared by 8-point serial dilution of a 2 μg/mL lambda working solution, which was in turn prepared through a 50-fold dilution of a 100 μg/mL stock solution in 1X TE buffer (10mM Tris-HCl, 1mM EDTA, pH7.5) supplied by the kit manufacturer. 50 μL of 1X TE buffer was added to each well of a 96-well plate followed by 50 μL of sample or standard. 100 μL of the Quant-iT PicoGreen reagent working solution was then added to each well and allowed to incubate for 2-5 minutes protected from light. Fluorescent measurements were then made using a Varioskan LUX multimode plate reader (ThermoFisher Scientific, MA, USA) with an excitation wavelength of 480 nm and emission wavelength of 520 nm. dsDNA content was calculated via standard curve according to kit manufacturer's

instructions.

5.2.7 ALP activity

To evaluate early osteogenic differentiation of the MC3T3-E1 cells, ALP activity was assessed using an alkaline phosphatase, diethanolamine detection kit (Sigma-Aldrich, MO, USA).

Cells lysates were used from the previously described proliferation assay. ALP measurements were performed according to manufacturer's instructions. Briefly, 5 μL of each test sample, including a ddH_2O blank, a 0.15 U/mL alkaline phosphatase enzyme control, and a similar enzyme control that underwent the previously described 3X freeze-thaw cycles for comparison, were added to the wells of a 96-well plate in duplicate. A premixed solution containing 245 μL reaction buffer and 5 μL of 0.67 M ρ-nitrophenol phosphate (pNPP) was subsequently added to each well. Absorbance values at 405 nm were read for 5 minutes at 37° C, from which each sample's linear rate of absorption was calculated and converted into ALP activity following the kit manufacturer's instructions. A maximum of 15 wells were read at once to ensure similar incubation time for all samples. For each scaffold assessed, ALP activity was normalized to the dsDNA content obtained from the PicoGreen assay for that same scaffold.

5.2.8 OCN content

OCN content was measured from the cell lysate using a mouse osteocalcin ELISA kit (MyBioSource, CA, USA). Briefly, 100 μL of standard or sample was added to

each well of a coated 96-well plate in duplicate in addition to 100 μL sterile PBS in duplicate to serve as a blank control. 10 μL of balance solution was added to each sample followed by 50 μL of conjugate (excluding the blank controls). Plates were incubated at 37° C for 1 hour. Plates were then washed 5 times with 1X wash solution followed by the addition of 50 μL substrate A and 50 μL of substrate B to each well including blank control. Plates were further incubated at 37° C for 15-20 minutes before the addition of 50 μL stop solution. The optical density of the wells was then read at 450 nm. OCN content for each scaffold was calculated via standard curve according to the kit manufacturer's instructions and normalized to the matching dsDNA content obtained from the PicoGreen assay for that same scaffold.

5.2.9 Statistics

Numerical data are presented as mean ± SD. DNA, ALP, and OCN results were analyzed using full-factorial two-way ANOVA, performed on rank transformed data to improve normality. This was followed by nonparametric Kruskal-Wallis tests and then Wilcoxon tests between individual pairs. Differences with $p \leq 0.05$ were considered statistically significant.

5.3 Results

5.3.1 Cell morphology and scaffold ultrastructure

The response of MC3T3-E1 pre-osteoblast cells to culture on aligned collagen fibril scaffolds following 0, 5, or 20 alternate soaking mineralization cycles was assessed using

SEM (Fig. 5.2). Cells on the unmineralized scaffolds exhibited mostly unidirectional cytoplasmic extension well-aligned with the direction of collagen fibrils after one day of culture (Fig. 5.2A). By day 7, the elongated cells had started to spread laterally (Fig. 5.2B). By 14 days, the cells had become confluent (Fig. 5.2C).

Cells on the 5 cycle mineralized scaffolds exhibited similar unidirectional cytoplasmic extension after one day of culturing, however the direction of elongation was more random due to the partial coverage of underlying collagen fibrils by mineral (Fig. 5.2D). After 7 days of culture, cells appeared more elongated and fusiform compared to cells on the unmineralized scaffolds (Fig. 5.2E vs. B). By 14 days, the cells had spread laterally taking on a polygonal morphology (Fig. 5.2F) appearing similar to those on the unmineralized scaffolds after 7 days of culture (Fig. 5.2B).

Cells grown on the 20 cycle mineralized scaffolds exhibited similar elongation patterns as cells grown on the 5 cycle scaffolds after one day of culture but with cellular extensions more commonly observed (Figs. 5.2G, 5.3A,D). By day 7, cells began to spread laterally, similar to what was observed on the 5 cycle mineralized scaffolds, with a small number of cells taking on a polygonal morphology (Figs. 5.2H, 5.3E). At 14 days, cell appearance had not changed appreciably compared to at 7 days (Figs. 5.2I, 5.3). Cells grown on the mineralized scaffolds exhibited close association with the underlying mineral phase at all timepoints, with cells gradually becoming more embedded and integrated with the mineral as culture time increased (Fig. 5.3).

Observed at all timepoints, cells on both the control and mineralized scaffolds possessed microvilli on their surfaces along with evidence of ECM production after 7 days (Fig. 5.4), indicating increased activity during the culturing period[319].

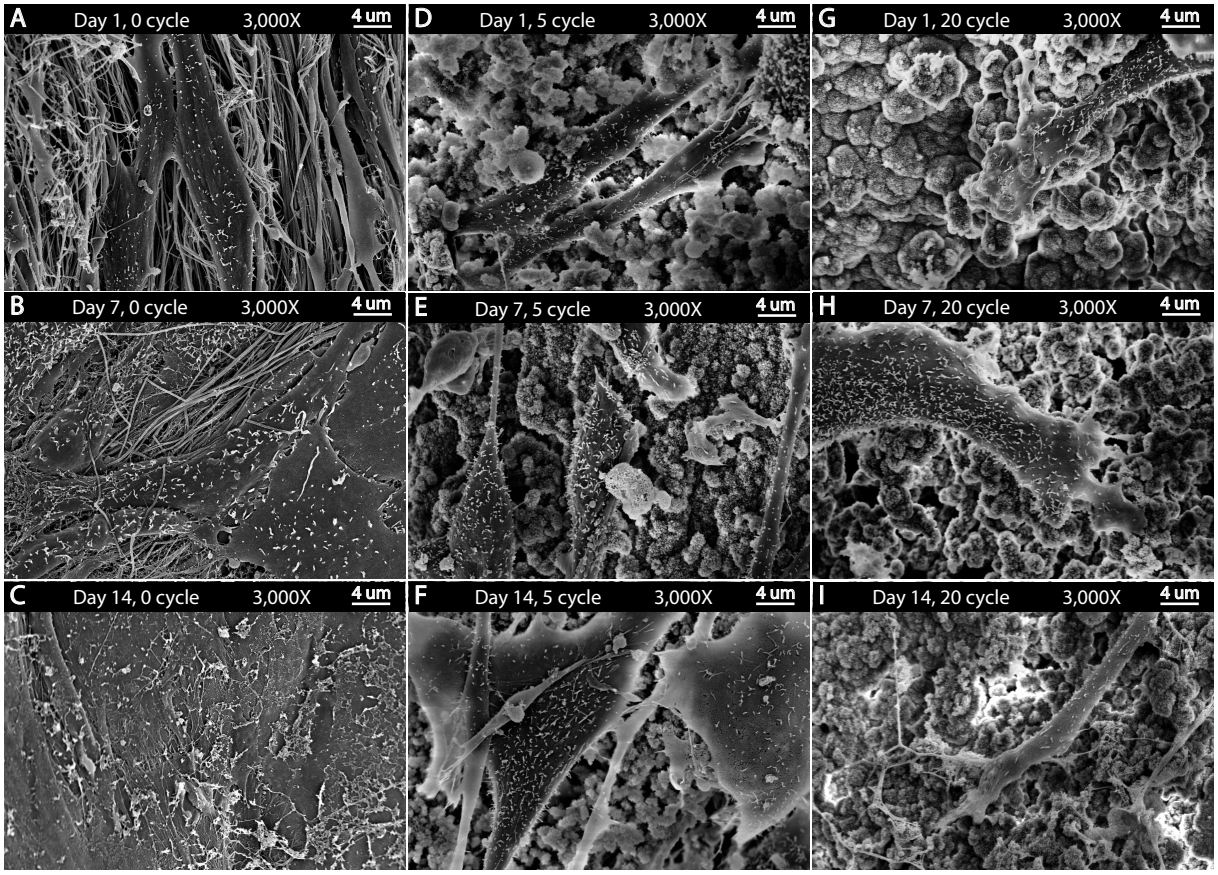

Figure 5.2: SEM images of MC3T3-E1 cells cultured on collagen scaffolds of varying mineral content, achieved via 0, 5, or 20 cycles of alternate soaking mineralization. A-C: On mineralized collagen scaffolds, cells had elongated by day 1, had begun to spread at day 7, and had reached confluence at day 14. D-F: On scaffolds treated with 5 mineralization cycles, cells elongated and spread, but spreading did not occur to the same extent as in controls. G-I: On scaffolds treated with 20 mineralization cycles, cells showed little spreading after 14 days.

5.3.2 Cell proliferation

On unmineralized scaffolds, DNA content did not change over 14 days of culture (Fig. 5.5A). With SEM observations having shown monolayer coverage of the unmineralized scaffolds by 14 days (Fig. 5.2C), the DNA and SEM results together suggest

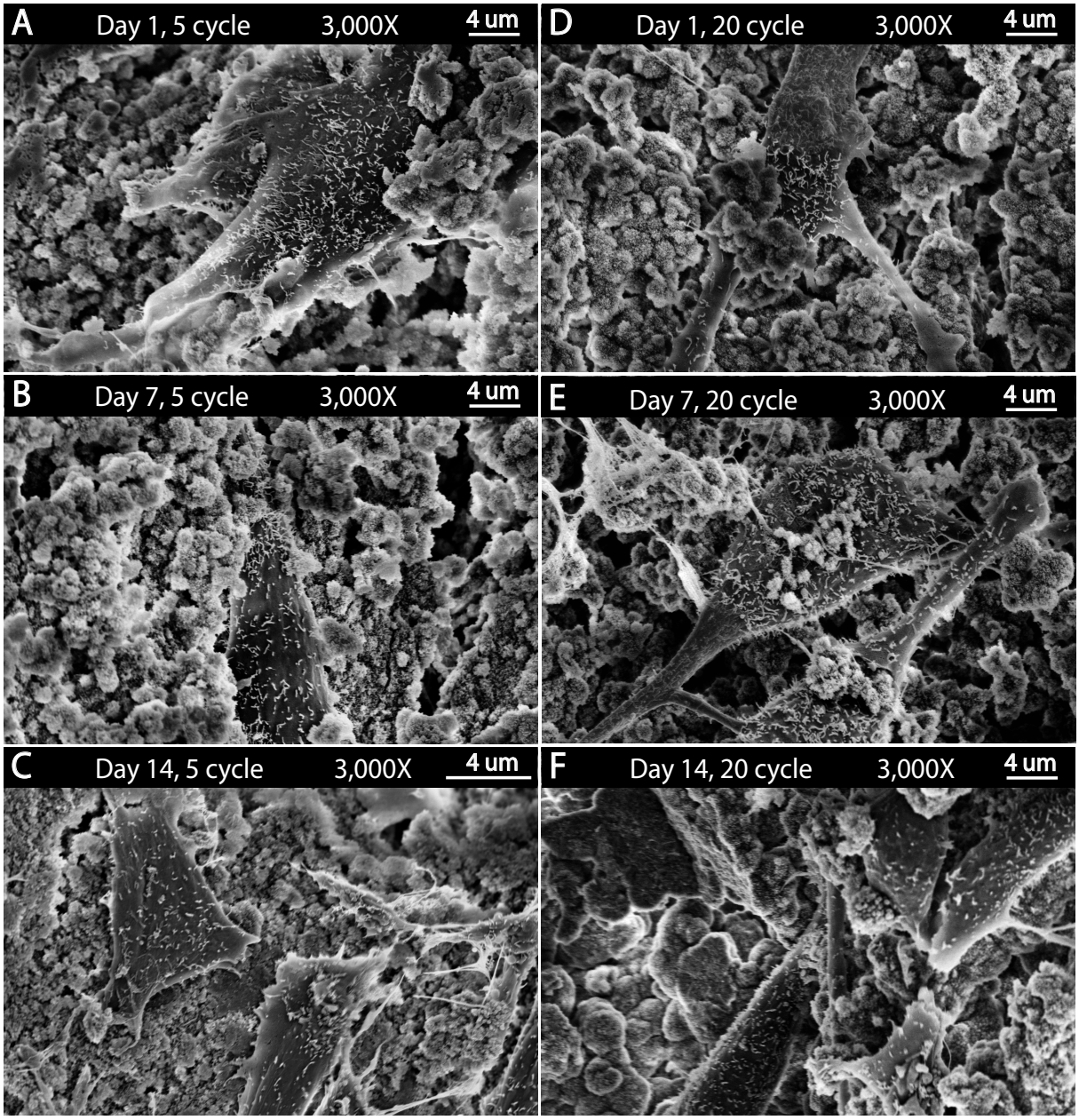

Figure 5.3: SEM images of MC3T3-E1 cells cultured on mineralized collagen scaffolds. A: 5 cycle mineralized collagen scaffold showing close association between cells and mineral after one day of culture. B: 5 cycle mineralized scaffold after 7 days of culture showing cells partially covered by mineral. C: 5 cycle mineralized scaffold after 14 days of culture. D: 20 cycle mineralized collagen scaffold showing similar cell-mineral interactions following one day of culture. E: 20 cycle mineralized scaffold after 7 day of culture. F: After 14 days of culture, some cells on scaffolds from the 20 mineralization cycle group were almost entirely covered by mineral.

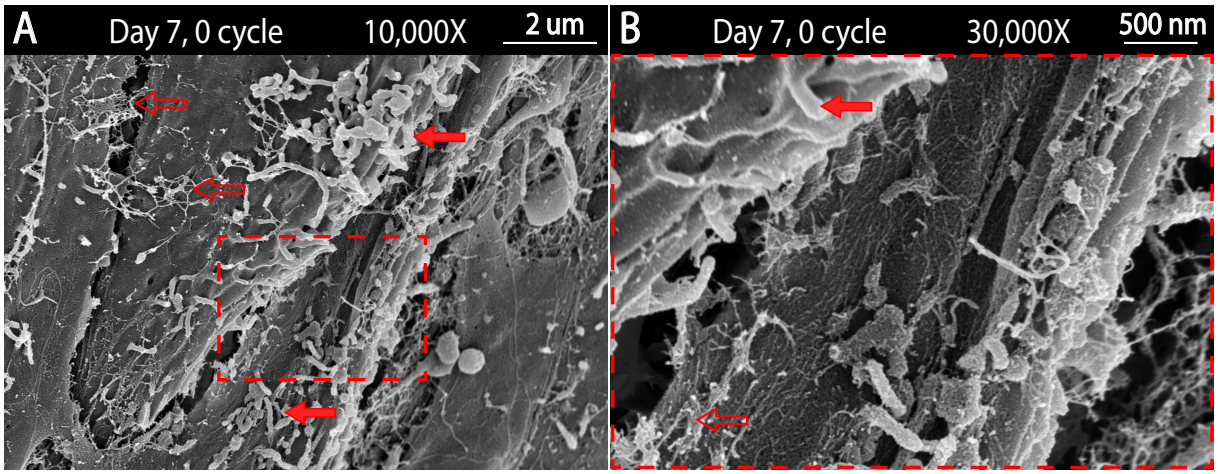

Figure 5.4: SEM images of MC3T3-E1 cells cultured on an unmineralized collagen scaffold for 7 days. A: Cells showing surface microvilli (solid red arrows) and evidence of ECM deposition (hollow red arrows). B: Magnified region of A. Both features, microvilli and ECM deposition, were also seen for the mineralized scaffolds.

that surface coverage was largely achieved via cell spreading over the 14 day culture duration.

On mineralized scaffolds, DNA content dropped significantly within the first 7 days of culture, and then remained unchanged to 14 days (Fig. 5.5A). This was consistent with SEM observations, showing a sparsity of cells after 7 days of culture on the 5 and 20 cycle mineralized scaffolds compared to the unmineralized scaffolds (Fig. 5.2E, H vs. B).

5.3.3 Cell differentiation

The potential for differentiation of the MC3T3-E1 pre-osteoblast cells on both unmineralized and mineralized collagen scaffolds was assessed by measuring ALP activity

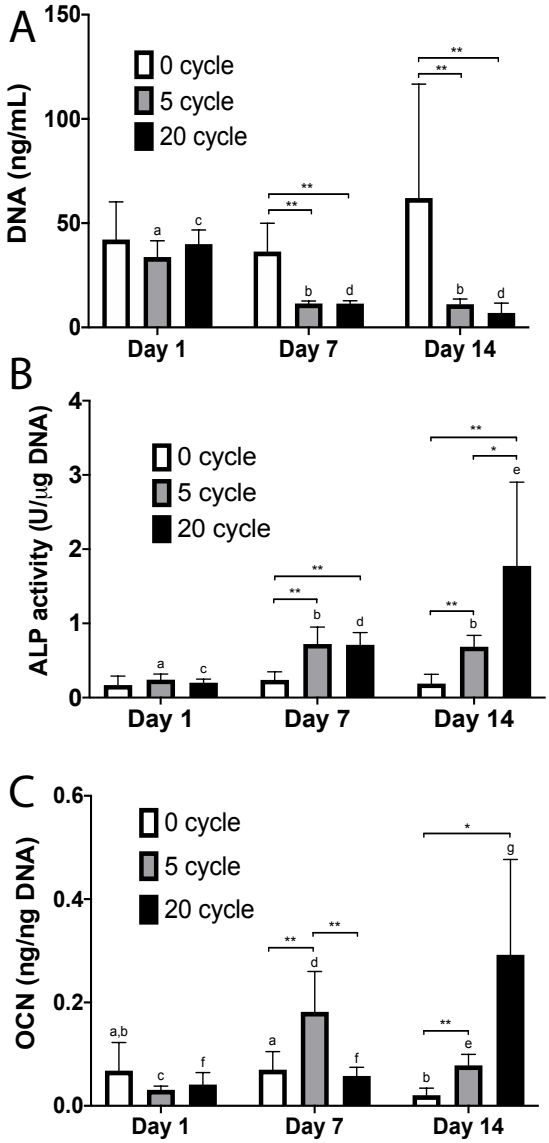

Figure 5.5: A. DNA measurements indicated that cell numbers remained consistent on unmineralized (0 cycle) scaffolds, while initially decreasing and then remaining constant for mineralized scaffolds (5 and 20 cycle). B. ALP activity normalized to DNA concentration showed increases for the mineralized scaffolds only, with a greater increase after 14 days of culture for the 20 cycle group compared to the 5 cycle group. C. OCN content normalized to DNA concentration similarly showed increases only for the cells cultured on mineralized scaffolds. After 14 days of culture, levels of OCN for the 20 cycle group nearly reached significance over the 5 cycle group with p=0.0552. Bars represent differences between treatment groups for a given culture time while letters represent differences between culture times for a given treatment group. *$p \leq 0.05$,**$p \leq 0.01$

.

and OCN production.

ALP enzyme activity is an early biomarker of osteoblast differentiation[320,321]. On unmineralized scaffolds, ALP activity did not change over the 14 days of culture (Fig. 5.5B). On mineralized scaffolds, ALP activity increased significantly for both the 5 and 20 cycle groups within the first 7 days of culture (Fig. 5.5B). While ALP activity did not change between 7 and 14 days of culture for the 5 cycle group, a significant increase was observed for the 20 cycle group (Fig. 5.5B).

To ensure that the freeze-thaw cycling used to lyse cells didn't negatively impact the ability to measure ALP activity, a test was done comparing the kit-provided enzyme control to the same enzyme control after undergoing 3X freeze-thaw cycles. No difference was found between ALP activity of the fresh enzyme controls vs. those that experienced freeze-thaw cycling (p=0.9889; n=9).

OCN production is thought to occur during the later stages of osteoblast differentiation[321]. On unmineralized scaffolds, OCN content did not increase during the 14 days of culture (Fig. 5.5C). OCN content increased significantly for the 5 cycle group within 7 days of culture followed by a decrease when measured at day 14 (Fig. 5.5C). For the 20 cycle group, OCN content was unchanged after 7 days of culture, but increased significantly after 14 days of culture, nearly reaching significance over the 5 cycle group (Fig. 5.5C).

5.4 Discussion

5.4.1 Visualization of cell morphology on scaffolds

Cell morphology is closely tied to a wide variety of cellular processes, including cell growth, cytoskeletal organization, cell differentiation, and gene expression[120]. For example, MSCs possessing a flattened and well-spread morphology are more likely to differentiate into osteoblasts and contribute to osteogenesis compared to cells more rounded in appearance, which are thought to become adipocytes[121–123]. This has been shown by Somaiah et al.[123] where MSCs were cultured on either uncoated tissue culture treated plastic or type I collagen coated tissue culture plates. Cells grown on the uncoated plastic were found to exhibit high levels of adipogenic differentiation, while the collagen coated surfaces enhanced cell proliferation and spreading, and promoted osteogenic differentiation[123].

In the current study, cells cultured on unmineralized collagen fibril scaffolds exhibited a flattened morphology and gradual cell spreading over time, with neighbouring cells coming into contact and forming a confluent monolayer within 14 days (Fig. 5.2A-C). Cells grown on the mineralized scaffolds showed a more elongated morphology along with overall lesser cell density (Fig. 5.2D-I). Cells cultured on the 5 cycle scaffolds appeared more polygonal-like after 14 days of culture compared to cells on the 20 cycle scaffolds (Figs. 5.2F, I, 5.3). Cells also appeared more elongated and spindle-like on the 20 cycle scaffolds as compared to the 5 cycle and unmineralized groups (Fig. 5.2). This resultant cell morphology may indicate less of an osteoblastic phenotype or may be a result of the highly mineralized surface of these scaffolds which may have required

the cells to spread from mineral peak-to-peak, bridging topographical gaps or pores, resulting in a 'stretched out' morphology. Cells were also observed within pores of the 20 cycle scaffolds with some extending under mineral clusters (Fig. 5.3D-F).

These morphological results, including cell flattening and spreading, are similar to those found by Cheng et al.[120] who cultured MC3T3-E1 cells on poly-dopamine functionalized graphene oxide substrates. Following 7 days of culturing, cells appeared flattened and well-spread, a trend similarly found in our study for cells grown on 0 and 5 cycle scaffolds and 20 cycle scaffolds to some extent. The authors also reported the resultant morphology of the MC3T3-E1 cells to be a product of the underlying surface morphology and structure[120]. For example, cells grown on bare glass exhibited reduced attachment, spreading, growth, and fewer microvilli and pseudopods than cells grown on the graphene oxide substrates[120]. This phenomenon of cells morphologically responding to underlying substrates was found in our study where cells favoured an initial elongated morphology in the direction of underlying collagen fibrils on the unmineralized scaffolds (Fig. 5.2A).

Cellular production of ECM was observed to begin on all scaffolds following 7 days of culture (Fig. 5.4). This observation resembles what was found by Quarles et al.[322] where extracellular matrix deposition by MC3T3-E1 cells was found to peak after 7 days of culture. In addition to ECM production, cells appeared to possess numerous microvilli on their surfaces (Fig. 5.4), pointing to heightened activity[319]. These findings are similar to what was observed by Cheng et al.[120], where an increase in microvilli and ECM formation occurred following 7 days of culturing MC3T3-E1 cells.

5.4.2 Cell proliferation and differentiation

dsDNA content was found to remain stable throughout the 14 days of cell culturing on the unmineralized collagen scaffolds (Fig. 5.5A). This is similar to what was found by Nijsure et al.[323], where the number of human osteosarcoma cells remained constant on unmineralized aligned-collagen scaffolds over 7 days of culturing. dsDNA content for mineralized scaffold groups was observed to decline after 7 days of culture (Fig. 5.5A). The increased relative cellular proliferation associated with unmineralized scaffolds compared to mineralized scaffolds may be due in part to the increased protein surface area available for cell adhesion. Pre-osteoblasts express the ability to adhere to collagen through RGD-dependent integrin binding[324]. This binding affinity is likely reduced when collagen fibrils are covered with mineral, which may result in a relative increase in cellular proliferation on unmineralized collagen scaffolds. In addition to this, osteogenic differentiation was observed to be greater for cells grown on the mineralized scaffolds compared to cells cultured on the unmineralized control scaffolds (described below) (Fig. 5.5A,B). It is known that the proliferation of MC3T3-E1 cells decreases during periods of differentiation, thus possibly accounting in-part for the lack of proliferation on mineralized scaffolds[322]. The decrease in dsDNA content observed for mineralized scaffold groups following 7 days of culture may indicate a degree of cell detachment or death on these scaffolds compared to the stationary dsDNA levels found on unmineralized scaffolds (Fig. 5.5A).

ALP is considered a prominent biomarker of early-stage bone formation[321,325]. In bone, ALP is a homodimeric glycoprotein enzyme thought to act as an inhibitor to the inhibitor of hydroxyapatite formation and growth, PPi, through its ability to cleave

PPi into inorganic phosphate[325,326]. ALP contains a calcium-binding domain site in addition to a region capable of binding matrix proteins, including type I collagen, and is found associated with the membranes of osteoblast secreted matrix vesicles in bone[325,327].

After one day of culturing, ALP activity was similar for all treatment groups (0, 5, and 20 cycles) (Fig. 5.5B). After 7 days of culture, cells on mineralized scaffolds exhibited significantly greater ALP activity than cells grown on unmineralized scaffolds; a trend that continued after 14 days of culturing (Fig. 5.5B). This increase in ALP activity observed for cells cultured only on mineralized collagen scaffolds could indicate increased early stage osteogenic differentiation for these cells[321]. This trend is consistent with results found by Xu et al.[328] where MSCs expressed increasing levels of ALP activity over 14 days of culturing, beginning on day 7 when grown on bioglass-collagen scaffolds. Further, Ngiam et al.[329] compared the ALP activity of osteoblasts when cultured on either a PLGA/collagen scaffold or a mineralized PLGA/collagen scaffold. After 7 days of culturing, ALP activity was significantly greater for cells grown on the mineralized scaffolds compared to the unmineralized scaffolds[329].

OCN is one of the most abundant NCPs found within bone[330,331]. Produced mainly by osteoblasts, OCN is a 5.6 kDa secreted protein that in its carboxylated form is one of the two main γ-carboxyglutamic acid (Gla) proteins in bone, the other being matrix Gla protein (MGP)[330,332]. The Gla residues of OCN align and bind to calcium ions in hydroxyapatite, which is thought to contribute to its role as an inhibitor of bone mineralization and as a bridge between the mineral and matrix portions of bone[330,331,333]. Due to its role as a regulator in bone mineralization, OCN

is commonly considered an important biomarker for bone formation, particularly late-stage osteoblast activity[321,334].

OCN content for cells cultured on the unmineralized scaffolds remained low for the 14 days of culture, while significant increases occurred for the mineralized scaffolds (Fig. 5.5C). In addition to the previously mentioned ALP results, increases in OCN content indicate that mineralized scaffolds better promoted osteogenic differentiation. Similar findings were reported by Chou et al.[335] who compared MC3T3-E1 growth and osteoblastic differentiation on PLGA and apatite-coated PLGA scaffolds. In that work OCN content increased for the mineral coated group compared to the uncoated group after 4 weeks of culture[335]. In another study by Lee et al.[336], the effect that mineralization had on the osteogenic activity of collagen-glycosaminoglycan scaffolds was evaluated using MSCs. It was found that mineralization of the scaffolds increased the expression of OCN after 14 days of culture, suggesting that mineralization may help cue cellular osteogenic differentiation[336].

The mechanical properties of substrate materials are critical factors in defining the resultant morphology and differentiation of adherent cells[119]. For example, Khatiwala et al.[280] observed increased proliferation, migration, and eventual osteoblastic differentiation of pre-osteoblast cells with increasing stiffness of collagenous hydrogels. From our previous work, progressive mineralization of collagen fibril templates by alternate soaking was shown to increase individual collagen fibril stiffness and macroscale scaffold flexural modulus in proportion to the number of mineralization cycles complete[197]. From the current study, it appears that the increase in scaffold mechanics moving from 5 to 20 mineralization cycles is sufficient to enhance

osteogenic differentiation of pre-osteoblasts, as measured by ALP activity and OCN content.

As is also demonstrated by the current work, there is a disadvantage to increased scaffold mineralization, with occlusion of collagen fibril surfaces by mineral appearing to significantly reduce cell adhesion. Considering how best to design future mineralized collagen scaffolds given these disparate effects of increasing mineralization may lead to the creation of new scaffolds with enhanced repair and regeneration potential.

5.5 Contributions

5.5.1 Author contributions

The original conception and experimental design of the research described in this chapter was carried out by myself with consultation by Dr. Samuel Veres. More specifically, tendon acquisition, decellularization, cryosectioning, collagen mineralization, SEM, and data analysis and presentation, including chapter writing and illustration, were completed myself. Culturing of cells, including the design and selection of culturing conditions, in addition to cell proliferation analysis, ALP activity analysis, and OCN content determination were all carried out myself with minor technical assistance from Darren Cole. Formal data analysis was carried out by myself and Dr. Samuel Veres.

5.5.2 Contributions to the field

It is crucial to the development of mineralized collagen devices for bone repair and regeneration that the method of mineralization used stimulate an osteogenic cellular response. Further, understanding how increasing levels of mineralization affect cellular response is important for the optimization of scaffold design. Knowledge on the *in vitro* osteogenic response of pre-osteoblast cells to mineralized scaffolds prepared from dense collagen templates is limited, in particular those prepared with varying degrees of mechanical stiffness. It was found in this work that the conditions necessary for an osteogenic response limit cellular proliferation. Therefore, when attempting to design mineralized collagen scaffolds, one should take into account that non-mineralized pathways will promote cell proliferation, while stiffer material regions will help promote an osteogenic response. This chapter additionally offers, for the first time, knowledge of the effects serial freeze-thawing has on the stability of ALP, which has since influenced manufacturer recommendations.

Chapter 6

Summary and Future Outlook

6.1 Clinical need and existing technologies

The clinical demand for bone grafting biomaterials is increasing as uses in traumatology, spinal surgery, tumor resection operations, oral and craniomaxillofacial surgery, and revision arthroplasty become more popular[337]. Part of the reason for the increasing rates of these procedures is due to our aging population, in addition to a population with increasing rates of chronic diseases[338]. For example, a reflection of this demographic shift can be seen in the numbers of hip and knee replacements from 2017-2018 in Canada, at nearly 130,000[339]. Compared to numbers from 2012-2013, this represents an overall increase of over 17%[339].

As was mentioned in Chapter 1, to repair injuries to bone that require surgical intervention, metallic implants are often used and/or the current gold standard bone grafting material, autologous bone, depending upon the region and indication. Metal-

lic implants offer heightened mechanical properties and easy availability, however, they lack biofunctionality and may result in many complications, such as migration and stress-shielding, requiring additional revision surgeries. In addition to this, in growing patients, eventual device retrieval may be required. Although autologous grafts offer many osteogenic advantages over most other materials, their availability is limited, and donor tissue harvesting may result in further complications.

In response to the need for alternative bone grafting materials, various research groups have focused their attention to the development of mineralized collagen-based materials. Although still in their relative clinical infancy compared to autologous or metallic implants, various iterations of these materials have been developed and approved for clinical use as shown in Table 1.2. As these materials advance further, considerations for not only their chemistry, but also for their structural features and both nano- and macromechanical properties are being taken further. As was mentioned in Chapters 1, 4, and 5, most mineralized collagen materials to-date fail to consider the importance of collagen fibril alignment, in addition to mechanical characteristics that may affect the cellular response to the material post-implantation. For these reasons, the work described herein aimed, and succeeded, at developing a mineralized collagen scaffold with controlled collagen fibril alignment and the ability to be easily tailored in regard to both nano- and macromechanics.

6.2 Summary of work completed

In accordance with the first thesis objective, a method for mineralizing decellularized sheets of bovine tendon was successfully developed. This method led to the close

integration of a mineral phase with collagen that resembled mineral found in bone. Through chemical and structural analysis, it was found that the prepared scaffold reasonably resembled both the chemical makeup and mineralized collagen microstructure found in bone. It was found that pAsp and citrate play important roles in determining crystal structure, findings not well reported previously. Evaluations of exogenous crosslinking agents were also conducted to assess their possible use towards the future construction of multilaminate scaffolds as outlined in the appendix. From this work, it was found that the natural crosslinking agent genipin can significantly increase collagen stability, indicating that it may possess some of the functional benefits of glutaraldehyde, while avoiding cytotoxic side effects.

As mentioned, most work done on the development of mineralized collagen scaffolds to-date fails to describe an ability to easily control scaffold mechanics over multiple scales. This design parameter is important if the scaffold is to be used throughout the body as mechanical demands vary greatly depending on the location and cause for surgical intervention. In order to address this gap in knowledge for the developed mineralized collagen scaffold described herein, both nano- and macromechanical testing was done using AFM and 3-point flexural testing, respectively, as set in the second thesis objective. From these experiments it was shown that both nano- and macromechanics can be easily controlled through modifications in the collagen mineralization process.

In order to validate the ability for this scaffold to promote bone repair, an *in vitro* investigation using MC3T3-E1 pre-osteoblastic cells was conducted, as was set in the third thesis objective. From this phenotypic and biochemical study, it was observed

that cells were able to adhere and spread on unmineralized and mineralized collagen scaffolds to some extent, with ECM production appearing following 7 days of culture on all treatment groups. It appeared from this work that an increase in scaffold mechanics, achieved through an increase in the number of mineralization cycles, results in enhanced osteogenic differentiation of cells, with no evidence of differentiation observed on unmineralized collagen, measured by ALP activity and OCN content. This, coupled with the knowledge that occlusion of the fibrillar collagen surface by mineral appears to reduce cell adhesion, will help to inform future scaffold design.

6.3 Future research goals and objectives

The overall goal of my doctoral thesis was to develop a novel mineralized-collagen scaffold for bone repair and regeneration. Through fundamental chemical, mechanical, structural, and *in vitro* experiments, promise towards this goal was achieved. In order to progress the research presented here further towards its clinical application, the following research directions and proposed steps are suggested. Briefly:

1. Selected area electron diffraction during TEM would allow for a more complete characterization of the mineral phase associated with individual collagen fibrils.

2. Extension to the *in vitro* culturing timeline from 14 to 21 days would allow for a more comprehensive evaluation to be done towards the differentiation profile of adherent MC3T3-E1 cells.

3. The addition of an *in vitro* collagen control group consisting of randomly oriented collagen fibrils in addition to a clinically available mineralized collagen

scaffold group would allow further comparisons to be made.

4. The preparation of multilaminate scaffolds through layering and exogenous crosslinking may allow for the production of more clinically relevant scaffolds.

5. A natural extension of this work towards possible clinic translation would be to conduct *in vivo* investigations, beginning with biocompatibility experiments and progressing towards clinical trials.

6. Looking towards possible alternative applications of the developed technology described herein, a possible research direction may be in the construction of scaffolds possessing regions of both mineralized and non-mineralized collagen for tendon/ligament to bone/tooth interfaces.

In order to better confirm the occurrence and type of intrafibrillar mineral formed from the described alternate soaking procedure, selected area electron diffraction methods may be used. Electron diffraction performed on mineralized collagen fibrils performed during TEM, such as that shown by Liu et al.[114] and Zhang et al.[340], would allow for a characterization of the crystal orientation as well as specific mineral phase. This would allow for a comparison to the crystal orientation and apatitic phase found within bone (*c*-axis parallel to the direction of the collagen fibril).

As a natural extension to the previously described *in vitro* work, further characterizations may be done through an increase to the duration in which cells are cultured on the prepared scaffolds. More specifically, with the addition of a 21-day timepoint to the existing 1, 7, and 14 days timepoints, a more complete evaluation of the osteogenic differentiation of MC3T3-E1 cells could be achieved. As OCN is considered

a late-stage differentiation marker for MC3T3-E1 cells, this timeline extension may show a more complete increasing trend in its expression over time. Additionally, as ALP activity is thought to be tied to earlier osteogenic differentiation, such a timeline extension may show its decline as levels of OCN increase further.

This work included a comparison between both mineralized and non-mineralized collagen scaffolds in regard to their ability both support the growth and osteogenic differentiation of MC3T3-E1 cells. An extension of this investigation would be to include alternative substrate materials for cells, such as sheets of randomly oriented collagen fibrils and/or existing clinically approved mineralized collagen scaffolds. The incorporation of randomly oriented collagen sheets in such an *in vitro* study would allow for a more in depth evaluation of how cells respond to changing fibrillar alignment including not only their growth patterns, but also their subsequent biochemical response. Comparisons between the scaffold described here and currently clinically approved scaffolds would better allow the scaffold described here to be placed amongst existing technologies.

The development of layered, mutli-sheet scaffolds may follow from the already developed and well-characterized single mineralized collagen sheets. Based upon preliminary investigations of crosslinking agents as outlined in the appendix, the natural crosslinker genipin may be used in this multilaminate scaffold construction. As mentioned in Chapter 1, and shown in Fig. 1.4, the orientation of collagen fibrils varies depending upon the location within the skeleton, and ultimately as a product of the specific loading requirements placed upon that bone region. Layering of aligned collagen fibril sheets may better allow scaffold mechanics and structure to be tailored

to specific donor tissue sites. The preparation of such multilaminate scaffolds may be done through the layering of sheets within a custom designed 3D printed mold containing a crosslinking agent, such as genipin. Once scaffolds are created, similar flexural testing experiments that were done on single sheets could be conducted, in addition to other relevant tests, such as delamination evaluations. Final design parameters should also be formulated in consultation with those who would be the end-stage users of such a device; clinicians. Through such consultations, practical design goals may become better recognized which would allow for a more streamlined clinical translation and a reduction in clinician rejection or apprehension.

Ultimately, in order for the scaffolds described herein to be translated to the clinic, *in vivo* evaluation must be conducted. These experiments would begin with an appropriate animal model in accordance with appropriate research ethics guidelines, such as those from the Canadian Council on Animal Care. Using this animal model, preliminary biocompatibility tests would be done, such as through implantation of the scaffold subcutaneously to elucidate the immunological response from the host in response to the material. This model would also allow for evaluations to be done in regard to the possibility of the scaffold contributing to ectopic bone formation. Following this, use of the scaffold for the repair of a non-critical size bone defect may be done to determine initial bone biocompatibility. Subsequently, or directly following subcutaneous implantation, a critical size defect model, such as the C57BL/6 mouse (from which MC3T3-E1 cells were established) calvarial bone defect model used by Zhang et al.[341], may be used to determine the ability for the scaffold to promote new bone growth in comparison to controls and existing devices. Evaluation may in-

clude micro-CT imaging of the defect region post-treatment in addition to histological characterizations. Once these investigations are complete and a better picture of how the developed scaffold presents itself within the body is obtained, controlled clinical investigations may begin to take place in accordance with established clinical testing guidelines outlined by Health Canada and other governing bodies.

Further, the application of the developed collagen mineralization procedure may be applied to the development of biomaterial grafts destined for alternative regions throughout the body. One such region may be at the interface between tendon and/or ligaments with bone and teeth where mineralized meets non-mineralized collagen. The need for such multiphasic scaffolds has been recently described in detail by Lausch et al.[190] where a central challenge to their production is achieving cohesion between layers. Due to the nature of how the collagen sheets are organized and mineralized in this work, it would be easy to mineralize only part of the tendon sheet, thus allowing for a seamless transition between scaffold regions. Additionally, due to the nature of the collagen material described here, that of bovine tendon origin, the collagenous phase already resembles highly the region in which it would intend to replace or repair.

6.4 Conclusion

The research work described herein not only highlights a novel method of preparing decellularized sheets of aligned mineralized collagen fibrils, it also allows for a better understanding of the mechanisms involved in collagen mineralization *in vitro*. I have presented, to the best of my knowledge, the first demonstration of the production of decellularized, naturally crosslinked and aligned, tendon-derived sheets of mineralized

collagen fibrils. I have shown that through alternate soaking mineralization of collagen sheets, mineral crystal morphology may be modified through the addition of various chemical additives, such as pAsp and citrate. This identification of collagen mineralization mechanisms may contribute and guide future work related to the development of mineralized collagen-based scaffolds for bone repair and regeneration.

Due to the growing clinical need for sustainable, reliable, safe, and functional bone repair materials, research towards their development is vital. This work focused upon three central objectives: first, to develop a method of producing mineralized collagen sheets in a bio-inspired way and to examine their chemical and structural properties compared to bone, second, to perform both nano- and macromechanical evaluations on the developed scaffolds, and finally to perform initial *in vitro* phenotypic and biochemical evaluations using MC3T3-E1 preosteoblastic cells grown on the prepared scaffolds. Each objective was successfully achieved and resulted in the development of a novel mineralized collagen scaffold capable of mechanical tailorability and the promotion of cellular osteogenic differentiation. Both mechanical and *in vitro* work was conducted on scaffolds prepared with varying exposures to the number of alternate soaking mineralization cycles. This comparison between groups, largely between scaffolds mineralized for either 0, 5 or 20 cycles, allows for design optimization to be performed where increased scaffold mineralization, and thus mechanics, was found to promote the osteogenic differentiation of pre-osteoblast cells, with however, reduced cell adhesion.

Questions still remain, such as the degree of biocompatibility of the described scaffold post implantation *in vivo* as well and the ability for the scaffold to promote bone repair

in a critical size bone defect model. These questions require the implementation of a *in vivo* model system, such as the previously mentioned C57BL/6 mouse model. Further, expansion to the already performed *in vitro* work described herein, largely in regard to culturing duration, may be of benefit prior to the commencement of *in vivo* investigations in order to better inform scaffold design parameters.

Appendix A

Genipin Crosslinking of Tendon Collagen

A.1 Genipin crosslinking

The following work explores the natural corsslinking agent genipin as a less cytotoxic alternative to glutaraldehyde for crosslinking tendon collagen, for the purpose of understanding whether it might be an appropriate method of creating multilaminate scaffolds.

A.1.1 Collagen acquisition and processing

Common digital extensor (CDE) tendons were dissected from the forelimbs of steers aged 24-36 months, killed for food at a local abattoir. Dissected tendons were stored in phosphate-buffered saline (PBS) solution at 4°C to await decellularization treatment,

which was started within 12 h of dissection.

Decellularization treatment was conducted following a method previously described by Woods and Gratzer[261]. Briefly, tendons were first exposed to a hypotonic 10 mM tris buffer containing serine and metalloprotease inhibitors, along with 1% penicillin/streptomycin and 1% amphotericin B for 36 h at room temperature. Tendons were then moved to a high saline 50 mM tris buffer containing 1% Triton X-100 along with antibiotics and protease inhibitors for 48 h at room temperature, followed by Hanks' buffer rinse and wash in a DNase/RNase solution. This was followed by a 48 h, room temperature soak in 1% Triton X-100 solution with 50 mM TRIZMA base and antibiotics. Finally, the tendon samples were rinsed in PBS with antibiotics and stored in a similar solution at 4°C until further use.

Decellularized tendons were cryosectioned using a Leica SM2000R sliding microtome. Tendons were cut into 20-mm-long segments, mounted on a steel block using optimal cutting temperature compound (Fisher Healthcare, Ottawa, ON), frozen in liquid nitrogen, and sectioned longitudinally to produce 200-μm-thick collagen sheets.

Sheets were subsequently exposed to either 0.1%, 0.3%, or 0.5% w/v GP or 0.3% v/v GTA at 37°C in PBS for 72h followed by rinsing in ddH_2O. Collagen sheets maintained under the same conditions but in PBS only served as controls.

A.1.2 Differential scanning calorimetry

Following their respective treatments, the thermal stabilities of the prepared collagen samples were assessed by DSC. For each treatment group (control, 0.1%, 0.3%, and

0.5% w/v GP), five collagen samples acquired from five different animals were assessed. For the second comparative study, between control, 0.3% w/v GP, and 0.3% v/v GTA, new samples from the same decellularized tendons were prepared for each treatment group. From the prepared samples, 2-mm-long subsamples were cut, blotted dry to remove excess surface liquid, and weighed. Wet weights of the subsamples ranged from 4-6 mg. Subsamples were gently pressed into the bottom of aluminum DSC pans and hermetically sealed. Each collagen subsample was run against an empty aluminum pan using a Q100 DSC (TA Instruments, New Castle, DE). Following equilibration at 20° C, the temperature was ramped to 100° C at 5° C/min. Following DSC runs, pans were pierced and dried in a vacuum desiccator overnight before being reweighed to acquire sample dry weight.

A.1.3 Presentation and statistics

Numerical data are presented as mean ± SD. Box plot whiskers show maximum/minimum values. Differences between groups were tested using one-way ANOVA with post hoc Tukey-Kramer HSD test, with results of $p \leq 0.05$ considered statistically significant.

A.1.4 Results

DSC was used to evaluate the thermal properties of the GP and GTA crosslinked collagen samples. Crosslinking with 0.3% and 0.5% w/v GP resulted in a statistically similar increase in both peak denaturation temperature (T_{peak}) and onset temperature (T_{onset}) of the collagen sheets compared treatment with 0.1% w/v GP (Figs. A.1A,

Table A.1: DSC data for collagen samples treated with varying concentrations of GP in PBS for 72h. T_{peak} and T_{onset} increased similarly for both 0.3% and 0.5% treated samples compared to those treated with 0.1% GP. *FWHM* and enthalpy values were statistically similar for all three concentrations of GP. Dissimilar letters indicate a significant difference between groups with $p \leq 0.05$.

Concentration of GP (w/v)	**Peak Temp. (°C)**	**Onset Temp. (°C)**	**FWHM (°C)**	**Enthalpy (J/g)**
0.1%	76.8 ± 0.6^{a}	75.6 ± 0.8^{c}	1.5 ± 0.3	8.9 ± 4.3
0.3%	78.1 ± 0.5^{b}	76.8 ± 0.6^{cd}	1.7 ± 0.1	11.9 ± 1.6
0.5%	78.5 ± 1.0^{b}	77.3 ± 1.0^{d}	1.7 ± 0.2	12.4 ± 2.1

A.2A,B). Enthalpy and Full-width half-max ($FWHM$) values, which measures the homogeneity of the collagen thermal stability and structure, remained statistically similar regardless of the concentration of GP used (Figs. A.2C,D, A.1).

Based on the above results, GP treatment of 0.3% w/v was chosen for comparison to GTA treatment. Treatment with 0.3% v/v GTA significantly increased T_{peak} and T_{onset} both in comparison to the native collagen and the GP crosslinked samples (Figs. A.3A,B, A.1B). $FWHM$ values were similar following both GP and GTA crosslinking (Figs. A.3C, A.1B, A.2). Specific enthalpy of denaturation, calculated based on dry sample weights, was statistically similar for all treatment groups (Figs. A.3D, A.1B).

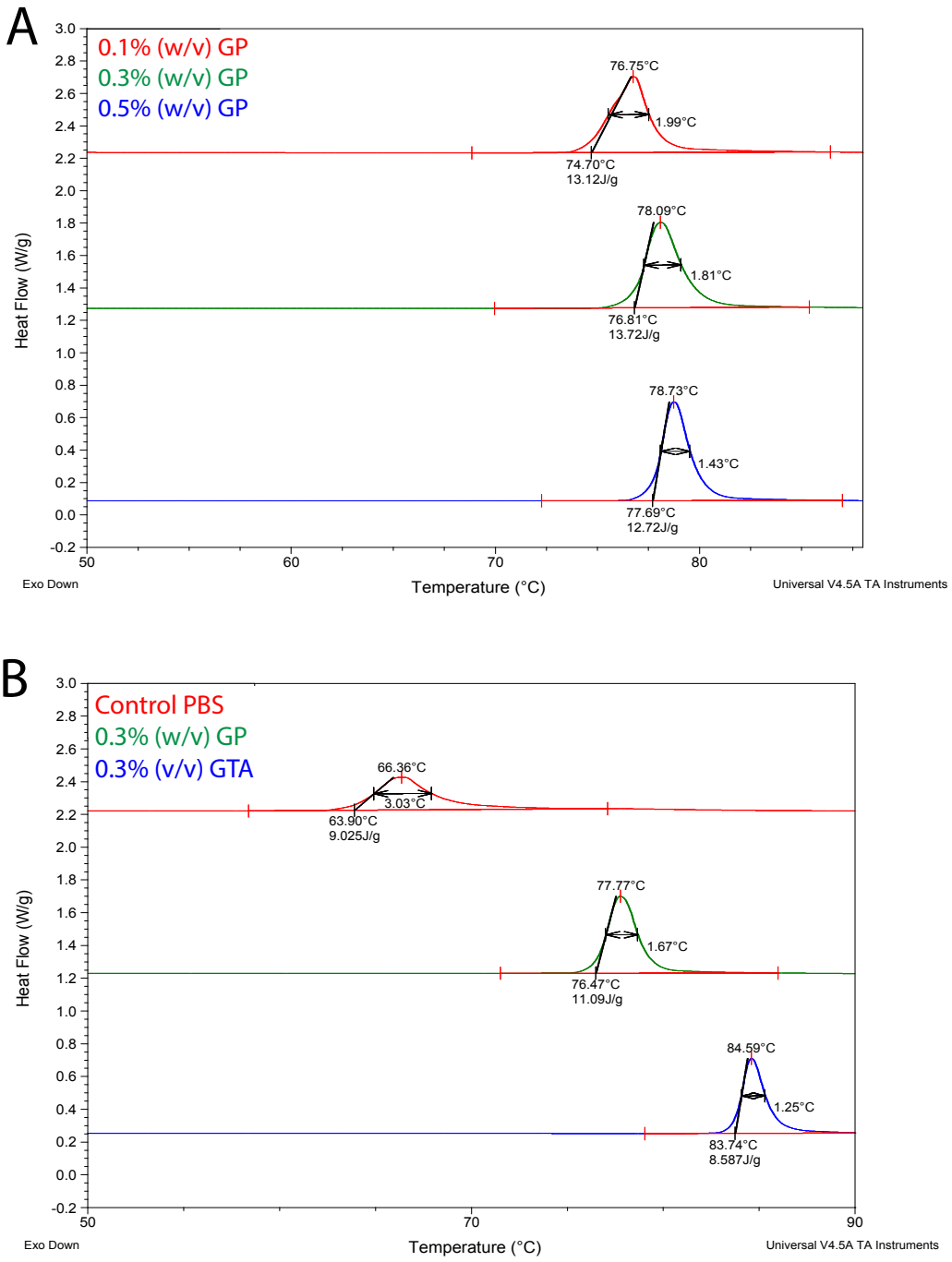

Figure A.1: Representative DSC endotherms of collagen scaffolds. A. Endotherms for collagen crosslinked with either 0.1%, 0.3%, or 0.5% (w/v) GP showing T_{peak}, T_{onset}, (*FWHM*), and enthalpy values. B. Endotherms comparing control collagen samples to those treated with 0.3% (w/v) GP and 0.3% (v/v) GTA.

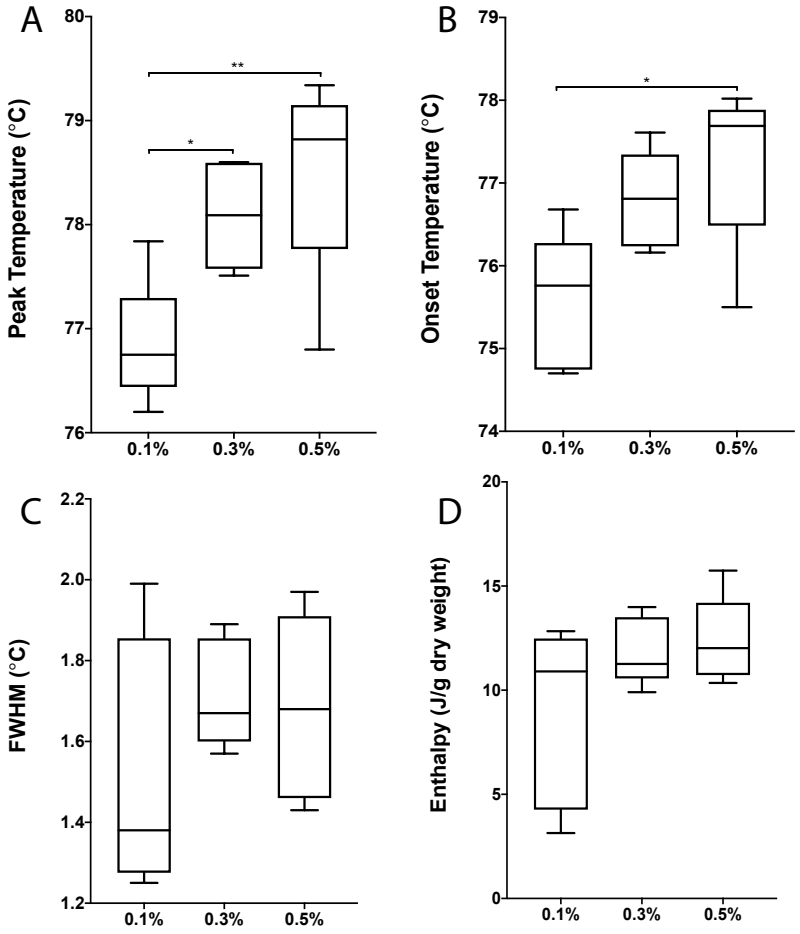

Figure A.2: A. DSC peak temperatures for bovine tendon collagen treated with varying w/v concentrations of genipin. B. DSC onset temperatures for sheets treated with genipin, C. *FWHM*, D. specific enthalpy of denaturation. Whiskers represent min/max values. *$p \leq 0.05$,**$p \leq 0.01$.

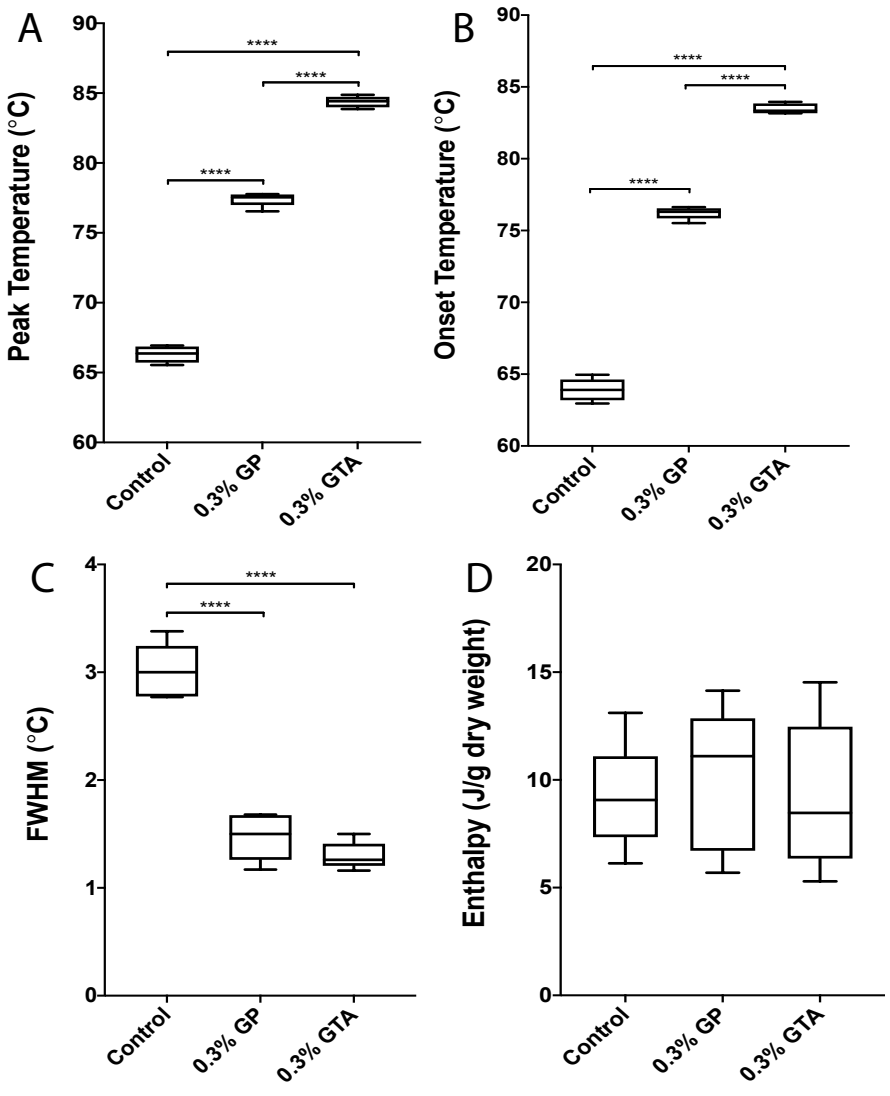

Figure A.3: A. DSC acquired peak temperatures for collagen obtained from bovine extensor tendons crosslinked with either 0.3% w/v GP of 0.3% v/v GTA, B. onset temperatures C. *FWHM*, D. specific enthalpy of denaturation. Whiskers represent min/max values. ****$p \leq 0.0001$.

Table A.2: DSC data for collagen samples treated with 0.3% w/v GP or 0.3% v/v GTA compared to untreated controls. Both GP and GTA treatment significantly increased T_{peak} and T_{onset} and decreased *FWHM*. Enthalpy values were statistically similar between all groups. Dissimilar letters indicate a significant difference between groups with $p \leq 0.05$.

	Peak Temp. (°C)	**Onset Temp. (°C)**	**FWHM (°C)**	**Enthalpy (J/g)**
Control	66.3 ± 0.6^{a}	63.9 ± 0.8^{d}	3.0 ± 0.3^{g}	9.2 ± 2.5
0.3% w/v GP	77.4 ± 0.5^{b}	76.2 ± 0.4^{e}	1.5 ± 0.2^{h}	10.0 ± 3.3
0.3% v/v GTA	84.4 ± 0.4^{c}	83.5 ± 0.4^{f}	1.3 ± 0.1^{h}	9.2 ± 3.5

Appendix B

Flexural Testing of Mineralized Collagen Scaffolds

B.1 3-point bending

The following appendix complements work presented in Chapter 4 through a presentation of detailed design parameters for the three-point bending system in addition to representative stress-strain curves for mineralization treatment groups. Hysteresis data for the three-point bending tests conducted in Chapter 4 is also presented.

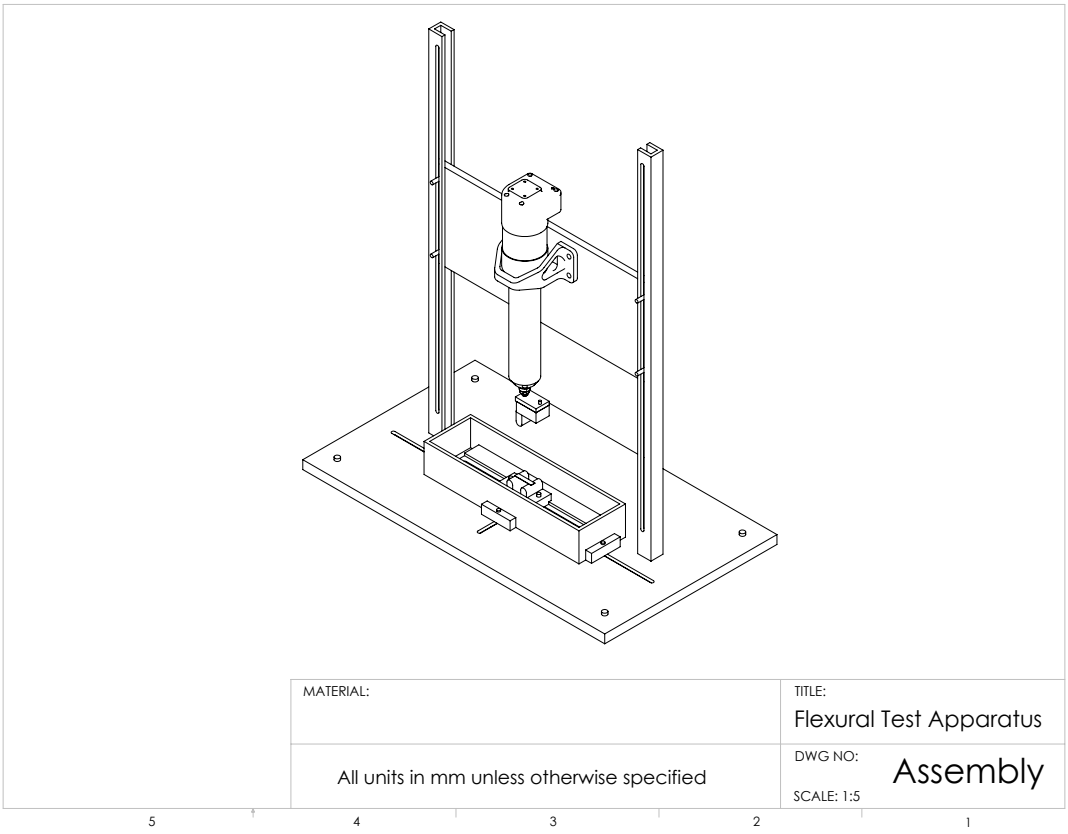

Figure B.1: Flexural test apparatus: assembly.

B.1.1 Custom-built electro-mechanical system component designs

The 3-point bending system consisted of a custom 316 stainless steel frame, Ultra Motion A1 series Servo Cylinder, Transducer Techniques GSO-1K load cell, and Transducer Techniques TMO-2 amplifier/conditioner module interfaced with a PC via a National Instruments NI 6351 DAQ board. Engineering drawings of the loading frame are shown in Figs. B.1 to B.16.

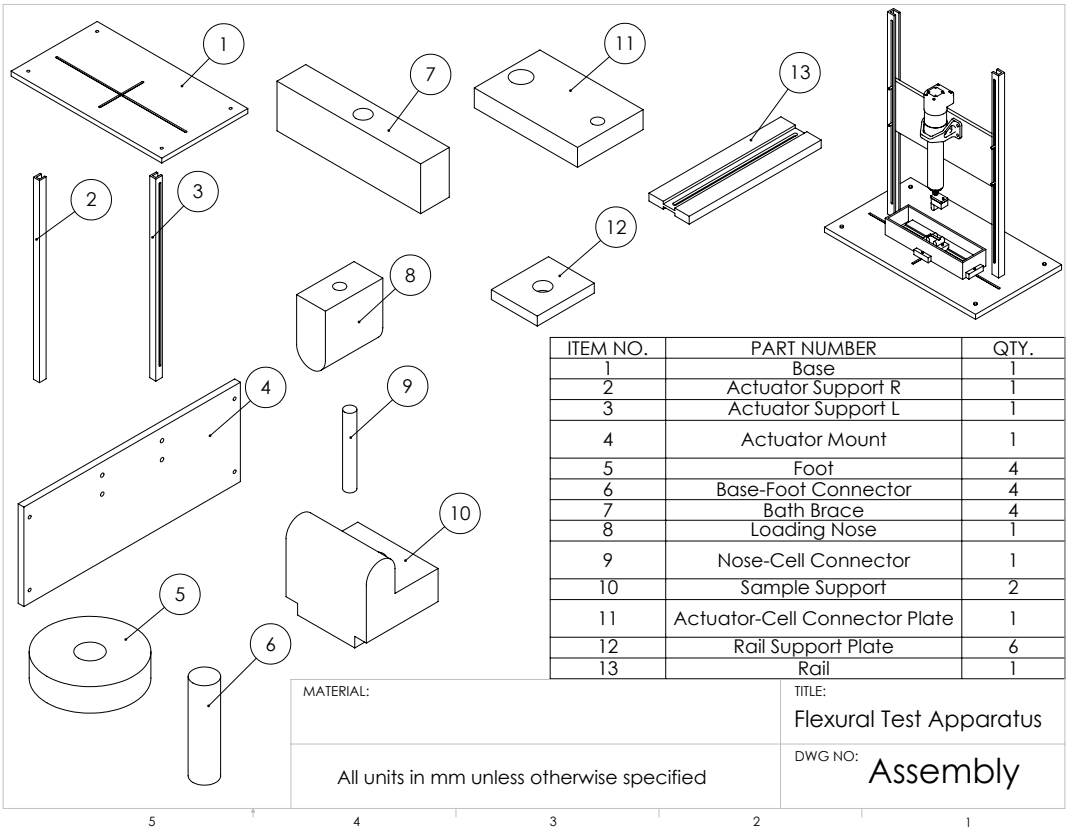

Figure B.2: Flexural test apparatus: assembly.

B.1.2 3-point bending system calibration

In order to confirm the movement accuracy of the Ultra Motion A1 series Servo Cylinder, its absolute position, as measured via the actuator's integrated Phase Index system, was compared against micrometer-measured actuator displacements during system commissioning. In order to calibrate the Transducer Techniques GSO-1K load cell, shunt calibration was used with linearity checked using a set of seven standard masses.

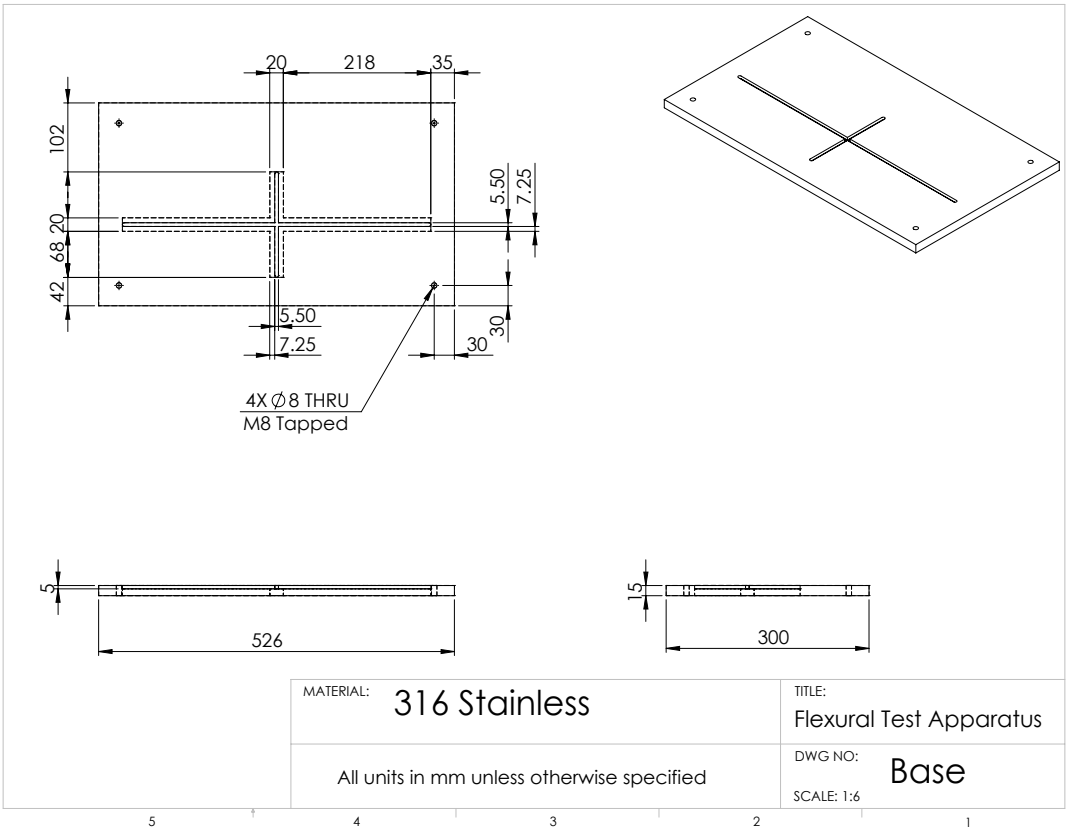

Figure B.3: Flexural test apparatus: base.

B.1.3 Hysteresis measurements

Representative stress-strain curves for the three sample groups tested in three-point bending are shown in (Fig. B.17). For the samples that underwent three-point bending, hysteresis was calculated as follows:

$$Hysteresis = (W_L - W_U)/W_L * 100$$

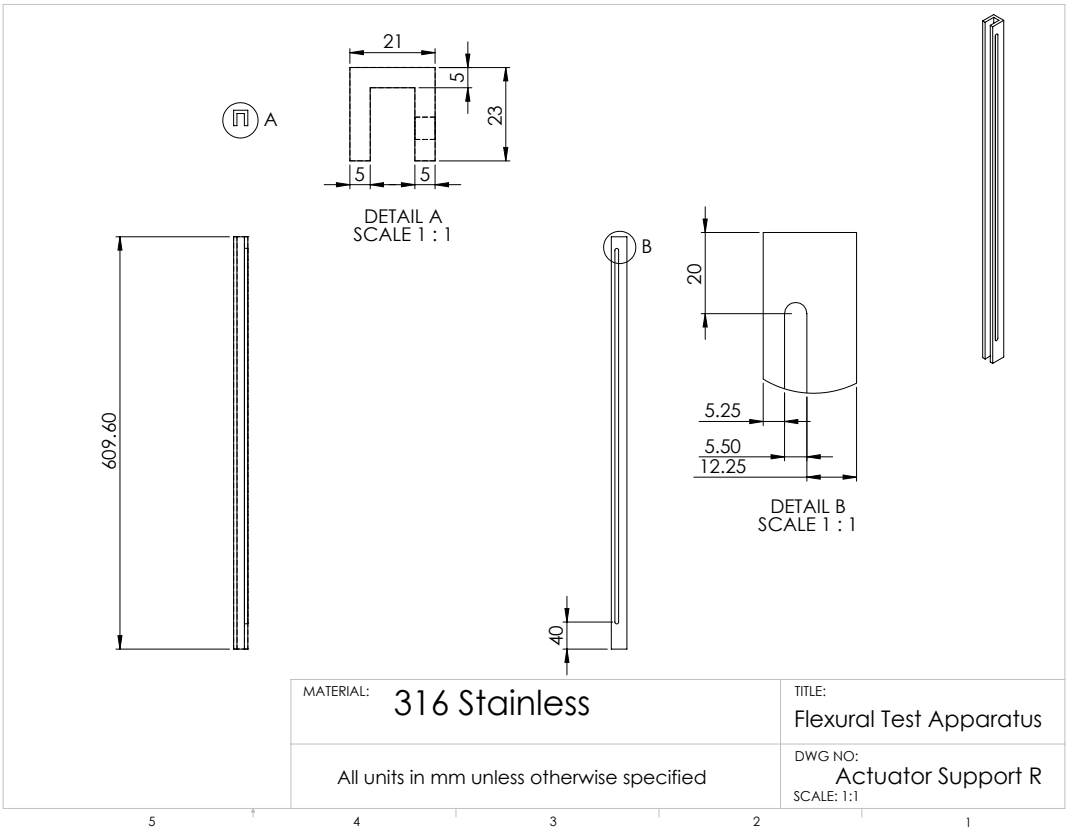

Figure B.4: Flexural test apparatus: actuator support R.

Where W_L and W_U refer to the areas below the loading and unloading regions of the stress-strain curves, respectively.

The final three loading cycles for each mineralized collagen scaffold were used for hysteresis measurements. These three values were then averaged for data analysis. From this, it was found that hysteresis increased significantly with an increase in the number of mineralization cycles to scaffolds (Fig. B.18). These data may indicate that like unmineralized tendon, interfibrillar sliding remained the main mechanism of

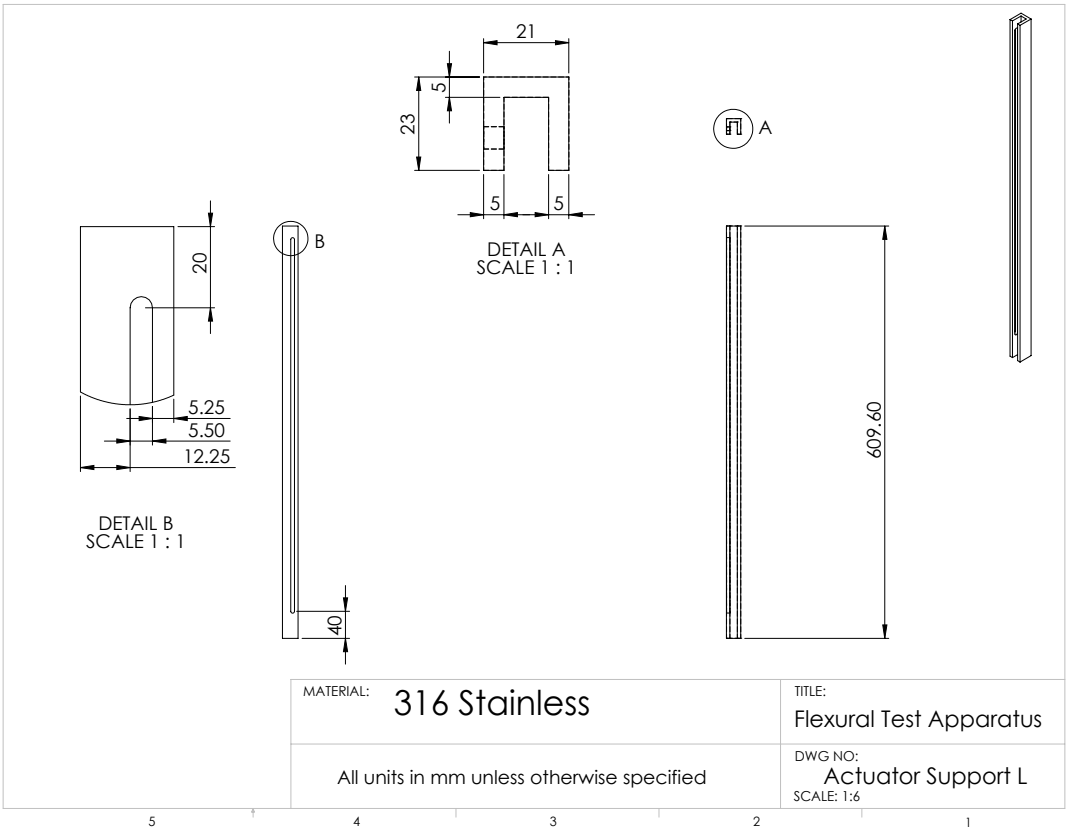

Figure B.5: Flexural test apparatus: actuator support L.

extension within the mineralized scaffolds, with greater levels of mineralization causing greater internal sliding friction and greater energy dissipation[342,343]. Differences between sample groups may additionally have been partly caused by differences in the surface charateristics of samples, leading to differences in friction between the scaffolds and fixed loading supports.

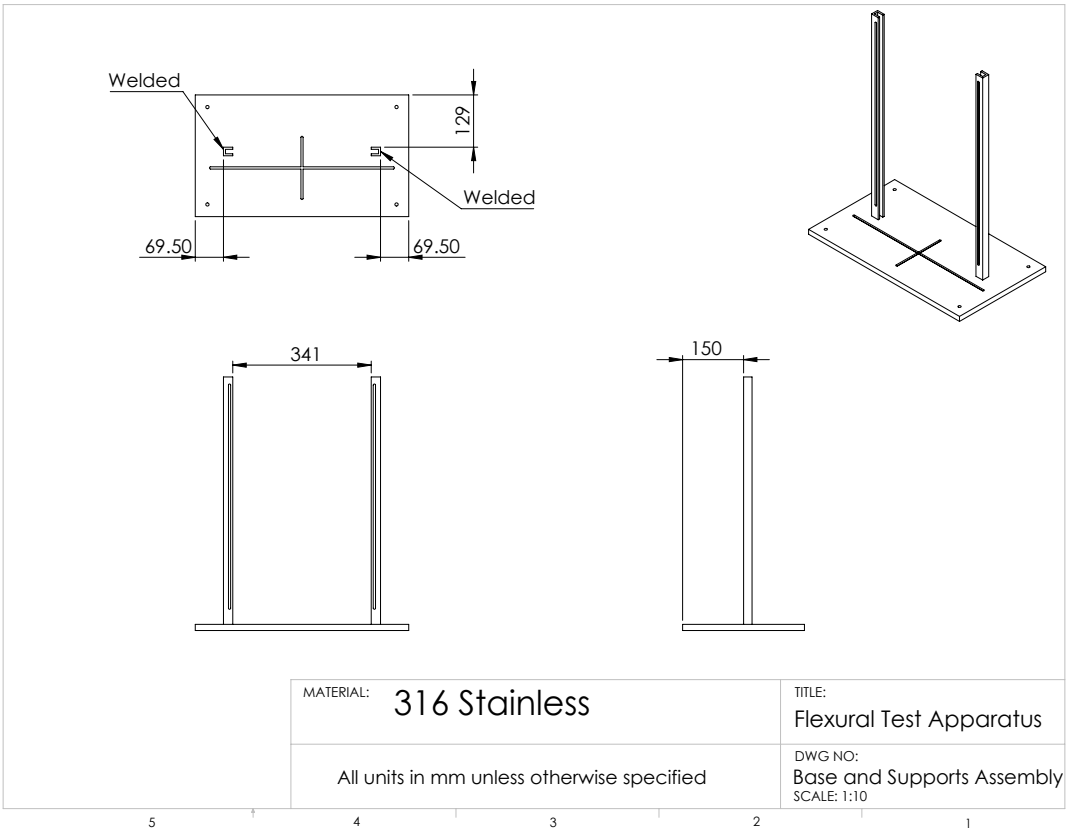

Figure B.6: Flexural test apparatus: base and supports assembl.

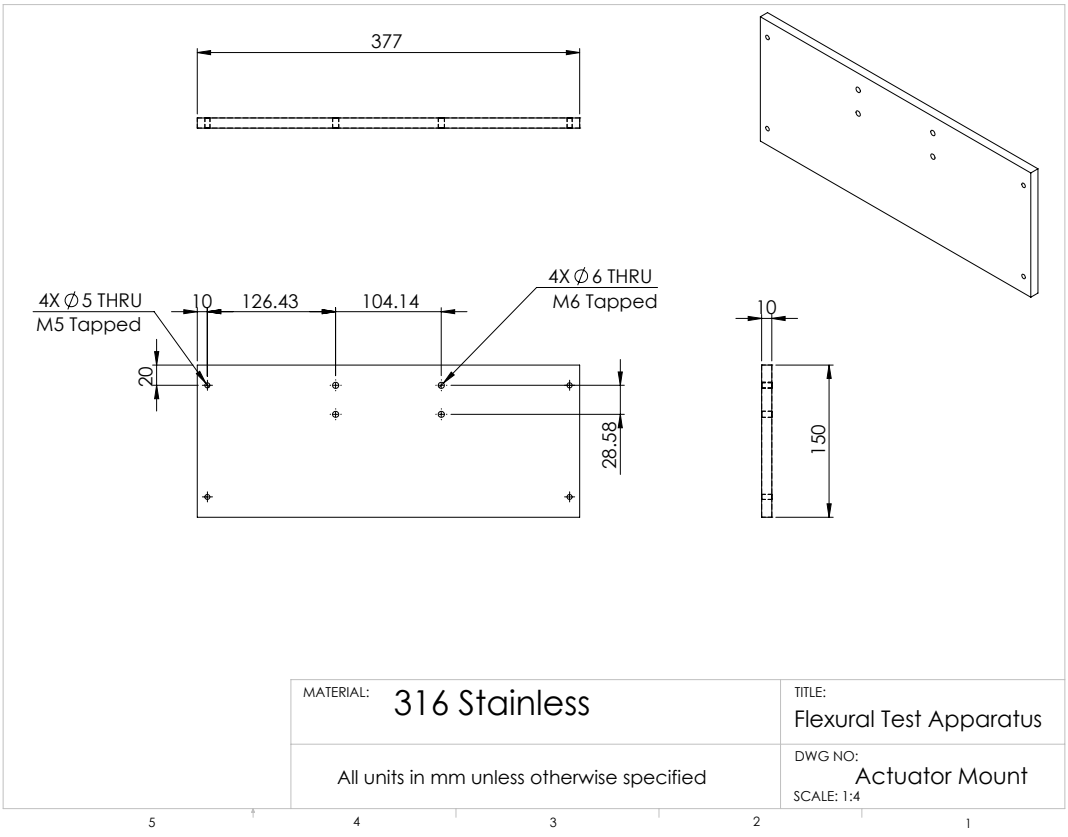

Figure B.7: Flexural test apparatus: actuator mount.

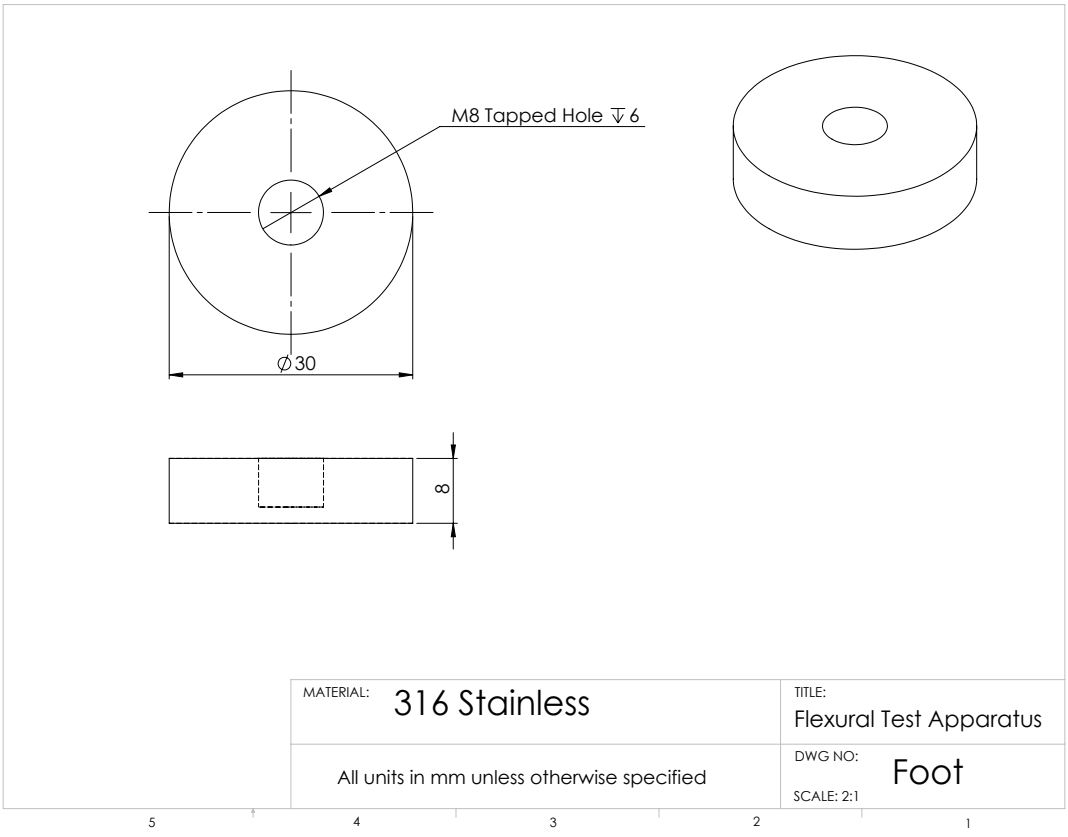

Figure B.8: Flexural test apparatus: foot.

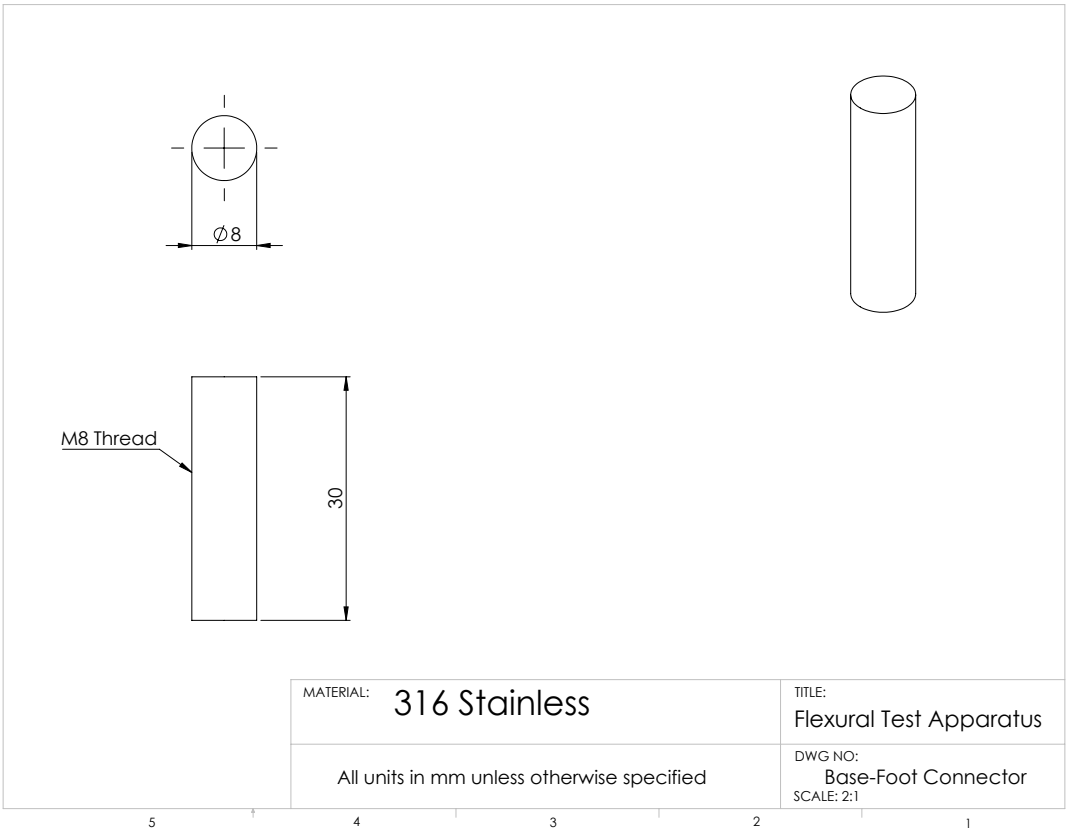

Figure B.9: Flexural test apparatus: base-foot connector.

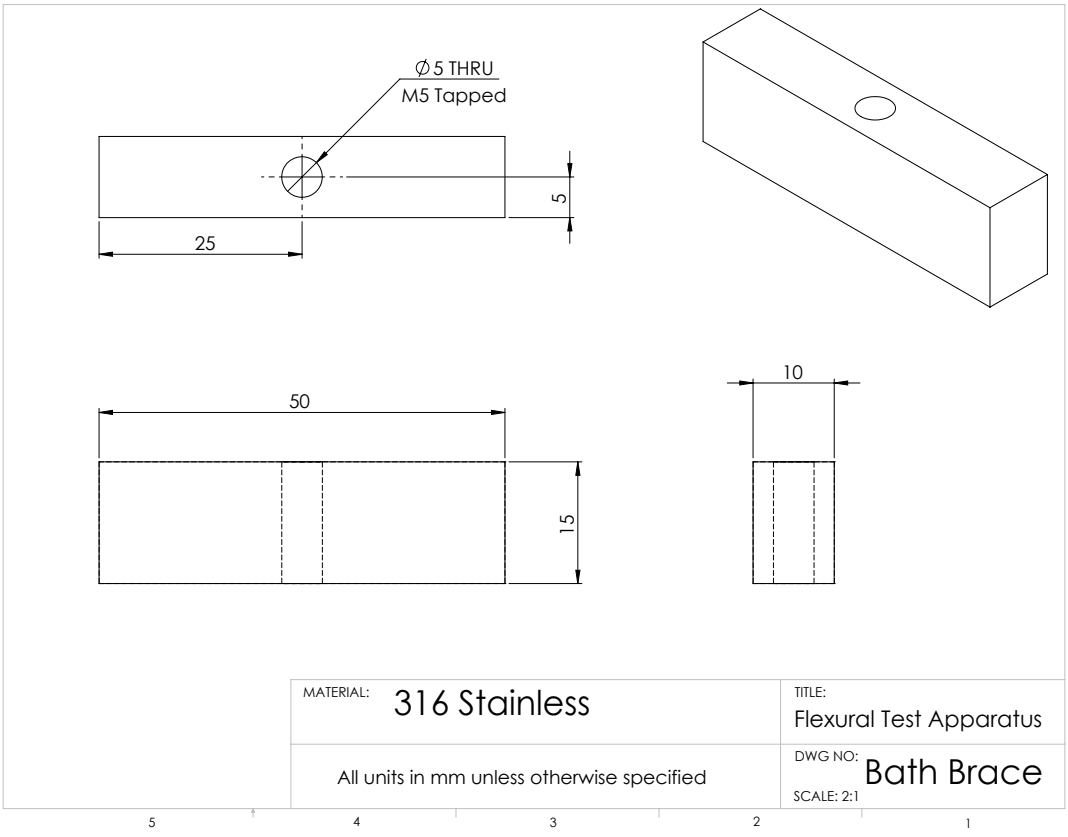

Figure B.10: Flexural test apparatus: bath brace.

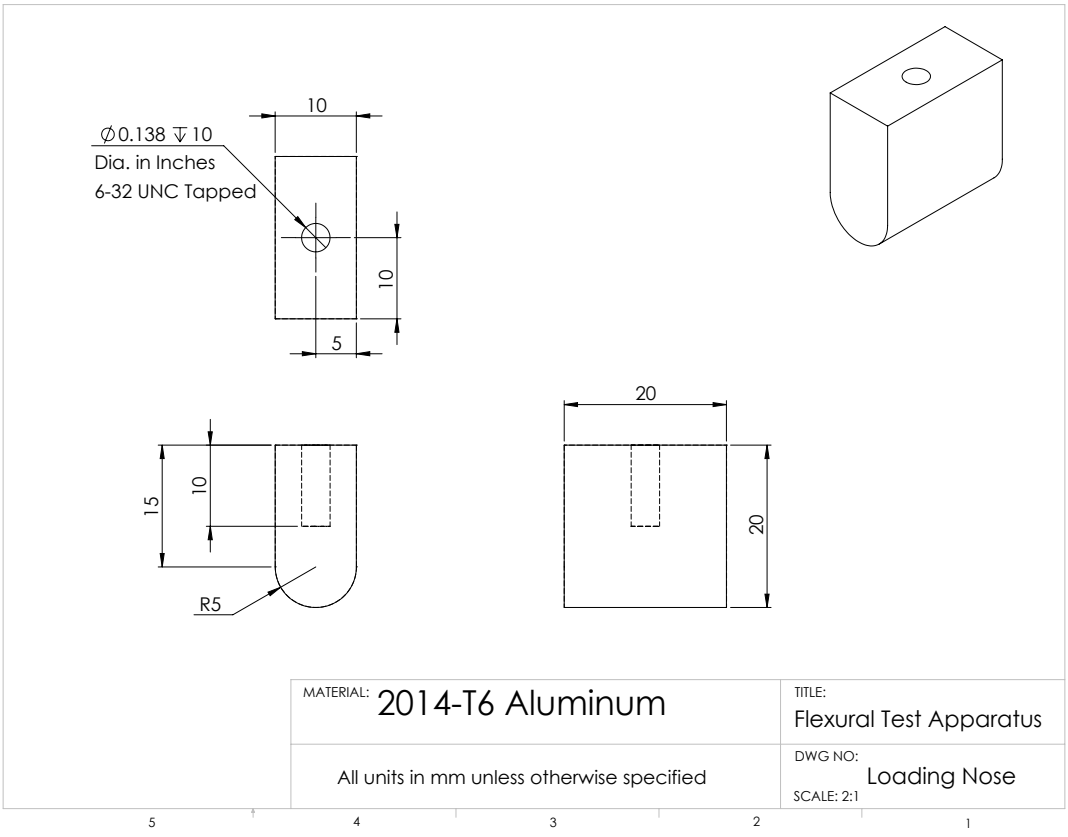

Figure B.11: Flexural test apparatus: loading nose.

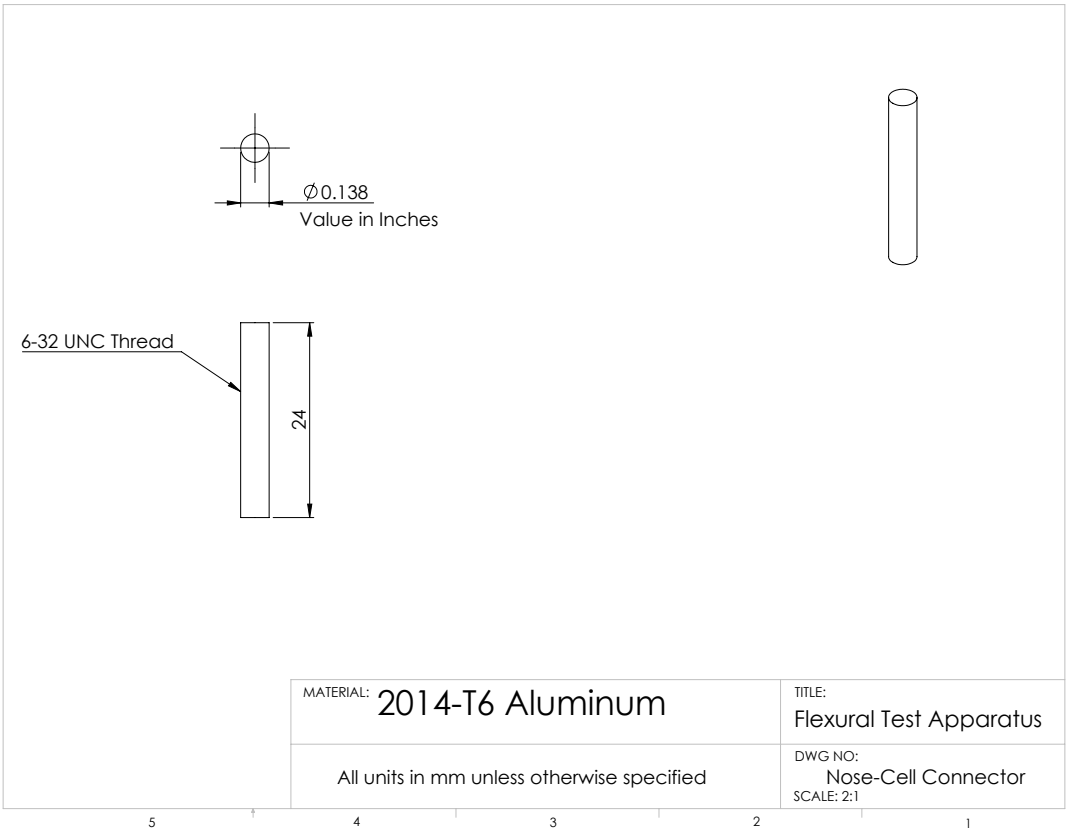

Figure B.12: Flexural test apparatus: nose-cell connector.

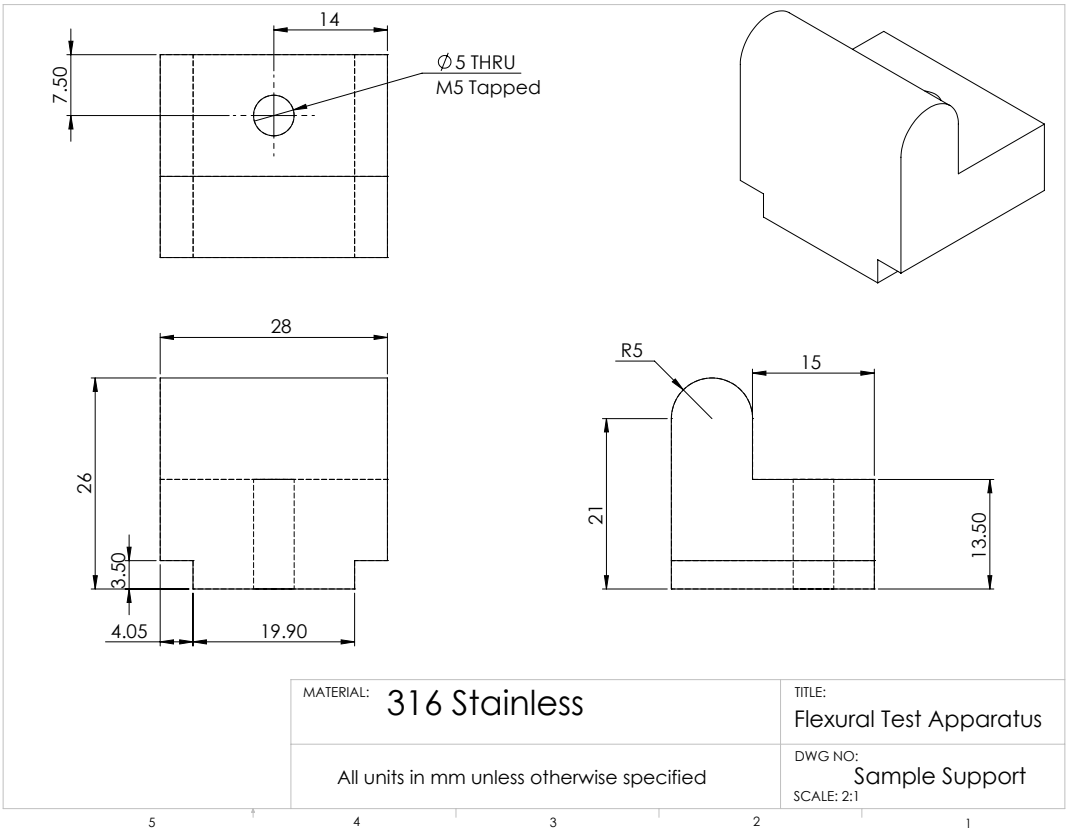

Figure B.13: Flexural test apparatus: sample support.

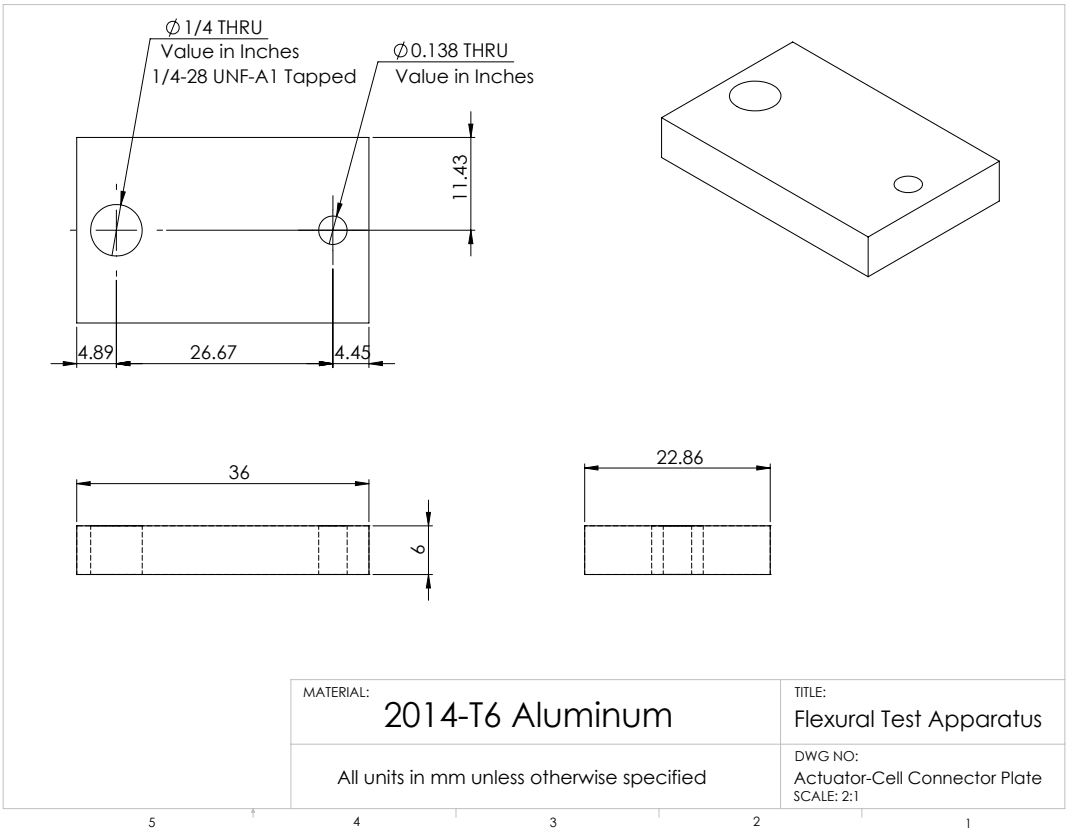

Figure B.14: Flexural test apparatus: actuator-cell connector plate.

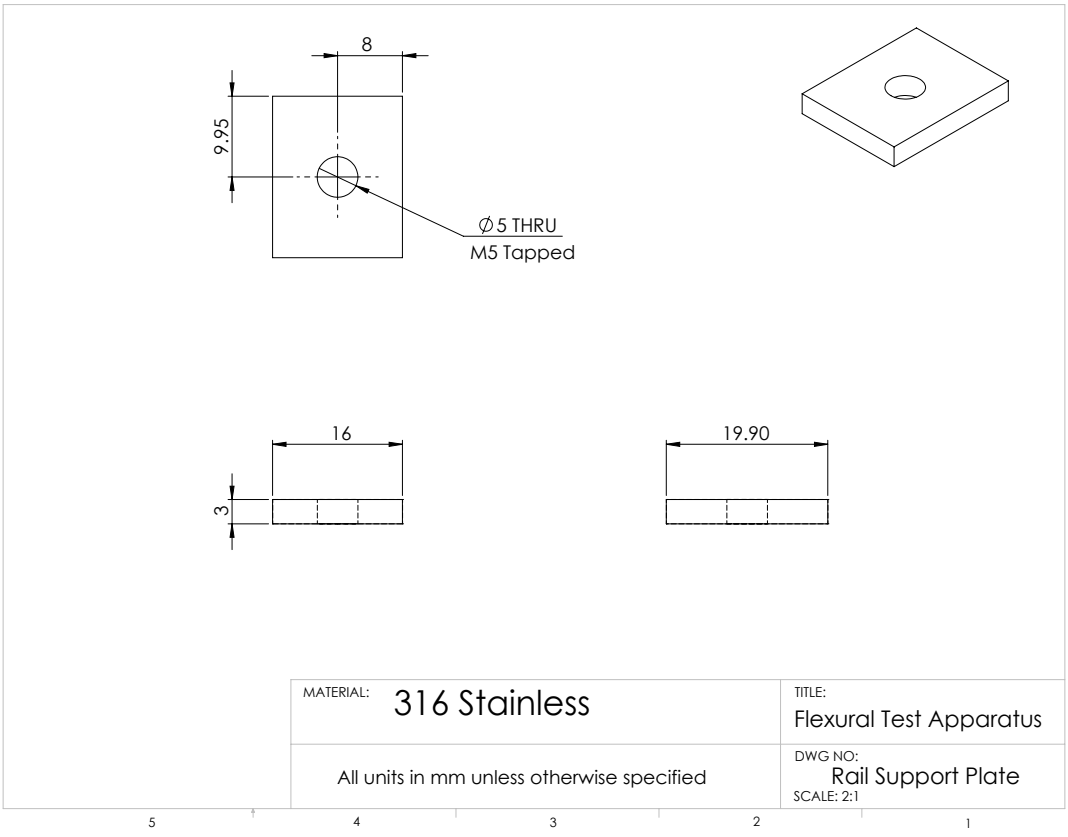

Figure B.15: Flexural test apparatus: rail support plate.

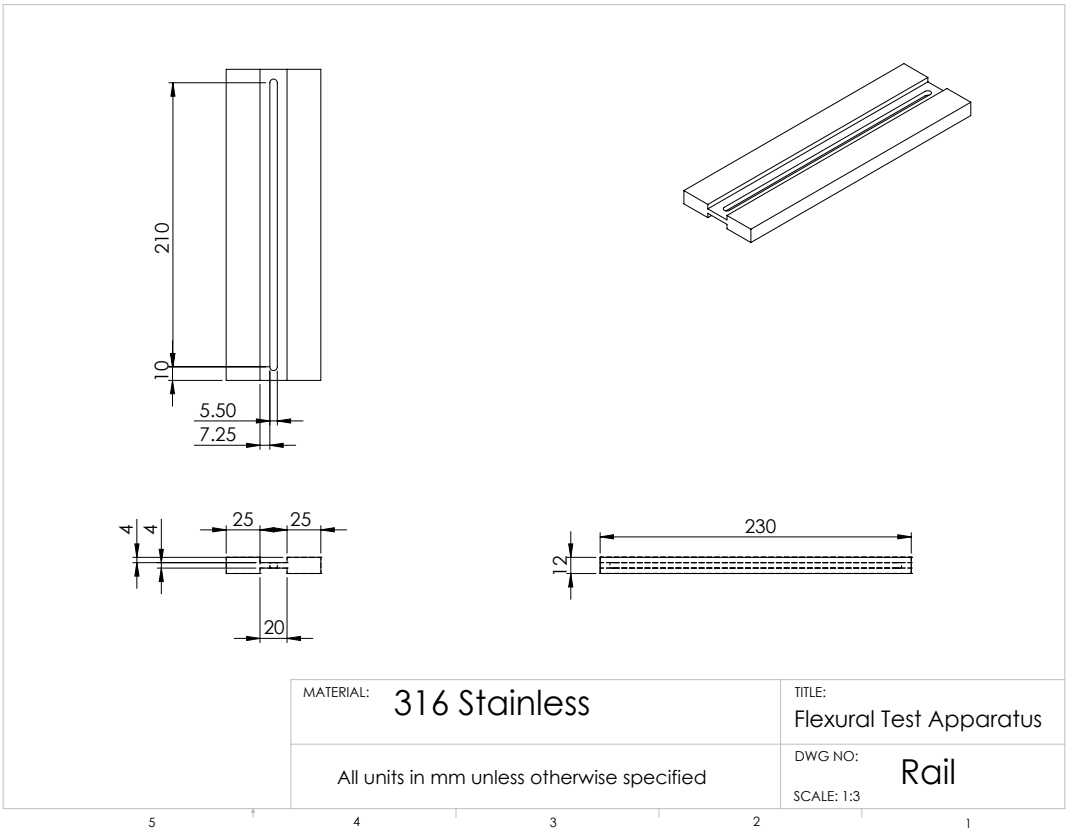

Figure B.16: Flexural test apparatus: rail.

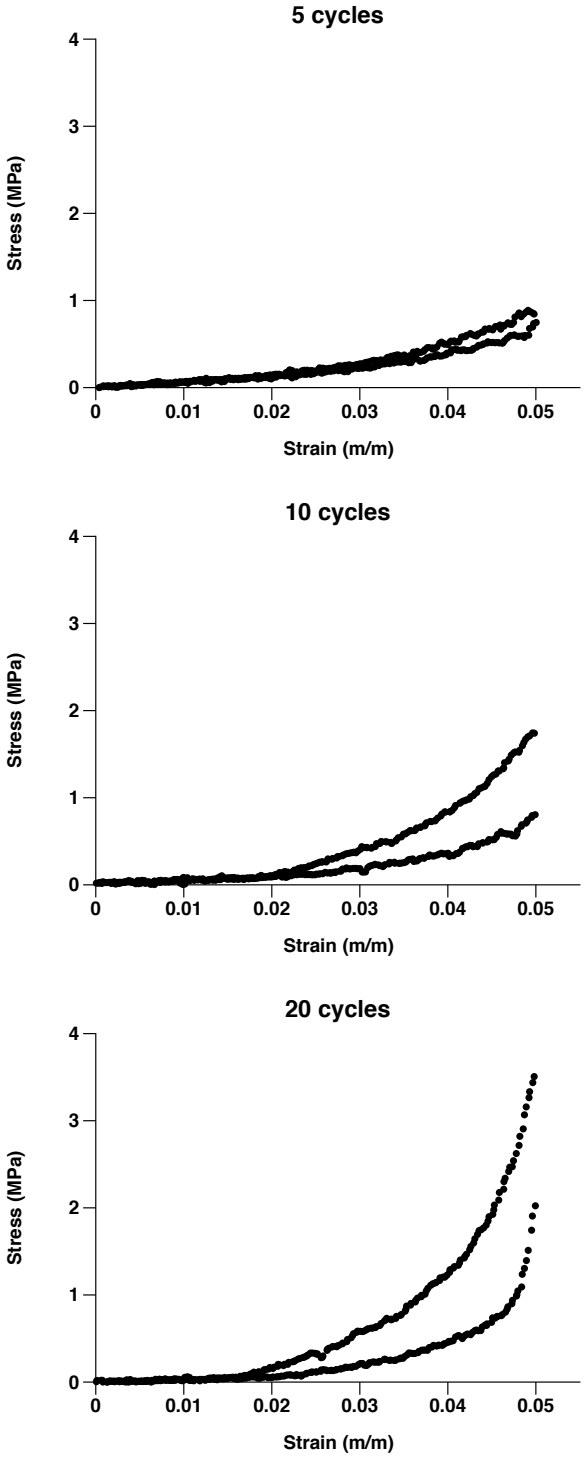

Figure B.17: Representative stress-strain curves obtained via 3-point bending of collagen scaffolds mineralized for either 5, 10, or 20 mineralization cycles.

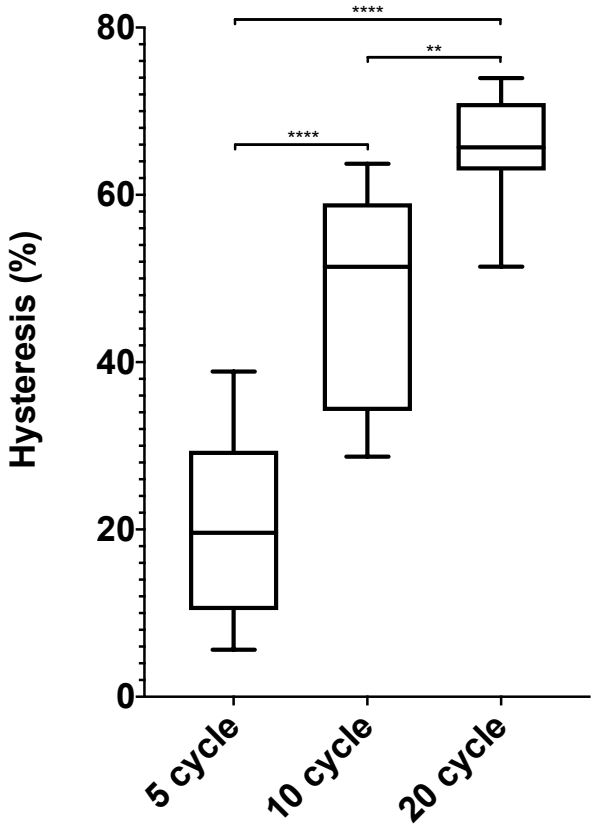

Figure B.18: Hysteresis in relation to the number of mineralization cycles collagen scaffolds were treated with. Whiskers indicate min/max values. $^{**}p \leq 0.01$, $^{****}p \leq 0.0001$.

Bibliography

[1] Zhi-Ye Qiu, Yun Cui, and Xiu-Mei Wang. Natural Bone Tissue and Its Biomimetic. In *Mineralized Collagen Bone Graft Substitutes*, pages 1–22. Elsevier, 2019.

[2] Usha Kini and B N Nandeesh. Physiology of Bone Formation, Remodeling, and Metabolism BT - Radionuclide and Hybrid Bone Imaging. pages 29–57. Springer Berlin Heidelberg, Berlin, Heidelberg, 2012. ISBN 978-3-642-02400-9. URL https://doi.org/10.1007/978-3-642-02400-9{_}2.

[3] Bart Clarke. Normal bone anatomy and physiology. *Clinical journal of the American Society of Nephrology*, 3(Supplement 3):S131–S139, 2008. ISSN 1555-9041.

[4] George Bou-Gharios, David Abraham, and Benoit de Crombrugghe. Type I collagen structure, synthesis, and regulation. In *Principles of bone biology*, pages 295–337. Elsevier, 2020.

[5] Matthew D Shoulders and Ronald T Raines. Collagen structure and stability. *Annual review of biochemistry*, 78:929–958, 2009. ISSN 0066-4154.

[6] Joseph P R O Orgel, Andrew Miller, Thomas C Irving, Robert F Fischetti, Andrew P Hammersley, and Tim J Wess. The in situ supermolecular structure of type I collagen. *Structure*, 9(11):1061–1069, 2001. ISSN 0969-2126.

[7] Ingomar Jäger and Peter Fratzl. Mineralized collagen fibrils: a mechanical model with a staggered arrangement of mineral particles. *Biophysical journal*, 79(4):1737–1746, 2000. ISSN 0006-3495.

[8] Xinhua Liu, Chi Zheng, Xiaomin Luo, Xuechuan Wang, and Huie Jiang. Recent advances of collagen-based biomaterials: Multi-hierarchical structure, modification and biomedical applications. *Materials Science and Engineering: C*, 99:1509–1522, 2019. ISSN 0928-4931. doi: https://doi.org/10.1016/j.msec.2019.02.070. URL http://www.sciencedirect.com/science/article/pii/S092849311831765X.

[9] Minqi Li, Tomoka Hasegawa, Hideo Masuki, Zhusheng Liu, Ying Guo, Reiko Suzuki, Tsuneyuki Yamamoto, Paulo H L Freitas, and Norio Amizuka. Ultrastructural assessment of mineral crystallization and collagen mineralization in bone. *Journal of Oral Biosciences*, 52(2):94–99, 2010. ISSN 1349-0079.

[10] Brigitte Wopenka and Jill D Pasteris. A mineralogical perspective on the apatite in bone. *Materials Science and Engineering: C*, 25(2):131–143, 2005. ISSN 0928-4931.

[11] Aleksandra Laskus and Joanna Kolmas. Ionic substitutions in non-Apatitic calcium phosphates. *International journal of molecular sciences*, 18(12):2542, 2017.

[12] Sang Soo Jee, Rajendra Kumar Kasinath, Elaine DiMasi, Yi-Yeoun Kim, and Laurie Gower. Oriented hydroxyapatite in turkey tendon mineralized via the polymer-induced liquid-precursor (PILP) process. *CrystEngComm*, 13(6):2077–2083, 2011.

[13] Fabio Nudelman, Alexander J Lausch, Nico A J M Sommerdijk, and Eli D Sone. In vitro models of collagen biomineralization. *Journal of structural biology*, 183 (2):258–269, 2013. ISSN 1047-8477.

[14] ZuFu Lu, Jiao Jiao Li, and Hala Zreiqat. Bone-Biomimetic Biomaterial and Cell Fate Determination. In *A Tissue Regeneration Approach to Bone and Cartilage Repair*, pages 119–146. Springer, 2015.

[15] S Weiner and P Zaslansky. Structure-mechanical function relations in bones and teeth. In *Learning from Nature How to Design New Implantable Biomaterialsis: From Biomineralization Fundamentals to Biomimetic Materials and Processing Routes*, pages 3–13. Springer, 2004.

[16] Robert A Robinson and Michael L Watson. Crystal-collagen relationships in bone as observed in the electron microscope. III. Crystal and collagen morphology as a function of age. *Annals of the New York Academy of Sciences*, 60(5): 596–630, 1955. ISSN 0077-8923.

[17] Aaron S Posner and Foster Betts. Synthetic amorphous calcium phosphate and its relation to bone mineral structure. *Accounts of Chemical Research*, 8(8): 273–281, 1975. ISSN 0001-4842.

[18] Sergey V Dorozhkin. Amorphous calcium (ortho) phosphates. *Acta Biomateri-*

alia, 6(12):4457–4475, 2010. ISSN 1742-7061.

[19] Julia Mahamid, Amnon Sharir, Lia Addadi, and Steve Weiner. Amorphous calcium phosphate is a major component of the forming fin bones of zebrafish: Indications for an amorphous precursor phase. *Proceedings of the National Academy of Sciences*, 105(35):12748–12753, 2008. ISSN 0027-8424.

[20] Shasha Yao, Biao Jin, Zhaoming Liu, Changyu Shao, Ruibo Zhao, Xiaoyu Wang, and Ruikang Tang. Biomineralization: From material tactics to biological strategy. *Advanced Materials*, 29(14):1605903, 2017. ISSN 0935-9648.

[21] Helmut Cölfen. Bio-inspired mineralization using hydrophilic polymers. In *Biomineralization II*, pages 1–77. Springer, 2006.

[22] Denis Gebauer and Helmut Cölfen. Prenucleation clusters and non-classical nucleation. *Nano Today*, 6(6):564–584, 2011. ISSN 1748-0132.

[23] Laurie B Gower. Biomimetic model systems for investigating the amorphous precursor pathway and its role in biomineralization. *Chemical Reviews*, 108(11): 4551–4627, 2008. ISSN 00092665. doi: 10.1021/cr800443h.

[24] J D Currey. The many adaptations of bone. *Journal of biomechanics*, 36(10): 1487–1495, 2003. ISSN 0021-9290.

[25] Steve Weiner and H Daniel Wagner. The material bone: structure-mechanical function relations. *Annual review of materials science*, 28(1):271–298, 1998. ISSN 0084-6600.

[26] Natalie Reznikov, Ron Shahar, and Steve Weiner. Bone hierarchical structure

in three dimensions. *Acta Biomaterialia*, 10(9):3815–3826, 2014. ISSN 1742-7061. doi: https://doi.org/10.1016/j.actbio.2014.05.024. URL http://www.sciencedirect.com/science/article/pii/S1742706114002360.

[27] Ridha Hambli and Abdelwahed Barkaoui. Physically based 3D finite element model of a single mineralized collagen microfibril. *Journal of Theoretical Biology*, 301:28–41, 2012. ISSN 0022-5193. doi: https://doi.org/10.1016/j.jtbi.2012.02.007. URL http://www.sciencedirect.com/science/article/pii/S0022519312000781.

[28] D T O'Connor, K I Elkhodary, Y Fouad, M S Greene, F A Sabet, J Qian, Y Zhang, W K Liu, and I Jasiuk. Modeling orthotropic elasticity, localized plasticity and fracture in trabecular bone. *Computational Mechanics*, 58(3): 423–439, 2016. ISSN 1432-0924. doi: 10.1007/s00466-016-1301-3. URL https://doi.org/10.1007/s00466-016-1301-3.

[29] Arun K Nair, Alfonso Gautieri, Shu-Wei Chang, and Markus J Buehler. Molecular mechanics of mineralized collagen fibrils in bone. *Nature communications*, 4:1724, 2013. ISSN 2041-1723.

[30] Kuangshin Tai, Hang J Qi, and Christine Ortiz. Effect of mineral content on the nanoindentation properties and nanoscale deformation mechanisms of bovine tibial cortical bone. *Journal of Materials Science: Materials in Medicine*, 16 (10):947–959, 2005. ISSN 1573-4838. doi: 10.1007/s10856-005-4429-9. URL https://doi.org/10.1007/s10856-005-4429-9.

[31] Lars Mulder, Jan Harm Koolstra, Jaap M J den Toonder, and Theo M G J

van Eijden. Relationship between tissue stiffness and degree of mineralization of developing trabecular bone. *Journal of Biomedical Materials Research Part A*, 84(2):508–515, 2008. ISSN 1549-3296.

[32] Adrian B Mann. Nanomechanical Properties of Solid Surfaces and Thin Films BT - Nanotribology and Nanomechanics I: Measurement Techniques and Nanomechanics. pages 391–437. Springer Berlin Heidelberg, Berlin, Heidelberg, 2011. ISBN 978-3-642-15283-2. doi: 10.1007/978-3-642-15283-2_9. URL https://doi.org/10.1007/978-3-642-15283-2{_}9.

[33] Abdelwahed Barkaoui, Brahim Tlili, Ana Vercher-Martínez, and Ridha Hambli. A multiscale modelling of bone ultrastructure elastic proprieties using finite elements simulation and neural network method. *Computer Methods and Programs in Biomedicine*, 134:69–78, 2016. ISSN 0169-2607. doi: https://doi.org/10.1016/j.cmpb.2016.07.005. URL http://www.sciencedirect.com/science/article/pii/S0169260716301109.

[34] Jacqueline H Cole and Marjolein C H van der Meulen. Whole bone mechanics and bone quality. *Clinical Orthopaedics and Related Research®*, 469(8):2139–2149, 2011. ISSN 0009-921X.

[35] Subrata Pal. *Design of artificial human joints & organs*. Springer, 2014. ISBN 146146255X.

[36] John D Currey. Role of collagen and other organics in the mechanical properties of bone. *Osteoporosis International*, 14(5):29–36, 2003. ISSN 0937-941X.

[37] Donald T Reilly and Albert H Burstein. The elastic and ultimate properties

of compact bone tissue. *Journal of Biomechanics*, 8(6):393–405, 1975. ISSN 0021-9290. doi: https://doi.org/10.1016/0021-9290(75)90075-5. URL http://www.sciencedirect.com/science/article/pii/0021929075900755.

[38] Peter Fratzl, H S Gupta, E P Paschalis, and P Roschger. Structure and mechanical quality of the collagen–mineral nano-composite in bone. *Journal of materials chemistry*, 14(14):2115–2123, 2004.

[39] J D Currey. Mechanical properties of bone tissues with greatly differing functions. *Journal of Biomechanics*, 12(4):313–319, 1979. ISSN 0021-9290. doi: https://doi.org/10.1016/0021-9290(79)90073-3. URL http://www.sciencedirect.com/science/article/pii/0021929079900733.

[40] John D Currey, Tomas Landete-Castillejos, J Estevez, Fernando Ceacero, Augusto Olguin, A Garcia, and Laureano Gallego. The mechanical properties of red deer antler bone when used in fighting. *Journal of Experimental Biology*, 212(24):3985–3993, 2009. ISSN 0022-0949.

[41] UWHD Akiva, H Daniel Wagner, and Steve Weiner. Modelling the three-dimensional elastic constants of parallel-fibred and lamellar bone. *Journal of Materials Science*, 33(6):1497–1509, 1998. ISSN 0022-2461.

[42] Hyoung Seop Kim, Sun Ig Hong, and Sun Jae Kim. On the rule of mixtures for predicting the mechanical properties of composites with homogeneously distributed soft and hard particles. *Journal of Materials Processing Technology*, 112(1):109–113, 2001. ISSN 0924-0136. doi: https://doi.org/10.1016/S0924-0136(01)00565-9. URL http://www.sciencedirect.com/

science/article/pii/S0924013601005659.

[43] John D Currey. *The mechanical adaptations of bones*. Princeton University Press, 2014. ISBN 1400853729.

[44] W Voigt. Ueber die Beziehung zwischen den beiden Elasticitätsconstanten isotroper Körper. *Annalen der Physik*, 274(12):573–587, jan 1889. ISSN 0003-3804. doi: 10.1002/andp.18892741206. URL https://doi.org/10.1002/andp.18892741206.

[45] Andras Reuss. Berechnung der fließgrenze von mischkristallen auf grund der plastizitätsbedingung für einkristalle. *ZAMM-Journal of Applied Mathematics and Mechanics/Zeitschrift für Angewandte Mathematik und Mechanik*, 9(1):49–58, 1929. ISSN 0044-2267.

[46] B K Sarkar. Estimation of composite strength by a modified rule of mixtures incorporating defects. *Bulletin of Materials Science*, 21(4):329–333, 1998. ISSN 0250-4707.

[47] Jae-Young Rho, Liisa Kuhn-Spearing, and Peter Zioupos. Mechanical properties and the hierarchical structure of bone. *Medical Engineering & Physics*, 20(2):92–102, 1998. ISSN 1350-4533. doi: https://doi.org/10.1016/S1350-4533(98)00007-1. URL http://www.sciencedirect.com/science/article/pii/S1350453398000071.

[48] Baohua Ji and Huajian Gao. Elastic properties of nanocomposite structure of bone. *Composites Science and Technology*, 66(9):1212–1218, 2006. ISSN

0266-3538. doi: https://doi.org/10.1016/j.compscitech.2005.10.017. URL http://www.sciencedirect.com/science/article/pii/S0266353805003714.

[49] Sabah Nobakhti and Sandra J Shefelbine. On the relation of bone mineral density and the elastic modulus in healthy and pathologic bone. *Current osteoporosis reports*, 16(4):404–410, 2018. ISSN 1544-1873.

[50] Iwona Jasiuk. Micromechanics of bone modeled as a composite material. In *Micromechanics and Nanomechanics of Composite Solids*, pages 281–306. Springer, 2018.

[51] Elham Alizadeh, Mehdi Dehestani, and Philippe Zysset. An efficient two-scale 3D FE model of the bone fibril array: comparison of anisotropic elastic properties with analytical methods and micro-sample testing. *Biomechanics and modeling in mechanobiology*, 2020. ISSN 1617-7959.

[52] P Zioupos and J D Currey. Changes in the Stiffness, Strength, and Toughness of Human Cortical Bone With Age. *Bone*, 22(1):57–66, 1998. ISSN 8756-3282. doi: https://doi.org/10.1016/S8756-3282(97)00228-7. URL http://www.sciencedirect.com/science/article/pii/S8756328297002287.

[53] J L Baker and C G Haugh. Mechanical properties of bone: a review. *Transactions of the ASAE*, 22(3):678–687, 1979.

[54] Steven A Goldstein, Douglas L Wilson, David A Sonstegard, and Larry S Matthews. The mechanical properties of human tibial trabecular bone as a function of metaphyseal location. *Journal of Biomechanics*, 16(12):965–969, 1983.

ISSN 0021-9290. doi: https://doi.org/10.1016/0021-9290(83)90097-0. URL http://www.sciencedirect.com/science/article/pii/0021929083900970.

[55] Johanna Warshaw, Timothy G Bromage, Carl J Terranova, and Donald H Enlow. Collagen fiber orientation in primate long bones. *The Anatomical Record*, 300(7):1189–1207, 2017. ISSN 1932-8486.

[56] Christopher M Riggs, L C Vaughan, G Paul Evans, L E Lanyon, and Alan Boyde. Mechanical implications of collagen fibre orientation in cortical bone of the equine radius. *Anatomy and embryology*, 187(3):239–248, 1993. ISSN 0340-2061.

[57] Rinaldo Florencio-Silva, Gisela Rodrigues da Silva Sasso, Estela Sasso-Cerri, Manuel Jesus Simões, and Paulo Sérgio Cerri. Biology of bone tissue: structure, function, and factors that influence bone cells. *BioMed research international*, 2015, 2015. ISSN 2314-6133.

[58] Mattia Capulli, Riccardo Paone, and Nadia Rucci. Osteoblast and osteocyte: Games without frontiers. *Archives of Biochemistry and Biophysics*, 561:3–12, 2014. ISSN 0003-9861. doi: https://doi.org/10.1016/j.abb.2014.05.003. URL http://www.sciencedirect.com/science/article/pii/S0003986114001520.

[59] Anna Teti. Bone development: overview of bone cells and signaling. *Current osteoporosis reports*, 9(4):264, 2011. ISSN 1544-1873.

[60] Koichi Matsuo and Naoko Irie. Osteoclast–osteoblast communication. *Archives of Biochemistry and Biophysics*, 473(2):201–209, 2008. ISSN 0003-9861. doi:

https://doi.org/10.1016/j.abb.2008.03.027. URL http://www.sciencedirect.com/science/article/pii/S0003986108001628.

[61] Agnes D Berendsen and Bjorn R Olsen. Bone development. *Bone*, 80:14–18, 2015. ISSN 8756-3282.

[62] Erik Holm, Jane E Aubin, Graeme K Hunter, Frank Beier, and Harvey A Goldberg. Loss of bone sialoprotein leads to impaired endochondral bone development and mineralization. *Bone*, 71:145–154, 2015. ISSN 8756-3282.

[63] J Gordon Betts, Peter DeSaix, Eddie Johnson, Jody E Johnson, Oksana Korol, Dean H Kruse, Brandon Poe, James A Wise, and Kelly A Young. Anatomy and physiology. 2014.

[64] Heiani Touaitahuata, Gaelle Cres, Sylvain de Rossi, Virginie Vives, and Anne Blangy. The mineral dissolution function of osteoclasts is dispensable for hypertrophic cartilage degradation during long bone development and growth. *Developmental biology*, 393(1):57–70, 2014. ISSN 0012-1606.

[65] J F Stoltz, D Dumas, X Wang, E Payan, D Mainard, F Paulus, G Maurice, P Netter, and S Muller. Influence of mechanical forces on cells and tissues. *Biorheology*, 37(1-2):3–14, 2000. ISSN 0006-355X.

[66] J Wolff. The law of transformation of bone. *Verlag von August Hirschwald*, 1892.

[67] Jean-François Stoltz, Jacques Magdalou, Daniel George, Yun Chen, Yinping Li, Natalia De Isla, Xiaohua He, and Yves Remond. Influence of mechan-

ical forces on bone: Introduction to mechanobiology and mechanical adaptation concept. *Journal of Cellular Immunotherapy*, 4(1):10–12, 2018. ISSN 2352-1775. doi: https://doi.org/10.1016/j.jocit.2018.09.003. URL http://www.sciencedirect.com/science/article/pii/S2352177518300086.

[68] S Weinbaum, S C Cowin, and Yu Zeng. A model for the excitation of osteocytes by mechanical loading-induced bone fluid shear stresses. *Journal of Biomechanics*, 27(3):339–360, 1994. ISSN 0021-9290. doi: https://doi.org/10.1016/0021-9290(94)90010-8. URL http://www.sciencedirect.com/science/article/pii/0021929094900108.

[69] Bettina M Willie, Elizabeth Zimmermann, Isabela Vitienes, Russell P Main, and Svetlana V Komarova. Bone adaptation: safety factors and load predictability in shaping skeletal form. *Bone*, page 115114, 2019. ISSN 8756-3282. doi: https://doi.org/10.1016/j.bone.2019.115114. URL http://www.sciencedirect.com/science/article/pii/S8756328219304077.

[70] Peter V Giannoudis, Thomas A Einhorn, and David Marsh. Fracture healing: the diamond concept. *Injury*, 38:S3–S6, 2007. ISSN 0020-1383.

[71] Rozalia Dimitriou, Eleftherios Tsiridis, and Peter V Giannoudis. Current concepts of molecular aspects of bone healing. *Injury*, 36(12):1392–1404, 2005. ISSN 0020-1383.

[72] K D Hankenson, K Gagne, and M Shaughnessy. Extracellular signaling molecules to promote fracture healing and bone regeneration. *Advanced drug delivery reviews*, 94:3–12, 2015. ISSN 0169-409X.

[73] Claudia Schlundt, Thaqif El Khassawna, Alessandro Serra, Anke Dienelt, Sebastian Wendler, Hanna Schell, Nico van Rooijen, Andreas Radbruch, Richard Lucius, and Susanne Hartmann. Macrophages in bone fracture healing: their essential role in endochondral ossification. *Bone*, 106:78–89, 2018. ISSN 8756-3282.

[74] Z Liu, F P Luyten, Johan Lammens, and Jan Dequeker. Molecular signaling in bone fracture healing and distraction osteogenesis. *Histology and histopathology*, 14(2):587–595, 1999. ISSN 0213-3911.

[75] Thomas A Einhorn and Louis C Gerstenfeld. Fracture healing: mechanisms and interventions. *Nature Reviews Rheumatology*, 11(1):45, 2015. ISSN 1759-4804.

[76] X Su, K Sun, F Z Cui, and W J Landis. Organization of apatite crystals in human woven bone. *Bone*, 32(2):150–162, 2003. ISSN 8756-3282.

[77] L B Gower. Biomimetic mineralization of collagen. In *Biomineralization and Biomaterials*, pages 187–232. Elsevier, 2016.

[78] Hang Ping, Hao Xie, Yamin Wan, Zhixiao Zhang, Jing Zhang, Mingyu Xiang, Jingjing Xie, Hao Wang, Weimin Wang, and Zhengyi Fu. Confinement controlled mineralization of calcium carbonate within collagen fibrils. *Journal of Materials Chemistry B*, 4(5):880–886, 2016.

[79] Bram Cantaert, Elia Beniash, and Fiona C Meldrum. Nanoscale confinement controls the crystallization of calcium phosphate: Relevance to bone formation. *Chemistry–A European Journal*, 19(44):14918–14924, 2013. ISSN 0947-6539.

[80] Gheorghe Tomoaia and Roxana-Diana Pasca. On the Collagen Mineralization. A Review. *Clujul medical (1957)*, 88(1):15–22, 2015. ISSN 1222-2119. doi: 10.15386/cjmed-359. URL https://www.ncbi.nlm.nih.gov/pubmed/26528042https://www.ncbi.nlm.nih.gov/pmc/articles/PMC4508610/.

[81] Benedetto Marelli, Chiara E Ghezzi, Yu Ling Zhang, Isabelle Rouiller, Jake E Barralet, and Showan N Nazhat. Fibril formation pH controls intrafibrillar collagen biomineralization in vitro and in vivo. *Biomaterials*, 37:252–259, 2015. ISSN 0142-9612.

[82] Ling Chen, Robin Jacquet, Elizabeth Lowder, and William J Landis. Refinement of collagen–mineral interaction: A possible role for osteocalcin in apatite crystal nucleation, growth and development. *Bone*, 71:7–16, 2015. ISSN 8756-3282.

[83] B L Foster, M Ao, C Willoughby, Y Soenjaya, E Holm, L Lukashova, A B Tran, H F Wimer, P M Zerfas, F H Nociti, K R Kantovitz, B D Quan, E D Sone, H A Goldberg, and M J Somerman. Mineralization defects in cementum and craniofacial bone from loss of bone sialoprotein. *Bone*, 78:150–164, 2015. ISSN 8756-3282. doi: https://doi.org/10.1016/j.bone.2015.05.007. URL http://www.sciencedirect.com/science/article/pii/S8756328215001787.

[84] Tomoka Hasegawa. Ultrastructure and biological function of matrix vesicles in bone mineralization. *Histochemistry and cell biology*, 149(4):289–304, 2018. ISSN 0948-6143.

[85] José Manuel Delgado-López, Federica Bertolotti, Jeppe Lyngsø, Jan Skov Peder-

sen, Antonio Cervellino, Norberto Masciocchi, and Antonietta Guagliardi. The synergic role of collagen and citrate in stabilizing amorphous calcium phosphate precursors with platy morphology. *Acta biomaterialia*, 49:555–562, 2017. ISSN 1742-7061.

[86] Jaime Gómez Morales, Raquel Fernández Penas, Cristóbal Verdugo-Escamilla, Lorenzo Degli Esposti, Francesca Oltolina, Maria Prat, Michele Iafisco, and Jorge Fernando Fernández Sánchez. Bioinspired Mineralization of Type I Collagen Fibrils with Apatite in Presence of Citrate and Europium Ions. *Crystals*, 9(1):13, 2019.

[87] Gloria Belén Ramírez-Rodríguez, José Manuel Delgado-López, Michele Iafisco, Monica Montesi, Monica Sandri, Simone Sprio, and Anna Tampieri. Biomimetic mineralization of recombinant collagen type I derived protein to obtain hybrid matrices for bone regeneration. *Journal of structural biology*, 196(2):138–146, 2016. ISSN 1047-8477.

[88] Wenhao Wang and Kelvin W K Yeung. Bone grafts and biomaterials substitutes for bone defect repair: A review. *Bioactive Materials*, 2(4):224–247, 2017. ISSN 2452-199X.

[89] Christian Rey, Christèle Combes, Christophe Drouet, and Melvin J Glimcher. Bone mineral: update on chemical composition and structure. *Osteoporosis International*, 20(6):1013–1021, 2009. ISSN 0937-941X.

[90] Laurie B Gower and Damian J Odom. Deposition of calcium carbonate films by a polymer-induced liquid-precursor (PILP) process. *Journal of Crystal Growth*,

210(4):719–734, 2000. ISSN 00220248. doi: 10.1016/S0022-0248(99)00749-6.

[91] Paul A Price, Damon Toroian, and Joo Eun Lim. Mineralization by inhibitor exclusion the calcification of collagen with fetuin. *Journal of Biological Chemistry*, 284(25):17092–17101, 2009. ISSN 0021-9258.

[92] Yan Liu, Young-Kyung Kim, Lin Dai, Nan Li, Sara O Khan, David H Pashley, and Franklin R Tay. Hierarchical and non-hierarchical mineralisation of collagen. *Biomaterials*, 32(5):1291–1300, 2011. ISSN 0142-9612.

[93] Matthew J Olszta, Xingguo Cheng, Sang Soo Jee, Rajendra Kumar, Yi-Yeoun Kim, Michael J Kaufman, Elliot P Douglas, and Laurie B Gower. Bone structure and formation: A new perspective. *Materials Science and Engineering: R: Reports*, 58(3-5):77–116, 2007. ISSN 0927-796X.

[94] Amir A Al-Munajjed, Niamh A Plunkett, John P Gleeson, Tim Weber, Christian Jungreuthmayer, Tanya Levingstone, Joachim Hammer, and Fergal J O'Brien. Development of a biomimetic collagen-hydroxyapatite scaffold for bone tissue engineering using a SBF immersion technique. *Journal of Biomedical Materials Research Part B: Applied Biomaterials: An Official Journal of The Society for Biomaterials, The Japanese Society for Biomaterials, and The Australian Society for Biomaterials and the Korean Society for Biomaterials*, 90(2): 584–591, 2009. ISSN 1552-4973.

[95] Stephen Weiner. Biomineralization: a structural perspective. *Journal of structural biology*, 163(3):229–234, 2008. ISSN 1047-8477.

[96] Dawei Zhang, Xiaowei Wu, Jingdi Chen, and Kaili Lin. The development of

collagen based composite scaffolds for bone regeneration. *Bioactive materials*, 3(1):129–138, 2018. ISSN 2452-199X.

[97] Ellis E Golub. Role of matrix vesicles in biomineralization. *Biochimica et Biophysica Acta (BBA)-General Subjects*, 1790(12):1592–1598, 2009. ISSN 0304-4165.

[98] L N Wu, B R Genge, G C Lloyd, and R E Wuthier. Collagen-binding proteins in collagenase-released matrix vesicles from cartilage. Interaction between matrix vesicle proteins and different types of collagen. *Journal of Biological Chemistry*, 266(2):1195–1203, 1991. ISSN 0021-9258.

[99] Anna Tampieri, Giancarlo Celotti, Elena Landi, Monica Sandri, Norberto Roveri, and Giuseppe Falini. Biologically inspired synthesis of bone-like composite: Self-assembled collagen fibers/hydroxyapatite nanocrystals. *Journal of Biomedical Materials Research - Part A*, 67(2):618–625, 2003. ISSN 00219304. doi: 10.1002/jbm.a.10039.

[100] Masanori Kikuchi, Soichiro Itoh, Shizuko Ichinose, Kenichi Shinomiya, and Junzo Tanaka. Self-organization mechanism in a bone-like hydroxyapatite/collagen nanocomposite synthesized in vitro and its biological reaction in vivo. *Biomaterials*, 22(13):1705–1711, 2001. ISSN 01429612. doi: 10.1016/S0142-9612(00)00305-7.

[101] M Gelinsky, P B Welzel, P Simon, A Bernhardt, and U König. Porous three-dimensional scaffolds made of mineralised collagen: Preparation and properties of a biomimetic nanocomposite material for tissue engineering of bone. *Chemical*

Engineering Journal, 137(1):84–96, 2008. ISSN 13858947. doi: 10.1016/j.cej.2007.09.029.

[102] Max M Villa, Liping Wang, Jianping Huang, David W Rowe, and Mei Wei. Bone tissue engineering with a collagenhydroxyapatite scaffold and culture expanded bone marrow stromal cells. *Journal of Biomedical Materials Research Part B: Applied Biomaterials*, 103(2):243–253, 2015.

[103] Daniel V Krogstad, Dongbo Wang, and Sheng Lin-Gibson. Kinetics of aggregation and crystallization of polyaspartic acid stabilized calcium phosphate particles at high concentrations. *Biomacromolecules*, 16(5):1550–1555, 2015. ISSN 1525-7797.

[104] Yimin Qiu, Erik Poppleton, Arya Mekkat, Hongtao Yu, Sourav Banerjee, Sandra E Wiley, Jack E Dixon, David L Kaplan, Yu-Shan Lin, and Barbara Brodsky. Enzymatic phosphorylation of ser in a Type I collagen peptide. *Biophysical journal*, 115(12):2327–2335, 2018. ISSN 0006-3495.

[105] Karl E Kadler, Yoshio Hojima, and D J Prockop. Assembly of collagen fibrils de novo by cleavage of the type I pC-collagen with procollagen C-proteinase. Assay of critical concentration demonstrates that collagen self-assembly is a classical example of an entropy-driven process. *Journal of Biological Chemistry*, 262(32): 15696–15701, 1987. ISSN 0021-9258.

[106] Garif Yalak and Bjorn R Olsen. Proteomic database mining opens up avenues utilizing extracellular protein phosphorylation for novel therapeutic applications. *Journal of translational medicine*, 13(1):1–11, 2015. ISSN 1479-5876.

[107] Gurpreet S Baht, Jason O'Young, Antonia Borovina, Hong Chen, Coralee E Tye, Mikko Karttunen, Gilles A Lajoie, Graeme K Hunter, and Harvey A Goldberg. Phosphorylation of Ser136 is critical for potent bone sialoprotein-mediated nucleation of hydroxyapatite crystals. *Biochemical Journal*, 428(3):385–395, 2010. ISSN 0264-6021.

[108] Xiaoke Li and Jiang Chang. Preparation of bone-like apatitecollagen nanocomposites by a biomimetic process with phosphorylated collagen. *Journal of Biomedical Materials Research*, 85A(2):293–300, 2008.

[109] H Y Ferrel Sung. Chemical phosphorylation of food proteins by sodium trimetaphosphate. *J Food Sci*, 47:716–724, 1982.

[110] Sang Soo Jee. *Development of collagen-hydroxyapatite nanostructured composites via a calcium phosphate precursor mechanism*. University of Florida, 2008. ISBN 110926450X.

[111] Taili T Thula, Douglas E Rodriguez, Myong Hwa Lee, Laura Pendi, Jacob Podschun, and Laurie B Gower. In vitro mineralization of dense collagen substrates: A biomimetic approach toward the development of bone-graft materials. *Acta Biomaterialia*, 7(8):3158–3169, 2011. ISSN 1742-7061. doi: https://doi.org/10.1016/j.actbio.2011.04.014. URL http://www.sciencedirect.com/science/article/pii/S174270611100170X.

[112] Harvey A Goldberg, Kevin J Warner, Michael C Li, and Graeme K Hunter. Binding of bone sialoprotein, osteopontin and synthetic polypeptides to hydroxyapatite. *Connective tissue research*, 42(1):25–37, 2001. ISSN 0300-8207.

[113] Yipin Qi, Zhou Ye, Alex Fok, Brian N Holmes, Montserrat Espanol, Maria-Pau Ginebra, and Conrado Aparicio. Effects of molecular weight and concentration of poly (acrylic acid) on biomimetic mineralization of collagen. *ACS biomaterials science & engineering*, 4(8):2758–2766, 2018. ISSN 2373-9878.

[114] Yan Liu, Nan Li, Yi-pin Qi, Lin Dai, Thomas E Bryan, Jing Mao, David H Pashley, and Franklin R Tay. Intrafibrillar collagen mineralization produced by biomimetic hierarchical nanoapatite assembly. *Advanced materials (Deerfield Beach, Fla.)*, 23(8):975–980, feb 2011. ISSN 1521-4095. doi: 10.1002/adma.201003882. URL https://pubmed.ncbi.nlm.nih.gov/21341310https://www.ncbi.nlm.nih.gov/pmc/articles/PMC3137871/.

[115] Taili T Thula, Felicia Svedlund, Douglas E Rodriguez, Jacob Podschun, Laura Pendi, and Laurie B Gower. Mimicking the nanostructure of bone: comparison of polymeric process-directing agents. *Polymers*, 3(1):10–35, 2011.

[116] Franklin R Tay and David H Pashley. Guided tissue remineralisation of partially demineralised human dentine. *Biomaterials*, 29(8):1127–1137, 2008. ISSN 0142-9612. doi: https://doi.org/10.1016/j.biomaterials.2007.11.001. URL http://www.sciencedirect.com/science/article/pii/S0142961207008940.

[117] Roel G M Breuls, Timothy U Jiya, and Theo H Smit. Scaffold stiffness influences cell behavior: opportunities for skeletal tissue engineering. *The open orthopaedics journal*, 2:103–109, may 2008.

[118] P J Prendergast, R Huiskes, and K Søballe. Biophysical stimuli on cells during tissue differentiation at implant interfaces. *Journal of Biomechanics*, 30(6):

539–548, 1997.

[119] Kaustabh Ghosh and Donald E Ingber. Micromechanical control of cell and tissue development: implications for tissue engineering. *Advanced Drug Delivery Reviews*, 59(13):1306–1318, 2007.

[120] Ju Cheng, Hongyan Liu, Bingjiang Zhao, Rong Shen, Di Liu, Jinpeng Hong, Hui Wei, Pinxian Xi, Fengjuan Chen, and Decheng Bai. MC3T3-E1 preosteoblast cell-mediated mineralization of hydroxyapatite by poly-dopamine-functionalized graphene oxide. *Journal of Bioactive and Compatible Polymers*, 30(3):289–301, 2015. ISSN 0883-9115.

[121] D Jhala, H Rather, and R Vasita. Polycaprolactone–chitosan nanofibers influence cell morphology to induce early osteogenic differentiation. *Biomaterials science*, 4(11):1584–1595, 2016.

[122] Rowena McBeath, Dana M Pirone, Celeste M Nelson, Kiran Bhadriraju, and Christopher S Chen. Cell shape, cytoskeletal tension, and RhoA regulate stem cell lineage commitment. *Developmental cell*, 6(4):483–495, 2004.

[123] Chinnapaka Somaiah, Atul Kumar, Darilang Mawrie, Amit Sharma, Suraj Dasharath Patil, Jina Bhattacharyya, Rajaram Swaminathan, and Bithiah Grace Jaganathan. Collagen promotes higher adhesion, survival and proliferation of mesenchymal stem cells. *PloS one*, 10(12), 2015.

[124] Adam J Engler, Shamik Sen, H Lee Sweeney, and Dennis E Discher. Matrix Elasticity Directs Stem Cell Lineage Specification. *Cell*, 126(4):677–689, 2006.

[125] V Campana, G Milano, E Pagano, M Barba, C Cicione, G Salonna, W Lattanzi, and G Logroscino. Bone substitutes in orthopaedic surgery: from basic science to clinical practice. *Journal of materials science. Materials in medicine*, 25 (10):2445–2461, oct 2014. ISSN 1573-4838. doi: 10.1007/s10856-014-5240-2. URL https://www.ncbi.nlm.nih.gov/pubmed/24865980https://www.ncbi.nlm.nih.gov/pmc/articles/PMC4169585/.

[126] W Arbuthnot Lane. Some remarks on the treatment of fractures. *British medical journal*, 1(1790):861, 1895.

[127] L E Lanyon. Functional strain as a determinant for bone remodeling. *Calcified tissue international*, 36(1):S56–S61, 1984. ISSN 0171-967X.

[128] Qizhi Chen. Biomaterials for bone tissue engineering. In *Emerging Trends in Cell and Gene Therapy*, pages 563–594. Springer, 2013.

[129] Safdar N Khan, Frank P Cammisa Jr, Harvinder S Sandhu, Ashish D Diwan, Federico P Girardi, and Joseph M Lane. The biology of bone grafting. *JAAOS-Journal of the American Academy of Orthopaedic Surgeons*, 13(1):77–86, 2005. ISSN 1067-151X.

[130] Ralph K Ghormley. Choice of bone graft methods in bone and joint surgery. *Annals of surgery*, 115(3):427, 1942.

[131] Gerald Zimmermann and Arash Moghaddam. Allograft bone matrix versus synthetic bone graft substitutes. *Injury*, 42:S16–S21, 2011. ISSN 0020-1383. doi: https://doi.org/10.1016/j.injury.2011.06.199. URL http://www.sciencedirect.com/science/article/pii/S0020138311003020.

[132] M Manyalich, A Navarro, J Koller, B Loty, A de Guerra, O Cornu, G Vabels, P M Fornasari, A N Costa, I Siska, M Hirn, N Franz, B Miranda, A Kaminski, I Uhrynowska, J Van Baare, E Trias, C Fernández, T de By, S Poniatowski, and R Carbonell. European Quality System for Tissue Banking. *Transplantation Proceedings*, 41(6):2035–2043, 2009. ISSN 0041-1345. doi: https://doi.org/10.1016/j.transproceed.2009.06.157. URL http://www.sciencedirect.com/science/article/pii/S0041134509008926.

[133] Christian Delloye, Olivier Cornu, V Druez, and Olivier Barbier. Bone allografts: what they can offer and what they cannot. *The Journal of bone and joint surgery. British volume*, 89(5):574–580, 2007. ISSN 0301-620X.

[134] Paul T Rubery. Enhancing allograft bone healing through gene therapy. *Spine*, 35(17):1640–1647, 2010. ISSN 0362-2436.

[135] Timothy T Roberts and Andrew J Rosenbaum. Bone grafts, bone substitutes and orthobiologics: the bridge between basic science and clinical advancements in fracture healing. *Organogenesis*, 8(4):114–124, 2012. ISSN 1547-6278.

[136] Fernando Judas, Maria Joao Saavedra, Alexandrina Ferreira Mendes, and Rui Dias. Cortical strut allografting in reconstructive orthopaedic surgery. 2011.

[137] Jordi Tomás Hernández and Kim Holck. Periprosthetic femoral fractures: When I use strut grafts and why? *Injury*, 46:S43–S46, 2015. ISSN 0020-1383. doi: https://doi.org/10.1016/j.injury.2015.08.012. URL http://www.sciencedirect.com/science/article/pii/S0020138315004842.

[138] Andrew P Van Houwelingen and Michael D McKee. Treatment of osteopenic

humeral shaft nonunion with compression plating, humeral cortical allograft struts, and bone grafting. *Journal of orthopaedic trauma*, 19(1):36–42, 2005. ISSN 0890-5339.

[139] Tim Rolvien, Mike Barbeck, Sabine Wenisch, Michael Amling, and Matthias Krause. Cellular Mechanisms Responsible for Success and Failure of Bone Substitute Materials. *International journal of molecular sciences*, 19(10):2893, sep 2018. ISSN 1422-0067. doi: 10.3390/ijms19102893. URL https://pubmed.ncbi.nlm.nih.gov/30249051https://www.ncbi.nlm.nih.gov/pmc/articles/PMC6213546/.

[140] Nicholas J Lash, Julian A Feller, Lachlan M Batty, Jason Wasiak, and Anneka K Richmond. Bone grafts and bone substitutes for opening-wedge osteotomies of the knee: a systematic review. *Arthroscopy: The Journal of Arthroscopic & Related Surgery*, 31(4):720–730, 2015. ISSN 0749-8063.

[141] Gerardo Presbítero, Marco A L Hernandez-Rodríguez, Geo R Contreras-Hernandez, José Félix Vilchez, Orlando Susarrey, and David Gutiérrez. Micro-damage distribution in fatigue fractures of bone allografts following gamma-ray exposure. *Acta of bioengineering and biomechanics*, 19(4):43–53, 2017. ISSN 1509-409X.

[142] Yingchao Su, Irsalan Cockerill, Yufeng Zheng, Liping Tang, Yi-Xian Qin, and Donghui Zhu. Biofunctionalization of metallic implants by calcium phosphate coatings. *Bioactive Materials*, 4:196–206, 2019. ISSN 2452-199X. doi: https://doi.org/10.1016/j.bioactmat.2019.05.001. URL http://www.sciencedirect.

com/science/article/pii/S2452199X19300222.

[143] Joy-anne N Oliver, Yingchao Su, Xiaonan Lu, Po-Hsuen Kuo, Jincheng Du, and Donghui Zhu. Bioactive glass coatings on metallic implants for biomedical applications. *Bioactive Materials*, 4:261–270, 2019. ISSN 2452-199X. doi: https://doi.org/10.1016/j.bioactmat.2019.09.002. URL http://www.sciencedirect.com/science/article/pii/S2452199X19300465.

[144] Qizhi Chen and George A Thouas. Metallic implant biomaterials. *Materials Science and Engineering: R: Reports*, 87:1–57, 2015. ISSN 0927-796X. doi: https://doi.org/10.1016/j.mser.2014.10.001. URL http://www.sciencedirect.com/science/article/pii/S0927796X14001077.

[145] Mitsuo Niinomi. *Metals for biomedical devices*. Woodhead publishing, 2019. ISBN 0081026676.

[146] Mohsen Taheri Andani, Narges Shayesteh Moghaddam, Christoph Haberland, David Dean, Michael J Miller, and Mohammad Elahinia. Metals for bone implants. Part 1. Powder metallurgy and implant rendering. *Acta Biomaterialia*, 10 (10):4058–4070, 2014. ISSN 1742-7061. doi: https://doi.org/10.1016/j.actbio.2014.06.025. URL http://www.sciencedirect.com/science/article/pii/S1742706114002724.

[147] Ricardo Tejero, Eduardo Anitua, and Gorka Orive. Toward the biomimetic implant surface: Biopolymers on titanium-based implants for bone regeneration. *Progress in Polymer Science*, 39(7):1406–1447, 2014. ISSN 0079-6700. doi: https://doi.org/10.1016/j.progpolymsci.2014.01.001. URL http:

//www.sciencedirect.com/science/article/pii/S0079670014000100.

[148] Vasiliki C Panagiotopoulou, Peter Varga, R Geoff Richards, Boyko Gueorguiev, and Peter V Giannoudis. Late screw-related complications in locking plating of proximal humerus fractures: A systematic review. *Injury*, 50 (12):2176–2195, 2019. ISSN 0020-1383. doi: https://doi.org/10.1016/j.injury.2019.11.002. URL http://www.sciencedirect.com/science/article/pii/S0020138319306989.

[149] Geetha Manivasagam, Durgalakshmi Dhinasekaran, and Asokamani Rajamanickam. Biomedical implants: corrosion and its prevention-a review. *Recent patents on corrosion science*, 2010. ISSN 1877-6108.

[150] Laura Leyssens, Bart Vinck, Catherine Van Der Straeten, Floris Wuyts, and Leen Maes. Cobalt toxicity in humans—A review of the potential sources and systemic health effects. *Toxicology*, 387:43–56, 2017. ISSN 0300-483X. doi: https://doi.org/10.1016/j.tox.2017.05.015. URL http://www.sciencedirect.com/science/article/pii/S0300483X17301555.

[151] Mohd Talha, Yucong Ma, Pardeep Kumar, Yuanhua Lin, and Ambrish Singh. Role of protein adsorption in the bio corrosion of metallic implants – A review. *Colloids and Surfaces B: Biointerfaces*, 176:494–506, 2019. ISSN 0927-7765. doi: https://doi.org/10.1016/j.colsurfb.2019.01.038. URL http://www.sciencedirect.com/science/article/pii/S0927776519300414.

[152] Takashi Takizawa, Noboru Nakayama, Hisao Haniu, Kaoru Aoki, Masanori Okamoto, Hiroki Nomura, Manabu Tanaka, Atsushi Sobajima, Kazushige

Yoshida, and Takayuki Kamanaka. Titanium fiber plates for bone tissue repair. *Advanced Materials*, 30(4):1703608, 2018. ISSN 0935-9648.

[153] Michael Schinhammer, Anja C Hänzi, Jörg F Löffler, and Peter J Uggowitzer. Design strategy for biodegradable Fe-based alloys for medical applications. *Acta Biomaterialia*, 6(5):1705–1713, 2010. ISSN 1742-7061. doi: https://doi.org/10.1016/j.actbio.2009.07.039. URL http://www.sciencedirect.com/science/article/pii/S1742706109003249.

[154] Hendra Hermawan, Dominique Dubé, and Diego Mantovani. Development of degradable Fe-35Mn alloy for biomedical application. In *Advanced Materials Research*, volume 15, pages 107–112. Trans Tech Publ, 2007. ISBN 0878494294.

[155] Sai Nievethitha Sethu, Subhapradha Namashivayam, Saravanan Devendran, Selvamurugan Nagarajan, Wei-Bor Tsai, Srinivasan Narashiman, Murugesan Ramachandran, and Moorthi Ambigapathi. Nanoceramics on osteoblast proliferation and differentiation in bone tissue engineering. *International journal of biological macromolecules*, 98:67–74, 2017. ISSN 0141-8130.

[156] P V Hatton, K Hurrell-Gillingham, and I M Brook. Biocompatibility of glass-ionomer bone cements. *Journal of dentistry*, 34(8):598–601, 2006. ISSN 0300-5712.

[157] Silvia Minardi, Bruna Corradetti, Francesca Taraballi, Monica Sandri, Jeffrey Van Eps, Fernando J Cabrera, Bradley K Weiner, Anna Tampieri, and Ennio Tasciotti. Evaluation of the osteoinductive potential of a bio-inspired scaffold mimicking the osteogenic niche for bone augmentation. *Biomaterials*, 62:128–

137, 2015. ISSN 18785905. doi: 10.1016/j.biomaterials.2015.05.011.

[158] Larry L Hench, R J_ Splinter, W C Allen, and T K Greenlee. Bonding mechanisms at the interface of ceramic prosthetic materials. *Journal of biomedical materials research*, 5(6):117–141, 1971. ISSN 0021-9304.

[159] Julian R Jones, Lisa M Ehrenfried, and Larry L Hench. Optimising bioactive glass scaffolds for bone tissue engineering. *Biomaterials*, 27(7):964–973, 2006. ISSN 0142-9612.

[160] Lutz-Christian Gerhardt and Aldo R Boccaccini. Bioactive glass and glass-ceramic scaffolds for bone tissue engineering. *Materials*, 3(7):3867–3910, 2010.

[161] Larry L Hench. Bioceramics: from concept to clinic. *Journal of the american ceramic society*, 74(7):1487–1510, 1991. ISSN 0002-7820.

[162] Yue Cai, Shuang Tong, Ran Zhang, Tong Zhu, and Xukai Wang. In vitro evaluation of a bone morphogenetic protein-2 nanometer hydroxyapatite collagen scaffold for bone regeneration. *Molecular medicine reports*, 17 (4):5830–5836, apr 2018. ISSN 1791-3004. doi: 10.3892/mmr.2018.8579. URL https://www.ncbi.nlm.nih.gov/pubmed/29436646https://www.ncbi.nlm.nih.gov/pmc/articles/PMC5866027/.

[163] Beom-Su Kim, Sun-Sik Yang, and Cheol Sang Kim. Incorporation of BMP-2 nanoparticles on the surface of a 3D-printed hydroxyapatite scaffold using an ϵ-polycaprolactone polymer emulsion coating method for bone tissue engineering. *Colloids and Surfaces B: Biointerfaces*, 170:421–429, 2018. ISSN

0927-7765. doi: https://doi.org/10.1016/j.colsurfb.2018.06.043. URL http://www.sciencedirect.com/science/article/pii/S0927776518304144.

[164] Kurosh Rezwan, Q Z Chen, J J Blaker, and Aldo Roberto Boccaccini. Biodegradable and bioactive porous polymer/inorganic composite scaffolds for bone tissue engineering. *Biomaterials*, 27(18):3413–3431, 2006. ISSN 0142-9612.

[165] Michael K Danquah and Ram I Mahato. *Emerging trends in cell and gene therapy*. Springer, 2013. ISBN 162703417X.

[166] Huiqiong Yan, Xiuqiong Chen, Meixi Feng, Zaifeng Shi, Dashuai Zhang, and Qiang Lin. Layer-by-layer assembly of 3D alginate-chitosan-gelatin composite scaffold incorporating bacterial cellulose nanocrystals for bone tissue engineering. *Materials Letters*, 209:492–496, 2017. ISSN 0167-577X.

[167] Sybele Saska, Lucas Novaes Teixeira, Paulo Tambasco de Oliveira, Ana Maria Minarelli Gaspar, Sidney José Lima Ribeiro, Younes Messaddeq, and Reinaldo Marchetto. Bacterial cellulose-collagen nanocomposite for bone tissue engineering. *Journal of Materials Chemistry*, 22(41):22102–22112, 2012.

[168] Jayachandran Venkatesan and Se-Kwon Kim. Chitosan composites for bone tissue engineering—an overview. *Marine drugs*, 8(8):2252–2266, 2010.

[169] Jayachandran Venkatesan, Ira Bhatnagar, Panchanathan Manivasagan, Kyong-Hwa Kang, and Se-Kwon Kim. Alginate composites for bone tissue engineering: a review. *International journal of biological macromolecules*, 72:269–281, 2015. ISSN 0141-8130.

[170] Karen B Chien, Emmanuella Makridakis, and Ramille N Shah. Three-dimensional printing of soy protein scaffolds for tissue regeneration. *Tissue Engineering Part C: Methods*, 19(6):417–426, 2013. ISSN 1937-3384.

[171] Simone S Silva, Marina I Santos, O P Coutinho, J F Mano, and R L Reis. Physical properties and biocompatibility of chitosan/soy blended membranes. *Journal of Materials Science: Materials in Medicine*, 16(6):575–579, 2005. ISSN 0957-4530.

[172] Hyeon Joo Kim, Ung-Jin Kim, Hyun Suk Kim, Chunmei Li, Masahisa Wada, Gary G Leisk, and David L Kaplan. Bone tissue engineering with premineralized silk scaffolds. *Bone*, 42(6):1226–1234, 2008. ISSN 8756-3282.

[173] Sarindr Bhumiratana, Warren L Grayson, Andrea Castaneda, Danielle N Rockwood, Eun S Gil, David L Kaplan, and Gordana Vunjak-Novakovic. Nucleation and growth of mineralized bone matrix on silk-hydroxyapatite composite scaffolds. *Biomaterials*, 32(11):2812–2820, 2011. ISSN 0142-9612.

[174] Chunmei Li, Charu Vepari, Hyoung-Joon Jin, Hyeon Joo Kim, and David L Kaplan. Electrospun silk-BMP-2 scaffolds for bone tissue engineering. *Biomaterials*, 27(16):3115–3124, 2006. ISSN 0142-9612.

[175] A K Lynn, I V Yannas, and W Bonfield. Antigenicity and immunogenicity of collagen. *Journal of Biomedical Materials Research Part B: Applied Biomaterials: An Official Journal of The Society for Biomaterials, The Japanese Society for Biomaterials, and The Australian Society for Biomaterials and the Korean Society for Biomaterials*, 71(2):343–354, 2004. ISSN 1552-4973.

[176] Alberto Di Martino, Michael Sittinger, and Makarand V Risbud. Chitosan: a versatile biopolymer for orthopaedic tissue-engineering. *Biomaterials*, 26(30): 5983–5990, 2005. ISSN 0142-9612.

[177] Hongxia Zhao and Weihuan Liang. A novel comby scaffold with improved mechanical strength for bone tissue engineering. *Materials Letters*, 194:220–223, 2017. ISSN 0167-577X.

[178] Jon A Rowley, Gerard Madlambayan, and David J Mooney. Alginate hydrogels as synthetic extracellular matrix materials. *Biomaterials*, 20(1):45–53, 1999. ISSN 0142-9612.

[179] E Alsberg, K W Anderson, A Albeiruti, R T Franceschi, and D J Mooney. Cell-interactive alginate hydrogels for bone tissue engineering. *Journal of dental research*, 80(11):2025–2029, 2001. ISSN 0022-0345.

[180] L Wang, R M Shelton, P R Cooper, M Lawson, J T Triffitt, and J E Barralet. Evaluation of sodium alginate for bone marrow cell tissue engineering. *Biomaterials*, 24(20):3475–3481, 2003. ISSN 0142-9612.

[181] Kuen Yong Lee and David J Mooney. Alginate: properties and biomedical applications. *Progress in polymer science*, 37(1):106–126, 2012. ISSN 0079-6700.

[182] C V M Rodrigues, P Serricella, A B R Linhares, R M Guerdes, R Borojevic, M A Rossi, M E L Duarte, and M Farina. Characterization of a bovine collagen–hydroxyapatite composite scaffold for bone tissue engineering. *Biomaterials*, 24(27):4987–4997, 2003. ISSN 0142-9612.

[183] Biman B Mandal, Ariela Grinberg, Eun Seok Gil, Bruce Panilaitis, and David L Kaplan. High-strength silk protein scaffolds for bone repair. *Proceedings of the National Academy of Sciences*, 109(20):7699–7704, 2012. ISSN 0027-8424.

[184] Cristina Correia, Sarindr Bhumiratana, Le-Ping Yan, Ana L Oliveira, Jeffrey M Gimble, Danielle Rockwood, David L Kaplan, Rui A Sousa, Rui L Reis, and Gordana Vunjak-Novakovic. Development of silk-based scaffolds for tissue engineering of bone from human adipose-derived stem cells. *Acta biomaterialia*, 8 (7):2483–2492, 2012. ISSN 1742-7061.

[185] Ryan K Roeder, Gabriel L Converse, Robert J Kane, and Weimin Yue. Hydroxyapatite-reinforced polymer biocomposites for synthetic bone substitutes. *Jom*, 60(3):38–45, 2008. ISSN 1047-4838.

[186] Istikamah Subuki, Nurzaimah Adnan, and Rahida Wati Sharudin. Biodegradable scaffold of natural polymer and hydroxyapatite for bone tissue engineering: A short review. In *AIP Conference Proceedings*, volume 2031, page 20019. AIP Publishing LLC, 2018. ISBN 0735417555.

[187] Sreepadmini Ragunathan, Gopu Govindasamy, D R Raghul, M Karuppaswamy, and R K VijayachandraTogo. Hydroxyapatite reinforced natural polymer scaffold for bone tissue regeneration. *Materials Today: Proceedings*, 2019. ISSN 2214-7853. doi: https://doi.org/10.1016/j.matpr.2019.07.712. URL http://www.sciencedirect.com/science/article/pii/S221478531932927X.

[188] Yao Wang, Ye Hua, Qian Zhang, Jie Yang, Hongjie Li, Ying Li, Man Cao, Qing Cai, Xiaoping Yang, and Xu Zhang. Using biomimetically mineralized collagen

membranes with different surface stiffness to guide regeneration of bone defects. *Journal of tissue engineering and regenerative medicine*, 12(7):1545–1555, 2018. ISSN 1932-6254.

[189] Zhen Zhang, Zheyi Li, Chengyao Zhang, Jiannan Liu, Yuxing Bai, Song Li, and Chenping Zhang. Biomimetic intrafibrillar mineralized collagen promotes bone regeneration via activation of the Wnt signaling pathway. *International journal of nanomedicine*, 13:7503, 2018.

[190] Alexander J Lausch, Lester C Chong, Hasan Uludag, and Eli D Sone. Multiphasic collagen scaffolds for engineered tissue interfaces. *Advanced Functional Materials*, 28(48):1804730, 2018. ISSN 1616-301X.

[191] Zhi-Ye Qiu, Yun Cui, Chun-Sheng Tao, Zi-Qiang Zhang, Pei-Fu Tang, Ke-Ya Mao, Xiu-Mei Wang, and Fu-Zhai Cui. Mineralized collagen: rationale, current status, and clinical applications. *Materials*, 8(8):4733–4750, 2015.

[192] Željka Perić Kačarević, Patrick Rider, Said Alkildani, Sujith Retnasingh, Marija Pejakić, Reinhard Schnettler, Martin Gosau, Ralf Smeets, Ole Jung, and Mike Barbeck. An introduction to bone tissue engineering. *The International Journal of Artificial Organs*, 43(2):69–86, 2020. ISSN 0391-3988.

[193] Petra Chocholata, Vlastimil Kulda, and Vaclav Babuska. Fabrication of Scaffolds for Bone-Tissue Regeneration. *Materials (Basel, Switzerland)*, 12(4):568, feb 2019. ISSN 1996-1944. doi: 10.3390/ma12040568. URL https://pubmed.ncbi.nlm.nih.gov/30769821https://www.ncbi.nlm.nih.gov/pmc/articles/PMC6416573/.

[194] Fergal J O'Brien. Biomaterials & scaffolds for tissue engineering. *Materials Today*, 14(3):88–95, 2011. ISSN 1369-7021. doi: https://doi.org/10.1016/S1369-7021(11)70058-X. URL http://www.sciencedirect.com/science/article/pii/S136970211170058X.

[195] Marcello Pilia, Teja Guda, and Mark Appleford. Development of composite scaffolds for load-bearing segmental bone defects. *BioMed research international*, 2013:458253, 2013. ISSN 2314-6141. doi: 10.1155/2013/458253. URL https://pubmed.ncbi.nlm.nih.gov/23984363https://www.ncbi.nlm.nih.gov/pmc/articles/PMC3745947/.

[196] Brian Wingender, Patrick Bradley, Neha Saxena, Jeffrey W Ruberti, and Laurie Gower. Biomimetic organization of collagen matrices to template bone-like microstructures. *Matrix Biology*, 52-54:384–396, 2016. ISSN 0945-053X. doi: https://doi.org/10.1016/j.matbio.2016.02.004. URL http://www.sciencedirect.com/science/article/pii/S0945053X16300154.

[197] Brendan H Grue and Samuel P Veres. Alternate Soaking Enables Easy Control of Mineralized Collagen Scaffold Mechanics from Nano- to Macro-scale. *Submitted for publication*, 2020.

[198] Emil H Schemitsch. Size matters: defining critical in bone defect size! *Journal of orthopaedic trauma*, 31:S20–S22, 2017. ISSN 0890-5339.

[199] JOHN P Schmitz and Jeffrey O Hollinger. The critical size defect as an experimental model for craniomandibulofacial nonunions. *Clinical orthopaedics and related research*, (205):299–308, 1986. ISSN 0009-921X.

[200] M Marzec, Justyna Kucińska-Lipka, Ilona Kalaszczyńska, and Helena Janik. Development of polyurethanes for bone repair. *Materials Science and Engineering: C*, 80:736–747, 2017. ISSN 0928-4931.

[201] Frank G Lyons, John P Gleeson, Sonia Partap, Karen Coghlan, and Fergal J O'Brien. Novel microhydroxyapatite particles in a collagen scaffold: a bioactive bone void filler? *Clinical Orthopaedics and Related Research®*, 472(4):1318–1328, 2014. ISSN 0009-921X.

[202] Andrew J Pugely, Emily B Petersen, Nicole DeVries-Watson, and Douglas C Fredericks. Influence of 45S5 bioactive glass in a standard calcium phosphate collagen bone graft substitute on the posterolateral fusion of rabbit spine. *The Iowa orthopaedic journal*, 37:193, 2017.

[203] Hellen Zheng, Yajun Bai, Mei-Shu Shih, Christiane Hoffmann, Fabian Peters, Christoph Waldner, and Wolf-Dietrich Hübner. Effect of a β-TCP collagen composite bone substitute on healing of drilled bone voids in the distal femoral condyle of rabbits. *Journal of Biomedical Materials Research Part B: Applied Biomaterials*, 102(2):376–383, 2014. ISSN 1552-4973.

[204] Giovanna Calabrese, Raffaella Giuffrida, Stefano Forte, Lucia Salvatorelli, Claudia Fabbi, Elisa Figallo, Massimo Gulisano, Rosalba Parenti, Gaetano Magro, and Cristina Colarossi. Bone augmentation after ectopic implantation of a cell-free collagen-hydroxyapatite scaffold in the mouse. *Scientific reports*, 6:36399, 2016. ISSN 2045-2322.

[205] Daniel W Weisgerber, Steven R Caliari, and Brendan A C Harley. Min-

eralized collagen scaffolds induce hMSC osteogenesis and matrix remodeling. *Biomaterials science*, 3(3):533–542, mar 2015. ISSN 2047-4849. doi: 10.1039/C4BM00397G. URL https://www.ncbi.nlm.nih.gov/pubmed/25937924https://www.ncbi.nlm.nih.gov/pmc/articles/PMC4412464/.

[206] Kai-Feng Lin, Shu He, Yue Song, Chun-Mei Wang, Yi Gao, Jun-Qin Li, Peng Tang, Zheng Wang, Long Bi, and Guo-Xian Pei. Low-temperature additive manufacturing of biomimic three-dimensional hydroxyapatite/collagen scaffolds for bone regeneration. *ACS applied materials & interfaces*, 8(11):6905–6916, 2016. ISSN 1944-8244.

[207] Elena Landi, Giandomenico Logroscino, Luca Proietti, Anna Tampieri, Monica Sandri, and Simone Sprio. Biomimetic Mg-substituted hydroxyapatite: from synthesis to in vivo behaviour. *Journal of Materials Science: Materials in Medicine*, 19(1):239–247, 2008. ISSN 0957-4530.

[208] Atsuro Yokoyama, Michael Gelinsky, Takao Kawasaki, Takao Kohgo, Ulla König, Wolfgang Pompe, and Fumio Watari. Biomimetic porous scaffolds with high elasticity made from mineralized collagenan animal study. *Journal of Biomedical Materials Research Part B: Applied Biomaterials: An Official Journal of The Society for Biomaterials, The Japanese Society for Biomaterials, and The Australian Society for Biomaterials and the Korean Society for Biomaterials*, 75(2):464–472, 2005.

[209] J C Goes, S D Figueiro, A M Oliveira, A. A.M. Macedo, C C Silva, N. M.P.S. Ricardo, and A. S.B. Sombra. Apatite coating on anionic and native collagen

films by an alternate soaking process. *Acta Biomaterialia*, 3(5):773–778, sep 2007. ISSN 17427061. doi: 10.1016/j.actbio.2007.02.008.

[210] E K Girija, Y Yokogawa, and F Nagata. Apatite formation on collagen fibrils in the presence of polyacrylic acid. *Journal of Materials Science: Materials in Medicine*, 15(5):593–599, 2004. ISSN 09574530. doi: 10.1023/B:JMSM.0000026101.53272.86.

[211] David Lickorish, John A M Ramshaw, Jerome A Werkmeister, Veronica Glattauer, and C Rolfe Howlett. Collagen–hydroxyapatite composite prepared by biomimetic process. *Journal of Biomedical Materials Research Part A: An Official Journal of The Society for Biomaterials, The Japanese Society for Biomaterials, and The Australian Society for Biomaterials and the Korean Society for Biomaterials*, 68(1):19–27, 2004. ISSN 1549-3296.

[212] Max M Villa, Liping Wang, Jianping Huang, David W Rowe, and Mei Wei. Bone tissue engineering with a collagen–hydroxyapatite scaffold and culture expanded bone marrow stromal cells. *Journal of Biomedical Materials Research Part B: Applied Biomaterials*, 103(2):243–253, 2015. ISSN 1552-4973.

[213] Wenying Liu, Yi Chun Yeh, Justin Lipner, Jingwei Xie, Hsing Wen Sung, Stavros Thomopoulos, and Younan Xia. Enhancing the stiffness of electrospun nanofiber scaffolds with a controlled surface coating and mineralization. *Langmuir*, 27(15):9088–9093, 2011. ISSN 07437463. doi: 10.1021/la2018105.

[214] Susan Liao, Fumio Watari, Motohiro Uo, Shoji Ohkawa, Kazuchika Tamura, Wei Wang, and Fuzhai Cui. The preparation and characteristics of a carbonated

hydroxyapatite/collagen composite at room temperature. *Journal of Biomedical Materials Research - Part B Applied Biomaterials*, 74(2):817–821, 2005. ISSN 00219304. doi: 10.1002/jbm.b.30315.

[215] Luis M Delgado, Yves Bayon, Abhay Pandit, and Dimitrios I Zeugolis. To Cross-Link or Not to Cross-Link? Cross-Linking Associated Foreign Body Response of Collagen-Based Devices. *Tissue Engineering - Part B: Reviews*, 21(3):298–313, 2015. ISSN 19373376. doi: 10.1089/ten.teb.2014.0290.

[216] Takako Ida, Masaru Kaku, Megumi Kitami, Masahiko Terajima, Juan Marcelo Rosales Rocabado, Yosuke Akiba, Masako Nagasawa, Mitsuo Yamauchi, and Katsumi Uoshima. Extracellular matrix with defective collagen cross-linking affects the differentiation of bone cells. *PloS one*, 13(9):e0204306, 2018. ISSN 1932-6203.

[217] M J Olszta, E P Douglas, and L B Gower. Scanning electron microscopic analysis of the mineralization of type I collagen via a polymer-induced liquid-precursor (PILP) process. *Calcified tissue international*, 72(5):583–591, 2003. ISSN 0171-967X.

[218] Terence Woods and Paul F Gratzer. Effectiveness of three extraction techniques in the development of a decellularized bone–anterior cruciate ligament–bone graft. *Biomaterials*, 26(35):7339–7349, 2005. ISSN 0142-9612.

[219] Li Sha Gu, Jongryul Kim, Young Kyung Kim, Yan Liu, Sabine H Dickens, David H Pashley, Jun Qi Ling, and Franklin R Tay. A chemical phosphorylation-inspired design for Type i collagen biomimetic remineralization. *Dental Mate-*

rials, 26(11):1077–1089, aug 2010. ISSN 01095641. doi: 10.1016/j.dental.2010.07.008.

[220] C Y Shen. Alkaline hydrolysis of sodium trimetaphosphate in concentrated solutions and its role in built detergents. *Industrial and Engineering Chemistry Product Research and Development*, 5(3):272–276, 1966. ISSN 01964321. doi: 10.1021/i360019a015.

[221] Tetsushi Taguchi, Miki Shiraogawa, Akio Kishida, and Mitsuru Akashi. A study on hydroxyapatite formation on/in the hydroxyl groups-bearing nonionic hydrogels. *Journal of Biomaterials Science, Polymer Edition*, 10(1):19–32, 1999. ISSN 0920-5063.

[222] Liga Berzina-Cimdina and Natalija Borodajenko. Research of calcium phosphates using Fourier transform infrared spectroscopy. *Infrared Spectroscopy-Materials Science, Engineering and Technology*, 12(7):251–263, 2012.

[223] Siwaporn Meejoo, Weerakanya Maneeprakorn, and Pongtip Winotai. Phase and thermal stability of nanocrystalline hydroxyapatite prepared via microwave heating. *Thermochimica Acta*, 447(1):115–120, 2006. ISSN 0040-6031.

[224] Arghavan Farzadi, Farhad Bakhshi, Mehran Solati-Hashjin, Mitra Asadi-Eydivand, and Noor Azuan abu Osman. Magnesium incorporated hydroxyapatite: Synthesis and structural properties characterization. *Ceramics International*, 40(4):6021–6029, 2014. ISSN 0272-8842.

[225] Abdullah Chandra Sekhar Talari, Marcela A Garcia Martinez, Zanyar Movasaghi, Shazza Rehman, and Ihtesham Ur Rehman. Advances in Fourier

transform infrared (FTIR) spectroscopy of biological tissues. *Applied Spectroscopy Reviews*, 52(5):456–506, 2017. ISSN 0570-4928.

[226] S Raynaud, E Champion, D Bernache-Assollant, and P Thomas. Calcium phosphate apatites with variable Ca/P atomic ratio I. Synthesis, characterisation and thermal stability of powders. *Biomaterials*, 23(4):1065–1072, 2002. ISSN 0142-9612.

[227] I Manjubala and M Sivakumar. In-situ synthesis of biphasic calcium phosphate ceramics using microwave irradiation. *Materials chemistry and physics*, 71(3): 272–278, 2001. ISSN 0254-0584.

[228] Sang Soo Jee, Lauren Culver, Yuping Li, Elliot P Douglas, and Laurie B Gower. Biomimetic mineralization of collagen via an enzyme-aided PILP process. *Journal of Crystal Growth*, 312(8):1249–1256, 2010. ISSN 0022-0248.

[229] Fabio Nudelman, Koen Pieterse, Anne George, Paul H H Bomans, Heiner Friedrich, Laura J Brylka, Peter A J Hilbers, Gijsbertus de With, and Nico A J M Sommerdijk. The role of collagen in bone apatite formation in the presence of hydroxyapatite nucleation inhibitors. *Nature materials*, 9(12):1004, 2010. ISSN 1476-4660.

[230] Doyoon Kim, Byeongdu Lee, Stavros Thomopoulos, and Young-Shin Jun. The role of confined collagen geometry in decreasing nucleation energy barriers to intrafibrillar mineralization. *Nature communications*, 9(1):962, 2018. ISSN 2041-1723.

[231] Changyu Shao, Ruibo Zhao, Shuqin Jiang, Shasha Yao, Zhifang Wu, Biao Jin,

Yuling Yang, Haihua Pan, and Ruikang Tang. Citrate improves collagen mineralization via interface wetting: a physicochemical understanding of biomineralization control. *Advanced Materials*, 30(8):1704876, 2018. ISSN 0935-9648.

[232] Y-Y Hu, A Rawal, and K Schmidt-Rohr. Strongly bound citrate stabilizes the apatite nanocrystals in bone. *Proceedings of the national academy of sciences*, 107(52):22425–22429, 2010. ISSN 0027-8424.

[233] Baoquan Xie and George H Nancollas. How to control the size and morphology of apatite nanocrystals in bone. *Proceedings of the National Academy of Sciences*, 107(52):22369–22370, 2010. ISSN 0027-8424.

[234] Michele Iafisco, Gloria Belén Ramírez-Rodríguez, Yuriy Sakhno, Anna Tampieri, Gianmario Martra, Jaime Gómez-Morales, and José Manuel Delgado-López. The growth mechanism of apatite nanocrystals assisted by citrate: relevance to bone biomineralization. *CrystEngComm*, 17(3):507–511, 2015.

[235] Guenter Matheis and John R Whitaker. Chemical phosphorylation of food proteins: an overview and a prospectus. *Journal of Agricultural and Food Chemistry*, 32(4):699–705, 1984. ISSN 0021-8561.

[236] Can-Peng Li, Hirofumi Enomoto, Yoko Hayashi, Hui Zhao, and Takayoshi Aoki. Recent advances in phosphorylation of food proteins: A review. *LWT-Food Science and Technology*, 43(9):1295–1300, 2010. ISSN 0023-6438.

[237] Xingguo Cheng, Philip L Varona, Matthew J Olszta, and Laurie B Gower. Biomimetic synthesis of calcite films by a polymer-induced liquid-precursor

(PILP) process: 1. Influence and incorporation of magnesium. *Journal of Crystal Growth*, 307(2):395–404, 2007. ISSN 0022-0248.

[238] Yael Politi, David R Batchelor, Paul Zaslansky, Bradley F Chmelka, James C Weaver, Irit Sagi, Steve Weiner, and Lia Addadi. Role of magnesium ion in the stabilization of biogenic amorphous calcium carbonate: A structure function investigation. *Chemistry of Materials*, 22(1):161–166, 2009. ISSN 0897-4756.

[239] John K Berg, Thomas Jordan, Yvonne Binder, Hans G Borner, and Denis Gebauer. Mg2+ tunes the wettability of liquid precursors of CaCO3: Toward controlling mineralization sites in hybrid materials. *Journal of the American Chemical Society*, 135(34):12512–12515, 2013. ISSN 0002-7863.

[240] Wolfgang Linhart, Fabian Peters, Wolfgang Lehmann, Karsten Schwarz, Arndt Friedrich Schilling, Michael Amling, Johannes Maria Rueger, and Matthias Epple. Biologically and chemically optimized composites of carbonated apatite and polyglycolide as bone substitution materials. *Journal of Biomedical Materials Research: An Official Journal of The Society for Biomaterials and The Japanese Society for Biomaterials*, 54(2):162–171, 2001. ISSN 0021-9304.

[241] J Moradian-Oldak, S Weiner, L Addadi, W J Landis, and W Traub. Electron imaging and diffraction study of individual crystals of bone, mineralized tendon and synthetic carbonate apatite. *Connective tissue research*, 25(3-4):219–228, 1991. ISSN 0300-8207.

[242] Grégory Chatelain, Damien Bourgeois, Johann Ravaux, Olivier Averseng,

Claude Vidaud, and Daniel Meyer. Alternate dipping preparation of biomimetic apatite layers in the presence of carbonate ions. *Biomedical Materials*, 9(1): 15003, 2013. ISSN 1748-605X.

[243] F C M Driessens, M G Boltong, O Bermudez, J A Planell, M P Ginebra, and E Fernandez. Effective formulations for the preparation of calcium phosphate bone cements. *Journal of Materials Science: Materials in Medicine*, 5(3):164–170, 1994. ISSN 0957-4530.

[244] George Fountos, Margaret Tzaphlidou, Evangelia Kounadi, and Dimitris Glaros. In vivo measurement of radius calcium/phosphorus ratio by X-ray absorptiometry. *Applied radiation and isotopes*, 51(3):273–278, 1999. ISSN 0969-8043.

[245] M Tzaphlidou and V Zaichick. Sex and age related Ca/P ratio in cortical bone of iliac crest of healthy humans. *Journal of radioanalytical and nuclear chemistry*, 259(2):347–349, 2004. ISSN 0236-5731.

[246] Sahar Mousa and Adly Hanna. Synthesis of nano-crystalline hydroxyapatite and ammonium sulfate from phosphogypsum waste. *Materials Research Bulletin*, 48 (2):823–828, 2013. ISSN 0025-5408.

[247] Ferdinand C M Driessens and R K Verbeeck. *Biominerals*. CRC Press, 1990. ISBN 0849352800.

[248] E Potier, J Noailly, and K Ito. Directing bone marrow-derived stromal cell function with mechanics. *Journal of biomechanics*, 43(5):807–817, 2010.

[249] Laura A Smith, Xiaohua Liu, Jiang Hu, and Peter X Ma. The Enhancement

of human embryonic stem cell osteogenic differentiation with nano-fibrous scaffolding. *Biomaterials*, 31(21):5526–5535, 2010.

[250] Peter X Ma, Victor J Chen, and Kyung Mi Woo. Nano-fibrous scaffolding architecture selectively enhances protein adsorption contributing to cell attachment. *Journal of biomedical materials research. Part A*, 67(2):531–537, nov 2003.

[251] Gwendolen C Reilly and Adam J Engler. Intrinsic extracellular matrix properties regulate stem cell differentiation. *Special Issue on Cell Mechanobiology*, 43 (1):55–62, 2010.

[252] Thomas J Webster, Celaletdin Ergun, Robert H Doremus, Richard W Siegel, and Rena Bizios. Enhanced osteoclast-like cell functions on nanophase ceramics. *Biomaterials*, 22(11):1327–1333, 2001. ISSN 0142-9612. doi: https://doi.org/10.1016/S0142-9612(00)00285-4. URL http://www.sciencedirect.com/science/article/pii/S0142961200002854.

[253] Matthew J Dalby, Nikolaj Gadegaard, Rahul Tare, Abhay Andar, Mathis O Riehle, Pawel Herzyk, Chris D W Wilkinson, and Richard O C Oreffo. The control of human mesenchymal cell differentiation using nanoscale symmetry and disorder. *Nature materials*, 6(12):997, 2007.

[254] J T Czernuszka and D A Wahl. Collagen-hydroxyapatite composites for hard tissue repair. *European cells & materials*, 11:43–56, mar 2006.

[255] Jan T Czernuszka, Chaozong Liu, Eleftherios Sachlos, and Denys A Wahl. Controlling the processing of collagen-hydroxyapatite scaffolds for bone tissue en-

gineering. *Journal of materials science. Materials in medicine*, 18(2):201–209, feb 2007.

[256] Dawei Zhang, Xiaowei Wu, Jingdi Chen, and Kaili Lin. The development of collagen based composite scaffolds for bone regeneration. *Bioactive materials*, 3 (1):129–138, sep 2017. ISSN 2452-199X. doi: 10.1016/j.bioactmat.2017.08.004. URL https://www.ncbi.nlm.nih.gov/pubmed/29744450https://www.ncbi.nlm.nih.gov/pmc/articles/PMC5935759/.

[257] Isabelle Denry and Liisa T Kuhn. Design and characterization of calcium phosphate ceramic scaffolds for bone tissue engineering. *Dental Materials*, 32(1):43–53, 2016. ISSN 0109-5641. doi: https://doi.org/10.1016/j.dental.2015.09.008. URL http://www.sciencedirect.com/science/article/pii/S0109564115004042.

[258] Brendan H Grue and Samuel P Veres. Use of tendon to produce decellularized sheets of mineralized collagen fibrils for bone tissue repair and regeneration. *Journal of Biomedical Materials Research Part B: Applied Biomaterials*, 2019. ISSN 1552-4973.

[259] S Heinemann, C Heinemann, M Jager, J Neunzehn, H P Wiesmann, and T Hanke. Effect of silica and hydroxyapatite mineralization on the mechanical properties and the biocompatibility of nanocomposite collagen scaffolds. *ACS applied materials & interfaces*, 3(11):4323–4331, 2011. ISSN 1944-8244.

[260] Grainne M Cunniffe, Glenn R Dickson, Sonia Partap, Kenneth T Stanton, and Fergal J O'Brien. Development and characterisation of a collagen nano-

hydroxyapatite composite scaffold for bone tissue engineering. *Journal of Materials Science: Materials in Medicine*, 21(8):2293–2298, 2010. ISSN 1573-4838. doi: 10.1007/s10856-009-3964-1. URL https://doi.org/10.1007/s10856-009-3964-1.

[261] Terence Woods and Paul F Gratzer. Effectiveness of three extraction techniques in the development of a decellularized boneanterior cruciate ligamentbone graft. *Dedicated to Canadian Biomaterials ResearchDedicated to Canadian Biomaterials Research*, 26(35):7339–7349, dec 2005.

[262] Anora K Burwell, Taili Thula-Mata, Laurie B Gower, Stefan Habeliz, Michael Kurylo, Sunita P Ho, Yung-Ching Chien, Jing Cheng, Nancy F Cheng, and Stuart A Gansky. Functional remineralization of dentin lesions using polymer-induced liquid-precursor process. *PloS one*, 7(6), 2012.

[263] Sang-Soo Jee, Taili T Thula, and Laurie B Gower. Development of bone-like composites via the polymer-induced liquid-precursor (PILP) process. Part 1: Influence of polymer molecular weight. *Acta Biomaterialia*, 6(9):3676–3686, 2010. ISSN 1742-7061. doi: https://doi.org/10.1016/j.actbio.2010.03.036. URL http://www.sciencedirect.com/science/article/pii/S1742706110001625.

[264] Bryan D Quan and Eli D Sone. The effect of polyaspartate chain length on mediating biomimetic remineralization of collagenous tissues. *Journal of The Royal Society Interface*, 15(147):20180269, 2018. ISSN 1742-5689.

[265] Benedikt R Neugirg, Sean R Koebley, Hannes C Schniepp, and Andreas Fery. AFM-based mechanical characterization of single nanofibres. *Nanoscale*, 8(16):

8414–8426, 2016.

[266] B V Derjaguin, V M Muller, and Yu.P Toporov. Effect of contact deformations on the adhesion of particles. *Journal of Colloid and Interface Science*, 53(2):314–326, 1975. ISSN 0021-9797. doi: https://doi.org/10.1016/0021-9797(75)90018-1. URL http://www.sciencedirect.com/science/article/pii/0021979775900181.

[267] T J Young, M A Monclus, T L Burnett, W R Broughton, S L Ogin, and P A Smith. The use of the PeakForceTM quantitative nanomechanical mapping AFM-based method for high-resolution Young's modulus measurement of polymers. *Measurement Science and Technology*, 22(12):125703, 2011. ISSN 0957-0233.

[268] H Buckle, J H Westbrook, and H Conrad. The science of hardness testing and its research applications. *American Society for Metals*, pages 453–491, 1973.

[269] ASTM International. ASTM D790-17 Standard Test Methods for Flexural Properties of Unreinforced and Reinforced Plastics and Electrical Insulating Materials., 2017.

[270] Majid Minary-Jolandan and Min Feng Yu. Nanomechanical heterogeneity in the gap and overlap regions of type I collagen fibrils with implications for bone heterogeneity. *Biomacromolecules*, 10(9):2565–2570, 2009. ISSN 15257797. doi: 10.1021/bm900519v.

[271] Stylianos V Kontomaris, Dido Yova, Andreas Stylianou, and Giorgos Balogian-

nis. The effects of UV irradiation on collagen D-band revealed by atomic force microscopy. *Scanning*, 37(2):101–111, 2015.

[272] O Chan, M J Coathup, A Nesbitt, C Y Ho, K A Hing, T Buckland, C Campion, and G W Blunn. The effects of microporosity on osteoinduction of calcium phosphate bone graft substitute biomaterials. *Acta Biomaterialia*, 8(7):2788–2794, 2012.

[273] Hiroshi Yamasaki and Hidetaka Sakai. Osteogenic response to porous hydroxyapatite ceramics under the skin of dogs. *Biomaterials*, 13(5):308–312, 1992.

[274] Huipin Yuan, Zongjian Yang, Yubao Li, Xingdong Zhang, J D de Bruijn, and K De Groot. Osteoinduction by calcium phosphate biomaterials. *Journal of Materials Science: Materials in Medicine*, 9(12):723–726, 1998.

[275] Ugo Ripamonti. Osteoinduction in porous hydroxyapatite implanted in heterotopic sites of different animal models. *Biomaterials*, 17(1):31–35, 1996.

[276] Borhane H Fellah, Olivier Gauthier, Pierre Weiss, Daniel Chappard, and Pierre Layrolle. Osteogenicity of biphasic calcium phosphate ceramics and bone autograft in a goat model. *Biomaterials*, 29(9):1177–1188, 2008.

[277] Richard J Miron, Yuang Shuang, Dieter D Bosshardt, Jordi Caballé-Serrano, Fatiha Chandad, and Yufeng Zhang. Osteogenic gene array of osteoblasts cultured on a novel osteoinductive biphasic calcium phosphate bone grafting material. *Clinical Oral Investigations*, 21(3):801–808, 2017. ISSN 14363771. doi: 10.1007/s00784-016-1825-0.

[278] Ting Wang, Xiaoyan Yang, Xin Qi, and Chaoyin Jiang. Osteoinduction and proliferation of bone-marrow stromal cells in three-dimensional poly (-caprolactone)/hydroxyapatite/collagen scaffolds. *Journal of translational medicine*, 13(1):152, 2015.

[279] Juliette van den Dolder and John A Jansen. The response of osteoblast-like cells towards collagen type I coating immobilized by p-nitrophenylchloroformate to titanium. *Journal of Biomedical Materials Research Part A: An Official Journal of The Society for Biomaterials, The Japanese Society for Biomaterials, and The Australian Society for Biomaterials and the Korean Society for Biomaterials*, 83(3):712–719, 2007.

[280] Chirag B Khatiwala, Shelly R Peyton, and Andrew J Putnam. Intrinsic mechanical properties of the extracellular matrix affect the behavior of pre-osteoblastic MC3T3-E1 cells. *American Journal of Physiology-Cell Physiology*, 290(6): C1640–C1650, 2006. ISSN 0363-6143.

[281] P L Leong and E F Morgan. Measurement of fracture callus material properties via nanoindentation. *Acta biomaterialia*, 4(5):1569–1575, sep 2008. ISSN 1742-7061. doi: 10.1016/j.actbio.2008.02.030. URL https://www.ncbi.nlm.nih.gov/pubmed/18400573https://www.ncbi.nlm.nih.gov/pmc/articles/PMC2575108/.

[282] Bradley T Estes, Jeffrey M Gimble, and Farshid Guilak. Mechanical Signals as Regulators of Stem Cell Fate. pages 91–126. Academic Press, 2004.

[283] Hongwei Lv, Lisha Li, Meiyu Sun, Yin Zhang, Li Chen, Yue Rong, and Yulin Li.

Mechanism of regulation of stem cell differentiation by matrix stiffness. *Stem cell research & therapy*, 6(1):103, 2015.

[284] Amanda M Malone, Ratul Narain, and Christopher R Jacobs. Biomechanical regulation of mesenchymal stem and progenitor cells and the implications for regenerative medicine. *Current Opinion in Orthopaedics*, 16(5):363–367, 2005.

[285] Yu-Ru V Shih, Kuo-Fung Tseng, Hsiu-Yu Lai, Chi-Hung Lin, and Oscar K Lee. Matrix stiffness regulation of integrin-mediated mechanotransduction during osteogenic differentiation of human mesenchymal stem cells. *Journal of Bone and Mineral Research*, 26(4):730–738, 2011.

[286] Laura Macri-Pellizzeri, Elena M De-Juan-Pardo, Felipe Prosper, and Beatriz Pelacho. Role of substrate biomechanics in controlling (stem) cell fate: implications in regenerative medicine. *Journal of tissue engineering and regenerative medicine*, 12(4):1012–1019, 2018. ISSN 1932-6254.

[287] Jin Hao, Yueling Zhang, Dian Jing, Yu Shen, Ge Tang, Shishu Huang, and Zhihe Zhao. Mechanobiology of mesenchymal stem cells: Perspective into mechanical induction of MSC fate. *Acta Biomaterialia*, 20:1–9, 2015.

[288] Robert J Kane and Ryan K Roeder. Effects of hydroxyapatite reinforcement on the architecture and mechanical properties of freeze-dried collagen scaffolds. *Journal of the Mechanical Behavior of Biomedical Materials*, 7:41–49, 2012. ISSN 1751-6161. doi: https://doi.org/10.1016/j.jmbbm.2011.09.010. URL http://www.sciencedirect.com/science/article/pii/S175161611100244X.

[289] Yan Liu, Dan Luo, Xiao-Xing Kou, Xue-Dong Wang, Franklin R Tay, Yin-Lin Sha, Ye-Hua Gan, and Yan-Heng Zhou. Hierarchical intrafibrillar nanocarbonated apatite assembly improves the nanomechanics and cytocompatibility of mineralized collagen. *Advanced Functional Materials*, 23(11):1404–1411, 2013. ISSN 1616-301X.

[290] M Balooch, S Habelitz, J H Kinney, S J Marshall, and G W Marshall. Mechanical properties of mineralized collagen fibrils as influenced by demineralization. *Journal of Structural Biology*, 162(3):404–410, 2008. ISSN 1047-8477. doi: https://doi.org/10.1016/j.jsb.2008.02.010. URL http://www.sciencedirect.com/science/article/pii/S104784770800035X.

[291] Fei Hang and Asa H Barber. Nano-mechanical properties of individual mineralized collagen fibrils from bone tissue. *Journal of the Royal Society Interface*, 8(57):500–505, 2010. ISSN 1742-5689.

[292] K Choi, J L Kuhn, M J Ciarelli, and S A Goldstein. The elastic moduli of human subchondral, trabecular, and cortical bone tissue and the size-dependency of cortical bone modulus. *Journal of Biomechanics*, 23(11):1103–1113, 1990. ISSN 0021-9290. doi: https://doi.org/10.1016/0021-9290(90)90003-L. URL http://www.sciencedirect.com/science/article/pii/002192909090003L.

[293] A Ascenzi, P Baschieri, and A Benvenuti. The bending properties of single osteons. *Journal of Biomechanics*, 23(8):763–771, 1990. ISSN 0021-9290. doi: https://doi.org/10.1016/0021-9290(90)90023-V. URL http://www.sciencedirect.com/science/article/pii/002192909090023V.

[294] S Lettry, B B Seedhom, E Berry, and M Cuppone. Quality assessment of the cortical bone of the human mandible. *Bone*, 32(1):35–44, 2003. ISSN 8756-3282. doi: https://doi.org/10.1016/S8756-3282(02)00921-3. URL http://www.sciencedirect.com/science/article/pii/S8756328202009213.

[295] Jik Hang Clifford Lee, Benjamin Ondruschka, Lisa Falland-Cheung, Mario Scholze, Niels Hammer, Darryl Chan Tong, and John Neil Waddell. An Investigation on the Correlation between the Mechanical Properties of Human Skull Bone, Its Geometry, Microarchitectural Properties, and Water Content. *Journal of Healthcare Engineering*, 2019, 2019. ISSN 2040-2295.

[296] J Rahmoun, A Auperrin, R Delille, H Naceur, and P Drazetic. Characterization and micromechanical modeling of the human cranial bone elastic properties. *Mechanics Research Communications*, 60:7–14, 2014. ISSN 0093-6413. doi: https://doi.org/10.1016/j.mechrescom.2014.04.001. URL http://www.sciencedirect.com/science/article/pii/S009364131400041X.

[297] Peter V Giannoudis and Haralampos T Dinopoulos. Autologous Bone Graft: When Shall We Add Growth Factors? *Foot and Ankle Clinics*, 15(4):597–609, 2010. ISSN 1083-7515. doi: https://doi.org/10.1016/j.fcl.2010.09.005. URL http://www.sciencedirect.com/science/article/pii/S1083751510000744.

[298] Yan Liu, Shuai Liu, Dan Luo, Zhenjie Xue, Xinan Yang, Lin Gu, Yanheng Zhou, and Tie Wang. Hierarchically staggered nanostructure of mineralized collagen as a bone-grafting scaffold. *Advanced Materials*, 28(39):8740–8748, 2016. ISSN

0935-9648.

[299] R David Roden. Principles of Bone Grafting. *Oral and Maxillofacial Surgery Clinics of North America*, 22(3):295–300, 2010. ISSN 1042-3699. doi: https://doi.org/10.1016/j.coms.2010.06.001. URL http://www.sciencedirect.com/science/article/pii/S1042369910000592.

[300] Hans Burchardt. The biology of bone graft repair. *Clinical orthopaedics and related research*, (174):28–42, 1983. ISSN 0009-921X.

[301] Alan S Herford and Jeffrey S Dean. Complications in Bone Grafting. *Oral and Maxillofacial Surgery Clinics of North America*, 23(3):433–442, 2011. ISSN 1042-3699. doi: https://doi.org/10.1016/j.coms.2011.04.004. URL http://www.sciencedirect.com/science/article/pii/S1042369911001014.

[302] Reena A Bhatt and Tamara D Rozental. Bone Graft Substitutes. *Hand Clinics*, 28(4):457–468, 2012. ISSN 0749-0712. doi: https://doi.org/10.1016/j.hcl.2012.08.001. URL http://www.sciencedirect.com/science/article/pii/S0749071212000972.

[303] James T Marino and Bruce H Ziran. Use of Solid and Cancellous Autologous Bone Graft for Fractures and Nonunions. *Orthopedic Clinics of North America*, 41(1):15–26, 2010. ISSN 0030-5898. doi: https://doi.org/10.1016/j.ocl.2009.08.003. URL http://www.sciencedirect.com/science/article/pii/S0030589809000881.

[304] Narayan Venkataraman, Sumidha Bansal, Pankaj Bansal, and Sarita Narayan.

Dynamics of bone graft healing around implants. *Journal of the International Clinical Dental Research Organization*, 7(3):40, 2015. ISSN 2231-0754.

[305] Dominique G Poitout. Biomechanics and biomaterials in orthopedics. 2004.

[306] Yue-Hui Zhang, Lei Shen, Jiang Shao, Dean Chou, Jia Song, and Jing Zhang. Structural Allograft versus Autograft for Instrumented Atlantoaxial Fusions in Pediatric Patients: Radiologic and Clinical Outcomes in Series of 32 Patients. *World Neurosurgery*, 105:549–556, 2017. ISSN 1878-8750. doi: https://doi.org/10.1016/j.wneu.2017.06.048. URL http://www.sciencedirect.com/science/article/pii/S1878875017309403.

[307] Naohiro Shibuya, Brandon K Holloway, and Daniel C Jupiter. A Comparative Study of Incorporation Rates between Non-xenograft and Bovine-based Structural Bone Graft in Foot and Ankle Surgery. *The Journal of Foot and Ankle Surgery*, 53(2):164–167, 2014. ISSN 1067-2516. doi: https://doi.org/10.1053/j.jfas.2013.10.013. URL http://www.sciencedirect.com/science/article/pii/S1067251613004924.

[308] Michael S Block. The Processing of Xenografts Will Result in Different Clinical Responses. *Journal of Oral and Maxillofacial Surgery*, 77(4):690–697, 2019. ISSN 0278-2391. doi: https://doi.org/10.1016/j.joms.2018.10.004. URL http://www.sciencedirect.com/science/article/pii/S0278239118311686.

[309] Elena García-Gareta, Melanie J Coathup, and Gordon W Blunn. Osteoinduction of bone grafting materials for bone repair and regeneration. *Bone*, 81:112–121, 2015. ISSN 8756-3282. doi: https://doi.org/10.1016/j.bone.

2015.07.007. URL http://www.sciencedirect.com/science/article/pii/S8756328215002793.

[310] David C Lobb, Brent R DeGeorge, and A Bobby Chhabra. Bone Graft Substitutes: Current Concepts and Future Expectations. *The Journal of Hand Surgery*, 44(6):497–505.e2, 2019. ISSN 0363-5023. doi: https://doi.org/10.1016/j.jhsa.2018.10.032. URL http://www.sciencedirect.com/science/article/pii/S0363502318307664.

[311] Araceli Cuellar and A Hari Reddi. Cell biology of osteochondromas: bone morphogenic protein signalling and heparan sulphates. *International orthopaedics*, 37(8):1591–1596, 2013. ISSN 0341-2695.

[312] Akiko Mizokami, Tomoyo Kawakubo-Yasukochi, and Masato Hirata. Osteocalcin and its endocrine functions. *Biochemical Pharmacology*, 132:1–8, 2017. ISSN 0006-2952. doi: https://doi.org/10.1016/j.bcp.2017.02.001. URL http://www.sciencedirect.com/science/article/pii/S0006295217300631.

[313] Jae Sam Lee, Jae Sung Lee, and William L Murphy. Modular peptides promote human mesenchymal stem cell differentiation on biomaterial surfaces. *Acta Biomaterialia*, 6(1):21–28, 2010. ISSN 1742-7061. doi: https://doi.org/10.1016/j.actbio.2009.08.003. URL http://www.sciencedirect.com/science/article/pii/S1742706109003304.

[314] A L Boskey, S Gadaleta, C Gundberg, S B Doty, P Ducy, and G Karsenty. Fourier transform infrared microspectroscopic analysis of bones of osteocalcin-deficient mice provides insight into the function of osteocalcin. *Bone*,

23(3):187–196, 1998. ISSN 8756-3282. doi: https://doi.org/10.1016/S8756-3282(98)00092-1. URL http://www.sciencedirect.com/science/article/pii/S8756328298000921.

[315] Ellis E Golub and Kathleen Boesze-Battaglia. The role of alkaline phosphatase in mineralization. *Current opinion in Orthopaedics*, 18(5):444–448, 2007.

[316] Dympna Harmey, Lovisa Hessle, Sonoko Narisawa, Kristen A Johnson, Robert Terkeltaub, and José Luis Millán. Concerted Regulation of Inorganic Pyrophosphate and Osteopontin by Akp2, Enpp1, and Ank: An Integrated Model of the Pathogenesis of Mineralization Disorders. *The American Journal of Pathology*, 164(4):1199–1209, 2004. ISSN 0002-9440. doi: https://doi.org/10.1016/S0002-9440(10)63208-7. URL http://www.sciencedirect.com/science/article/pii/S0002944010632087.

[317] Andreas Hammerl, Carlos E Diaz Cano, Elena M De-Juan-Pardo, Martijn van Griensven, and Patrina S P Poh. A growth factor-free co-culture system of osteoblasts and peripheral blood mononuclear cells for the evaluation of the osteogenesis potential of melt-electrowritten polycaprolactone scaffolds. *International journal of molecular sciences*, 20(5):1068, 2019.

[318] THOMAS J FANGMAN and MARCIA CARLSON SHANNON. CHAPTER 105 - Diseases of the Puerperal Period. pages 789–794. W.B. Saunders, Saint Louis, 2007. ISBN 978-0-7216-9323-1. doi: https://doi.org/10.1016/B978-072169323-1.50108-2. URL http://www.sciencedirect.com/science/article/pii/B9780721693231501082.

[319] Beatrice Yue. Biology of the extracellular matrix: an overview. *Journal of glaucoma*, page S20, 2014.

[320] Chuanglong He, Fan Zhang, Lijun Cao, Wei Feng, Kexin Qiu, Yanzhong Zhang, Hongsheng Wang, Xiumei Mo, and Jinwu Wang. Rapid mineralization of porous gelatin scaffolds by electrodeposition for bone tissue engineering. *Journal of Materials Chemistry*, 22(5):2111–2119, 2012.

[321] Wei Huang, Shuying Yang, Jianzhong Shao, and Yi-Ping Li. Signaling and transcriptional regulation in osteoblast commitment and differentiation. *Frontiers in bioscience: a journal and virtual library*, 12:3068, 2007.

[322] L Darryl Quarles, Daniel A Yohay, Laura W Lever, Rashmi Caton, and Richard J Wenstrup. Distinct proliferative and differentiated stages of murine MC3T3-E1 cells in culture: An in vitro model of osteoblast development. *Journal of Bone and Mineral Research*, 7(6):683–692, 1992. ISSN 0884-0431.

[323] Madhura P Nijsure, Meet Pastakia, Joseph Spano, Michael B Fenn, and Vipuil Kishore. Bioglass incorporation improves mechanical properties and enhances cell-mediated mineralization on electrochemically aligned collagen threads. *Journal of Biomedical Materials Research Part A*, 105(9):2429–2440, 2017. ISSN 1549-3296.

[324] Anna V Taubenberger, Maria A Woodruff, Huifen Bai, Daniel J Muller, and Dietmar W Hutmacher. The effect of unlocking RGD-motifs in collagen I on pre-osteoblast adhesion and differentiation. *Biomaterials*, 31(10):2827–2835, 2010. ISSN 0142-9612. doi: https://doi.org/10.1016/j.biomaterials.

2009.12.051. URL http://www.sciencedirect.com/science/article/pii/S0142961209014380.

[325] Sunita Sardiwal, Per Magnusson, David J A Goldsmith, and Edmund J Lamb. Bone Alkaline Phosphatase in CKD–Mineral Bone Disorder. *American Journal of Kidney Diseases*, 62(4):810–822, 2013. ISSN 0272-6386. doi: https://doi.org/10.1053/j.ajkd.2013.02.366. URL http://www.sciencedirect.com/science/article/pii/S0272638613005866.

[326] Etienne Mornet. Hypophosphatasia. *Best Practice & Research Clinical Rheumatology*, 22(1):113–127, 2008. ISSN 1521-6942. doi: https://doi.org/10.1016/j.berh.2007.11.003. URL http://www.sciencedirect.com/science/article/pii/S152169420700126X.

[327] H Clarke Anderson, Joseph B Sipe, Lovisa Hessle, Rama Dhamyamraju, Elisa Atti, Nancy P Camacho, and José Luis Millán. Impaired Calcification Around Matrix Vesicles of Growth Plate and Bone in Alkaline Phosphatase-Deficient Mice. *The American Journal of Pathology*, 164(3):841–847, 2004. ISSN 0002-9440. doi: https://doi.org/10.1016/S0002-9440(10)63172-0. URL http://www.sciencedirect.com/science/article/pii/S0002944010631720.

[328] Caixia Xu, Peiqiang Su, Xiaofeng Chen, Yongchun Meng, Weihua Yu, Andy Peng Xiang, and Yingjun Wang. Biocompatibility and osteogenesis of biomimetic Bioglass-Collagen-Phosphatidylserine composite scaffolds for bone tissue engineering. *Biomaterials*, 32(4):1051–1058, 2011. ISSN 0142-9612. doi: https://doi.org/10.1016/j.biomaterials.2010.09.068. URL http:

//www.sciencedirect.com/science/article/pii/S0142961210012810.

[329] Michelle Ngiam, Susan Liao, Avinash J Patil, Ziyuan Cheng, Casey K Chan, and S Ramakrishna. The fabrication of nano-hydroxyapatite on PLGA and PLGA/collagen nanofibrous composite scaffolds and their effects in osteoblastic behavior for bone tissue engineering. *Bone*, 45(1):4–16, 2009. ISSN 8756-3282. doi: https://doi.org/10.1016/j.bone.2009.03.674. URL http://www.sciencedirect.com/science/article/pii/S8756328209012708.

[330] Meredith L Zoch, Thomas L Clemens, and Ryan C Riddle. New insights into the biology of osteocalcin. *Bone*, 82:42–49, 2016. ISSN 8756-3282. doi: https://doi.org/10.1016/j.bone.2015.05.046. URL http://www.sciencedirect.com/science/article/pii/S8756328215002355.

[331] Mathieu Ferron and Julie Lacombe. Regulation of energy metabolism by the skeleton: Osteocalcin and beyond. *Archives of Biochemistry and Biophysics*, 561:137–146, 2014. ISSN 0003-9861. doi: https://doi.org/10.1016/j.abb.2014.05.022. URL http://www.sciencedirect.com/science/article/pii/S0003986114001878.

[332] Paul A Price, Marshall R Urist, and Yoko Otawara. Matrix Gla protein, a new γ-carboxyglutamic acid-containing protein which is associated with the organic matrix of bone. *Biochemical and Biophysical Research Communications*, 117(3):765–771, 1983. ISSN 0006-291X. doi: https://doi.org/10.1016/0006-291X(83)91663-7. URL http://www.sciencedirect.com/science/article/pii/0006291X83916637.

[333] O Berezovska, G Yildirim, W C Budell, S Yagerman, B Pidhaynyy, C Bastien, M C H van der Meulen, and T L Dowd. Osteocalcin affects bone mineral and mechanical properties in female mice. *Bone*, 128:115031, 2019. ISSN 8756-3282. doi: https://doi.org/10.1016/j.bone.2019.08.004. URL http://www.sciencedirect.com/science/article/pii/S8756328219303114.

[334] Yun Shen, Yiting Xu, and Yuqian Bao. Interaction among skeleton, body fat and cardiovascular diseases mediated by osteocalcin. *Obesity Medicine*, 17:100184, 2020. ISSN 2451-8476. doi: https://doi.org/10.1016/j.obmed.2020.100184. URL http://www.sciencedirect.com/science/article/pii/S245184762030004X.

[335] Yu-Fen Chou, James C Y Dunn, and Benjamin M Wu. In vitro response of MC3T3-E1 preosteoblasts within three-dimensional apatite-coated PLGA scaffolds. *Journal of Biomedical Materials Research Part B: Applied Biomaterials: An Official Journal of The Society for Biomaterials, The Japanese Society for Biomaterials, and The Australian Society for Biomaterials and the Korean Society for Biomaterials*, 75(1):81–90, 2005. ISSN 1552-4973.

[336] Justine C Lee, Clifford T Pereira, Xiaoyan Ren, Weibiao Huang, David Bischoff, Daniel W Weisgerber, Dean T Yamaguchi, Brendan A Harley, and Timothy A Miller. Optimizing Collagen Scaffolds for Bone Engineering: Effects of Cross-linking and Mineral Content on Structural Contraction and Osteogenesis. *The Journal of craniofacial surgery*, 26(6):1992–1996, sep 2015. ISSN 1536-3732. doi: 10.1097/SCS.0000000000001918. URL https://pubmed.ncbi.nlm.nih.gov/26147021https://www.ncbi.nlm.nih.gov/pmc/articles/PMC4871115/.

[337] Hoon-Sang Sohn and Jong-Keon Oh. Review of bone graft and bone substitutes with an emphasis on fracture surgeries. *Biomaterials Research*, 23(1):9, 2019. ISSN 2055-7124. doi: 10.1186/s40824-019-0157-y. URL https://doi.org/10.1186/s40824-019-0157-y.

[338] Victor Martin and Ana Bettencourt. Bone regeneration: Biomaterials as local delivery systems with improved osteoinductive properties. *Materials Science and Engineering: C*, 82:363–371, 2018. ISSN 0928-4931. doi: https://doi.org/10.1016/j.msec.2017.04.038. URL http://www.sciencedirect.com/science/article/pii/S0928493117303636.

[339] Canadian Institute for Health Information. Hip and Knee Replacements in Canada, 2017-2018. Canadian Joint Replacement Registry Annual Report. Technical report, CIHI, Ottawa, ON, 2019.

[340] Wei Zhang, Xiao-juan Luo, Li-na Niu, Hong-ye Yang, Cynthia K Y Yiu, Li-qun Zhou, Jing Mao, Cui Huang, David H Pashley, and Franklin R Tay. Biomimetic intrafibrillar mineralization of type I collagen with intermediate precursors-loaded mesoporous carriers. *Scientific reports*, 5:11199, 2015. ISSN 2045-2322.

[341] Xiaojin Zhang, Yan Li, Y Eugene Chen, Jihua Chen, and Peter X Ma. Cell-free 3D scaffold with two-stage delivery of miRNA-26a to regenerate critical-sized bone defects. *Nature Communications*, 7(1):10376, 2016. ISSN 2041-1723. doi: 10.1038/ncomms10376. URL https://doi.org/10.1038/ncomms10376.

[342] R Puxkandl, I Zizak, O Paris, J Keckes, W Tesch, S Bernstorff, P Purslow, and P Fratzl. Viscoelastic properties of collagen: synchrotron radiation investi-

gations and structural model. *Philosophical Transactions of the Royal Society of London. Series B: Biological Sciences*, 357(1418):191–197, 2002. ISSN 0962-8436.

[343] Julia Liu, Debashish Das, Fan Yang, Andrea G Schwartz, Guy M Genin, Stavros Thomopoulos, and Ioannis Chasiotis. Energy dissipation in mammalian collagen fibrils: Cyclic strain-induced damping, toughening, and strengthening. *Acta biomaterialia*, 80:217–227, oct 2018. ISSN 1878-7568. doi: 10.1016/j.actbio.2018.09.027. URL https://pubmed.ncbi.nlm.nih.gov/30240954https://www.ncbi.nlm.nih.gov/pmc/articles/PMC6510236/.